Understanding the role of group 2 innate lymphoid cells and mucosal cytokines in urinary tract injury and infection

Guy John-Malcolm Cameron

B.BiomedSc(Hons)

School of Biomedical Sciences and Pharmacy

College of Health, Medicine and Wellbeing

University of Newcastle, Australia.

April 2021

A thesis submitted in fulfilment of the requirements for the degree of Doctor of Philosophy in Immunology and Microbiology

This research was supported by an Australian Government Research Training Program (RTP) Scholarship

Statement of originality

I hereby certify that the work embodied in the thesis is my own work, conducted under normal supervision. The thesis contains no material which has been accepted, or is being examined, for the award of any other degree or diploma in any university or other tertiary institution and, to the best of my knowledge and belief, contains no material previously published or written by another person, except where due reference has been made. I give consent to the final version of my thesis being made available worldwide when deposited in the University's Digital Repository, subject to the provisions of the Copyright Act 1968 and any approved embargo.

Guy John-Malcolm Cameron

Acknowledgement of authorship

I hereby certify that the work embodied in this thesis contains published paper/s/scholarly work of which I am a joint author. I have included as part of the thesis a written declaration endorsed in writing by my supervisor, attesting to my contribution to the joint publication/s/scholarly work.

By signing below, I confirm that Guy Cameron significantly contributed to the data acquisition, analysis and interpretation; drafting of the manuscript; and final approval of the papers/publications entitled:

Cameron GJM, et al. Emerging therapeutic potential of group 2 innate lymphoid cells in acute kidney injury. J Pathol. 2019;248(1):9-15.

Cameron, GJM, et al. Group 2 Innate Lymphoid Cells Are Redundant in Experimental Renal Ischemia-Reperfusion Injury. Front Immunol. 2019;10:826.

Cameron GJM, et al. Systemic interleukin-33 increased the severity of uropathogenic Escherichia coli-induced pyelonephritis and impaired kidney function in mice. JCI Insight. 2021.

Cameron GJM, et al. Treatment with recombinant interleukin-22 protects against uropathogenic Escherichia coli-induced pyelonephritis in mice. Immunol Cell Biol. 2021.

Dr. Malcolm Ronald Starkey

Manuscripts arising from this thesis

1.1 Published at time of submission

Cameron GJM, Jiang SH, Loering S, Deshpande AV, Hansbro PM, Starkey MR. Emerging therapeutic potential of group 2 innate lymphoid cells in acute kidney injury. J Pathol. 2019;248(1):9-15

Cameron GJM, Cautivo KM, Loering S, Jiang SH, Deshpande AV, Foster PS, McKenzie ANJ, Molofsky AB, Hansbro PM, Starkey MR. Group 2 Innate Lymphoid Cells Are Redundant in Experimental Renal Ischemia-Reperfusion Injury. Front Immunol. 2019;10:826.

1.2 Unpublished at time of submission

Cameron GJM, Cautivo KM, Lawrence BM, Loering S, Deshpande AV, Bhatt NP, Collison AM, Foster PS, Deshpande AV, Molofsky AB, Starkey MR. Systemic interleukin-33 increased the severity of uropathogenic Escherichia coli-induced pyelonephritis and impaired kidney function in mice. JCI Insight. 2021.
This article underwent peer review at Kidney Int and peer feedback has been incorporated into this thesis where appropriate.

Cameron GJM*, Lawrence BM*, Loering S, Deshpande AV, Bhatt NP, Collison AM, Foster PS, Deshpande AV, Starkey MR. Treatment with recombinant interleukin-22 protects against uropathogenic Escherichia coli-induced pyelonephritis in mice. Immunol Cell Biol. 2021.
*** equal contribution, co-first author*. *This article underwent peer review at Am J Physiol Renal Physiol and peer feedback has been incorporated into this thesis where appropriate.*

Other publications during candidature for PhD

Donovan C*, Starkey MR*, Kim RY, Rana BMJ, Barlow JL, Jones B, Haw TJ, Mono Nair P, Budden K, **Cameron GJM**, Horvat JC, Wark PA, Foster PS, McKenzie, ANJ, Hansbro PM. Roles for T/B lymphocytes and ILC2 in experimental chronic obstructive pulmonary disease. J Leukoc Biol. 2019;105(1):143-50. ***** *equal contribution, co-first author*

Loering S, **Cameron GJM**, Starkey MR[#], Hansbro PM[#]. Lung development and emerging roles for type 2 immunity. J Pathol. 2019;247(5):686-96. # *co-senior author*

Starkey MR, Plank MW, Casolari P, Papi A, Pavlidis S, Guo Y, **Cameron GJM**, Haw TJ, Tam A, Obiedat M, Donovan C, Hansbro NG, Nguyen DH, Nair PM, Kim RY, Horvat JC, Kaiko GE, Durum SK, Wark PA, Sin DD, Caramori G, Adcock IM, Foster PS, Hansbro PM. IL-22 and its receptors are increased in human and experimental COPD and contribute to pathogenesis. Eur Respir J. 2019;54(1).

Loering S, **Cameron GJM**, Bhatt NP, Belz GT, Foster PS, Hansbro PM, Starkey MR. Differences in pulmonary group 2 innate lymphoid cells are dependent on mouse age, sex and strain. Immunol Cell Biol. 2020.

Conference publications during candidature for PhD

The 3rd International conference on innate lymphoid cells, Tokyo 2018 (*Poster*). *Presented by the supervisory team*

47th Annual Scientific Meeting of the Australasian Society for Immunology, Perth 2018 (*Poster*). *Presented by the supervisory team*

25th edition of the International Society of Nephrology's World Congress of Nephrology, Melbourne 2019 (*Poster*). *Presented by the candidate*

NSW Annual Scientific Meeting for the Australian Society for Medical Research, Newcastle 2019 (*Oral*). *Presented by the candidate*

Dedication

I dedicate this body of work to Rebecca. You inspired me to be a kinder, healthier, and all-round better person each and every day. Without your love, support and encouragement throughout my pursuit of knowledge, completion of this thesis would not have been possible.

Acknowledgements

First and foremost, I would like to thank my current and previous supervisors; Doctor Malcolm Starkey, Professor Phil Hansbro, Doctor Aniruddh Deshpande, Professor Paul Foster and Doctor Adam Collison. Without them, this project would not have been possible.

I also wish to acknowledge the many other mentors from the Hunter Medical Research Institute and University of Newcastle who have provided valuable advice throughout the course of my research.

In addition, I acknowledge Ben Lawrence whom I worked side-by-side with during his honours project. Without him, parts of this thesis would not have been accomplished.

I'd like to extend this acknowledgement to the funding bodies, international collaborators and the co-authors of my publications who made this project possible.

Furthermore, I want to acknowledge everyone at the Wollotuka Institute, their support was crucial for helping me get through the difficult times, ranging from supervisory changes to the impact of the COVID-19 pandemic on my experimental plans.

Finally, a very sincere thank you is extended to my family, friends, and other laboratory colleagues.

Table of contents

List of figures

List of tables

List of abbreviations

AAM: Alternatively activated macrophage

ABR: Australian Bioresources

AKI: Acute kidney injury

AREG: Amphiregulin

BUN: Blood urea nitrogen

CCL: C-C motif chemokine ligand

CFU: Colony forming units

CXCL: C-X-C motif chemokine ligand

*e*GFR: Estimated glomerular filtration rate

ELISA: Enzyme-linked immunosorbent assay

FimH: Type I fimbrin D-mannose specific adhesin

G-CSF: Granulocyte colony stimulating factor

GFR: Glomerular filtration rate

IBC: Intracellular bacterial communities

ICOS: Inducible T-cell costimulator

ICU: Intensive care units

IFN: Interferon

IHC: Immunohistochemistry

IL: Interleukin

ILC: Innate lymphoid cells

ILC1: Group 1 innate lymphoid cells

ILC2: Group 2 innate lymphoid cells

ILC3: Group 3 innate lymphoid cells

IRI: Ischemia reperfusion injury

iT_{reg}: Induced regulatory T-lymphocytes

LOD: Limit of detection

LYVE1: lymphatic endothelial hyaluronan receptor-1

MFI: Median fluorescence intensity

MHCII: Major histocompatibility complex class II

NK: Natural killer cells

NKT: Natural killer T cells

NMU: Neuromedin U

PAS: Periodic acid-Schiff

PBS: Phosphate buffered saline

PCN: Peritubular capillary network

PCT: Proximal convoluted tubule

PFA: Paraformaldehyde

PPE: Personal protective equipment

qPCR: Quantitative real-time polymerase chain reaction

QIR: Quiescent intracellular reservoirs

SEM: Standard error of the mean

SMA: Smooth muscle actin

STAT: Signal transducer and activator of transcription

TCR: T cell receptor

*t*GFR: Transcutaneous glomerular filtration rate

T_H: T helper cells

T_H1: T helper type 1 cells

T_H2: T helper type 2 cells

T_H17: T helper type 17 cells

T_H22: T helper type 22 cells

TLR: Toll-like receptor

TNF: Tumor necrosis factor alpha

T_{reg}: Regulatory T cells

TSLP: Thymic stromal lymphopoietin

t-SNE: t-distributed stochastic neighbor embedding

UO: Ureter obstruction

UTI: Urinary tract infection

Synopsis

Acute kidney injury remains a global challenge, and despite the availability of dialysis and transplantation, can be fatal. Individuals who survive an acute kidney injury are at increased risk of developing chronic kidney disease and end-stage renal failure. Acute injury of the kidney may occur from sterile inflammation associated with lack of blood flow and oxygenation termed ischemia, and from ascending urinary tract infections termed pyelonephritis. Understanding the fundamental mechanisms underpinning the pathophysiology of acute kidney injury is critical for future development of novel strategies for diagnosis and treatment.

A growing body of evidence indicates that amplifying type II immunity may have therapeutic potential in sterile kidney injury and disease. Of particular interest are a recently described subset of innate lymphocytes called group 2 innate lymphoid cells. Group 2 innate lymphoid cells are crucial tissue-resident immune cells that maintain homeostasis and regulate tissue repair at multiple organ sites, including the kidney. They are also critical mediators of type 2 immune responses following infection and injury.

The existing literature suggests that activation of group 2 innate lymphoid cells and production of a local type 2 immune milieu is protective against sterile kidney injury and the associated pathology. Several studies used a gain-of-function approach whereby administration of alarmins such as interleukin-33 prior to and/or after injury. Yet, it is unknown whether the specific depletion of the group 2 innate lymphoid cells would impair the ability of the kidney to repair or whether the injury would be exaggerated if a loss-of-function approach were used.

However, in the context of non-sterile kidney injury far less is known about type II immune pathways. Whilst the interleukin-33 is increased in the urinary bladder following infection in

pre-clinical models, the effect of exogenous interleukin-33 is yet to be explored in this context. Before considering interleukin-33 or other type II immunotherapies for sterile kidney injury, it is essential to explore the role of these factors in a non-sterile context due to the global prevalence of urinary tract infections.

In **Chapter 3** of this thesis, I characterised the phenotype of group 2 innate lymphoid cells in the kidney and contrasted them against the same cells in the lung in terms of cell surface antigen expression and key type II cytokines, interleukin-5 and interleukin-13. Next, I demonstrated that these cells can be identified in cleared tissue sections using cytokine reporter mice and determined that these cells are primarily localised around the vasculature of the mouse kidney. Finally, I performed specific loss-of-function studies using a range of genetically modified mice, which were constitutively deficient in group 2 innate lymphoid cells, and others which were conditionally depleted of these cells by administration of the diphtheria toxoid; and found that reduction of these cells does not impact on the severity of sterile kidney injury induced by surgical blood flow restriction and ischemia.

In **Chapter 4**, I confirmed reports from others and found that the interleukin-33 was increased during uropathogenic *Escherichia coli* infection in the urinary bladder and kidney, respectively. Next, I demonstrated that administration of the recombinant mouse interleukin-33 prior to infection was sufficient to exaggerate the proportion of animals with kidney infection, termed pyelonephritis. Yet interestingly, it did not alter the kinetics of bladder infection, termed cystitis. Additionally, I discovered that *Escherichia coli*-induced pyelonephritis caused a noteworthy kidney injury, as seen in tissue histopathology; and kidney function was impaired, as measured by transcutaneous glomerular filtration rate. Similar to the kidney, I found that group 2 innate lymphoid cells in the bladder can be identified using interleukin-5 reporter systems. Yet there were some inherent differences in the cell surface markers between these

two tissues as determined by unsupervised clustering from flow cytometry. Whilst group 2 innate lymphoid cells were found in the urinary bladder and were localised around the vasculature, specific depletion of these cells by diphtheria toxoid did not induce any obvious phenotype during infection. Finally, I observed that the interleukin-22 levels were decreased following infection with exogenous interleukin-33 pre-treatment.

In **Chapter 5**, I found that the interleukin-22 protein was largely undetectable in the urinary bladder under homeostatic conditions, was highly variable in the kidney, and that the levels were unchanged by circadian rhythm or sex. However, low interleukin-22 low levels were correlated with worse infection in the kidney. Next, I demonstrated that the urinary bladder and kidney express the membranous receptor to respond to interleukin-22, and found that systemic administration of the recombinant cytokine was sufficient to activate downstream pathways in the kidney only. Finally, I demonstrated that exogenous interleukin-22 was protective against pyelonephritis in almost all cases when administered 12 hours after infection, yet the pre-treatment regime was ineffective.

Within this thesis, several knowledge gaps around our understanding of type II immunity and the function of group 2 innate lymphoid cells was investigated in the urinary bladder and kidney. I demonstrated the phenotype of group 2 innate lymphoid cells was unique between the urinary bladder and kidney under homeostatic conditions. I also determined that interleukin-5 reporter systems were able to be used to pinpoint the location of these cells in both tissues, and that the group 2 innate lymphoid cells are localised around the vasculature. Using a combination of loss- and gain-of-function approaches the function of these cells was explored with sterile kidney injury, and urinary tract infection models. Overall, I find that depletion of these cells using diphtheria toxoid cause no significant changes in kidney injury, yet exogenous interleukin-33 caused a phenotype of exaggerated kidney infection with

concurrent low interleukin-22 levels. Finally, I discovered that exogenous interleukin-22 was sufficient to protect against kidney infection.

Chapter 1: General introduction

Some of the content in this chapter has been previously published as:

> **Cameron GJM**, Jiang SH, Loering S, Deshpande AV, Hansbro PM, Starkey MR. Emerging therapeutic potential of group 2 innate lymphoid cells in acute kidney injury. J Pathol. 2019;248(1):9-15

Cameron GJM and Starkey MR conceptualised the manuscript. Cameron GJM drafted the manuscript and figures. Jiang SH, Loering S, Deshpande AV, Hansbro PM and Starkey MR provided critical review of the manuscript.

> **Cameron GJM**, Cautivo KM, Loering S, Jiang SH, Deshpande AV, Foster PS, McKenzie ANJ, Molofsky AB, Hansbro PM, Starkey MR. Group 2 Innate Lymphoid Cells Are Redundant in Experimental Renal Ischemia-Reperfusion Injury. Front Immunol. 2019;10:826.

Cameron GJM and Starkey MR conceptualised the manuscript. Cautivo KM and Molofsky AB performed the flow cytometry and immunofluorescence using Il5$^{td\text{-}tomatoCre}$Rosa26-CAG-RFP mice. Cameron GJM performed all other aspects including the surgical model, flow cytometry, histological assessment, gene expression analysis, data analysis and drafted the manuscript. Loering S assisted with animal monitoring and flow cytometry. Jiang SH and Deshpande AV provided clinical insight for study design and surgical technique. McKenzie ANJ created, supplied and advised on the use of ILC2-deficient & -depleted and Il13td tomato mice. Foster PS supplied and advised on the use of Il5venus reporter line. Foster PS and Hansbro PM advised on experimental design.

1.1 The mammalian kidney

The mammalian kidneys have an important role in maintaining homeostasis through the removal of excess ions and waste from the blood, as urine [1]. The nephrons that perform filtering of the blood are contained across the cortex and medulla regions of the kidneys (**Figure 1**) [1]. Each nephron is made up of a glomerulus, a series of micro vessels where the filtering of blood occurs, and the tubule which receives the filtrate [1]. In humans, the blood enters the kidney by the renal artery, lobular vessels, then arcuate vessels that perfuse the kidney (**Figure 1**) [1]. The afferent arteriole branches from the lobular artery which supplies unfiltered blood to the glomerulus, whereas the efferent arteriole removes the 'filtered' blood (**Figure 1**) [1]. This filtrate is either removed as urine or is retained by the body by reabsorption into the blood [1]. For excess ions, it is the concentration gradient that determines whether reabsorption into the peritubular capillary network or retention in the tubule takes place (**Figure 1**) [1]. The portion of filtrate which is to be expelled travels to collecting duct, papilla, calyxes, then ureter (**Figure 1**) [1]. On average there are approximately 1 million nephrons in the adult human kidney, the number varies between individuals and gradually decreases with age, eventually this loss of nephrons impairs kidney function [2-5]. Kidney injury, however, may cause further loss of nephrons, which accelerates the process [6]. This process puts increased pressure on each of the remaining nephrons as each is required to work harder and filter an greater volume of blood to maintain homeostasis [6]. Often this loss of nephrons is unnoticed until serious symptoms develop, yet >70% of the kidney function may be lost by that stage making prevention and intervention difficult [6-8].

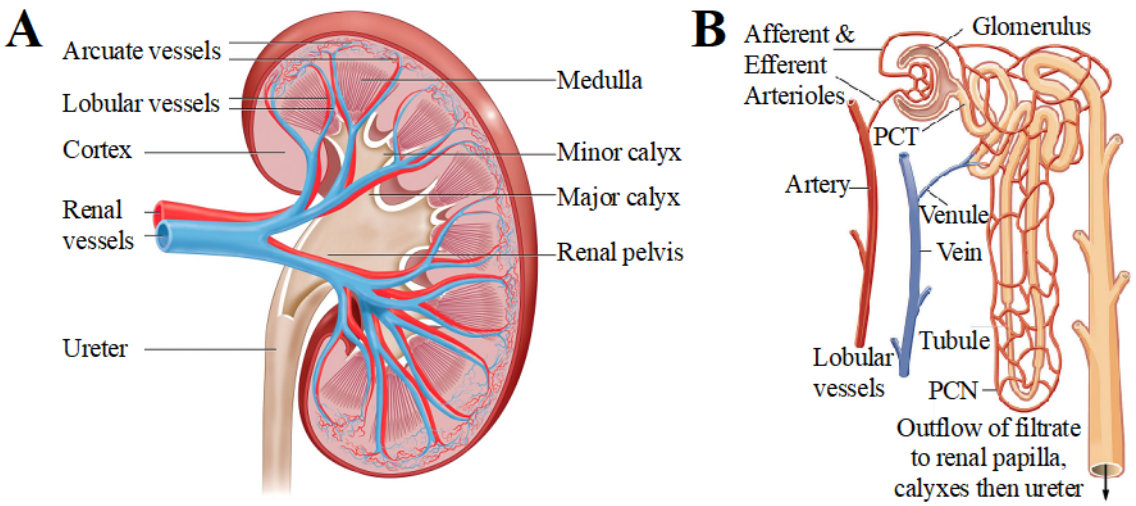

Figure 1: Mammalian kidney anatomy

A)°The gross anatomy of the mammalian kidney in longitudinal cross-section and **B)**°schematic representation of the functional unit of the kidney, the nephron. Proximal convoluted tubule = PCT; peritubular capillary network = PCN. Adapted from [1].

1.1.1 Acute kidney injury (AKI)

AKI, an abrupt decline in kidney function, is a common disorder with profound effects on mortality and morbidity [9]. Approximately 13 million people in the US are affected by acute kidney injury (AKI) each year and of these approximately 2 million cases are fatal [5]. Meta-analysis of epidemiological studies demonstrated that the pooled incidence of AKI in hospital patients is 22% and AKI is independently associated with up to a 16-fold increase in the risk of death [10-12]. Indeed, the overall mortality of patients with AKI requiring renal replacement therapy was 46% [11]. Acute injury and chronic disease are strongly interrelated with patients recovering from AKI at increased risk of chronic kidney disease, and individuals with chronic kidney disease have a substantially increased risk of AKI [13]. AKI can arise from a diverse array of pathophysiologic processes including: haemodynamic compromise, nephrotoxic injury, autoimmune glomerulonephritis and urine outflow obstruction; reviewed in [6]. A

common cause of AKI, however, is kidney ischemia which induces hypoxic cell death in the most metabolically active components of the kidney, the tubular epithelium [14], reviewed extensively in [15]. The tubular epithelial injury results in necrosis and shedding of epithelia from the basement membrane, a process recognised as histopathological lesions termed acute tubular necrosis [15-17]. Occlusion of tubular space by necrotic epithelial tissue results in glomerular injury and obsolescence [18]. The subsequent reduction in the number of functional nephrons, the complex comprising of afferent and efferent arteriole, glomerulus, tubule and collecting duct, leads to reduced glomerular blood flow and filtration, retention of waste products and impaired homeostasis of major electrolytes in the systemic circulation [17-19].

The Kidney Disease Improving Global Outcomes (KDIGO) initiative proposed the definition of AKI as an elevation in serum creatinine within the prior week or by a reduction in urine output sustained over six hours [20]. However, the recognition that increasing severity of AKI is associated with elevated risks of chronic kidney disease and mortality, the risk, injury, failure, loss, end stage (RIFLE) criteria were proposed to identify and grade injury based on the magnitude of serum creatinine rise and urine output reduction [21]. When renal function is impaired for ≥three months the patient may be defined as having chronic kidney disease [22]. Therefore, a therapeutic window for reducing chronic kidney disease exists by preventing AKI in high-risk patients and improving regeneration, or repair, of the kidney following AKI. Importantly, the available therapies for AKI are of a supportive nature and do not act to treat the injury itself [23, 24]. Hence, there is a clear need for an improved understanding of the cellular mechanisms that underpin the pathogenesis of AKI and chronic kidney disease.

1.1.2 Epidemiology of AKI

Despite the availability of therapies for end-stage kidney disease such as dialysis and transplantation, AKI alone is still responsible for over a million deaths per year [5, 9, 11, 23]. AKI also increases the risk of chronic kidney disease, renal failure and systemic consequences [4, 5, 7, 20, 25-27]. The Australian Bureau of Statistics report found 1 in 10, or approximately 1.7 million, Australians who are at least 18 years old had indicators of chronic kidney disease; although surprisingly it was only 6.1% of these people who had previously received a diagnosis of chronic kidney disease [28]. The difficulty arises due to the impossibility of delineating between AKI and chronic kidney disease if utilising a single time point. Whilst it is possible some people with chronic kidney disease are unaware of the condition since it has yet to cause any major symptoms, one could speculate that the tests have identified AKI instead [28].

Several prospective cohort studies suggested that sexual dimorphism exists for AKI since there have been data finding males had an increased risk of developing AKI [29-34]. The prevalence of AKI is greatly increased in critically ill patients and in paediatric patients [23, 35]. Within intensive care units (ICU), the rate of AKI is highly variable around the world and has been reported as low as 22%, but can be as high as 67% in other areas [24, 36]. This variability may be partially explained by the multifactorial causes of AKI, some being far more prevalent in certain geographical locations [9]. However, it is quite possible that inconsistencies in diagnostic criteria are another hurdle for accurate reporting [37].

1.1.3 AKI aetiology

AKI in humans can be the result of obstructions in urinary output, exposure to chemicals that are nephrotoxic, or genetic polymorphisms [6, 27]. Nevertheless, AKI is most commonly the

result of acute tubular necrosis, where ischemia is a common cause [18, 19]. Ischemic injuries may occur from impaired kidney perfusion causing hypoxia [18, 19]. Whilst ischemic AKI is multifactorial, some common factors which drive this include sepsis, trauma which triggers haemorrhage, medications that may be prescribed and cardiovascular disease, (**Figure 2**) [17]. It is the hypoxic state induced by AKI and subsequent reduction in the number of nephrons that are functional, which leads to a reduction in kidney function [6]. As a consequence, the waste and excess ions may be increased in concentration in systemic circulation [17-19].

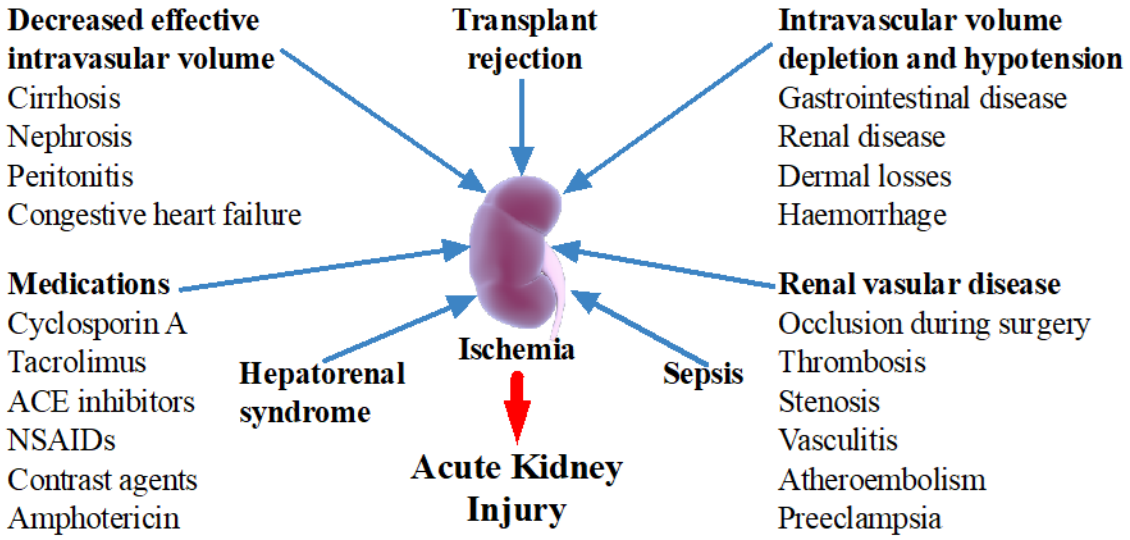

Figure 2: Renal ischemia can cause an AKI

Acute kidney injury (AKI) from renal ischemia may be driven by prescribed medications, sepsis haemorrhage, cardiovascular disease, amongst many other reasons. Adapted from [17].

1.1.4 Histopathology in AKI

One of the most consistent histological features of AKI is acute tubular necrosis [17, 38]. This necrosis is identified at irregular intervals throughout the tissue which is known as 'skip

lesions' and are predominantly found in the proximal convoluted tubules in the outer medulla region of the kidney [17, 38, 39]. Typically, AKI will not present with glomerular pathology, however, in cases of nephrotoxic chemical exposure or underlying genetic issue there may be glomerular involvement [38, 40]. Assessment of histopathology in renal biopsies requires experience since the features are subtle to the untrained eye. The difficulty is intensified by being constrained to 2-dimensions using light microscopy [37, 38, 41]. Acute tubular necrosis can be identified by a disrupted epithelial layer and/or basement membrane with sloughing of structural cells, dilation of the tubules or an obstruction which is present inside the tubules [17, 38, 39]. These features can be visualised using relatively inexpensive and common staining techniques such as hematoxylin and eosin (H&E) and periodic acid–Schiff (PAS) [17, 38, 39, 42]. However, assessment by biochemical testing is preferred since biopsies are invasive [17, 38, 39, 43].

1.1.5 Diagnostic criteria for AKI

Kidney function impairment from AKI can be assessed by analysing factors in the blood and urine [38]. A waste marker in the serum, named creatinine, is used routinely to calculate the estimated glomerular filtration rate (*e*GFR) in patients [38]. The concentration of creatinine is increased following AKI, which can used to determine that the estimated *e*GFR has decreased and therefore kidney function is impaired [38]. Clinical diagnosis of AKI is made when serum creatinine is either increased by $\geq 26.5 \mu mol \cdot L^{-1}$ over 48 hours or 1.5 times higher than the known baseline levels for that patient; additionally, where urinary output is $\leq 0.5 mL \cdot kg^{-1} \cdot h^{-1}$ [38]. However, the baseline levels of creatinine and urinary output vary based on water intake, weight, physical activity, muscle mass, age, gender and other factors; hence alternative markers have been proposed [44]. Urea is used in pre-clinical experimental models and in clinical

practice; often converted as blood urea nitrogen (BUN) [21, 38, 40, 42-47]. Like creatinine, BUN may also be changed by factors independent of GFR [21, 38, 40, 42-47]. Yet at baseline and with AKI, BUN concentration is higher than creatinine making it useful when large volumes of blood can't be obtained, essential for human infants and experimental models utilising small animals [21, 38, 40, 42-47].

1.1.6 Progression from AKI to chronic disease

Ischemic injury and acute impairment of kidney function drive the development of chronic disease and ultimately lead to renal failure (**Figure 3**). In essence, chronic disease is defined by the same criteria as AKI lasting ≥three months [38, 41]. Several studies have determined that the severity and number of AKI have been linked to progression to chronic disease [48-53]. Therefore, a therapeutic window exists to try to identify patients who have an increased risk of AKI, and to intervene following AKI to prevent further complications (**Figure 3**). An early indicator of chronic disease can be seen histologically by observing collagen deposition and fibrosis of the tissue by utilising stains such as Masson's trichrome [40]. In order to intervene, pre-clinical experimental models of kidney injury are utilised to gain a greater understanding of the pathophysiology of AKI.

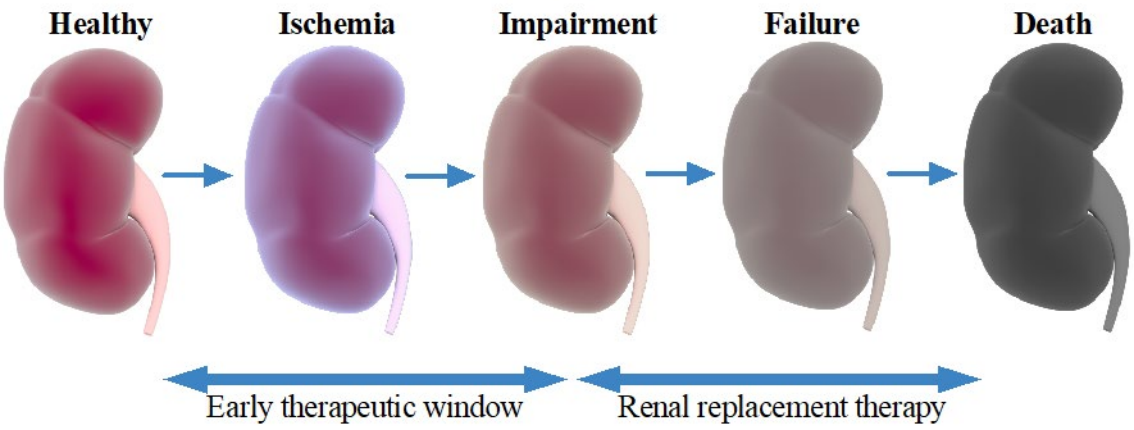

Figure 3: Renal ischemia can progress to chronic impairment and kidney failure

The ischemic acute kidney injury can progress to impairment of kidney function and eventually kidney failure may occur. Therefore, an early therapeutic window exists to prevent the progression of AKI prior to renal replacement therapy by identifying AKI and patients who are at risk. Adapted from [54].

1.1.7 Experimental models of AKI

Canines have been used extensively in the past due to similarity to humans in renal structure and function [55, 56]. Yet rodents are commonly utilised due to ease of genetic manipulation with CRISPR, short generational timeframe and small size, allowing for easier husbandry [39]. Male mice are typically used due to their increased susceptibility to models of renal ischemia [57, 58]. To induce ischemia, renal ischemia reperfusion injury (IRI) models are particularly relevant as they appropriately model AKI in trauma and kidney transplantation patients [39, 59]. The models of IRI differ in execution but are widely used; they involve temporary obstruction of the renal vessels, which prevents blood flow to the kidney [58, 60, 61]. Dependent on mouse strain and severity of the injury the timing of ischemia varies from 20 to 30 minutes [58, 60, 61]. The ischemia may be induced either in one or both of the kidneys termed unilateral and bilateral IRI, respectively [58, 60, 61]. A contralateral nephrectomy may

be performed to remove one kidney entirely to prevent compensation, improving the accuracy of assessing AKI features [58, 60, 61]. Whilst a contralateral nephrectomy does not recapitulate human disease it may be required in order to induce an injury in one kidney, which is akin to human AKI, since rodents are extremely resilient [58, 60, 61].

Surgical models of ureter obstruction (UO) induce an injury by preventing voiding of urine [62, 63]. Typically a permanent ligation of the ureter is performed unilaterally [62, 63]. Although a complete obstruction is not often present in humans, the model produces a reliable injury [64-69]. However, the UO model may be inadequate for studying the normal repair processes following AKI [62, 63]. Yet, the strength of the UO model lies in studying chronic injury and preventing the progression to complete renal failure [62, 63].

There are also chemical-induced models of AKI, the most popular choice involves administration of doxorubicin systemically [70, 71]. In rodents this compound causes a robust kidney injury and inflammation, which progresses to fibrosis [70, 71]. This model has similarities to the human disease named focal segmental glomerulosclerosis [70, 71]. Whilst the model is useful for ascertaining new therapeutic targets and for evaluating new treatments for prevention of fibrosis, the model may not be appropriate depending on the scientific question since the model is driven by a systemic chemical exposure and is not localised to the kidneys itself [72-74].

1.1.8 Immunity and interleukin-33 (IL-33)

During an ischemic injury in the IRI model, the kidney cells, in particular the proximal convoluted tubules, are starved of oxygen due to the high mitochondria density [14, 17]. The tubules become damaged by oxidative stress from H_2O_2, OH^- and $ONOO^-$ [75-79]. Oxidative

stress drives inflammation, dysfunction of the endothelial microvasculature and necrotic cell death in the kidneys [75, 76, 79]. During cell death, factors termed alarmins are released, including thymic stromal lymphopoietin (TSLP), interleukin (IL)-25 and IL-33 which activate the innate immune system causing the accumulation of immune cells which are either resident to, or can be recruited from the circulation [80-82].

IL-33 is constitutively expressed in human and mouse epithelial nuclei from virtually all tissue sites, yet the endothelium is considered the primary cellular source in humans; however, the IL-33 protein is substantially lower in the endothelium of mice in comparison to their epithelial expression [83-86]. Between both species the IL-33 protein is comprised of two domains which are evolutionarily conserved, named the C- and N-terminal domains [87]. The C-terminal domain, sometimes called the IL-1-like cytokine domain, contains a β-trefoil fold similar to the IL-1 superfamily members IL-1α, IL-1β and IL-18 [88, 89]. The N-terminal domain, sometimes referred to as the nuclear domain, contains a chromatin-binding-motif allowing the formation of a complex between IL-33 and histone proteins H2A and H2B [87, 90]. IL-33 exhibits its effect by binding to the interleukin-1 receptor-like 1 membranous receptor named ST2, which allows the interaction between ST2 and the IL-1 superfamily co-receptor/accessory protein IL-1RAP or IL-1AP for human and mouse, respectively [88, 89]. The IL-33 C-terminal domain binds to all three of the immunoglobulin-like sites of ST2, yet only two of these sites are critical for the binding affinity [88, 89]. ST2 can be expressed on a wide range of immune and non-immune cells under homeostatic conditions, ST2 expression can also be induced on subsets of immune cells, which allows it to play diverse roles in type I and type II immunity [91-94].

IL-33 may drive a protective antiviral type I immune response targeting natural killer (NK) cells, NKT cells, $CD8^+$ cytotoxic T-cells and $CD4^+$ T-helper type 1 cells (T_H1) by induced ST2 expression [95-99]. Although, IL-33 is best known for the deleterious allergic and anti-

pathogen protective type II immune responses, which is often orchestrated primarily by the production of the IL-5 and IL-13 cytokines [93, 94]. These are mediated by ST2 expression on neutrophils, macrophages, eosinophils, basophils, mast cells, dendritic cells, $CD4^+$ T-helper type 2 cells (T_H2), B-cells, regulatory T cells (T_{reg}), and subsets of lymphoid cells which have innate functions [95, 100-128].

1.2 Innate lymphoid cells (ILC)

ILC can be categorised into three major subtypes based the profile of transcription factors, and by their production of specific effector cytokines [129]. The group 1 ILC (ILC1) lineage are involved in type I immunity [130]. ILC1 resemble T_H1 as they produce interferon (IFN)-γ and express the transcription factor T box 21 [130]. The ILC1 are made up of natural killer (NK) cells and non-NK ILC1 [130]. Group 2 ILC (ILC2) are involved in type II immunity [119, 120]. ILC2 resemble T_H2 predominantly due to their effector cytokines IL-5 and IL-13; yet, they can also produce IL-4 and IL-9 [119, 120]. Additionally, ILC2 are known by their expression of the GATA binding protein 3 for their development [119, 120]. Group 3 ILC (ILC3) and have critical roles in type III immunity [131, 132]. ILC3 are functionally similar to the T_H17 and T_H22 subsets of T-lymphocytes [131, 132]. The ILC3 are best characterised by their IL-17 and IL-22 production, in addition to the expression of RAR-related orphan receptor gamma [131, 132].

1.2.1 Natural and inflammatory ILC2

ILC2 are rare immune cells, but they are potent innate producers of type 2 cytokines in response to epithelial-derived alarmins, particularly IL-25, IL-33 and TSLP [119, 120] (**Figure 4**). ILC2

are also required for the development of effective T_H2-mediated adaptive immune responses [133]. ILC2 have been suggested to exist in distinct states depending on the cytokines which drive their activation [134]. Under homeostatic conditions, natural ILC2 are resident in most tissues, including the kidney and respond primarily to IL-33 [135]. Indeed, natural ILC2 are defined as expressing the IL-33 receptor, ST2 [120]. Inflammatory ILC2, however, are difficult to detect under homeostatic conditions but are rapidly induced in response to IL-25 [136]. The inflammatory ILC2 represent a subpopulation of ILC2 that are ST2 negative [136]. There is evidence of plasticity between ILC states and it has been proposed that inflammatory ILC2 can act as progenitors for natural ILC2 or even ILC3 [136, 137]. These findings indicate that the tissue resident pool of natural ILC2 may be replenished by inflammatory ILC2 and that resident cells may change in response to certain insults.

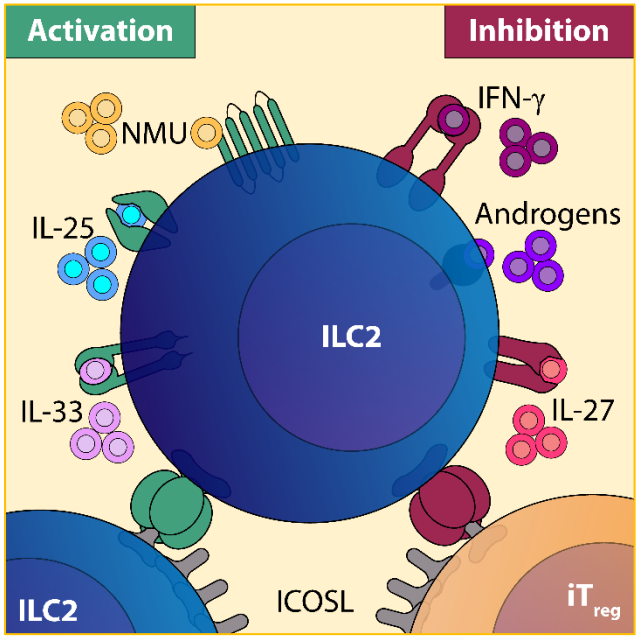

Figure 4: Factors that regulate ILC2 function

Crucial factors and associated receptors that modulate group 2 innate lymphoid cells (ILC2), to activate (green) or inhibit (red) their survival, proliferation and cytokine production. For

acute kidney injury, increasing the activity of neuromedin U (NMU), interleukin (IL)-25, IL-33 and thymic stromal lymphopoietin (TSLP), and decreasing the activity of androgens, IL-27 and interferon-γ (IFN-γ) may be advantageous. Inducible T-cell costimulator (ICOS), however, can be excitatory for ILC2-ILC2 or inhibitory for induced regulatory T-lymphocytes (iT_{reg})-ILC2 interactions depending on co-stimulatory factors from the host cell.

1.2.2 ILC2 coordinate innate and adaptive immune responses

ILC2 are resident in murine and human kidneys, and exhibit similar type 2 effector cytokine profiles [117, 138]. IL-4 is produced by ILC2 in response to alarmins from epithelia, helminth infection or activation of pattern recognition receptors [139, 140]. Interestingly, ILC2 express the IL-4 receptor and are sensitive to IL-4 through positive feedback, which can further enhance ILC2 activation and cytokine production [141]. IL-5 is constitutively produced by ILC2 in adult mammals, which is required to maintain homeostasis of eosinophils, and in turn, maintain homeostasis of macrophages [135, 138]. ILC2 also produce significant amounts of IL-13, which is required for the recruitment of eosinophils [133, 138]. Additionally, IL-13 induces the production of mucins that are required for tissue homeostasis [141-144]. IL-4 and IL-13 are also critical for the polarisation of macrophages towards the alternatively activated state (AAM; also known as M2), which can dampen excessive inflammatory immune responses and aid with epithelial recovery following insults within the kidney and other organs [145, 146].

ILC2 express the inducible T-cell co-stimulator (ICOS) in addition to its ligand (ICOSL mouse; ICOSLG human) and ICOS-ICOSL interactions between ILC2-ILC2, or ILC2 and T_H lymphocytes enhance cytokine production (**Figure 4**) [118, 147, 148]. However, ICOS-ICOSL interactions between ILC2 and induced regulatory T (iT_{reg}) cells has the opposite effect (**Figure 4**) [149]. ILC2 have also been demonstrated to induce the expansion of T_H2 and T_{reg} *via* the

expression of the costimulatory molecule TNF superfamily member 4 (TNFSF4; OX40L) [150]. Through the production of IL-13, ILC2 can increase the activation of T_H2 cells indirectly through dendritic cells that produce the T-cell attracting chemokine CCL17 [133, 151]. Additionally, IL-13 can recruit macrophages and other phagocytes to the area and cause dendritic cells to migrate to the lymph nodes and prime naïve T-cells to differentiate into T_H2 cells [151, 152]. The interaction between ILC2 and T cell subsets is complex and tightly regulated to allow heterogeneous function in different contexts and locations.

In addition to cytokines, ILC2 also produce the growth factor amphiregulin (AREG), which promotes tissue repair [153, 154]. In the lung, AREG is essential for the resolution of tissue homeostasis following viral respiratory infection [155]. Excessive AREG signalling can drive fibrosis in tissues such as the lung and kidney, and AREG inhibition may be beneficial in this context [156, 157]. Recent literature suggests that AREG is also produced by kidney ILC2 and is renoprotective [158]. ILC2 have also been shown to express the antigen presenting molecule major histocompatibility complex class II (MHCII) [152, 159]. This allows them to act as antigen presenting cells (APCs) to stimulate the adaptive immune system [152, 159]. Recent advances have shown that ILC2 can be neuronally regulated, specifically by the neuropeptide neuromedin U (NMU), which signals through the surface NMU receptor 1 (NMUR1) to drive their activation and expansion (**Figure 4**) [160-162].

There is also a growing body of evidence suggesting ILC2 exhibit sexual dimorphism. Depending on the tissue ILC2 express androgen and oestrogen receptors and this signalling can alter the activity of these cells (**Figure 4**) [163-167]. Androgens can act to suppress lung ILC2 and even prevent differentiation of bone marrow progenitors, opposite to the effect of oestrogen on uterine ILC2 [163-167]. Interestingly, multiple reports have found male mice have less tissue-resident ILC2 within multiple organs, though it is not yet known whether this

is the case in humans [163, 165, 167]. Male mice are also more susceptible to kidney injury [57, 168]. It is currently unknown whether this discrepancy in the number of ILC2 under homeostatic conditions in males is causal or merely coincidental. Immune-related factors and signalling pathways such as IFN-γ, IL-27 and signal transducer and activator of transcription (STAT)1 can also suppress the activity of ILC2 (**Figure 4**) [169-171]. This may be a mechanism of how pathogens can suppress host repair responses. These immune-related factors may also prove to be avenues for regulating ILC2 activity depending on the disease context (**Figure 4**); similar to that described for type II-mediated allergic diseases [172].

1.2.3 ILC2 as a potential cellular therapy in renal injury

ILC2 have recently been shown to have protective effects in mouse models of IRI [173]. Administration of recombinant mouse (rm)IL-25 prior to IRI induction resulted in the expansion and activation of ILC2, which reduced tubular damage, BUN and serum creatinine following IRI [173]. To further confirm the role of ILC2 in AKI, ILC2 were isolated from naïve mice and stimulated *ex vivo* with rmIL-25 [173]. These activated inflammatory ILC2 were then adoptively transferred into recipient mice one day prior to the induction of IRI [173]. Mice that received inflammatory ILC2 had significantly reduced tubular damage, BUN and serum creatinine levels [173]. However, it is difficult to conclude whether ILC2 are constitutively renoprotective without the introduction of exogenous rmIL-25 [173]. Furthermore, inflammatory ILC2 are predominantly responsive to IL-25 and are not considered to be the resident population of ILC2 within peripheral tissues [136].

Following this initial study, the role of ILC2 were investigated in a model of doxorubicin-induced nephropathy [174]. A similar approach was used to activate ILC2 in this model, however, the cytokine IL-33 was administered for 5 days, starting the day after doxorubicin

administration [174]. Administration of rmIL-33 induced partial protection against the typical features of doxorubicin-induced nephropathy, such as tubular inflammation and fibrotic-like remodelling [174]. It was demonstrated that these effects occur independently of adaptive immunity using mice deficient in T and B cells (*Rag2*$^{-/-}$), and mice deficient in T, B and ILC (*Rag2*$^{-/-}$*Il2rcg*$^{-/-}$) [174]. However, it is also possible that non-ILC, ST2 expressing cells such as basophils, eosinophils and mast cells may have important roles in protection against renal insult [95, 123, 175-177]. As the ILC-deficient animals lacked T and B cells in addition to all ILC subsets, not just ILC2, it is difficult to conclude that ILC2 are required [174]. In this study, IL-33-activated ILC2 were also able to induce an AAM phenotype consistent with the mechanism of protection following rmIL-25 administration [173, 174]. Importantly, ILC2 have been found in human kidney biopsies, which identifies the potential for these cells to be targeted in humans [174]. However, alterations in ILC2 number, function and phenotype in human kidney disease requires further investigation.

The potential complementary effects of IL-2 and IL-33 were investigated using models of chemical-induced injury, by doxorubicin and cisplatin, in addition to IRI [178]. Pre-treatment with a combination of rmIL-2 and rmIL-33 before inducing an injury was protective by a mechanism involving ILC2 and T_{reg} activation [178]. Furthermore, superior protection was achieved by means of a new hybrid cytokine named IL233, formed by fusing recombinant components of IL-2 & IL-33 [178]. In some experiments, IL233 was sufficient to prevent animals from becoming moribund following IRI, while all vehicle-treated mice were culled within 3-4 days following injury as a humane intervention [178]. These results are exciting proof-of-principal evidence for prophylactic treatment and intermediate intervention, although it is unlikely this particular therapy will be a viable option in humans. The main challenges are that IL-33 has multiple targets and cannot currently be administered directly to the kidney without the use of invasive techniques. For patients with type II-mediated allergic diseases,

such as asthma, systemic activation of ILC2 and other IL-33 responsive cells would likely be detrimental and potentially life-threatening.

Most recently the therapeutic potential of ILC2 in IRI has been further elucidated [158]. rmIL-33 treatment or transfer of rmIL-33-stimulated ILC2 was sufficient to significantly reduce serum creatinine, tubular injury and increase survival to 100% out to 28 days post-injury [158]. In other studies, treatment with rmIL-33, or recombinant human IL-33 in humanised mice, prior to injury, induced similar protective effects, although only the day following injury was assessed [158]. Loss-of-function studies were also performed by depletion of ILC2 in T/B cell-deficient (*Rag1*$^{-/-}$) mice by treatment with anti-CD90 [158]. These studies demonstrated that the protective effect of IL-33 was significantly diminished in the absence of ILC2 [158]. However, these mice were also depleted of other CD90 expressing cells, including T_{reg} cells, which may also be critical for this renoprotection [123, 158, 179]. Furthermore, a complex bidirectional relationship exists between ILC2 and T_{reg} [123, 158, 179]. This concept is supported by studies examining the IL233 hybrid cytokine [178]. Interestingly, depletion of ILC2 and other CD90 expressing cells did not worsen the severity of injury suggesting that ILC2 may not be required for effective recovery from IRI [158].

Our understanding of the innate immune system and its role in the resolution and repair of tissue injury is increasing. However, it is far from complete and further characterization of the immunological interactions, particularly in kidney disease, is required for translation into clinical practice. Recent studies provide a strong rationale to further explore the role of ILC2 in AKI. Whilst these provide substantial steps forward in our understanding of the immunology of AKI, it is also important to consider that *in vivo* or *ex vivo* stimulated cells may establish an artificial state that is not representative of their normal functions in human AKI patients. Collectively, these studies show that artificially increasing ILC2 provides protection from AKI

and decreases pathology (**Table 1**). Since *Rag1*$^{-/-}$, *Rag2*$^{-/-}$ and *Rag2*$^{-/-}$*Il2rcg*$^{-/-}$ mice are deficient in T and B lymphocytes, the next important step is to show that the effects are maintained by selective depletion of ILC2 whilst preserving the adaptive populations; an approach described by Oliphant, *et al.* [159]. This is particularly important as a recent report suggests ILC may be redundant since there was no susceptibility to any particular human disease in patients with ILC lymphopenia [180]. There are also conflicting reports which suggest that therapeutic use of IL-33 may be detrimental in AKI.

Table 1: Methods of *in vivo* group 2 innate lymphoid cell expansion in experimental AKI

Method of expansion	**Timing**	**Model used**	**Ref**
5 days of 0.3µg rmIL-25. 2 x 10^5 ILC2.	Prophylactic	Bilateral IRI 30min, 1 day endpoint.	[173]
5 days of 0.4µg rmIL-33.	Therapeutic	Doxorubicin 12mg kg^{-1}, 14 day endpoint.	[174]
5 days of 66pmol rmIL-2 & rmIL-33. 5 days of 66pmol IL233.	Both	Bilateral IRI 24 & 26min, 1, 9 & 28 day endpoints. Cisplatin 20mg kg^{-1}, 4 day endpoint. Doxorubicin 10mg kg^{-1}, 4 day endpoint.	[178]
5 days 0.3µg rmIL-33. 1 x 10^6 ILC2.	Both	Bilateral IRI 30 & 38min (35min *Rag*$^{-/-}$ only), 1 & 28 day endpoints.	[158]

Summary of the main experimental approaches of group 2 innate lymphoid cells (ILC2) adoptive transfer and administration of recombinant mouse (rm) cytokines to activate and expand kidney ILC2 either before (prophylactic) or after (therapeutic) the induction of injury. 8-12 week old, male, wild-type BALB/c or C57BL/6 mice were used in each study unless specified. In each study, expanding ILC2 was deemed beneficial.

1.2.4 Therapeutic potential of IL-33-induced ILC2 activation

Using a cisplatin model, rmIL-33 treatment was detrimental and led to increased serum creatinine and histopathology [181]. Administration of a soluble form of the IL-33 receptor, rmST2, significantly reduced these features [181]. Consistent results were achieved using rmIL-33 and soluble rmST2 within an IRI model, and a similar conclusion was reached using unilateral ureter obstruction [182, 183]. Mice deficient in IL-33 or ST2 (*Il33*$^{-/-}$ or *Il1rl1*$^{-/-}$) were partially protected against the remodelling and fibrotic changes following injury, and *Il33*$^{-/-}$ mice were also protected against features of injury following IRI [183, 184].

The dosage of rmIL-33, length of administration and/or the type of renal injury may drastically alter the response exhibited to be advantageous or deleterious. rmIL-33 treatment was beneficial at a dose of 0.3µg per day for five days, but was detrimental at a lower dose of 0.05µg per day for 14 days [158, 182]. Whilst both studies utilized models of IRI, there were differences in the ischemia timeframe and in the surgery itself [158, 182]. These contrasting conclusions could potentially be explained by the composition of the immune cells within the kidney and circulation at the time of IL-33 treatment. It is emerging that diverse microbiomes in experimental animals in different facilities have a substantial impact on immune responses in multiple contexts. One way around this may be to perform similar studies in germ-free mice and mice that are "wild-type" with diverse microbiomes.

1.3 The urinary bladder

The urinary bladder is located in the pelvis; it is a muscular organ which acts as to store urine until excretion [185]. During the stretch response, the superficial cells which line the bladder, the urothelium, causes an activation of sensory nerve and central nervous system which

indicates that the bladder needs voiding [186]. Micturition, the act of conscious voiding of the bladder, requires activation of the detrusor muscle and relaxation of the urethral sphincters, allowing urine excretion through the urethra [185]. The urothelium is the lining of transitional epithelial cells in the proximal urethra, ureters and the urinary bladder [185]. It is made up of 3 layers; the basal, intermediate and superficial urothelial cells [185]. This barrier is the first line of defence against pathogens, which may regenerate after being damaged [187, 188]. Underneath these layers is the connective tissue and muscularis [185]. It is known that a urinary microbiome exists and that tissue resident immune cells are present, yet the role of these in urothelial repair is not yet understood [189].

1.3.1 Urinary tract infection (UTI)

UTI is a general term that describes an infection at any part of the urinary tract; colloquially it is used in place of the medical term cystitis, an infection of the urinary bladder (**Figure 5**) [190]. Pyelonephritis, an infection of the kidney, is less likely but is medically far more serious (**Figure 5**) [190]. Whilst UTI's are common in the overall population, with approximately 150 million people experiencing UTI's each year, the incidence is higher in paediatric care [191, 192]. Approximately 1 in 10 children develop a UTI, and of these roughly a third will have recurrent infections [193, 194]. Women are disproportionally affected and are >40 times greater risk of UTI [195]. Half of all women develop a UTI throughout their lifetime and a third of these cases necessitate treatment before 24 years of age. Additionally, a quarter of women who have had an infection will suffer from recurrent infections [196]. Children have a higher risk of UTI and are more likely to develop renal scaring as a result, which may pose a threat to the functioning and development of the kidneys [194, 197, 198]. Vesicoureteral reflux is where urine flows the wrong way, bladder into ureters and sometimes the kidneys.

This condition is more often diagnosed in children, which further increases the rate of developing further UTI's and renal scarring [194]. The urethra is shorter in women, it's theorised that this makes it easier for the bacteria to colonise the urinary bladder; however, the urethral length hypothesis is largely considered to be outdated since length is not correlated with increased incidence of UTI [195, 199]. Furthermore, this subject has been recently reviewed in detail with sex-based immune differences theorised to be a better explanation [200].

There are many risk factors for UTI, some specific to women or men. Changes to the urinary tract environment by menopause can increase the risk of infection due to the reduced amount of circulating oestrogen [201]. Frequent sexual activity and delayed voiding bladder after sexual intercourse also increases risk due to proximity of urethral and vaginal orifices [202]. Additionally, there are intrinsic differences immunological responses between males and females during UTI [203]. Medical procedures, in particular catheterisation, can also increase risk [201]. Comorbidities such as diabetes mellitus with immune system suppression, can have more severe UTI with an increased complication rate [204, 205]. The elderly are typically more immunocompromised and potentially explains the increased UTI incidence [206]. Other abnormalities like kidney stones or an enlarged prostate also increase risk of UTI due to blockage and reduced flushing of the tract, allowing pathogens to colonise [207].

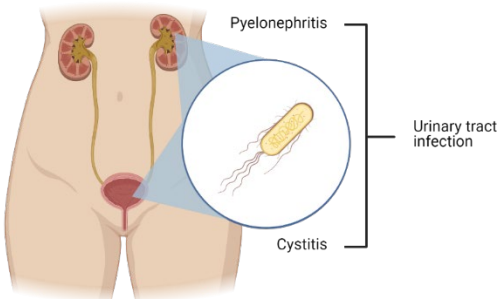

Figure 5: Urinary tract infection, cystitis, and pyelonephritis

Schematic representation of the urinary tract defining infection of the bladder as cystitis and infection of the kidney as pyelonephritis. Created with BioRender.com.

1.3.2 Classification of UTI

Different classifications exist for UTI which can vary between countries. Guidelines have been established by the Infectious Diseases Society of America and the Centres for Disease Control & Prevention, in addition to other entities [208, 209]. The guidelines classified UTI broadly into uncomplicated and complicated types with several overlapping clinical presentations. This has been refined by the European Association of Urology, Section of Infections in Urology. First described in 2011, a uniform classification system was proposed known as ORENUC; "**O** – N**O** known risk factor; **R** – risk for **R**ecurrent UTI, but without risk of more severe outcome; **E** – **E**xtraurogenital risk factors; **N** – relevant **N**ephropathic diseases; **U** – **U**rological resolvable (transient) risk factors; **C** – permanent external urinary **C**athether and non resolved urological risk factors" [210]. In essence, this classification is based on clinical presentation, the anatomical level, grade of severity, risk factors and the appropriateness of antimicrobial therapy (**Table 2**) [210]. This classification has been adopted into the 2021 Urological Infections Guidelines by the European Association of Urology and will be further referred to and discussed in this thesis to classify UTI henceforth [211].

Table 2: Summary of criteria for assessment and characterisation of UTI

Clinical presentation	UTI location: Urethritis, Cystitis, Pyelonephritis, Urosepsis, Male specific (epididymitis, vesiculitis, orchitis, prostatitis)
Specificity of symptoms	Cystitis and lower tract: dysuria, frequency, urgency, suprapubic pain. Pyelonephritis and upper tract: fever, tenderness at costovertebral angle, flank pain,
Severity of symptoms	Mild/Moderate/Severe (no validated scoring system) or Septic
Possible risk factors	Sex (if female: pre/post-menopausal or pregnant), Age, Catheterisation, Immunosuppressive conditions, Kidney disease, Diabetes mellitus
Pathogen/causative agent	Pathogen type, Bacterial/pathogen load, Antimicrobial susceptibility or resistance, Virulence factors
Acquisition circumstance	Community, Hospital, Private practice, Residential accommodation (nursing home)
Therapeutic options	Susceptible to commonly used antimicrobials, Limited susceptibility, Multi-resistant and appropriate antimicrobials are either not available, or are not easily available

Adapted from [210].

Acute, recurrent or sporadic lower and upper UTI are typically termed uncomplicated; uncomplicated cystitis and pyelonephritis, respectively (**Figure 6**) [211]. However, uncomplicated UTI is limited to women who are not pregnant and have no anatomical or functional aberrations in their urinary tract (**Table 2**) [211]. Complicated UTI are all other cases, essentially it is used to pronounce the risk that the infection may take a more complicated course (**Figure 6**) [211]. This involves UTI in pregnant women, men, patients with urinary tract abnormalities, UTI from urinary catheters, in patients with conditions such as kidney disease, diabetes, or who are immunocompromised (**Table 2**) [211]. Urosepsis is a life threatening condition whereby organ dysfunction is caused by insufficient immune responses by the host to the uropathogen and can originate from infection of any part of the urinary tract and from the male specific reproductive tissues (**Figure 6**) [211]. Whereas recurrence of infection is termed recurrent UTI which is used to describe where there has been at three or more UTI in a year, or two in six months (**Figure 6**) [211]. Catheter-associated UTI is used to

describe infections where a catheter is currently, or has been in place in the last two days (**Figure 6**) [211]. Often in recurrent UTI, the same bacterium is the causative agent [212, 213]. Since the same bacterial species is capable of causing recurrent infections, this may indicate that the memory immune responses are ineffective in these tissues.

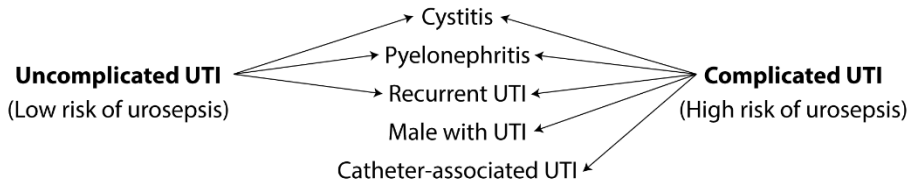

Figure 6: Classifications of uncomplicated and complicated UTI

Adapted from [211].

1.3.3 Aetiology of UTI

Diagnosis of UTI is typically based on concentration of bacteria $>10^4$ colony forming units (CFU) per mL of urine [214]. The gold standard remains bacterial culturing methods in agar and although a comprehensive urinary microbiome exists it will typically not grow on standard media [215, 216]. The uropathogenic *Escherichia coli* species account for between 80 and 90% UTI globally [217, 218]. An *Escherichia coli* infection progresses rapidly since the replication period is only 20 minutes. When untreated, bacteria can ascend to the ureter and cause acute or chronic pyelonephritis by colonising one, or both of the kidneys [219]. Pyelonephritis is serious and can cause an acute swelling due to inflammation and immune cell infiltration; these processes can even cause irreversible damage, predisposing to chronic kidney disease [220, 221].

1.3.4 Symptoms of UTI

Asymptomatic cystitis is not uncommon, although even if the patients are not aware of the situation, they will usually have experienced an increased frequency to urinate small volumes of urine, termed oliguria [217]. During UTI, this innate response makes sense as an attempt to remove pathogens from the urinary tract along with the urine. Often there is a purulent discharge which is indicative of the immune cells fighting this infection. Symptoms include cloudy or odorous urine, blood in the urine, pelvic pain and experiencing a stinging sensation around the urethra during urination [222, 223]. Whilst pyelonephritis presents similar symptoms, it is distinguished from cystitis by the addition of pain localised to the flank, nausea, fatigue and fever [224].

1.3.5 Pyelonephritis and kidney complications

Pyelonephritis can cause renal scarring and chronic kidney disease, which can result in hypertension [225]. Recurrent UTI has a 12 times increased risk of developing renal scaring than after a single infection; therefore being able to intervene in high-risk patients is incredibly important since this also increases the risk of pyelonephritis and subsequent acute kidney injury or kidney damage [226]. Urosepsis is another complication from pyelonephritis; this is a life-threatening situation where the bacteria enter the bloodstream rapidly, causing septic shock in addition to multiorgan failure [227]. Therefore, there is a need to be able to effectively treat UTI and prevent recurrent infections, not only due to the symptoms of the acute phase of infection but to prevent the far more serious complications resulting from pyelonephritis.

1.3.6 Current therapies and limitations

Whilst infections are often self-limiting, most cases are treated with antibiotics; the reasoning is two-fold, it is impossible to determine the course of infection in a patient where they do not have a previous history, and the risk of complications outweigh both the financial cost and adverse symptoms following treatment [228]. Yet, immediately after the consultation, patients often start an oral antibiotic regime before the results of their bacterial cultures and testing of antibiotic sensitivity [229]. This results in antibiotics being prescribed which are ineffective against the against the bacteria, meanwhile the bacteria are largely free to continue multiplying and wreaking havoc. Antibiotics commonly prescribed are those which are broad-spectrum, the most popular includes: fosfomycin, nitrofurantoin and a combination of trimethoprim and sulfamethoxazole [230-232]. Trimethoprim-sulfamethoxazole has been efficacious in several clinical trials; though if antibiotic resistance is suspected, nitrofurantoin is the preferred option [233, 234].

Both nitrofurantoin and fosfomycin are sufficient options since they report minimal resistance in the literature [234]. Although trimethoprim-sulfamethoxazole typically tolerated well, it can cause an imbalance to the bowel microbiome [235]. There are also rare but serious adverse events such as hypoglycaemia and hyperkalaemia, which have been reported [236, 237]. Trimethoprim-sulfamethoxazole can also interfere with warfarin treatment, which is typically prescribed to thin the blood and prevent clotting, hence, in these patients would increase the risk of haemorrhage [238]. Whilst being extremely effective, nitrofurantoin is limited by side-effects such as nausea, vomiting and stomach aches which are twice as likely compared with trimethoprim-sulfamethoxazole [239]. This is why it is not recommended for patients <4 months old, since these side-effects and subsequent dehydration are much more serious in early life [239]. Ampicillin and other β-lactam agents are not recommended because of antimicrobial

resistance rates but can be considered if other therapies can't be used [234]. Oral formulations of antibiotics are most common due to bioavailability, ability to penetrate the tissue and renal elimination characteristics [240].

Trimethoprim-sulfamethoxazole acts to prevent biosynthesis of nucleic acids, yet nitrofurantoin causes damage to bacterial genetic material, which impacts protein synthesis, whereas fosfomycin disrupts the synthesis of bacterial cell walls [230]. A typical antibiotic regime lasts between 3 and 5 days for uncomplicated cystitis, yet the choice will differ for cases of pyelonephritis or other complicated infections [190, 241]. Using an experimental model system in mice, *in vivo* has found that bladder reservoirs are not fully depleted following extended treatment regimes, demonstrating the ability of the bacteria to persist after antibiotics treatment and remerge causing recurrent infections [242]. However, these studies introduced antibiotics in drinking water and therefore, the dosage cannot be accurately controlled, it is also possible that the water may have a bad taste due to the antibiotics which could mean the animals are consuming a smaller volume to fluid. Therefore, it is plausible that administration by another route, for example oral gavage or injection, may provide new insights in these pre-clinical model systems to combat antimicrobial resistance.

1.3.7 Antibiotic resistance

A major concern for the treatment of UTI is the increasing rate of antibiotic resistance [243, 244]. Resistance to ampicillin is most prevalent, whereas nitrofurantoin is far less likely due to being less prescribed [229]. Studies which utilise *in vitro* models of cystitis commonly use a uropathogenic *Escherichia coli* strain, known as UTI89, have found it most sensitive to nitrofurantoin; yet *in vivo* models in mice with this same strain found the reservoirs in bladder tissue were not completely removed irrespective of the antibiotic agent [245]. Though the

concentration of bacteria in the urine may be reduced or ablated by antibiotic treatment, the titres in bladder and kidney tissue are not necessarily gone [246]. Indeed, uropathogenic *Escherichia coli* have the ability to form intracellular bacterial communities (IBC) which may explain their persistence in the urinary tract following antibiotic treatment [247]. Several studies demonstrate that resistance can vary depending on the region vary greatly depending on geographical location is unknown whether this is the result of differences in prescription and medical policies [248]. Yet the one thing which is clear is that the threat of antibiotic resistance further emphasises the need for new therapies, one possibility yet to be explored is targeting our immune system using immunotherapies rather than targeting the bacteria directly.

1.3.8 Pathogenesis of uropathogenic *Escherichia coli*

Uropathogenic *Escherichia coli* are gram-negative, facultative anaerobic bacilli which cause >80% of UTI [217, 249]. Primarily the pathogenesis begins with the pathogen residing in the gut, accidental introduction to the external urethra and ascension from the urethra into the urinary bladder [217, 243]. These bacteria evolved strategies that increase adherence to urothelium and resist the flushing action of urine; preventing the elimination of bacteria by bladder voiding. Using type 1 pili, these bacteria adhere to the urothelium and forming a biofilm [250]. The type I fimbrin D-mannose specific adhesin (FimH) acts to bind to the receptor of the uroplakin complex resulting in phosphorylation, preventing expulsion during bladder voiding [251, 252]. FimH also allows bacteria to invade the superficial urothelial cells during the acute infection and form IBC as they rapidly replicate; at the later stages of infection bacteria may invade the underlying layer of urothelium forming quiescent intracellular reservoirs (QIR) of low levels <10 bacterium [247, 253]. Therefore, it is essential to mount an

effective immune response to UTI in the early phase of infection and in IBC, else the bacteria may be able to remain dormant in QIR leading to recurrent infection [212, 247, 253].

1.3.9 Virulence factors of uropathogenic *Escherichia coli*

Uropathogenic *Escherichia coli* have several virulence factors including: type-1 pili, flagellum, siderophores, toxins, capsule and the lipopolysaccharide membrane [243, 254]. FimH is critical for the adherence to, and invasion of the urothelium by stimulating the host cell to create an envelope around the bacteria by rearranging actin cytoskeletal rearrangements [231, 254]. The bacteria can be seen enveloped within the urothelial cells, using scanning electron microscopy; yet adherence assays which utilise FimH knock outs demonstrate the invasion capacity is severely diminished [254]. Ultimately, this is the major virulence factor whereby bacteria can remain after voiding of the urinary bladder [255].

Other factors such as the flagellum allow for movement and migration along the urinary tract; whereas the purpose of siderophores is to scavenge iron, a critical factor for growth of the bacteria [256-258]. Bacterial toxins can also impair the ability of the cell to have control over cell cycle processes and programmed cell death pathways known as apoptosis; these factors include alpha-haemolysin, cytotoxic necrotising factor 1 and auto-transporter toxins [257]. Ultimately the induction of apoptosis provides the nutrients to multiply and assists to provide the bacteria a new host cell [259-263]. It is the capsule that surrounds uropathogenic *Escherichia coli*, which protects against phagocytosis, being engulfed and destroyed by the host immune cells [264]. An important factor is lipopolysaccharide which is contained within the outer membrane of which can increase the ability to colonise, evade antibiotics also the immune response of the host [265, 266]. Therefore, we need to enhance our understanding of

the pathophysiology of UTI, particularly the immune-driven responses, in order to establish new therapeutics in the future.

1.3.10 Responses to infection in the urinary bladder

A defence mechanism of the urinary bladder is shedding of the urothelium, the removal of pockets of most superficial epithelial lining, where pathogens have adhered; this process is extremely effective for most acute infections [267]. Where the cells are infected, caspase 3- and caspase 8-dependent apoptosis occurs [268, 269]. The superficial urothelium is regenerated rapidly following this process, as either a result of proliferation of the basal progenitor, and/or stem cells [269]. This process is crucial since this also gives bacteria the opportunity to invade deeper into the tissue and form QIR where they are largely safe from host immunity since they remain at low levels and are not replicating [253, 270]. During this process, the regenerated tissue is often not identical; typically there is hyperplasia which is identified histologically as a thickened appearance to the urothelial layers [213]. In pyelonephritis, however, there can be the development of clusters of debris known as casts [271]. Additionally, there is often accumulation of white blood cells, which are important for dealing with the bacteria yet these processes also drive collateral damage as a consequence [271]. Based on findings from a chronic murine UTI model with concurrent pyelonephritis, it is probable that multiple immune factors are also accountable for driving changes such as fibrosis, which somewhat mimics the renal scarring in seen in paediatric human studies [272].

Uncomplicated cystitis, requiring intervention, causes an initial severe inflammatory response; this may be an important factor, which determines whether the infection is able to drive chronic inflammation or recurrent infections [213]. Antimicrobial responses to uropathogenic *Escherichia coli* are largely triggered by toll-like receptor 4 (TLR4) activation on the

superficial epithelial cells [273, 274]. Major downstream antimicrobial pathways are driven by the pro-inflammatory cytokines IL-6 and IL-8 [275, 276]. TLR4 also drives tumor necrosis factor alpha (TNF) production, contributing to the general inflammation and aids with mounting an effective immune response [274]. Yet it is important to consider that an *in vitro* study found these same cytokines also increased the ability of the bacteria to grow, but reduced in biofilm formation; therefore, more studies are required [277]. Furthermore, activation of these TLR4 pathways enhanced antimicrobial peptides that intercalate and disrupt bacterial membranes causing cell death, including β-defensin 1 and cathelicidin [278, 279].

Cytokines and cells from both arms of the immune system, the innate and adaptive, are crucial to limit the spread of uropathogenic *Escherichia coli* [280]. The acute phase requires activation of innate immune cells, in particular, the neutrophils and macrophages [280]. Neutrophils have a critical role to phagocytose bacteria in the early stages of infection; while the $Ly6C^-$ macrophages attract the $Ly6C^+$ macrophages and also the neutrophils due to the production of C-X-C motif chemokine ligands (CXCL)1, CXCL2, CXCL6 and others [280]. Yet, it is the role of the $Ly6C^+$ macrophages to conduct TNF release, which forces the $Ly6C^-$ macrophages to release large amounts of CXCL2 [280]. This massive CXCL2 signal allows for the neutrophils to navigate and migrate throughout urothelium in order to seek out and engulf the loose bacteria [280]. Yet there is contradictory evidence on the role of neutrophils, since decreasing the number of neutrophils circulating and in the bladder through neutralisation of granulocyte colony stimulating factor (G-CSF) in infection actually decreased the bladder bacterial burden, opposite of what would be anticipated [281]. Although the authors found that macrophage-activating cytokines were concomitantly increased including C-C motif chemokine ligand (CCL)2, also known as monocyte chemoattractant protein 1, and IL-1β which suggests that the role of macrophages may be equally as important in this context [281]. In contract to this work, additional studies depleted bladder resident macrophages prior to

primary UTI which led to a substantial decrease in bacterial load during secondary UTI [282]. Indeed, the increase in bacterial clearance was lymphocyte dependent since macrophages were found to be the principal antigen presenting cell in the context of a challenge infection [282]. Although, many other pro-inflammatory chemokines are also significantly upregulated post-infection, including the CXCL5, CXCL9 and CCL2 [283]. Other studies found IL-8 in the urine was increased and positively correlated with neutrophils during infection, however, the authors found this approach was more specific as an indicator of pyelonephritis [284]. IL-8 assisted to allow neutrophil migration through the urothelium during infection and anti-IL-8 was sufficient to prevent this behaviour [285]. Increasing the knowledge of the urinary immune system is critical to discover the next phase of therapeutics.

1.3.11 Experimental models of pyelonephritis

Experimental models of cystitis commonly use the UTI89 strain in typical laboratory mice strains like C57BL/6. Pyelonephritis models rely on utilizing specific strains such as C3H/HeJ, which are deficient in TLR4, and the C3H/HeN and C3H/HeOuJ, which are TLR4 sufficient yet are prone to vesicoureteral reflux [286]. However, there may be sufficient rationale to generate a robust pyelonephritis model on a C57BL/6 background since it would have the benefit of allowing the assessment of conventional genetic knock-out studies. Additionally, more complex studies are possible using cre-recombinase for ablation of genes, or even specific cells, during a selected timeframe by administration of Tamoxifen or Diphtheria toxoid. Other popular methods of inducing pyelonephritis are achieved by the introduction of more virulent *Escherichia coli* strains such as CFT073, isolated from a patient with urosepsis [287], or by utilizing models of superinfection, which typically involve a secondary inoculation of bacteria in the early phase of infection [288].

1.4 IL-33, emerging immunotherapies and UTI

During experimental UTI, IL-33 is increased in the urinary bladder whereas IL-5 is increased in the bladder and serum [213, 265]. One report found IL-33 protein levels were increased in female and male mice, yet exogenous rmIL-33 administration did not affect bacterial load in male mice utilising a cystitis model [203]. Similar studies were performed female mice, but instead using a loss-of-function approach whereby a neutralising anti-IL-33 was administered, yet once again there was no discernible alternations to bacterial load, which is the major readout [203]. These results identify a potential knowledge gap around the role of IL-33 in the context of UTI. There are conditions whereby IL-33 may be exaggerated and UTI is predominantly a condition that affects female humans; therefore, I was interested in knowing the effect of IL-33 exaggeration during UTI in female mice. Since in other tissues, IL-5 production is largely driven by IL-33 signalling through ILC2, I theorise that a similar mechanism is at play in the urinary bladder (**Figure 7**).

If an important role is identified for IL-33 in UTI, there may be the possibility of repurposing existing immunotherapies. REGN3500 (Regeneron Pharmaceuticals) is a monoclonal antibody that inhibits the human IL-33 protein. REGN3500 is currently under investigation in a phase 4 clinical trial (trial # NCT04701983) for the treatment of chronic obstructive pulmonary disease. Clinical safety and pharmacokinetic studies have already been completed as well as trials in atopic dermatitis (trial # NCT03738423) and asthma (trial # NCT02999711). Although the immunology of the urinary bladder has been extensively studied, the role of IL-33 in UTI is limited. Yet, IL-33 may be an attractive therapeutic target for severe UTI based on the preliminary data from the preclinical proof-of-principal studies. However, additional *in vivo* data is required before considering the repurposing of this novel immunotherapy for the treatment of cystitis or pyelonephritis.

IL-10 is another factor driven by IL-33 and is produced by $CD45^{+}$ monocytes which drives anti-inflammatory pathways, aiming to limit collateral damage to the host [283]. IL-10 dampens the inflammatory processes in macrophages, dendritic cells and other monocytes and even cells of the adaptive immune system including T_H1 and T_H17 [289]. IL-10 is appealing as a biomarker since it's been found in the urine >7-fold increased during UTI [283]. Using a classical knockout system in mice, deficiency in IL-10 exacerbated cystitis with >10-fold bacterial load in the bladder and >30-fold in kidneys during the early phases of infection [283]. Similarly, a pre-treatment approach of anti-IL-10 neutralising antibody therapy before infection resulted in exacerbation of bacterial load [283]. Yet, many additional cytokines and chemokines act to facilitate the recruitment or instruction of innate and adaptive immune cells in the context of UTI [285].

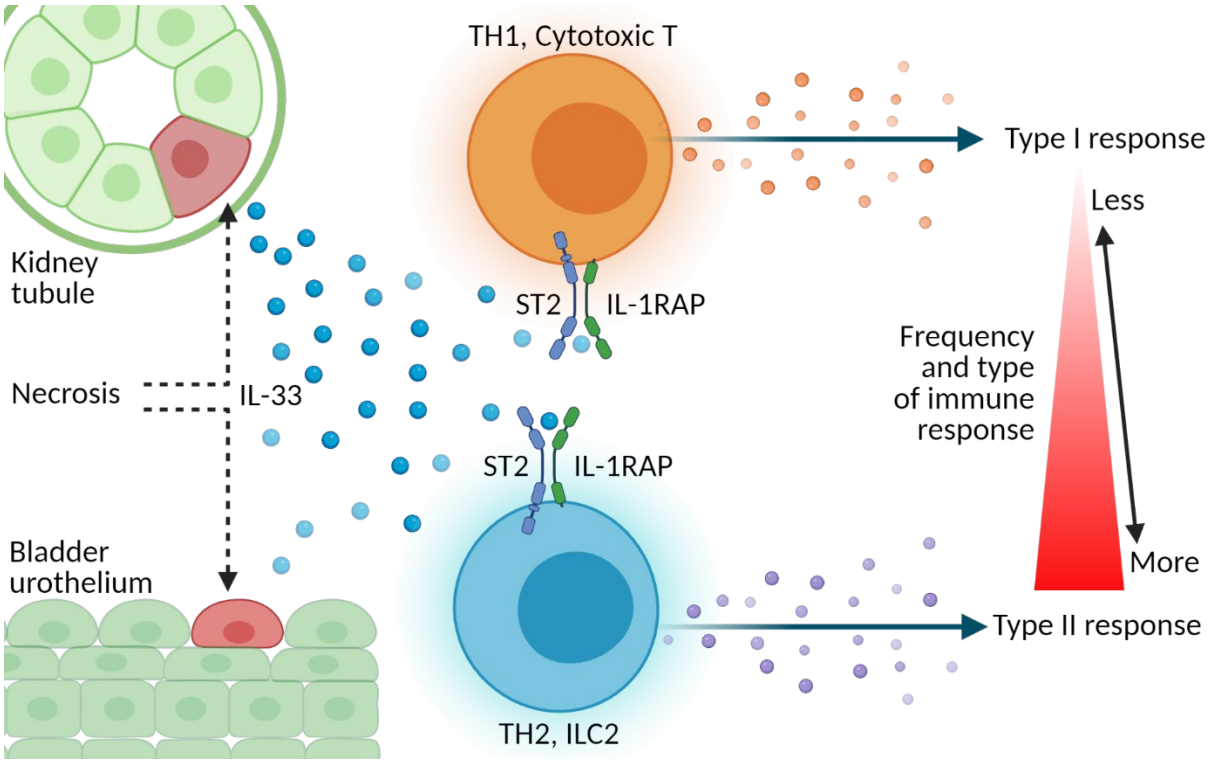

Figure 7: IL-33 is released following cell death and induces a type II immune response

Interleukin (IL)-33 is released during necrosis of epithelial cells in multiple tissue sites including the kidney tubules and the urinary bladder urothelium. IL-33 can induce a type I or II response through binding the IL-33 receptor (ST2) and forming a complex with the IL-1 receptor accessory protein (IL-1RAP). Type I response is induced by immune cells such as $CD4^+$ T-helper type 1 (T_H1) and CD8+ cytotoxic T-cells. However, IL-33 primarily induces a type II response targeting $CD4^+$ T-helper type 2 (T_H2) and group 2 innate lymphoid cells (ILC2). Created with BioRender.com.

1.5 IL-17A, IL-22 and IL-22 emerging immunotherapies

In other mucosal tissues such as the gastrointestinal tract and lung IL-17A has a major role to induce pro-inflammatory immune responses [290, 291]. IL-17A can be produced by T_H17 cells or γδ T cells which induces the early defence against bacterial infection and protective immunity in other systems [292-294]. IL-17A activates neutrophils which are critical for protection against pathogens, but also can drive autoimmune diseases like allergic encephalomyelitis [294-296]. IL-17A has been investigated using *in vitro* and *in vivo* models with transcript and protein levels increased in the bladder by UTI [203, 297]. Whilst IL-17A is required for the appropriate clearance of bacteria in UTI, treatment with rmIL-17A was not able to reduce bacterial load [203]. Yet, the protective features of IL-17A may be explained by investigation of the closely associated cytokine, IL-22 [298].

IL-22 is a member of the IL-10 family, primarily targeting epithelial cells at barrier sites, including lung, gastrointestinal tract and skin [299]. IL-22 can induce differing effects depending on the tissue site and context of expression [299]. IL-22 can prevent epithelial damage and promote epithelial integrity by inducing the proliferation of epithelial cells,

increasing tissue regeneration and inhibiting apoptosis in mucosal tissues [300-302]. IL-22 can induce antimicrobial peptide production at barrier sites, some of the best known include including S100A7 to A9, β-defensin 2 & 3, regenerating IIIβ & γ; each assisting in regulation of microbiota and prevention of colonisation [302-307]. Since IL-22 levels have been found to be dysregulated during inflammation, there is some evidence suggesting it is a physiological mediator which acts to upregulate the repair of tissue; yet other studies found a pro-inflammatory role, therefore, it may have a multifaceted role [304, 308]. Another cytokine, IL-23, potently stimulates IL-22 production and has been shown to be an early regulator of IL-22 by γδ T cells, $CD4^+$ T cells and monocytes [306, 309]. However, there are some conflicting reports on the role of IL-22 in chronic inflammation [310-315]. IL-22 was detrimental in chronic obstructive pulmonary disease models with increased levels observed with poor outcomes and IL-$22^{-/-}$ animals having better lung function in these models [310]. Increased IL-22 is associated with autoimmune inflammatory diseases, including Crohn's disease, psoriasis, and rheumatoid arthritis, which may indicate IL-22 is detrimental [312-315]. Yet, in the case of the chronic inflammatory skin disease acne inversa, the opposing conclusions were made [311]. Overexpression of IL-10 was found to inhibit the IL-22 cytokine, the expression of the membrane-bound IL-22 receptor was reduced, and the IL-22 binding protein which mops up the cytokine was increased, which suggests that insufficient IL-22 levels can also drive chronic inflammation [311]. Therefore, it is plausible that the contrasting results are indicative that IL-22 needs to be tightly regulated; like the phenomenon known as the Goldilocks principle, the IL-22 levels may need to be 'just right' and any deviation is negative. In addition, at some mucosal sites IL-22 protein levels fluctuate in mice, with decreased levels observed at night [316].

An emerging immunotherapy exists in the form of a human recombinant IL-22 IgG2-Fc named F-652 (Generon BioMed), which aims to mimic the protective effects of endogenous IL-22. F-

652 is currently under investigation in a phase IIa clinical trial (trial # NCT02406651) for the treatment of graft vs host disease. Clinical safety and pharmacokinetic studies have already been completed as well as a trial in alcoholic hepatitis (trial # NCT02655510). IL-22 may be an attractive novel therapeutic target for severe UTI due to its dual antimicrobial and tissue-protective effects in other tissue sites. Yet, before considering repurposing of F-652, preclinical *in vivo* proof-of-principal studies are required to determine if IL-22 may be suitable as a novel therapy for the treatment of cystitis and pyelonephritis. Furthermore, the role of IL-22 in the context of UTI has not been explored to date.

1.5.1 Cell types which produce IL-22

Primarily, lymphocytes are responsible for producing IL-22, these include: group 3 innate lymphoid cells (ILC3), mucosal associated invariant T cells, NKT cells, γδ T cells and $T_H17/22$ cells [304, 310]. Interestingly, ILC3 and γδ T cells are increased in the bladder during experimental UTI; yet the functional role is not known [203, 317]. In these models, a deficiency in some cell types which can produce IL-22 also increased susceptibility to UTI [318]. However, myeloid cells like macrophages, dendritic cells and neutrophils are also capable of producing IL-22 in some circumstances (**Figure 8**) [304]. Therefore, it is difficult to evaluate the contribution of IL-22 in UTI since it has not been specifically targeted in these models.

1.5.2 IL-22 receptors and signalling pathway

The primary receptor which binds IL-22 and performs downstream signalling is a heterodimer consisting of the IL-22 receptor subunit alpha 1 (IL-22Rα, encoded by *IL22RA1*) and the IL-10 receptor subunit beta (IL-10Rβ, *IL10RB*) [319]. Whilst IL-22Rα is shared by IL-20 and IL-

24, IL-10Rβ is required for IL-10 and IL-26 signalling [320, 321]. The high binding affinity of IL-22 to the receptor is through IL-22Rα; there is no affinity for the IL-10Rβ alone [322]. This is sensible considering IL-10Rβ is expressed ubiquitously on the membrane of many cells, whereas IL-22Rα is restricted to epithelia (**Figure 8**) [323, 324]. IL-22Rα is known to be expressed in the urinary bladder and kidney; in the kidney, the expression is restricted to the tubular epithelium, with negligible signal from the glomeruli in mice [324, 325].

The IL-22 subunit alpha 2 is commonly referred to as the IL-22 binding protein (IL-22BP, encoded by *IL22RA2*) [304]. This is a soluble form of IL-22 receptor which has antagonist properties and effectively outcompetes and blocks the interaction of IL-22 with its cell surface receptor since it has 1000-fold higher affinity than the membrane receptor IL-22Rα [304, 326, 327]. IL-22BP is primarily produced by dendritic cells in response to TNF, yet, can also be produced by eosinophils, macrophages, and by $CD4^+$ T cells [326, 328, 329]. IL-22BP is expressed by mucosal sites including: the skin, gastrointestinal tract, lung and urinary bladder (**Figure 8**) [327]. Suppression of IL-22BP increases IL-22 signalling, which in gastrointestinal tract has been shown to be detrimental [330].

When IL-22 binds the heterodimer, it signals through a known pathway of janus kinase 1 and tyrosine kinase 2 activation, then leading to signal transducers and activators of transcription (STAT) phosphorylation [330]. Specifically, STAT3 is essential for the IL-22 downstream pathways, but STAT1/STAT5 pathways are also activated to a lesser extent [330]. STAT3 regulates many pathways including: apoptosis, proliferation, immune cell maturation and inflammation [331]. One *in vitro* study uropathogenic *Escherichia coli* decreased the phosphorylation of STAT3 in human bladder cells [332].

1.5.3 IL-22 in the kidney

In the kidney, utilising a pre-clinical model of unilateral UO, IL-22 from infiltrating immune cells induced progressive kidney remodelling, enhanced tubular epithelial integrity and barrier function [333]. Using models of IRI, IL-22 enhanced repair of the tubular epithelium and ameliorated the acute injury [324]. IL-22 was found to be increased in the cortex within an experimental glomerulonephritis model, yet deletion of IL-22 did not alter the pathophysiology [334]. Whilst the current data suggests IL-22 is protective in the kidney, the function is likely to be context dependent based on other organs and therefore, further study is still required.

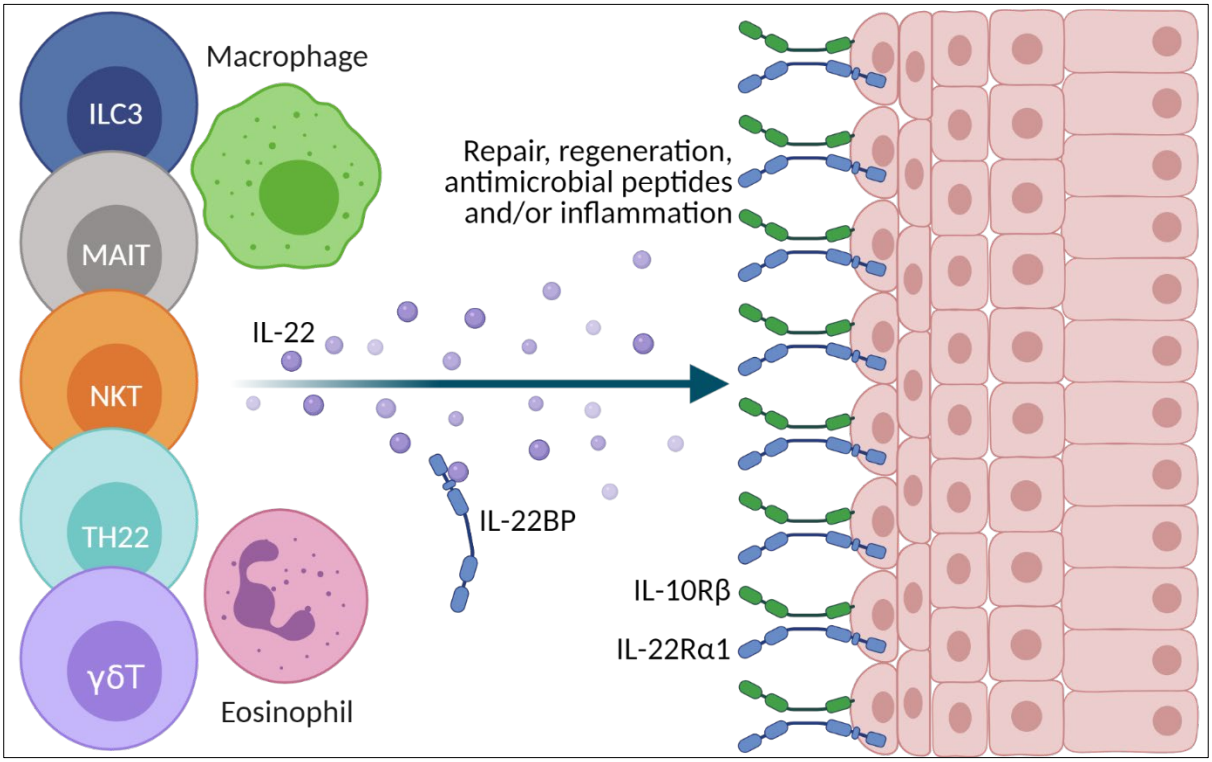

Figure 8: IL-22 cellular sources and primary receptors

Interleukin (IL)-22 can be produced by group 3 innate lymphoid cells (ILC3), mucosal-associated invariant T cells (MAIT), natural killer T cells (NKT), T helper 22 cells (T_H22), γδT-cells, macrophages and neutrophils. IL-22 can bind to the soluble binding protein (IL-

22BP) which acts as a decoy receptor, or the membranous IL-22 receptor alpha 1 (IL-22Rα) in conjunction with the IL-10 receptor beta (IL-10Rβ). When binding the membrane receptor, IL-22 can induce tissue repair, regeneration, production of antimicrobial peptides and can stimulate proinflammatory cascades. Adapted from [335]. Created with Biorender.com.

1.6 Rationale for Chapter 3

Amplification of ILC2 using IL-33 may be effective in attenuating the deleterious consequences of AKI in preclinical models. However, since IL-33 may be both beneficial and detrimental, more specific strategies are required to target ILC2 to delineate their role in kidney injury and disease. The crucial next step is to investigate whether these strategies are sufficient to prevent or delay the progression to chronic disease and end-stage renal failure. It is also plausible that ILC2-activating therapies could be detrimental if assessed at later time points due to the exacerbation of fibrosis as a result of uncontrolled AAM activation. If indeed ILC2-activating therapies are proven to be effective in the prevention of chronic disease, there is still the issue of targeting therapeutics directly to ILC2 and only within the kidney. I envision that future therapeutic strategies could involve isolating circulating immune cells, such as ILC2, from patients followed by *ex vivo* stimulation to promote activation and translocation to the kidney, and finally re-introduction to the patient. However, further studies are required to better define the diverse function of ILC2 in kidney injury and disease.

1.6.1 Hypothesis

I hypothesised that ILC2, are required in the mammalian kidney for sufficient repair and recovery following an injury. The objective was to perform loss-of-function studies and determine whether this exaggerated the severity of sterile kidney injury by utilising a model of IRI.

1.6.2 Aims

1. To assess the phenotype of murine kidney ILC2 and determine their localisation in the tissue.
2. To establish a sterile surgical AKI murine model by performing a contralateral nephrectomy with unilateral IRI, then characterise the phases of injury and recovery.
3. To examine if specific deficiency or depletion of ILC2 negatively impacted the severity of experimental injury using the IRI model.

1.7 Rationale for Chapter 4

Whilst an IL-33 immunotherapy appears like an attractive future option for sterile AKI, there has been little consideration of the effect of such therapeutics on non-sterile conditions. Several studies demonstrate the dysregulation of IL-33 occurs within pre-clinical models of experimental UTI, but the functional relevance has not yet been explored. It is understood that cystitis increases the transcript and protein levels of IL-33 in the urinary bladder, and that IL-33 is released following cell death in the urinary bladder and kidney. However, given the prevalence of UTI globally, the function of IL-33 in the context of UTI must be explored before any IL-33 immunotherapy can be considered for use since there is the potential that the effect of IL-33 differs between sterile and non-sterile forms of injury.

1.7.1 Hypothesis

I hypothesised that IL-33 release from the bladder is required for effective immune responses during cystitis and may contribute to the regeneration of the urothelium. I proposed that excess

exogenous IL-33 would be protective in this context and would reduce the bacterial load and prevent pyelonephritis.

1.7.2 Aims

1. To assess the phenotype of urinary bladder ILC2 and determine their localisation in the tissue.
2. To establish a murine model of uropathogenic *Escherichia coli* cystitis which also induces pyelonephritis.
3. To investigate the function of ILC2 in the urinary bladder and assess the impact of IL-33 treatment in experimental UTI using the cystitis model.

1.8 Rationale for Chapter 5

Antibiotic-resistant uropathogenic bacterial strains are being increasingly seen in UTI, with the majority of these being uropathogenic *Escherichia coli*. Alternative approaches to antibiotics are needed to continue to treat UTI and prevent the risk of pyelonephritis. One such avenue may be immunotherapies. The cytokine IL-22 is crucial for protection at mucosal sites; however, it has not yet been explored in UTI.

1.8.1 Hypothesis

I hypothesised that the IL-22 protein is crucial in the urinary tract for host immunity in the context of UTI. I proposed that exogenous IL-22 would aid the host in clearing the bacteria, reducing the bacterial load in the urinary bladder and kidney.

1.8.2 Aims

1. To assess IL-22 protein levels at various phases of infection within an experimental murine model of uropathogenic *Escherichia coli*-induced cystitis.
2. To confirm that the urinary bladder and kidney express the membranous IL-22 receptor and evaluate whether systemic administration of rmIL-22 can reach these tissues.
3. To determine if a prophylactic or therapeutic treatment regime is most suitable for the introduction of exogenous IL-22 and to assess the therapeutic potential of IL-22 in UTI.

Chapter 2: Methods and materials

Some of the content in this chapter has been previously published as:

> **Cameron GJM**, Jiang SH, Loering S, Deshpande AV, Hansbro PM, Starkey MR. Emerging therapeutic potential of group 2 innate lymphoid cells in acute kidney injury. J Pathol. 2019;248(1):9-15

Cameron GJM and Starkey MR conceptualised the manuscript. Cameron GJM drafted the manuscript and figures. Jiang SH, Loering S, Deshpande AV, Hansbro PM and Starkey MR provided critical review of the manuscript.

> **Cameron GJM**, Cautivo KM, Loering S, Jiang SH, Deshpande AV, Foster PS, McKenzie ANJ, Molofsky AB, Hansbro PM, Starkey MR. Group 2 Innate Lymphoid Cells Are Redundant in Experimental Renal Ischemia-Reperfusion Injury. Front Immunol. 2019;10:826.

Cameron GJM and Starkey MR conceptualised the manuscript. Cautivo KM and Molofsky AB performed the flow cytometry and immunofluorescence using Il5$^{td\text{-}tomato Cre}$Rosa26-CAG-RFP mice. Cameron GJM performed all other aspects including the surgical model, flow cytometry, histological assessment, gene expression analysis, data analysis and drafted the manuscript. Loering S assisted with animal monitoring and flow cytometry. Jiang SH and Deshpande AV provided clinical insight for study design and surgical technique. McKenzie ANJ created, supplied and advised on the use of ILC2-deficient & -depleted and Il13td tomato mice. Foster PS supplied and advised on the use of Il5venus reporter line. Foster PS and Hansbro PM advised on experimental design.

2.1 Usage of animals

2.1.1 General introduction

The work that took place within this thesis would not have been possible without the *in vivo* models using mice. Every effort was made to reduce the numbers of animals required for experiments, to reduce the possibility of harm and to maximise the data obtained from each sample which was collected from these animals. During this thesis, several procedures and protocols were established by the candidate at the Hunter Medical Research Institute and at the University of Newcastle prior to obtaining any data or testing hypotheses; this chapter outlines some the procedures which were critical for obtaining the results seen in later chapters.

2.1.2 Animal care, ethics and husbandry

The University of Newcastle's animal care and ethics committee strictly oversaw the usage of animals and approved all procedures under ethics #A-2017-700. Animals were bred at Australian Bioresources (Moss Vale) and were relocated to the Hunter Medical Research Institute (New Lambton Heights) by JetPets at least one week prior to starting any procedures. Animals were received by trained staff from the University's animal services unit and were divided up based on sex and genotype, then were allocated into enclosures at random. The animal services staff were external to the researchers who would perform the studies and therefore allowed for randomisation to be performed between enclosures ensuring that animals were mixed between interventions. All animals were housed in individually ventilated enclosures and the airflow for the enclosures was passed through high efficiency HEPA filters. Co-housing of animals in the same experimental groups was performed to prevent anxiety, the female animals were housed up to 4 animals per enclosure and the males typically only 2 per

enclosure to minimise the risk of fighting. Each of the rooms which housed the animal enclosures was certified as physical containment level 2 and maintained the animals as specific pathogen free. There were two separate rooms for housing of animals for studies with and without infectious agents used, each with separate procedures room to ensure there was no cross-contamination. Movement between these areas required showering, changing of clothes and new personal protective equipment (PPE). The day/night cycle of each room was maintained automatically at a strict 12-hour timeframe, with lights on at 6am. The animal services unit staff performed the day to day general husbandry and ensured the animals had an environment which was not soiled, and that the animals had access to standard laboratory chow and water *ad libitum*.

The candidate was responsible to monitor the health status of animals frequently, as a minimum twice per day after any receiving any intervention. To do this, animals were handled within a class II biosafety cabinet with vertical laminar air flow and were assessed for weight, facial signs, behavioural changes, and other features depending on the intervention.

2.2 Establishment of surgical models

2.2.1 Training, aseptic techniques and protocol approval

Before submitting ethics applications, the candidate consulted with, and received one on one training with a paediatric urological surgeon from the John Hunter Hospital to develop aseptic techniques. This was essential as the candidate had no prior experience of surgery, and although these types of surgical procedures have been conducted at other research laboratories, they needed to be established at the Hunter Medical Research Institute and the University of Newcastle. The candidate learned about how surgery is performed in humans, gained

experience with using surgical instruments and received training on techniques such as suturing. Before the procedures received full approval, the surgical techniques were performed extensively on mouse cadavers. Once the candidate demonstrated competence with cadavers, initial approval was given for a 5 mouse pilot study which was supervised by two members of the animal care and ethics committee, one an animal welfare officer who was also a trained veterinarian, the other independent researcher with experience using other invasive procedures. The pilot study was also observed by the paediatric urological surgeon and the chief investigator of the project. During the pilot study, all animals survived the procedure and a report was submitted to the animal care and ethics committee detailing the circumstances of the surgery and recovery which was used to develop the protocol and monitoring criteria. In this protocol, intraperitoneal injection of 75mg kg^{-1} ketamine, in combination with 1mg kg^{-1} medetomidine in sterile saline was used for anaesthesia.

Interim approval was received, yet soon after an adverse event was encountered whereby some animals did not awaken from anaesthesia. The protocol was temporarily suspended, post-mortem revealed no surgical error or trauma and the likely cause was deemed to be an anaesthetic overdose. Hence a new protocol for anaesthesia was designed and submitted to the committee. Under the new protocol, anaesthesia was achieved by 4% isoflurane in 1 litre of oxygen min^{-1} in an anaesthetic chamber, then maintenance with 1%, up to a maximum 2.5% isoflurane continuously using a rodent sized face mask. Although this required specialised equipment and greatly restricted throughput, it allowed for superior control of anaesthesia depth. Additionally, the animals recovered from anaesthesia quicker, and were resuming normal behaviours sooner than the injected anaesthetic regime. Again, the protocol was reviewed and gained interim approval. This time the protocol demonstrated 100% survival in the pilot study and received the full approval. The anaesthetic record and monitoring checklist

designed by the candidate specific for this project is included; a new document was completed for each animal undergoing surgery to record the status of every animal daily (**Figure 9**).

Anaesthetic record - Acute Kidney Injury in mice – DURING SURGERY MONITORING

Project Title: Understanding how immune cells repair the kidney after injury **Chief Investigator:** A/Prof Jay Horvat

ACEC Approval Number: A-2017-700 **Box Number/s:** **No. Mice in group:** **Individual ID:**

Group (Sham or AKI)

Genotype:

Marked by:

Analgesic premedication	Induction of anaesthesia	Maintenance of anaesthesia
Time:	**Time:**	**Time:** to
Drug: Buprenorphine	**Drug:** Isoflurane	**Drug:** Isoflurane
Dose: 0.1mg/kg	**Dose:** 4.0% in oxygen	**Dose:** 1.0 to 2.5% in oxygen
Volume:	**Volume:** 1L per min	**Volume:** 1L per min
Route of administration: s.c.	**Route of administration:** inhaled	**Route of administration:** inhaled

Weight (prior to analgesic):

Misc details:

Surgery start time (time of first incision):

Surgery finish time (dermal adhesive applied):

Important to reassess the condition of the animal during surgery, where safe to do so. Include comments and time of any events (e.g. time of clamp application and removal).												
Time												
Foot pinch reflex (Y/N)												
Ear pinch reflex (Y/N)												
Respiratory rate (Fast/Normal/Slow)												
Comments												

Monitoring Checklist - Acute Kidney Injury in mice – IMMEDIATE MONITORING POST-SURGERY

Project Title: Understanding how immune cells repair the kidney after injury **Chief Investigator:** A/Prof Jay Horvat

ACEC Approval Number: A-2017-700 **Box Number/s:** **No. Mice in group:** **Individual ID:**

NOTE: place an 'x' against any clinical signs that are present. Use the intervention instructions at the base of the sheet to ensure that the correct action is taken. **NAD**- No abnormalities detected.

Date													
Time													
Observer Initials													
NAD													
Weight (grams)													
% of starting weight													
Category 1 signs													
Ruffled fur													
Decreased activity													
Shallow or increased respiratory rate													
Isolated from cagemates													
Abnormal gait													
Irritation and/or over grooming at surgical site													
Category 2 signs													
Thin or dehydrated													
Ungroomed													
Unusually docile or aggressive													
Hunched posture													
Change to faeces													
Abdominal swelling													
Abnormalities and/or infection (pus) at injection site/s (from i.p or s.c)													
Category 3 signs													
Emaciated													
Pale or cyanotic ears/nose/feet													
Gasping respiration													
Unresponsive to stimulus													
Swelling of and/or severe bleeding from surgical site													
Comments													

Monitoring Checklist - Acute Kidney Injury in mice - DAILY MONITORING POST SURGERY

Project Title: Understanding how immune cells repair the kidney after injury **Chief Investigator:** A/Prof Jay Horvat

ACEC Approval Number: A-2017-700 **Box Number/s:** **No. Mice in group:** **Individual ID:**

NOTE: place an 'x' against any clinical signs that are present. Use the intervention instructions at the base of the sheet to ensure that the correct action is taken. **NAD**- No abnormalities detected.

Date													
Time													
Observer Initials													
NAD													
Weight (grams)													
% of starting weight													
Category 1 signs													
Ruffled fur													
Decreased activity													
Shallow or increased respiratory rate													
Isolated from cagemates													
Abnormal gait													
Irritation and/or over grooming at surgical site													
Category 2 signs													
Thin or dehydrated													
Ungroomed													
Unusually docile or aggressive													
Hunched posture													
Change to faeces													
Abdominal swelling													
Abnormalities and/or infection (pus) at injection site/s (from i.p or s.c)													
Category 3 signs													
Emaciated													
Pale or cyanotic ears/nose/feet													
Gasping respiration													
Unresponsive to stimulus													
Swelling of and/or severe bleeding from surgical site													
Comments													

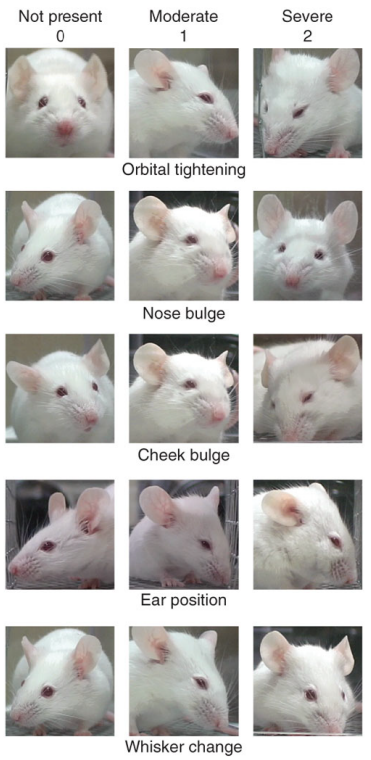

NAD- no action

Category 1- monitor again in 4 hours, if not improved seek advice from CI or veterinarian

Category 2- contact Chief investigator and veterinarian for advice

Category 3- euthanize immediately. Ensure post mortem performed. Submit adverse event report to ACEC

More than 15% weight loss- euthanize immediately

Any combination of signs-

More than two signs in any one category- Contact Chief investigator and veterinarian for advice

Signs from more than one category- Treat as for higher of the categories which the signs belong to

Guidelines to Use of Monitoring Checklist

1. Use the general Animal Services monitoring checklist (provided in the procedures/treatment record folder – red folder) to record monitoring information twice weekly until animals enter the active research protocol.
2. Once a procedure has been performed on an animal use this specific checklist.
3. Ensure all monitoring checklists are held in the red folders in the room in which the animals are held.
4. Monitor animals in accordance with and as frequently as required by the Animal Care and Ethics approval.
5. Where an abnormal clinical sign in an animal has been detected, use the Animal Services Unit provided "sick' card to identify the cage.
6. Where an abnormal clinical sign in an animal has been detected make a notation in the ASU provided checklist in the red folder of the action taken. Make sure the animal identification is included in this notation.

Image from: Langford, D. J. *et al.* Coding of facial expressions of pain in the laboratory mouse. *Nat. Methods* **7,** 447–449 (2010).
"In the Mouse Grimace Scale, intensity of each feature is coded on a three-point scale. For each of the five features, images of mice exhibiting behaviour corresponding to the three values are shown".

Figure 9: Monitoring checklist for surgery

2.2.2 Preparation for surgery

Microbiological screening was performed on the surgical environment pre- and post-sterilisation to ensure sterilisation procedures were sufficient. The day prior to surgery, animals were anaesthetised briefly to remove the dorsal skin of fur using an electric razor. Subcutaneous 0.1mg kg^{-1} buprenorphine was administered for analgesia 30 minutes prior to surgery. Hypothermia was prevented by keeping the animals on a heat mat during procedures, and the recovery area contained a heat lamp. Poly visc ointment was applied to the eyes to prevent drying out during procedures. The dorsal skin was cleaned using a povidone-iodine solution then chlorhexidine 3 times before the surgery. A sterile surgical drape was used to ensure that the sterilised instruments could not become contaminated by touching other areas of the mouse

during the procedure. The candidate performed every surgery and was assisted at all times. The assistant was required to fill the monitoring sheets and start or stop timers for certain phases of the procedure. Surgery was performed on a maximum 4 male mice per day but staggered such two animals were being worked on at once, with the first incision at approximately 9am.

2.2.3 Renal unilateral IRI surgery

Contralateral nephrectomy of the right kidney and ischemia of the left kidney was performed. The kidneys were exposed by an incision in the dorsal skin at the midline. Next, lateral flank incisions were made, parallel to the spine. The right kidney vessels were ligated with 5/0 vicryl suture using a double surgical knot, and then 3 single knots. This was repeated on a medial section of vessel as a precaution to reduce the risk of adversity. The kidney was removed after confirming a lack of blood supply visualised by a darkened appearance to the tissue. The site was irrigated with warmed sterile saline and 5/0 vicryl suture was used to close the right flank muscle. The left kidney vessels were restricted of blood flow for 29 minutes by using a sterilised vascular clamp (**Figure 10**). The site was irrigated with warmed sterile saline, covered with the skin and gauze for protection and heat maintenance. Ischemia was assessed regularly during this timeframe, on one occasion the ischemia was not present, the clamp was removed, some adipose tissue was excised carefully and after clamp reposition the timer was restarted. Kidney reperfusion was observed once the clamp was removed (**Figure 10**). The site was irrigated with warmed sterile saline and 5/0 vicryl suture was used to close the left flank muscle and the skin. Dermal adhesive was applied to the skin for added protection and infection control. As a control, sham operations were performed which were identical in timing and procedures except the vascular clamp was not applied; sham operations involved contralateral nephrectomy but not the IRI.

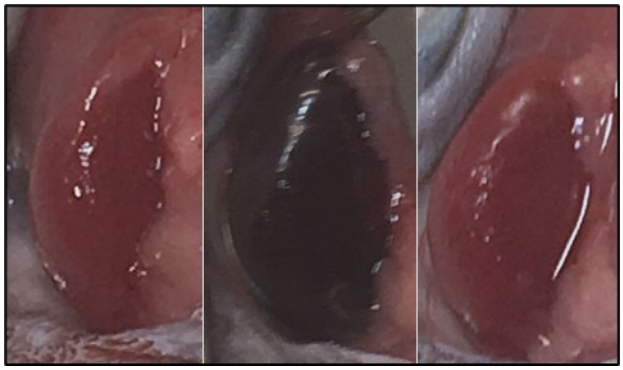

Figure 10: Closeup of the same kidney before, during and after unilateral ischemia

The normal appearance of the mouse kidney (left), the appearance is darkened after clamp application to the vessels (middle), and after the clamp is released reperfusion occurs and the kidney returns to the normal colour (right).

2.2.4 Renal bilateral IRI surgery

An additional model was established to maximise throughput, whereby IRI was induced in both kidneys. The kidneys were exposed by an incision in the dorsal skin at the midline and lateral flank incisions, as described earlier. The vessels of the left and right kidney were simultaneously restricted of blood flow for up to 30 minutes by using sterilised vascular clamps (**Figure 11**). The site was irrigated with warmed sterile saline, covered with the skin and gauze for protection and heat maintenance. Ischemia was assessed regularly, as described earlier. Kidney reperfusion was observed once the clamps were removed (**Figure 11**). The site was irrigated with warmed sterile saline and 5/0 vicryl suture was used to close the left flank muscle and the skin. Dermal adhesive was applied to the skin for added protection and infection control. As a control, sham operations were performed which were identical in timing and procedures except the vascular clamp was not applied; sham operations involved the externalisation of the kidneys but not the IRI. This model was developed after the completion of the studies in **Chapter 3** and would have been used further if funding was obtained.

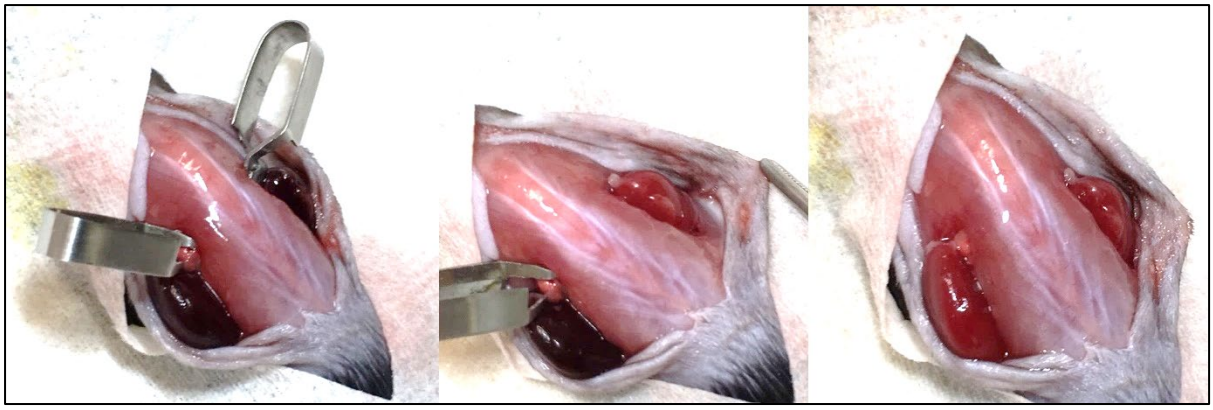

Figure 11: Appearance of the same kidneys during bilateral ischemia and reperfusion

The appearance of the kidneys during bilateral ischemia (left), after one clamp is released (middle), and both clamps are released reperfusion occurs and the kidneys return to the normal colour (right).

2.2.5 Post-operative monitoring

Animals were closely monitored by the candidate who performed each surgery. As an absolute minimum this was over an 8-hour period immediately after the surgery, and on two separate occasions daily on every subsequent day, as per the ethical requirements. Additional subcutaneous buprenorphine was provided every 8-12 hours, as required by the animal. Typically, 3 days post-surgery animals were weaned off the analgesic. There were no signs of infection nor was there need to perform a humane intervention based on the checklist (**Figure 9**). Skin irritation was observed since as animals recovered, they scratched at the external skin sutures. This was consistent between surgical groups and was monitored closely by the candidate and the animal welfare officer.

2.3 Establishment of infectious procedures

2.3.1 Training, infectious procedures and protocol approval

Before submitting ethics applications, the candidate again consulted with the paediatric urological surgeon from the John Hunter Hospital. Like the surgical procedures, the urinary tract infection protocol was established at the Hunter Medical Research Institute and the University of Newcastle by the candidate. Approval for the use of the uropathogenic *Escherichia coli* clinical isolate UTI89 was received from Prof. Scott Hultgren, who's lab originally isolated the bacteria. A stab culture was then obtained from Prof. Mark Schembri which was subcultured and glycerol stocks were created. Extensive culturing experiments were performed to ensure a known amount of the bacterium could be reproducibly administered in subsequent experiments. Additionally, mouse cadavers were extensively used to gain competence in the transurethral infection technique. To gain competence, trypan blue dye was administered to the bladder by the transurethral route and was found localised to the bladder with no obvious stain in the ureters or kidney, demonstrating competence in the technique. Initially, the catheter was fashioned from a 29G needle covered by 0.5mm polyethylene tubing, as described [336]. However, to prevent harm the protocol was further refined to use a flexible shielding from a BD Insyte-N™ Autoguard™ shielded IV catheter, as described [337].

Initial approval was given for a 5 mouse pilot study which was supervised by the animal welfare officer/veterinarian of the animal care and ethics committee. The protocol was reviewed, gained interim approval a then the full study was performed which received the full approval. The anaesthetic record and monitoring checklist designed by the candidate specific for this project is included; a new document was completed for each animal undergoing urinary tract infection, and was used to record the status of every animal daily (**Figure 12**).

Anaesthetic record – Urinary Tract Infection in mice – MONITORING DURING ANAESTHESIA/INOCULATION

Project Title: Understanding how immune cells repair the kidney after injury **Chief Investigator:** A/Prof Jay Horvat

ACEC Approval Number: A-2017-700 **Box Number/s:** **No. Mice in group:** **Individual ID:**

Group (UTI, PBS, etc)

Genotype:

Marked by:

Weight (prior to analgesic):

Analgesic premedication	Induction of anaesthesia	Maintenance of anaesthesia
Time:	**Time:**	**Time:** to
Drug: Buprenorphine	**Drug:** Isoflurane	**Drug:** Isoflurane
Dose: 0.1mg/kg	**Dose:** 4.0% in oxygen	**Dose:** 1.0 to 2.5% in oxygen
Volume:	**Volume:** 1L per min	**Volume:** 1L per min
Route of administration: s.c.	**Route of administration:** inhaled	**Route of administration:** inhaled

Misc details:

Important to reassess the condition of the animal during procedure, where safe to do so. Include comments and time of any events.													
Time													
Foot pinch reflex (Y/N)													
Ear pinch reflex (Y/N)													
Respiratory rate (Fast/Normal/Slow)													
Comments (include isoflurane %)													

Monitoring Checklist – Urinary Tract Infection in mice – IMMEDIATE MONITORING POST-INOCULATION

Project Title: Understanding how immune cells repair the kidney after injury **Chief Investigator:** A/Prof Jay Horvat

ACEC Approval Number: A-2017-700 **Box Number/s:** **No. Mice in group:** **Individual ID:**

NOTE: place an 'x' against any clinical signs that are present. Use the intervention instructions at the base of the sheet to ensure that the correct action is taken. **NAD**- No abnormalities detected.

Date													
Time													
Observer Initials													
NAD													
Weight (grams)													
% of starting weight													
Category 1 signs													
Ruffled fur													
Decreased activity													
Shallow or increased respiratory rate													
Isolated from cagemates													
Abnormal gait													
Irritation and/or over grooming around urethra													
Category 2 signs													
Thin or dehydrated													
Excessive drinking and/or excessive urination													
Ungroomed													
Unusually docile or aggressive													
Hunched posture													
Change to faeces													
Abdominal swelling													
Abnormalities and/or infection (pus) at injection site/s (from i.p or s.c)													
Category 3 signs													
Emaciated													
Pale or cyanotic ears/nose/feet													
Gasping respiration													
Unresponsive to stimulus													
Swelling of and/or severe bleeding from urethra													
Comments													

Monitoring Checklist – Urinary Tract Infection in mice - DAILY MONITORING POST-INOCULATION

Project Title: Understanding how immune cells repair the kidney after injury **Chief Investigator:** A/Prof Jay Horvat

ACEC Approval Number: A-2017-700 **Box Number/s:** **No. Mice in group:** **Individual ID:**

NOTE: place an 'x' against any clinical signs that are present. Use the intervention instructions at the base of the sheet to ensure that the correct action is taken. **NAD**- No abnormalities detected.

Date													
Time													
Observer Initials													
NAD													
Weight (grams)													
% of starting weight													
Category 1 signs													
Ruffled fur													
Decreased activity													
Shallow or increased respiratory rate													
Isolated from cagemates													
Abnormal gait													
Irritation and/or over grooming around urethra													
Category 2 signs													
Thin or dehydrated													
Excessive drinking and/or excessive urination													
Ungroomed													
Unusually docile or aggressive													
Hunched posture													
Change to faeces													
Abdominal swelling													
Abnormalities and/or infection (pus) at injection site/s (from i.p or s.c)													
Category 3 signs													
Emaciated													
Pale or cyanotic ears/nose/feet													
Gasping respiration													
Unresponsive to stimulus													
Swelling of and/or severe bleeding from urethra													
Comments													

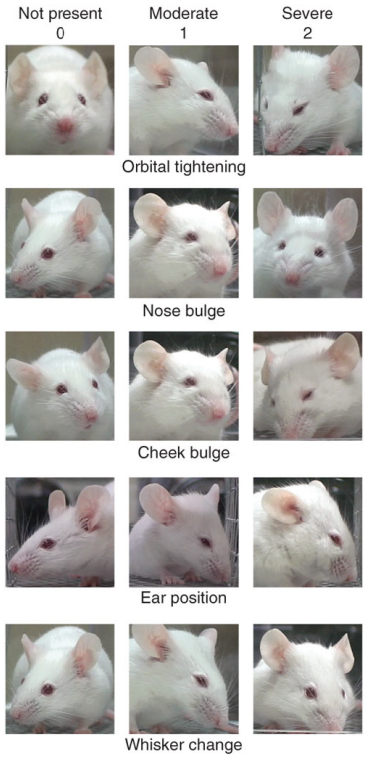

NAD- no action

Category 1- monitor again in 4 hours, if not improved seek advice from CI or veterinarian

Category 2- contact Chief investigator and veterinarian for advice

Category 3- euthanize immediately. Ensure post mortem performed. Submit adverse event report to ACEC

More than 15% weight loss- euthanize immediately

Any combination of signs-

More than two signs in any one category- Contact Chief investigator and veterinarian for advice

Signs from more than one category- Treat as for higher of the categories which the signs belong to

Guidelines to Use of Monitoring Checklist

1. Use the general Animal Services monitoring checklist (provided in the procedures/treatment record folder – red folder) to record monitoring information twice weekly until animals enter the active research protocol.

2. Once a procedure has been performed on an animal use this specific checklist.

3. Ensure all monitoring checklists are held in the red folders in the room in which the animals are held.

4. Monitor animals in accordance with and as frequently as required by the Animal Care and Ethics approval.

5. Where an abnormal clinical sign in an animal has been detected, use the Animal Services Unit provided "sick' card to identify the cage.

6. Where an abnormal clinical sign in an animal has been detected make a notation in the ASU provided checklist in the red folder of the action taken. Make sure the animal identification is included in this notation.

Image from: Langford, D. J. *et al.* Coding of facial expressions of pain in the laboratory mouse. *Nat. Methods* **7,** 447–449 (2010).
"In the Mouse Grimace Scale, intensity of each feature is coded on a three-point scale. For each of the five features, images of mice exhibiting behaviour corresponding to the three values are shown".

Figure 12: Monitoring checklist for urinary tract infection

2.3.2 Preparation of bacterial inoculum

Uropathogenic *Escherichia coli* clinical isolate UTI89 stock was stored in 20% glycerol at -80˚C. UTI89 was streaked onto LB agar and incubated statically overnight at 37°C. Static incubation is critical for type 1 pili expression on the bacteria [336]. 10mL of sterile LB broth was inoculated with a single colony of UTI89 from the agar plate and incubated overnight with the above conditions. 25µL of this was subcultured into 25mL of fresh broth and incubated overnight. The culture was centrifuged for 5 minutes at 4,122x*g* at 4°C. The supernatant was discarded and 10mL of sterile phosphate buffered saline was used to resuspend the bacteria. Optical density was measured at 600nm (OD_{600nm}) and a dilution series was performed to reach 0.4 OD_{600nm}, which was approximately 10^7 CFU, determined empirically (**Figure 13**). Agar plates were incubated for 16 hours before CFU determination.

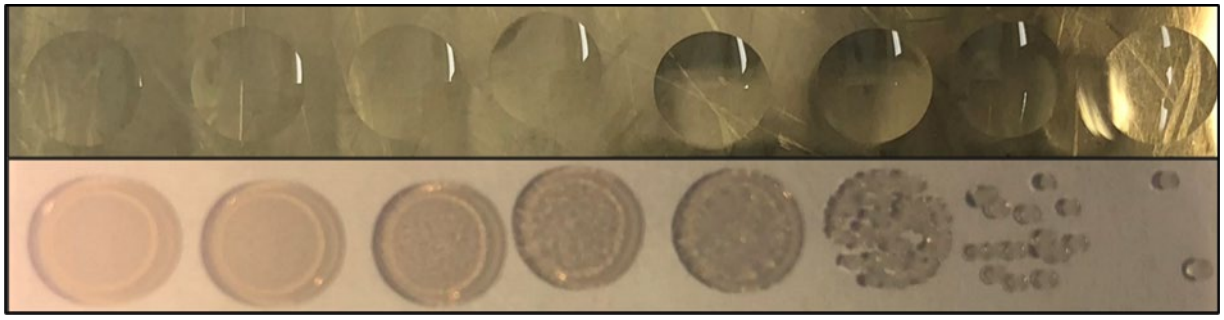

Figure 13: Bacterial spots and growth from undiluted to 10^7-fold diluted inoculum

Serial dilution of bacterial inoculum from undiluted (far left) to 10^7-fold diluted (far right). Each of the 10uL spots is 10 times more diluted then the one to the left. The 10uL spots on LB agar are shown before drying (top) and after 16 hours of incubation (bottom). After incubation the individual bacterial colonies were counted at a dilution where they were discernible from one another then were used to calculate the colony forming units per mL (CFU mL^{-1}). In this example, the second from the right 10uL spot was the most appropriate to count, ≈18 clearly

defined colonies. The spot to the left is unable to be counted, whereas to the right of this only has 2 colonies, as expected since it is 10x more dilute.

2.3.3 Transurethral inoculation

Subcutaneous 0.1mg kg^{-1} buprenorphine was administered for analgesia 30 minutes prior to surgery. Hypothermia was prevented by keeping the animals on a heat mat during procedures, and the recovery area contained a heat lamp. Poly visc ointment was applied to the eyes to prevent drying out during procedures. The induction of anaesthesia was identical to that described for surgery, using isoflurane. Once anaesthetised, anaesthesia was maintained using a specialised multi-animal breather nose cone system (EZ Systems, Palmer, United States). The urinary bladders were voided by applying pressure to the lower abdomen before inoculation. The urethra was then cleaned with 70% ethanol, which had an added benefit of dampening the fur and improving visibility of the external urethra.

The refined urinary tract infection protocol utilised a BD Insyte-N™ Autoguard™ shielded IV catheter, where the needle was ejected and discarded, leaving behind the flexible shielding which was repurposed for a female mouse urinary catheter. The makeshift catheter was lubricated then inserted into urethra at a 45-degree angle, then lowered parallel to the mouse to avoid the pelvic bone (**Figure 14**). 50µL of the inoculum was administered slowly to ensure retention in the urinary bladder. The catheter was slowly retracted from the urethra, leaving behind the inoculum. Anaesthesia was continued for 20 minutes, preventing immediate voiding of the inoculum and allowing for infection to occur.

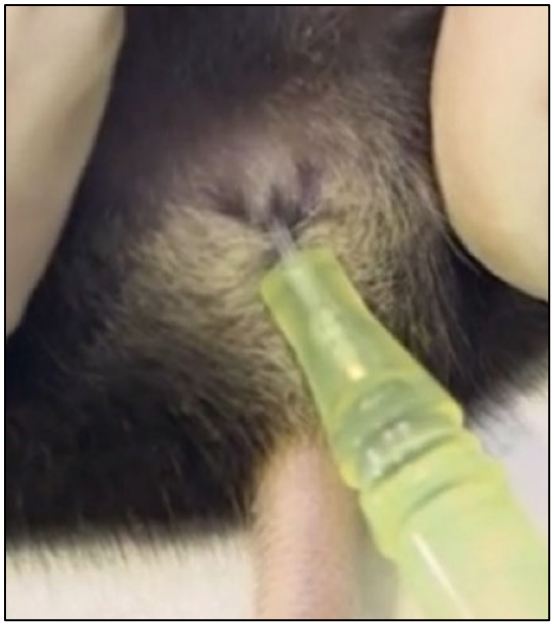

Figure 14: Closeup of the female mouse external urethra during transurethral inoculation

The mouse urethra can be seen with a makeshift urinary catheter inserted, the catheter was fashioned using the shielding ejected from a BD Insyte-N™ Autoguard™ shielded IV catheter.

2.3.4 Post-infection monitoring

Animals were closely monitored by the candidate who performed each infection. As an absolute minimum this was over a 2-hour period immediately after the procedure, and on two separate occasions daily on every subsequent day, as per the ethical requirements. Additional subcutaneous buprenorphine was able to be provided every 8-12 hours, as required by the animal, yet it was typically not required. In the base model, without rmIL-33, there was no adversity nor was there need to perform a humane intervention (**Figure 12**).

2.4 Recombinant mouse (rm) treatments

2.4.1 rmIL-33

Animals received 0.5µg of rmIL-33 (cat# 580508 [BioLegend, San Diego, United States]) at day -6, -4 and -2 with day 0 being the date of infection or 200µL of the vehicle phosphate buffered saline (PBS) *via* intraperitoneal injection, as described [338].

2.4.2 rmIL-22

For pre- and post-infection treatments, animals received 0.5µg of rmIL-22 (cat# 582-ML-010/CF [R&D Systems]) daily or 200µL of the vehicle PBS *via* intraperitoneal injection, as described [339]. Treatments which took place at 12hpi typically occurred at 9:20pm±1 hour.

2.5 Kidney function

2.5.1 Transcutaneous glomerular filtration rate (*t*GFR) measurement

Dorsal fur was removed using an electric razor and depilation cream. Measurements were obtained by attaching a mini version of the *t*GFR device (MediBeacon gmbH, Mannheim, Germany) [340]. Mice were anaesthetised and the background fluorescence was measured for 3 minutes, an intravenous bolus of 50mg kg^{-1} FITC-Sinistrin (cat# 29389090; MediBeacon gmbH) was administered, and fluorescence decay was measured for a further 90 minutes. Data was read from the device using MB lab 2 software and was analysed using MB Studio software using a three-compartment model with linear baseline correction to obtain FITC-Sinistrin half-life in minutes (min) which the software used to determine *t*GFR as mL min^{-1} 100g bw^{-1}, using

the improved kinetic model as described [341]. Due to funding constraints, the devices were only able to be obtained after completion of **Chapter 3**. The technology was validated using the bilateral IRI model, which caused a severe injury with loss of kidney function 1 day after surgery (**Figure 15**).

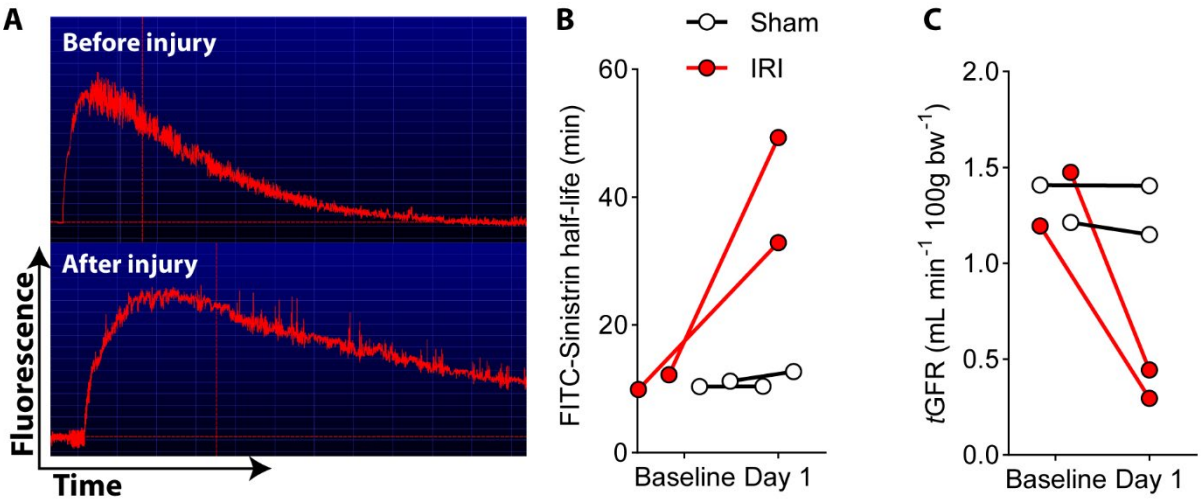

Figure 15: Transcutaneous glomerular filtration rate (*t*GFR) measurement

A) Baseline fluorescence was measured, measurement was continued for 90 minutes after intravenous administration of 50mg kg^{-1} of FITC-Sinistrin before and after bilateral IRI and in sham surgical controls. **B)** Fluorescence curves were used to obtain the half-life of FITC-Sinistrin, which was used to calculate the **C)** *t*GFR.

2.6 Histological techniques

2.6.1 Standard histological staining and scoring

Tissues were fixed by storing in formalin for 24 to 48 hours. 4µm, longitudinally cut bladder and kidney sections were stained with H&E, PAS and/or Masson's trichrome. Histopathology

was quantified by visualising dilation of tubules, cell death/sloughing of cells or cast formation by a single blinded investigator using a well-established semi-quantitative method [342], with minor alterations as described [158]. An average was taken of the score from duplicate PAS stained sections from each animal. A score of 0 = 0% of tubules were affected by the above histopathological features; 1 = 1-10%; 2 = 11-25%; 3 = 26-50%; 4 = 51-75%; 5 = 76-100%.

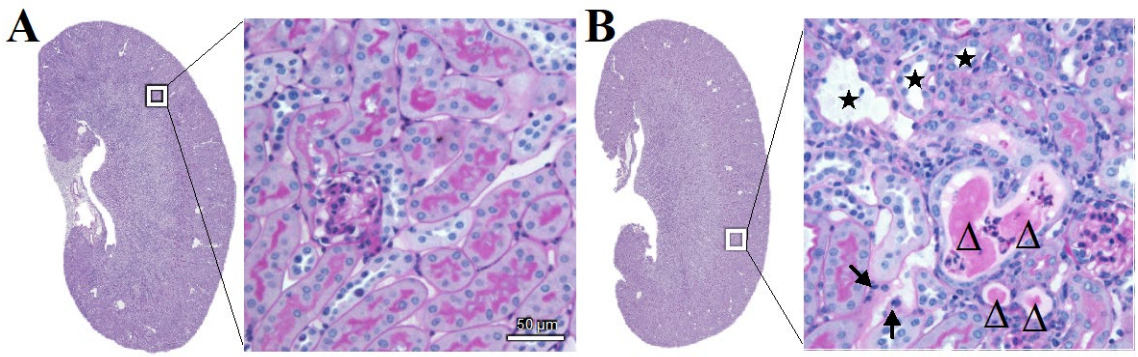

Figure 16: Kidney histopathology and features of acute tubular necrosis

Periodic acid-Schiff-stained longitudinal kidney sections from **A)** sham and **B)** unilateral IRI 24-hours post-surgery, magnified region demonstrates histopathology features of acute tubular necrosis including cell death/sloughing of cells, dilated tubules and casts; ↘, ★ and **Δ**, respectively.

2.6.2 Assessment of tubular collagen deposition

Collagen deposition was assessed using Masson's trichrome and collagen was identified as methyl blue content between adjacent tubules. A colour threshold was applied to better visualise the methyl blue content (**Figure 17**). Fiji v2.0.0-rc-61 software, built on ImageJ (National Institute of Health) was used to display hue's between 155-180 (**Figure 17**). Since the blood vessels contained significant collagen, exclusion was performed by freehand drawing

around each blood vessel, using the 'perimeter expansion tool' until the entire perivascular content was selected, and the hue's 155-180 were removed (**Figure 17**). This process allowed for an unbiased and easy approach to determine whether the collagen content was changed following kidney injury.

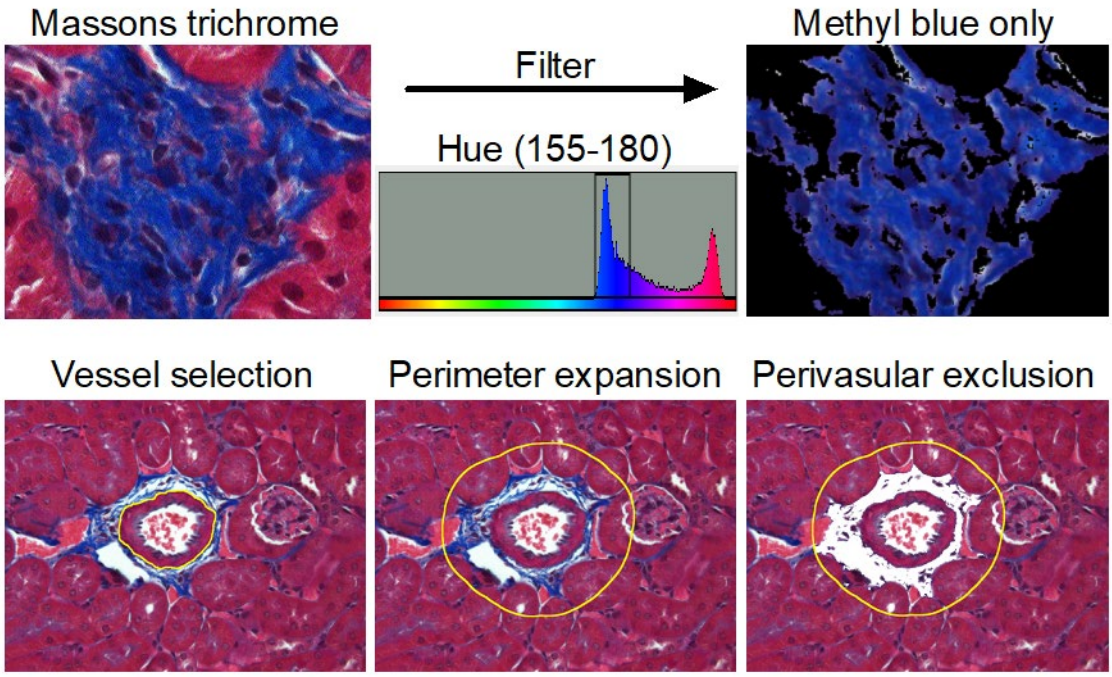

Figure 17: Visualisation of methyl blue component of masons trichrome

Methods for masons trichrome stained kidney sections to retain methyl blue content (top), and removal of the perivascular associated methyl blue content (bottom).

2.7 Immunohistochemistry (IHC)

2.7.1 Fluorescent IHC of ILC2

Il5$^{\text{td-tomatoCre}}$; Rosa26-CAG-RFP reporter-tracker mice were euthanised and perfused intracardially with 1x phosphate buffered saline (PBS) and then 4% paraformaldehyde (PFA)

in PBS. Bladder and kidneys were removed and kept in fresh 4% PFA for 24 hours at 4°C and then washed in 1xPBS. 300μm kidney sections were prepared using a vibratome, bladders were not sectioned. Subsequently, samples were incubated in permeabilization buffer (1x PBS/0.2% Triton X-100/0.3M glycine) then blocked in PBS/0.2% Triton X-100/5% donkey serum at 4°C overnight. Samples were washed in PBS/0.2% Tween-20 once, then incubated with primary antibodies diluted in PBS/0.2% Tween-20/3% donkey serum at room temperature until the next day. Next, samples were washed in PBS/0.2% Tween-20 for 30 minutes, 3-4 times, then incubated with secondary antibodies diluted in PBS/0.2% Tween-20/3% donkey serum at room temperature for 6-8 hours. Samples were washed in PBS/0.2% Tween-20 for 1 day and then dehydrated in an ascending ethanol series (20%, 30%, 50%, 70%, 95%, 100%), 10 minutes each step. Finally, kidney sections were cleared by soaking in methyl salicylate (M-2047; Sigma-Aldrich, Castle Hill, Australia) and then mounted in fresh methyl salicylate onto a concave coverslip or chamber. Images were captured with Nikon A1R laser scanning confocal including 405, 488, 561, and 650 laser lines for excitation and imaging with 16X/0.8 or 25X1.1, NA Plan Apo long working distance water immersion objectives. Z steps were acquired every 6μm. Images were processed with ImageJ (NIH, Bethesda, MD, US) and Bitplane Imaris software v8 (Andor Technology PLC, Belfast, N. Ireland). Surface reconstructions of alpha smooth muscle-labelled blood vessels were performed with Imaris. Surface module and pseudocoloured based on their characteristic architecture and volume to visualize large arteries and veins. The following antibodies and dilutions were used: Living Colors anti-DsRed Rabbit Polyclonal Pan Antibody (1:500; TaKaRa, Mountain View, USA), goat polyclonal anti-alpha smooth muscle actin antibody (1:200; Abcam, Cambridge, UK), eFluor 660 LYVE1 monoclonal Antibody (1:300, clone ALY7, eBioscience), armenian hamster anti-mouse CD3 antibody (1:100, clone 145-2C11, Biolegend), Alexa Fluor® 488 donkey anti-goat IgG (H+L),

Alexa Fluor® 555 donkey anti-rabbit IgG (H+L) Alexa Fluor® 647 goat anti-hamster IgG (H+L) cross-adsorbed (1:400, ThermoFisher Scientific).

2.7.2 Standard and fluorescent IHC of IL-22 receptors

For fluorescent IHC, sections were incubated with primary (cat# MAB42941 [R&D Systems, Minneapolis, United States]) and secondary (cat# AB150157 [Abcam]) antibodies at 1:100 concentration, as described [310]. For standard light microscopy IHC, primary and secondary (cat# MAB42941 & HAF005 [R&D Systems]) were used at 1:100 concentration. DAPI mounting media (cat# 00-4959-52 [Thermo Fisher Scientific) and hematoxylin (cat# MHS1-100ML [Sigma-Aldrich]) counterstain was used for fluorescent and standard IHC, respectively.

2.8 Gene and protein expression

2.8.1 RNA and protein extraction

Each step of the RNA and protein extraction was completed on ice at ≈4°C unless stated otherwise. For the experiments in **Chapter 3**, half of the right kidney was diluted in 400µL of PBS then homogenised with a TissueLyser LT™ (Qiagen, Chadstone Centre, Australia), typically 2 minutes at 50 oscillations per second was sufficient. For the experiments in **Chapter 4** & **Chapter 5**, urinary bladder and kidney pairs were homogenised in 800 and 1000µL, respectively, using a TissueLyser II™ (Qiagen) at 30Hz for 3 minutes. In each experiment, 200µL of tissue homogenate 200µL of 2xprotein buffer solution, 1xPhosSTOP™ tablet and 1xcOmplete™ tablet in 5mL of PBS (Sigma-Aldrich, Castle Hill, NSW). Samples were vortexed then centrifuged for 10 minutes at 10,000x*g*. The supernatant was kept at -80°C prior

to ELISA, described in later sections. In **Chapter 4** & **Chapter 5**, 200µL of homogenised sample was removed for quantification of CFU. The remainder of the sample was diluted with 1mL of TRI Reagent® (Sigma-Aldrich) and physical homogenisation was repeated. Samples were incubated at room temperature for 5 minutes then centrifuged for 10 minutes at 12,000x*g*. The supernatant was diluted with 250µL of chloroform (Sigma-Aldrich) in **Chapter 3**, and 500uL in **Chapter 4** & **Chapter 5**. After vortexing, the samples were incubated at room temperature for 10 minutes then centrifuged for 15 minutes at 12,000x*g*. The supernatant was diluted with 500µL of isopropanol (Sigma-Aldrich) in **Chapter 3**, and 1000µL in **Chapter 4** & **Chapter 5**. After vortexing, the samples were incubated at room temperature for 10 minutes then centrifuged for 10 minutes at 12,000x*g*. Without disrupting the pellet, the supernatant was discarded. The pellet was carefully washed with 1ml of 75% ethyl alcohol (Sigma-Aldrich), centrifuged for 5 minutes at 10,000x*g*. The washing step was repeated twice before air-drying the pellet at room temperature. The pellet was re-suspended in 100µL of UltraPure™ H_2O (Thermo-Fisher Scientific, North Ryde, NSW) in **Chapter 3**, and 10 or 100µL in **Chapter 4** & **Chapter 5** for bladders and kidneys, respectively. Samples were kept at -80°C prior to reverse transcription.

2.8.2 Reverse transcription

A Nanodrop2000™ (Thermo-Fisher Scientific) was used for spectrophotometry to assess RNA yield. UltraPure™ H_2O was used to dilute 5µL of sample to a concentration of 125ng°µL^{-1}. 8µL of diluted RNA, approximately 1000ng total, was DNAse treated by incubation with DNAse I Mix, containing 1µL DNAse I amplification and 1µL of 10x DNAse Reaction Buffer (Sigma-Aldrich) for 15min at room temp. Chemical inactivation was performed by adding 1µL of DNAse I STOP Solution (Sigma-Aldrich). Using a T100™ thermal cycler (BioRad

Laboratories, Gladesville, Australia), the samples were incubated at 70°C for 10 minutes then 65°C for 5 minutes to for heat-based inactivation of DNAse I Mix and to denature the RNA. 2µL of Primer dNTP Mix was added (1µL Random Primers [50ng°µL^{-1} Hexamers; ThermoFisher], 1µL dNTP's [10mM per base; BioLine]) and were incubated at 37°C for 2 minutes. 7µL of MMLV Master Mix was added (4µL 5x First Strand Reaction Buffer, 2µL DTT [100mM], 1µL H_2O; [ThermoFisher]) and was incubated at 25°C for 10 minutes. 1µL of MMLV reverse transcriptase was added (200U; ThermoFisher) and the samples were incubated at 37°C 50 minutes then 70°C 15 minutes for the generation of cDNA (**Table 3**). Samples were kept at 4°C before dilution with 79µL of H_2O and storage at -80°C until required for assessment of gene expression.

Table 3: Thermal cycling conditions for generation of cDNA

Condition	Description
70°C 10 minutes (mins) 65°C 5mins	Heat-based inactivation of DNAse I Mix, denaturation of RNA (maximise annealing efficiency of primers, prevent non-specific hydrolysis or degradation and unravel secondary structures)
37°C 2mins	Annealing of primers
25°C 10mins	Annealing of primers
37°C 50mins	Reverse Transcription (optimum temperature for MMLV enzyme)
70°C 15mins	Inactivation of enzyme
4°C	cDNA ready for dilution with H_2O

2.8.3 Real-time quantitative polymerase chain reaction (qPCR)

A CFX96™ and CFX384 Touch™ (Bio-Rad Laboratories) was used for SYBR based qPCR. 2µL of cDNA was added to 10.5µL of the qPCR Master Mix (6.25µL iTaq™ Universal SYBR® Green Supermix, 3.25µL of Ultrapure H_2O, 0.5µL of forward & 0.5µL of reverse primers specific for the target gene) and was repeated for each target gene of interest. Gene expression was normalised relative to the to the expression of *Actb* in that sample on the same physical plate. Whilst *Actb* and *Hprt* genes are commonly used for normalisation, *Actb* was superior in my hands since it was more consistent and was detected at higher abundance in bladder samples (**Figure 18**). Cycle conditions were set as per standard operating procedures for qPCR (**Table 4**).

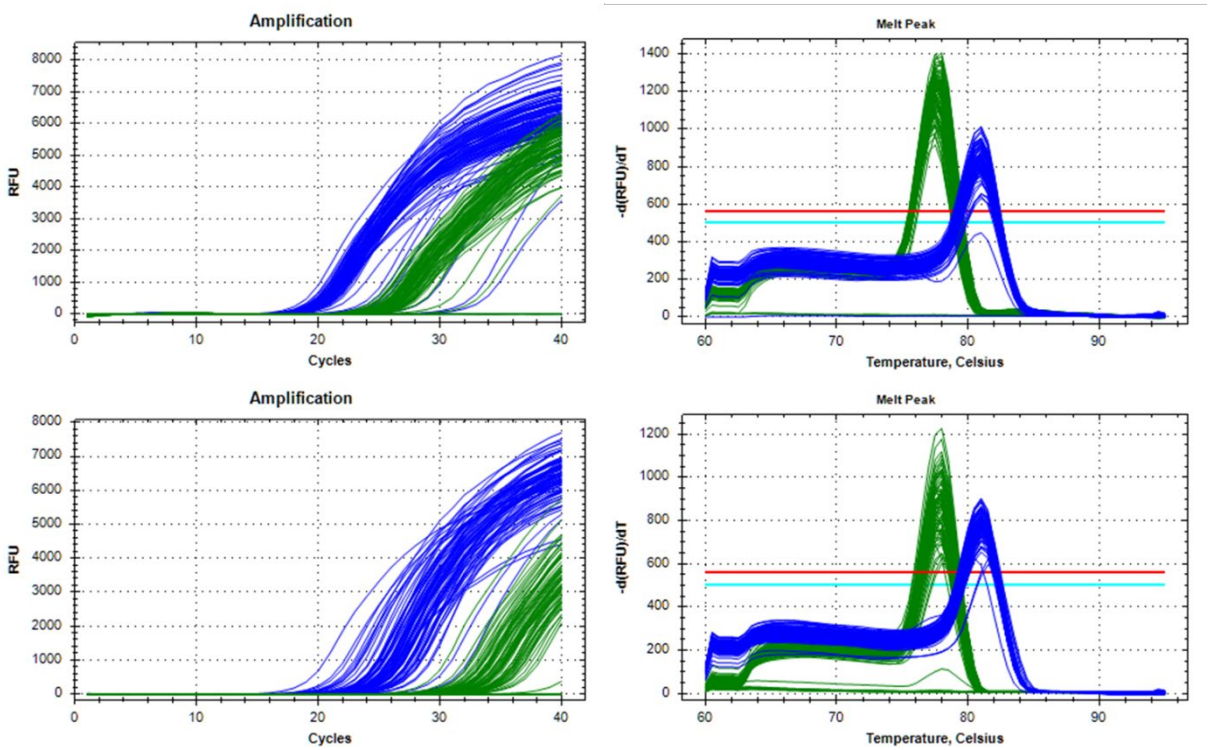

Figure 18: *Actb* outperformed *Hprt* in the bladder but were consistent in the kidney

Actb (Blue) and *Hprt* (green) in the kidney (top) and Bladder (bottom). *Actb* was quantified using regression at an earlier cycle (left) and was more consistent. Both *Actb* and *Hprt* showed a single product being formed in the melt peaks (right).

Table 4: Cycle conditions for qPCR

Step	Temp (°C)	Time	Special conditions
1	50	2 min	
2	95	2 min	
3	95	15 sec	
4	60	1 min	Repeat step 3 & 4, 40 times
5	60-95	30 sec	Dissociation (Melting) curve

2.8.4 RT^2 profiler array

RT^2 Profiler™ PCR Array Mouse Extracellular Matrix & Adhesion Molecules and an Inflammatory Response & Autoimmunity (Qiagen) was performed as per manufacturer's instructions and data was uploaded then analysed by the online tool, available from: https://dataanalysis.qiagen.com/pcr/arrayanalysis.php. This array allows profiling of 84 genes in a maximum 4 samples, therefore, equal amounts of cDNA for each replicate in a group were pooled from mice on following IRI or UTI, compared to sham procedures. For each target, the fold change in cDNA pooled from experimental intervention biological replicates was compared to the sham expression.

2.9 Biochemical analysis

2.9.1 Blood collection

Immediately after confirmed euthanasia, whole blood was collected by cardiac puncture. Samples were left to clot at room temperature for 20 minutes. Samples were centrifuged at 3,000x*g* for 10 minutes at 4°C and the supernatant, serum, was removed and stored at -80°C.

2.9.2 Enzyme-linked immunosorbent assay (ELISA)

ELISA was performed using commercially available kits, the method varied slightly between each assay, but was performed as per the protocol which can be looked up using the provided catalogue numbers. Protein samples from homogenised organs were assessed for IL-33 (cat# 436407; BioLegend) protein levels, the limit of detection for this assay was 4pg mL^{-1} IL-22 protein levels were measured using quantitative ELISA (cat# 436304 [BioLegend, San Diego, United States]), the limit of detection for this assay was 2pg mL^{-1}. IL-5 (cat# 431204; BioLegend) protein levels were measured in serum. The limit of detection for this assay was 15pg mL^{-1}. STAT3 pY705 was detected in protein samples and represented as a proportion of total STAT3 in using semi-quantitative ELISA kit (cat# AB126458 [Abcam, Melbourne, Australia]).

2.9.3 Chemistry analyser

BUN (cat# 98-11070-01 [IDEXX Laboratories, Rydalmere, Australia]) was measured in serum supernatants using a Catalyst One veterinary chemistry analyser. This involved insertion of a single use BUN slide and loading the serum sample into the analyser compartment.

2.10 Assessment of colony forming units (CFU)

200µL of homogenised urinary bladder samples in PBS was set aside for CFU determination. A serial dilution from undiluted to 10^7-fold diluted was performed. 10uL of each dilution was spotted onto LB agar, with 5 technical replicates and colonies were counted for CFU after 16 hours of incubation (**Figure 13**). CFU mL^{-1} was calculated using the following formula:

$$\text{CFU} = \frac{\text{Raw count}}{\text{Number of replicates}} \times 10^{\text{Dilution factor}} \times \frac{\text{Total volume of sample}}{\text{Volume spotted}}$$

2.11 Flow cytometry

2.11.1 Equipment & antibodies

Data was collected using a BD LSR Fortessa X20 flow cytometer™ (BD biosciences) and was analysed using FlowJo v10.5.3 (Tree Star, Ashland, USA). software. Typical voltages for each channel are contained in **Table 5**. All details of the antibodies are listed in **Table 6**.

Table 5: Typical voltages and parameter setup for flow cytometry

Parameter	Voltage	Log	A	H	W
FSC	150		x	x	x
SSC	240		x	x	x
BB515	523	x	x		
PerCP-Cy5-5	595	x	x		
BV421	400	x	x		
BV510	470	x	x		
BV650	634	x	x		

BV711	568	x	x		
APC	528	x	x		
APC-Alexa 700	517	x	x		
APC-Cy7	546	x	x		
PE-CF594	593	x	x		
PE-Cy7	551	x	x		

Table 6: All antibodies used for flow cytometry

Antigen	Product code	Clone	Fluorophore	Dilution factor	Source
CD11b	557960	M1/70	AF700	100	BD Biosciences
CD3	561388	17A2	AF700	100	BD Biosciences
CD45R (B220)	557957	RA3-6B2	AF700	100	BD Biosciences
LY-6G/C (GR-1)	557979	RB6-8C5	AF700	100	BD Biosciences
NK-1.1	560515	PK136	AF700	100	BD Biosciences
TER-119	560508	TER-119	AF700	100	BD Biosciences
CD3	100236	17A2	APC	100	Biolegend
IL-33R (ST2)	17-9335-82	RMST2-2	APC	50	eBioscience
CD90.2	561641	53-2.1	APC-Cy7	200	BD Biosciences
Viability	565388	-	APC-Cy7	1000	BD Biosciences
CD45	564279	30-F11	BUV395	400	BD Biosciences
CD278 (ICOS)	565886	C398.4A	BV421	100	BD Biosciences
CD4	100516	RM4-5	BV421	200	Biolegend
CD4	563106	RM4-5	BV510	300	BD Biosciences
CD8a	563068	53-6.7	BV510	300	BD Biosciences
TCR-αβ	563221	H57-597	BV510	300	BD Biosciences

TCR-γδ	563218	GL3	BV510	300	BD Biosciences
CD90.2	140318	53-2.1	BV605	400	Biolegend
CD11b	101259	M1/70	BV650	200	Biolegend
KLRG1	740553	2F1	BV650	100	BD Biosciences
CD4	100557	RM4-5	BV711	200	Biolegend
CD8a	100750	53-6.7	BV785	200	Biolegend
CD11b	101206	M1/70	FITC	200	Biolegend
NK1.1	108706	PK136	FITC	200	Biolegend
CD49b	108918	DX5	Pacific Blue	300	Biolegend
CD127 (IL-7Rα)	562419	SB/199	PE-CF594	100	BD Biosciences
CD19	115520	6D5	PE-Cy7	200	Biolegend
CD25	552880	PC61	PE-Cy7	50	BD Biosciences
CD45	550994	30-F11	PerCP-Cy5.5	200	BD Biosciences
IL-13	-	-	Td-tomato (PE)	-	Reporter mice
IL-5	-	-	Venus (BB515)	-	Reporter mice

2.11.2 Isolation and staining of cells

Whole tissues were added to a gentleMACS C tube (Miltenyi Biotec, Macquarie Park, NSW) with 5mL of digestion buffer containing: 10µL DNAse I at 200U mL^{-1}, 100µL collagenase IV at 1mg mL^{-1} and 4.9mL of Hanks salt solution (Sigma-Aldrich). A gentleMACS™ dissociator (Miltenyi Biotec) was used to create the single cell suspensions. Single-cell suspensions were prepared as described in "Preparation of single-cell suspensions from mouse lung with Collagenase D treatment" (Miltenyi Biotec GmbH, 2008; Bergisch Gladbach, Germany). Cells were blocked with Fc block (purified anti-mouse CD16/32; Biolegend, San Diego, USA) for

30 minutes and stained with fluorescently-conjugated antibodies against target cell surface antigens (**Table 6**). Staining and washing steps were performed with BSA stain buffer (BD Biosciences, North Ryde, Australia).

2.11.3 t-distributed stochastic neighbor embedding (t SNE)

t-SNE was performed on gated populations of single cell events from flow cytometry. Using the random down sampling plugin, the number of events in each sample was normalized to equal the lowest, rounded down to the nearest 10 events. All populations were combined into one .fcs file by concatenating the down sampled populations. The t-SNE analysis was performed on the concatenated sample containing the gated populations combined from each biological replicate belonging to the same group for a single tissue type. For this, the compensated channels that were not used for gating were assessed under the following t-SNE settings: Iteration 1000, Perplexity 20, Eta 224. Histograms were used to show the differential expression of cell surface antigens and cytokines in the tissues.

2.12 Statistical analysis

In **Chapter 3**, data were analysed with GraphPad Prism software v8.02 using non-parametric unpaired t-tests (Mann-Whitney U-test). $P<0.05$ was set as threshold for determining statistically significant differences. * $P<0.05$, ^{ns} not significant. All data are expressed as mean ± standard error of the mean (SEM). In each analysis there were n=4-8 replicates per group and results were representative of at least two experiments. Sample size for each experiment is described in the corresponding figure legend.

In **Chapter 4** & **Chapter 5**, data were analysed with GraphPad Prism software v9.1.0. Statistical tests, sample size and number of experiments are described in each of the corresponding figure legends. Raw P-values were shown for enhanced interpretation of these data, since the models of urinary tract infection induced a highly variable response, unlike the IRI surgical models used in **Chapter 3** which were highly consistent.

Chapter 3: Evidence of group 2 innate lymphoid cell redundancy during ischemia-reperfusion injury in mice

Some results in this chapter have been previously published as:

> **Cameron GJM**, Cautivo KM, Loering S, Jiang SH, Deshpande AV, Foster PS, McKenzie ANJ, Molofsky AB, Hansbro PM, Starkey MR. Group 2 Innate Lymphoid Cells Are Redundant in Experimental Renal Ischemia-Reperfusion Injury. Front Immunol. 2019;10:826.

Cameron GJM and Starkey MR conceptualised the manuscript. Cautivo KM and Molofsky AB performed the flow cytometry and immunofluorescence using Il5$^{td\text{-}tomatoCre}$Rosa26-CAG-RFP mice. Cameron GJM performed all other aspects including the surgical model, flow cytometry, histological assessment, gene expression analysis, data analysis and drafted the manuscript. Loering S assisted with animal monitoring and flow cytometry. Jiang SH and Deshpande AV provided clinical insight for study design and surgical technique. McKenzie ANJ created, supplied and advised on the use of ILC2-deficient & -depleted and Il13td tomato mice. Foster PS supplied and advised on the use of Il5venus reporter line. Foster PS and Hansbro PM advised on experimental design.

3.1 Abstract

Acute kidney injury (AKI) can be fatal and is a well-defined risk factor for the development of chronic kidney disease. Group 2 innate lymphoid cells (ILC2) are innate producers of type-2 cytokines and are critical regulators of homeostasis in peripheral organs. However, the knowledge of their function in the kidney is relatively limited. Recent evidence suggests that increasing ILC2 numbers by systemic administration of recombinant interleukin (IL)-25 or IL-33 protects against renal injury. Whilst ILC2 can be induced to protect against ischemic- or chemical-induced AKI, the impact of ILC2 deficiency or depletion on the severity of renal injury is unknown. Firstly, the phenotype and location of ILC2 in the kidney was assessed under homeostatic conditions. Kidney ILC2 constitutively expressed high levels of IL-5 and were located in close proximity to the renal vasculature. To test the functional role of ILC2 in the kidney, an experimental model of renal ischemia-reperfusion injury (IRI) was used and the severity of injury was assessed in wild-type, ILC2-reduced, ILC2-deficient and ILC2-depleted mice. Surprisingly, there were no differences in histopathology, collagen deposition or mRNA expression of injury-associated (*Lcn2*), inflammatory (*Cxcl1*, *Cxcl2* and *Tnf*) or extracellular matrix (*Col1a1*, *Fn1*) factors following IRI in the absence of ILC2. These data suggest the absence of ILC2 does not alter the severity of renal injury, suggesting possible redundancy. Therefore, other mechanisms of type II-mediated immune cell activation likely compensate in the absence of ILC2. Hence, a loss of ILC2 is unlikely to increase susceptibility to, or severity of AKI.

3.2 Introduction

Acute kidney injury (AKI) and its associated pathologies have profound effects on human health [10]. A common cause of AKI is renal ischemia, which primarily affects the tubular epithelium due to the high mitochondrial density and metabolic activity in these cells [14]; reviewed in [15, 17]. Acute tubular necrosis impairs waste excretion, alters water and electrolyte imbalance, and causes robust inflammatory responses, reviewed in [17]. Influx of neutrophils and monocytes contributes to the injury, however other innate immune cells can facilitate the return to homeostasis [343]; reviewed in [344]. Innate lymphoid cells (ILC) are a recent addition to this family and are categorized into 3 groups based on the transcription factors that are required for their development and by the effector cytokines they produce [129]. Group 2 ILC (ILC2) are potent producers of type 2 cytokines, predominantly interleukin (IL)-5 and IL-13 [119, 120]. These cells also promote tissue recovery following insult in multiple organs and have diverse functions *in vivo* [345]. For example, following respiratory viral infection with influenza virus, ILC2 co-ordinate repair of the airway epithelium by producing the growth factor amphiregulin (AREG) [155]. More recently ILC2 have been investigated in models of renal injury including ischemia-reperfusion injury (IRI), and nephrotoxic chemical-induced injury with doxorubicin or cisplatin [158, 173, 174, 178, 346]. Renal IRI is typically achieved by temporarily restricting blood flow to the kidney for 20-30 minutes, modelling trauma from transplant or surgical intervention [58, 59, 61, 347, 348].

Collectively, these studies show that *in vivo* administration of recombinant mouse cytokines that activate ILC2, namely IL-25 or IL-33, is sufficient to reduce the severity of tubular epithelial cell injury [158, 173, 174, 178, 346]. Similar results have been achieved with adoptive transfer of *ex vivo* activated ILC2 [158, 173]. Whilst ILC2 can be artificially induced to proliferate and protect against the deleterious consequences of experimental renal injury, the

impact of ILC2-deficiency remains incompletely understood. Indeed, other immune cells, which have complex interactions with the ILC2 such as regulatory T cells ($T_{reg)}$ and alternatively activated macrophages (AAM; also known as M2) are critical for this renoprotective effect [16, 179, 349, 350]. In this study, I sought to further characterise ILC2 phenotype in the kidney, their location within this organ and determine their functional role in IRI using a loss-of-function approach. Here, I found that kidney ILC2 constitutively express IL-5 and are primarily located in close proximity to the renal vasculature, within the adventitia. Additionally, I demonstrate that a reduction, deficiency or depletion of ILC2 had minimal impact on the severity of IRI. Whilst activation of ILC2 and the associated amplification of local type II immunity has been previously shown to reduce the deleterious consequences of AKI, my results reveal that comparable injury occurs in the absence of ILC2, suggesting that ILC2 may be redundant in IRI when other compensatory immune cells such as T cells are present.

3.3 Methods

3.3.1 Mice

8-12-week-old male wild-type (WT; C57BL/6JAusb), vehicle (saline-treated *Icos*$^{dtr/+}$*Cd4*$^{cre/+}$), ILC2-reduced (*Rora*$^{fl/+}$*Il7r*$^{cre/+}$), ILC2-deficient (*Rora*$^{fl/fl}$*Il7r*$^{cre/+}$), ILC2-depleted (Diphtheria toxoid-treated [DTx] *Icos*$^{dtr/+}$ *Cd4*$^{cre/+}$) and IL-5/IL-13 dual reporter mice (*Il5*$^{venus/+}$*Il13*$^{td\text{-}tomato/+}$) mice were obtained from Australian Bioresources (Moss Vale, Australia). *Il5*$^{td\text{-}tomatoCre}$; Rosa26-CAG-RFP reporter-tracker mice were obtained from Jackson Labs (ref# 030926 and 007914). All mice that underwent surgery were housed under specific pathogen free, physical containment 2 conditions, in individually ventilated cages. Mice were exposed to normal room

air within a sterilized environment during surgery. Mice were allowed one week to acclimatise before experiments were started and were maintained on a 12-hour day/night cycle with access to standard laboratory chow and water *ad libitum*.

3.3.2 Flow cytometry and t-distributed stochastic neighbor embedding (t-SNE) analysis

Kidneys and lungs were collected from reporter mice. Single-cell suspensions were prepared as described in "Preparation of single-cell suspensions from mouse lung with Collagenase D treatment" (Miltenyi Biotec GmbH, 2008; Bergisch Gladbach, Germany). Cells were blocked with Fc block (purified anti-mouse CD16/32; Biolegend, San Diego, USA) for 30 minutes and stained with fluorescently-conjugated antibodies against target cell surface antigens (**Table 7**, **Table 8**). Staining and washing steps were performed with BSA stain buffer (BD Biosciences, North Ryde, Australia). Samples were acquired on a BD LSR Fortessa X20 flow cytometer. Flow cytometry data were analysed using FlowJo v10.5.3 (Tree Star, Ashland, USA). The t-SNE was performed on ILC2 ($CD45^+Lineage^-[TCR^-[TCR\alpha\beta^-TCR\gamma\delta^-CD8^-CD4^-]CD11b^-GR\text{-}1^-B220^-TER\text{-}119^-CD3^-NK\text{-}1.1^-]IL7R\alpha^+$ $CD90.2^+ST2^+FSC^{low}SSC^{low}$ single cells). Using the random down sampling plugin, the number of events in each sample was normalized to equal the lowest, rounded down to the nearest 10 events. All populations were combined into one .fcs file by concatenating the down sampled populations. The t-SNE analysis was performed on the concatenated sample containing the gated populations from all kidney and lung samples combined. For this, the compensated channels that were not used for gating were assessed under the following t-SNE settings: Iteration 1000, Perplexity 20, Eta 224. Histograms were used to show the differential expression of cell surface antigens and cytokines in the lung and kidney.

Table 7: Flow cytometry antibodies and channels used to detect GM mouse reporter constructs for assessing group 2 innate lymphoid cells

Antigen	Product code	Clone	Fluorophore	Dilution factor	Source
CD278 (ICOS)	565886	C398.4A	BV421	100	BD Biosciences
TCR-αβ	563221	H57-597	BV510	300	BD Biosciences
TCR-γδ	563218	GL3	BV510	300	BD Biosciences
CD4	563106	RM4-5	BV510	300	BD Biosciences
CD8a	563068	53-6.7	BV510	300	BD Biosciences
KLRG1	740553	2F1	BV650	100	BD Biosciences
CD45	550994	30-F11	PerCP-Cy5.5	200	BD Biosciences
CD127 (IL-7Rα)	562419	SB/199	PE-CF594	100	BD Biosciences
CD25	552880	PC61	PE-Cy7	50	BD Biosciences
IL-33R (ST2)	17-9335-82	RMST2-2	APC	50	eBioscience
CD11b	557960	M1/70	AF700	100	BD Biosciences
LY-6G/C (GR-1)	557979	RB6-8C5	AF700	100	BD Biosciences
CD45R (B220)	557957	RA3-6B2	AF700	100	BD Biosciences
TER-119	560508	TER-119	AF700	100	BD Biosciences
CD3	561388	17A2	AF700	100	BD Biosciences
NK-1.1	560515	PK136	AF700	100	BD Biosciences
CD90.2	561641	53-2.1	APC-Cy7	200	BD Biosciences
IL-5	-	-	Venus (BB515)	-	Reporter mice
IL-13	-	-	Td-tomato (PE)	-	Reporter mice

Table 8: Flow cytometry antibodies for assessing group 2 innate lymphoid cells in conjunction with T helper type 2 cells

Antigen	Product code	Clone	Fluorophore	Dilution factor	Source
CD45	564279	30-F11	BUV395	400	BD Biosciences
CD90.2	140318	53-2.1	BV605	400	Biolegend
CD3	100236	17A2	APC	100	Biolegend
CD4	100557	RM4-5	BV711	200	Biolegend
CD8a	100750	53-6.7	BV785	200	Biolegend
CD49b	108918	DX5	Pacific Blue	300	Biolegend
CD19	115520	6D5	PE-Cy7	200	Biolegend
CD11b	101259	M1/70	BV650	200	Biolegend
IL-5	-	-	Td-tomato (PE)	-	Reporter mice

3.3.3 Immunofluorescence

Il5$^{\text{td-tomatoCre}}$; Rosa26-CAG-RFP reporter-tracker mice were euthanised and perfused intracardially with 1x phosphate buffered saline (PBS) and then 4% paraformaldehyde (PFA) in PBS. Kidneys were removed and kept in fresh 4% PFA for 24 hours at 4°C and then washed in 1xPBS. 300µm sections were prepared using a vibratome. Subsequently, tissue sections were incubated in permeabilization buffer (1x PBS/0.2% Triton X-100/0.3M glycine) then blocked in PBS/0.2% Triton X-100/5% donkey serum at 4°C overnight. Samples were washed in PBS/0.2% Tween-20 once, then incubated with primary antibodies diluted in PBS/0.2% Tween-20/3% donkey serum at room temperature until the next day. Next, samples were washed in PBS/0.2% Tween-20 for 30 minutes, 3-4 times, then incubated with secondary

antibodies diluted in PBS/0.2% Tween-20/3% donkey serum at room temperature for 6-8 hours. Samples were washed in PBS/0.2% Tween-20 for 1 day and then dehydrated in an ascending ethanol series (20%, 30%, 50%, 70%, 95%, 100%), 10 minutes each step. Finally, kidney sections were cleared by soaking in methyl salicylate (M-2047; Sigma-Aldrich, Castle Hill, Australia) and then mounted in fresh methyl salicylate onto a concave coverslip or chamber. Images were captured with Nikon A1R laser scanning confocal including 405, 488, 561, and 650 laser lines for excitation and imaging with 16X/0.8 or 25X1.1, NA Plan Apo long working distance water immersion objectives. Z steps were acquired every 6µm. Images were processed with ImageJ (NIH, Bethesda, MD, US) and Bitplane Imaris software v8 (Andor Technology PLC, Belfast, N. Ireland). Surface reconstructions of alpha smooth muscle-labelled blood vessels were performed with Imaris. Surface module and pseudocolored based on their characteristic architecture and volume to visualize large arteries and veins. The following antibodies and dilutions were used: Living Colors anti-DsRed Rabbit Polyclonal Pan Antibody (1:500; TaKaRa, Mountain View, USA), goat polyclonal anti-alpha smooth muscle actin antibody (1:200; Abcam, Cambridge, UK), eFluor 660 LYVE1 monoclonal Antibody (1:300, clone ALY7, eBioscience), armenian hamster anti-mouse CD3 antibody (1:100, clone 145-2C11, Biolegend), Alexa Fluor® 488 donkey anti-goat IgG (H+L), Alexa Fluor® 555 donkey anti-rabbit IgG (H+L) Alexa Fluor® 647 goat anti-hamster IgG (H+L) cross-adsorbed (1:400, ThermoFisher Scientific).

3.3.4 Unilateral ischemia-reperfusion injury

Surgical anaesthesia was induced by 4% isoflurane inhalation and maintained with continuous 1-1.5% isoflurane inhalation through a nose cone. Throughout the procedure, mice were kept on a surgical platform maintained at 37°C by a digital thermostat-controlled heat mat.

Nephrectomy of the right kidney was performed in all animals. To induce unilateral ischemia the vessels of the left kidney were clamped near the renal pedicle for 29-minutes using a non-traumatic sterile vascular clamp (Coherent Scientific; Hilton, Australia) applying sufficient force to prevent blood flow to and from the kidney without irreversible damage to the vessels. Uniform and rapid reperfusion of the kidney was observed after removing the vascular clamp in all mice. The muscle and skin wounds were closed using a 5/0 vicryl suture (Johnson & Johnson Medical, North Ryde, NSW), the skin was then sealed using dermal adhesive (Provet, Charlestown, Australia) to protect the wound and prevent infection. Control animals were subjected to a sham operation with identical anaesthesia time and received only a contralateral nephrectomy. For effective analgesia mice received 0.1mg kg^{-1} of buprenorphine subcutaneously 30 minutes prior to the operation and then 0.05-0.1mg kg^{-1} every 8-12 hours, as required. Animals were typically weaned off analgesia by 4 days post-surgery without any signs of pain or distress as defined by facial characteristics using the standard mouse grimace scale; as described [351]. All mice survived to the pre-determined endpoint.

3.3.5 Depletion of ILC2 *in vivo*

ILC2 were depleted in *Icos*$^{dtr/+}$*Cd4*$^{cre/+}$ mice by intraperitoneal injection of 0.025 mg kg^{-1} of DTx (Sigma-Aldrich) as previously described [159]. DTx was administered 30 minutes prior to surgery and daily thereafter until the endpoint. To confirm ILC2-depletion, a subset of naïve animals received DTx for 3 days. Control *Icos*$^{dtr/+}$*Cd4*$^{cre/+}$ mice received intraperitoneal saline injection.

3.3.6 Histology

Excised kidneys were immediately sectioned in half longitudinally through the hilum. Half was fixed in 10% buffered formalin, containing 4% formaldehyde for 24 hours before temporary storage in 10% ethanol, paraffin embedding and sectioning. 4μm, longitudinally cut sections were stained with periodic acid-Schiff (PAS) and Masson's trichrome. Histopathology was quantified by visualizing dilation of tubules, apoptosis or cast formation by a single blinded investigator using a well-established semi-quantitative method [342], with minor alterations as described [158]. An average was taken of the score from duplicate PAS stained sections from each animal. A score of 0 = 0% of tubules were affected by the above histopathological features; 1 = 1-10%; 2 = 11-25%; 3 = 26-50%; 4 = 51-75%; 5 = 76-100%. Collagen deposition was assessed using Masson's trichrome and collagen was identified as methyl blue content between adjacent tubules.

3.3.7 RNA extraction, reverse transcription and qPCR

Half of one kidney was retained for gene expression analysis. The tissue was homogenised in 400μL of PBS using a TissueLyser LT™ (Qiagen, Chadstone Centre, Australia) through 50 oscillations per second for 2 minutes. 200μl of the sample was removed for other analyses. 1mL of TRI Reagent® (Sigma-Aldrich) was added to the remaining 200μl of the sample, which received a further 50 oscillations per second for 1-2 minutes until completely homogenised. Following 5 minutes of incubation at room temperature and centrifugation at 12,000x*g* for 10 minutes, the supernatant was extracted and vortexed with 250μL of chloroform (Sigma-Aldrich). After incubating for 10 minutes at room temperature and centrifugation at 12,000x*g* for 15 minutes, the supernatant was extracted and vortexed with 500μL of 70% isopropanol (Sigma-Aldrich). The sample was incubated again for 10 minutes at room temperature then

was centrifuged at 12,000x*g* for 10 minutes. The supernatant was discarded without disrupting the RNA-rich pellet. The pellet was washed twice with 1mL of 75% RNA-grade ethanol (Sigma-Aldrich), centrifuged at 10,000x*g* for 5 minutes and the supernatant was discarded each time. The pellet was air-dried at room-temperature briefly before re-suspending in 80-100µL of UltraPure™ DNase/RNase-free double distilled water (ddH_2O; Thermo-Fisher Scientific) and was then stored at -80°C prior to reverse transcription. Immediately prior to reverse transcription, RNA yield was determined by spectrophotometric assessment using a Nanodrop2000™ (Thermo-Fisher Scientific). 5µL of each sample was diluted in ddH_2O such that 1000ng of RNA was loaded per sample. Following DNAse (Sigma-Aldrich) treatment, cDNA was generated using the M-MLV (Thermo-Fisher Scientific, North Ryde. Australia) enzyme standard operating procedures using a T100™ thermal cycler (BioRad Laboratories, Gladesville, Australia). Using SYBR based methodology, qPCR was performed using CFX384 Touch™ (BioRad Laboratories) as per standard operating procedures. Each primer set was gradient tested to determine the optimal temperature for amplification (**Table 9**). Cycle quantification was interpreted using regression for each target, gene expression was normalized relative to hypoxanthine guanine phosphoribosyl transferase (*Hprt*). Melt curves were assessed for signs of primer dimerization and non-specific amplification. On every plate, at least one negative control and no-template control was used for each target to ensure contamination was not present within each master mix or the ddH_2O used.

Table 9: qPCR primer sequences

Target	Forward primer (5`-3`)	Reverse primer (5`-3`)
Areg	TTGCTGCTGGTCTTAGGCTC	TGGTCCCCAGAAAGCGATTC
Arg1	GGCAGAGGTCCAGAAGAATG	GTGAGCATCCACCCAAATG
Ccl20	AGACGCCTCTTCCTTCGAGAGC	TGCTTTGGATCAGCGCACACA
Ccl5	TGGCTCGGACACTCCCTG	GGGTTGGCACACACTTGGCGG
Col1a1	CTTCACCTACAGCACCCTTGTG	TGACTGTCTTGCCCCAAGTTC
Cxcl1	GCTGGGATTCACCTCAAGAA	CTTGGGGACACCTTTTAGCA
Cxcl10	CCAAGTGCTGCCGTCATTTTC	TCCCTATGGCCCTCATTCTCA
Cxcl2	TGCTGCTGGCCACCAACCAC	AGTGTGACGCCCCCAGGACC
Fn1	GCACTGCTGCTGATTCAAGTTC	AGTTGCTCCTGGCTGGTATG
Hprt	AGGCCAGACTTTGTTGGATTTGAA	CAACTTGCGCTCATCTTAGGCTTT
Lcn2	TACAATGTCACCTCCATCCTGG	CCACTTGCACATTGTAGCTCT
Mrc1	CATGGATGTTGATGGCTACTGG	CCATAGAAAGGAATCCACGCAGT
Nos2	AGCGAGGAGCAGGTGGAAGACT	CCATAGGAAAAGACTGCACCGAA
Tnf	TCTGTCTACTGAACTTCGGGGTGA	TTGTCTTTGAGATCCATGCCGTT

3.3.8 RT^2 profiler array

RT² Profiler™ PCR Array Mouse Extracellular Matrix & Adhesion Molecules (Qiagen) was performed as per manufacturer's instructions and data was uploaded then analysed by the online tool, available from: https://dataanalysis.qiagen.com/pcr/arrayanalysis.php. This array allows profiling of 84 genes in a maximum 4 samples, therefore, equal amounts of cDNA for each replicate in a group were pooled from WT mice on day 1, 3 or 7 following IRI, and sham

pooled from each replicate from each of these timepoints. For each target, the fold change following IRI was compared to sham expression.

3.3.9 Statistical analysis

All data were analysed with GraphPad Prism software v8.02 using non-parametric unpaired t-tests (Mann-Whitney U-test). $P<0.05$ was set as threshold for determining statistically significant differences. * $P<0.05$, ^{ns} not significant. All data are expressed as mean ±SEM. In each analysis there were n=4-8 replicates per group and results were representative of at least two experiments. Sample size for each experiment is described in the corresponding figure legend.

3.4 Results

A detailed analysis of renal ILC2 phenotype and location under homeostatic conditions was performed (**Figure 19A-F**). There were significantly more ILC2 ($CD45^+Lineage^-IL\text{-}7R\alpha^+CD90.2^+ST2^+FSC^{low}SSC^{low}$ single cells), in the kidney compared to the lung when represented as a percentage of total $CD45^+$ single cells (**Figure 20A**). t-SNE analysis of kidney and lung ILC2 showed unique clustering, although these clusters were not entirely distinct from one another (**Figure 20B**). However, kidney ILC2 had markedly lower expression of CD25, consistent expression of ICOS and KLRG1, but higher expression of IL-5 compared to lung ILC2 (**Figure 20C**). Kidney ILC2 had higher constitutive expression of IL-5 than IL-13 (**Figure 20D**). ILC2 were determined to be the major IL-5 producing cell type in the kidney, with a negligible contribution from T helper type-2 (T_H2) cells (**Figure 20E**). Therefore, IL-5 was used as a surrogate marker to identify the location of ILC2 within the mouse kidney, as

has been described for multiple peripheral organs [135, 138, 338]. This was achieved by utilizing mice that express an IL-5 linked cre-recombinase crossed to a Rosa-tdtomato lineage tracker (**Figure 21A,B**) [135, 138].

IL-5 positive cells, predominantly ILC2, were found throughout the kidney, but were primarily localized to the major vasculature, as visualised with alpha smooth muscle actin (α-SMA) positive staining (**Figure 22A**), consistent with a recent report [338]. ILC2 were found to be associated with both interlobular and arcuate renal vessels in the cortex and medullary regions, as shown by lymphatic endothelial hyaluronan receptor-1 (LYVE1) expression (**Figure 22B**). Further imaging demonstrated that very few of the $CD3^+$ cells, predominantly T_H2 cells, contributed to the endogenous $IL\text{-}5^+$ signal (**Figure 22C**). ILC2 were identified in the adventitia of the vessel using pseudocolored surface reconstructions of the arterial α-SMA.

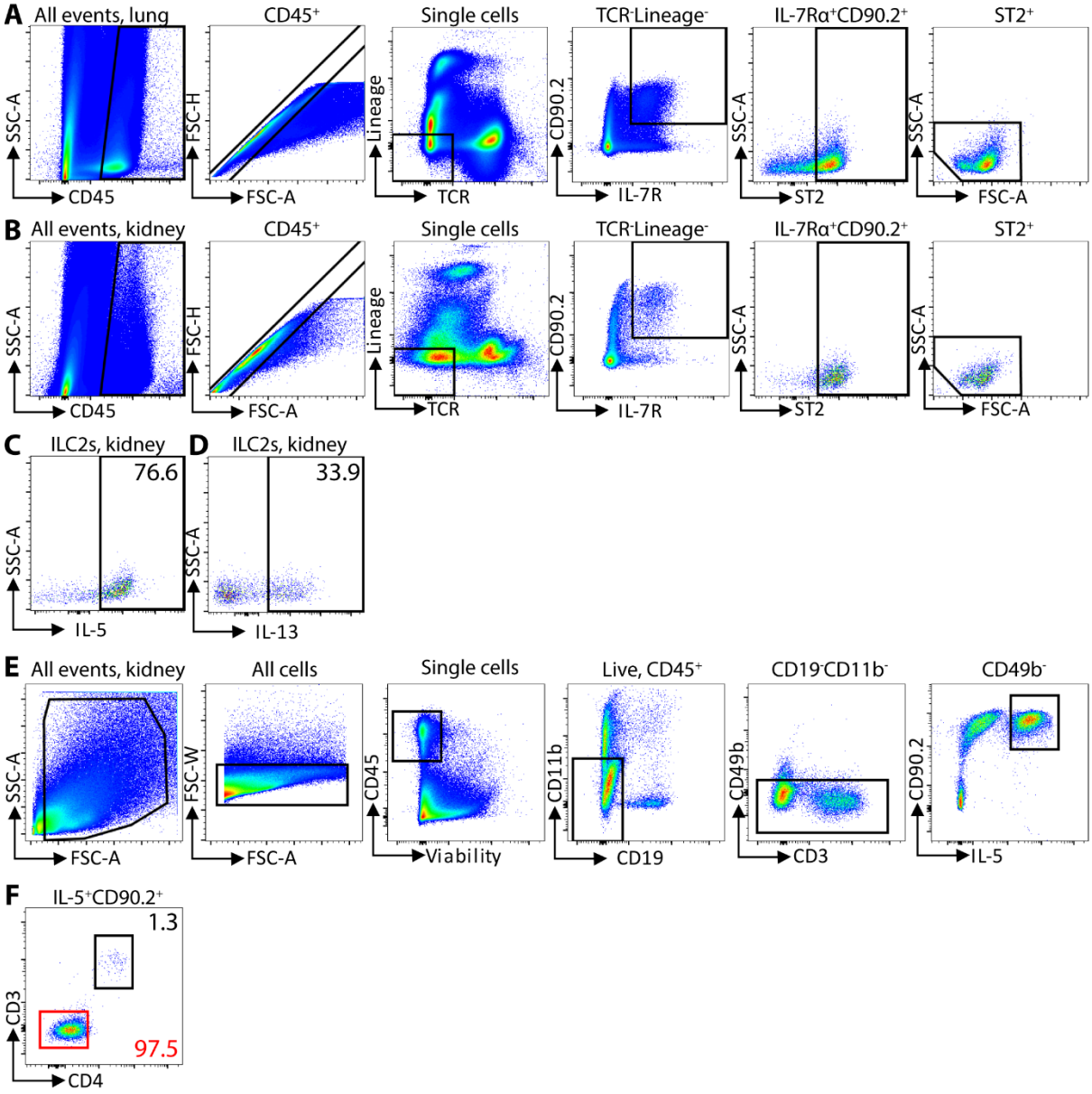

Figure 19: Flow cytometry gating strategy for ILC2 and T_H2s

(A) Lung and **(B)** kidney single cell suspensions from *Il5*$^{venus/+}$*Il13*$^{td\text{-}tomato/+}$ mice, n=8, were gated for ILC2 (CD45$^+$Lineage$^-$[TCR$^-$[TCRαβ$^-$TCRγδ$^-$CD8$^-$CD4$^-$]CD11b$^-$GR-1$^-$B220$^-$TER-119$^-$CD3$^-$NK-1.1$^-$]IL-7Rα$^+$CD90.2$^+$ST2$^+$FSC^{low}SSC^{low} single cells). **(C)** Representative FACS plots of IL-5 and **(D)** IL-13 expression in kidney ILC2. **(E)** Gating strategy demonstrating the proportion of CD45$^+$CD19$^-$CD11b$^-$CD49b$^-$CD90.2$^+$IL-5$^+$ single cells which were consistent with **(F)** ILC2 (CD3$^-$CD4$^-$) and T_H2s (CD3$^+$CD4$^+$) in kidney single cell suspensions from *Il5*$^{td\text{-}tomatoCre}$; Rosa-CAG-RFP mice, n=8.

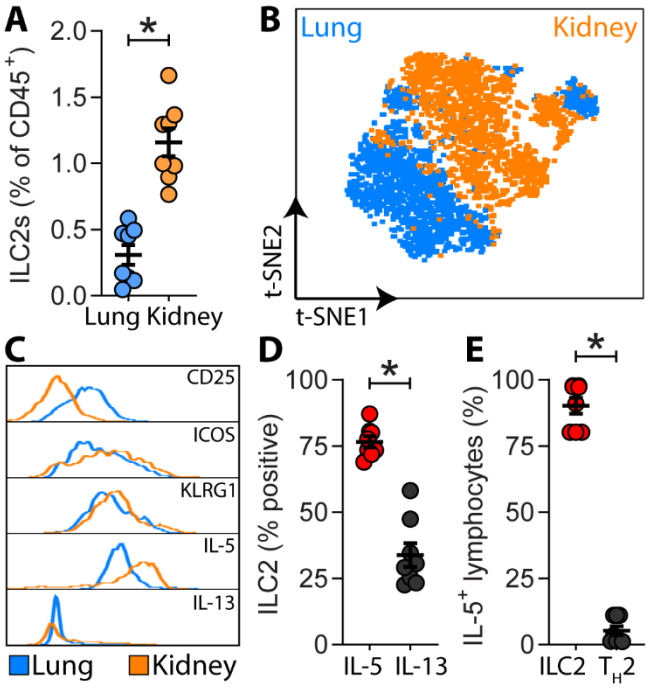

Figure 20: ILC2 are present in the kidney and have a unique signature compared to lung ILC2

(A) ILC2($CD45^+Lineage^-[TCR^-[TCR\alpha\beta^-TCR\gamma\delta^-CD8^-CD4^-]CD11b^-GR\text{-}1^-B220^-TER\text{-}119^-CD3^-NK\text{-}1.1^-]IL\text{-}7R\alpha^+CD90.2^+ ST2^+FSC^{low}SSC^{low}$ single cells) in kidney and lung single cell suspensions from naïve $Il5^{venus/+}Il13^{td\text{-}tomato/+}$ mice, n=8. **(B)** Comparison of lung and kidney ILC2 by t-distributed stochastic neighbor embedding (t-SNE) analysis based on the cell surface antigens CD25, ICOS, KLRG1 and the type 2 effector cytokines IL-5 and IL-13. **(C)** Differential expression of ILC2-associated cell surface antigens and type II effector cytokines. **(D)** Percentage of $IL\text{-}5^+$ and $IL\text{-}13^+$ renal ILC2. **(E)** Proportions of $CD45^+CD19^-CD11b^-CD49b^-CD90.2^+IL\text{-}5^+$ single cells which were consistent with ILC2 ($CD3^-CD4^-$) and T_H2s ($CD3^+CD4^+$) in kidney single cell suspensions from $Il5^{td\text{-}tomatoCre}$; Rosa-CAG-RFP mice, n=8. All data are expressed as mean ±SEM. * $P<0.05$ by Mann-Whitney U-test.

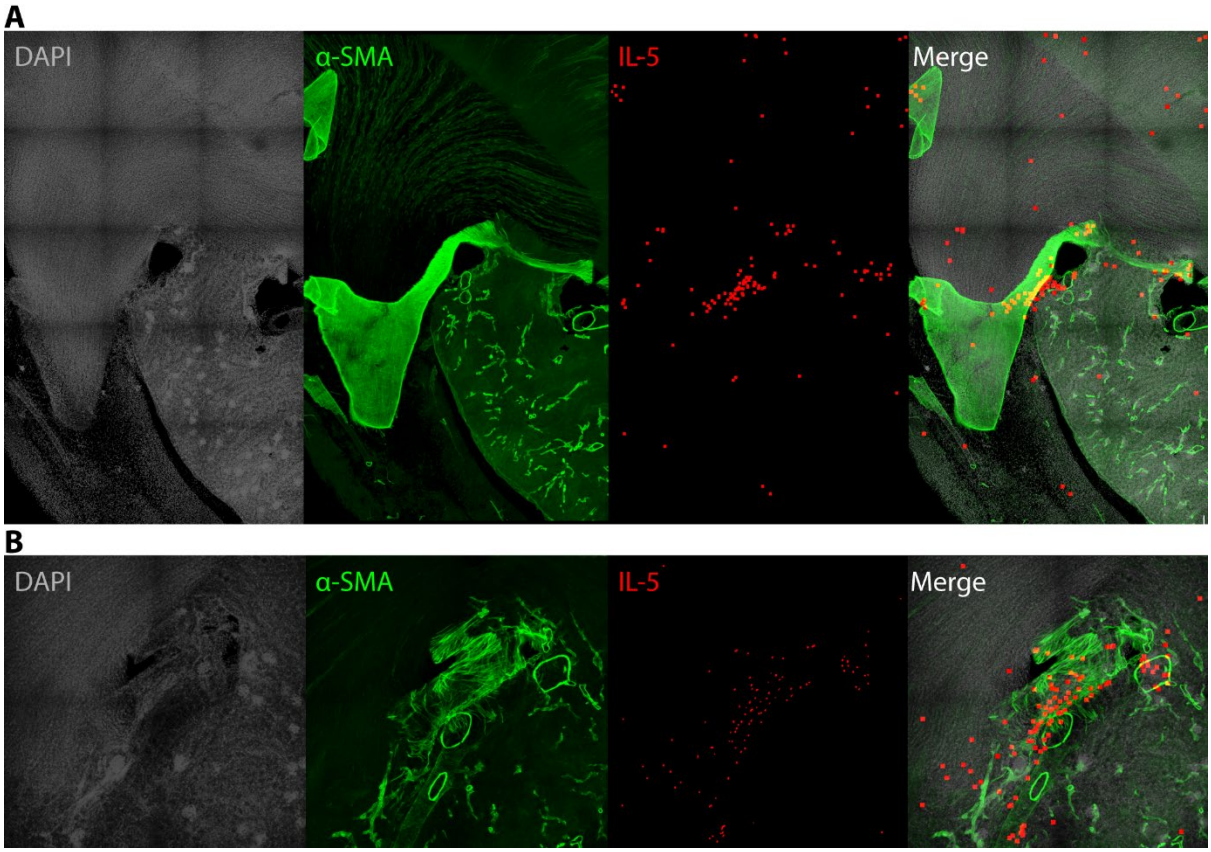

Figure 21: Immunofluorescence imaging of IL-5^{+} cells in the kidney

Kidney sections from *Il5*$^{\text{td-tomatoCre}}$; Rosa26-CAG-RFP mice were stained with DAPI, α-SMA and DsRed to visualize nuclei, smooth muscle actin and IL-5, respectively. **(A)** Visualization of broad regions of the mouse kidney, IL-5^{+} staining was identified in the calyx, capsule, cortex and medulla. **(B)** IL-5^{+} staining was localized to blood vessels in the kidney. DsRed identified IL-5^{+} cells and imaris software identified maximum projection surfaces and enhanced the pixel area for ease of visualization.

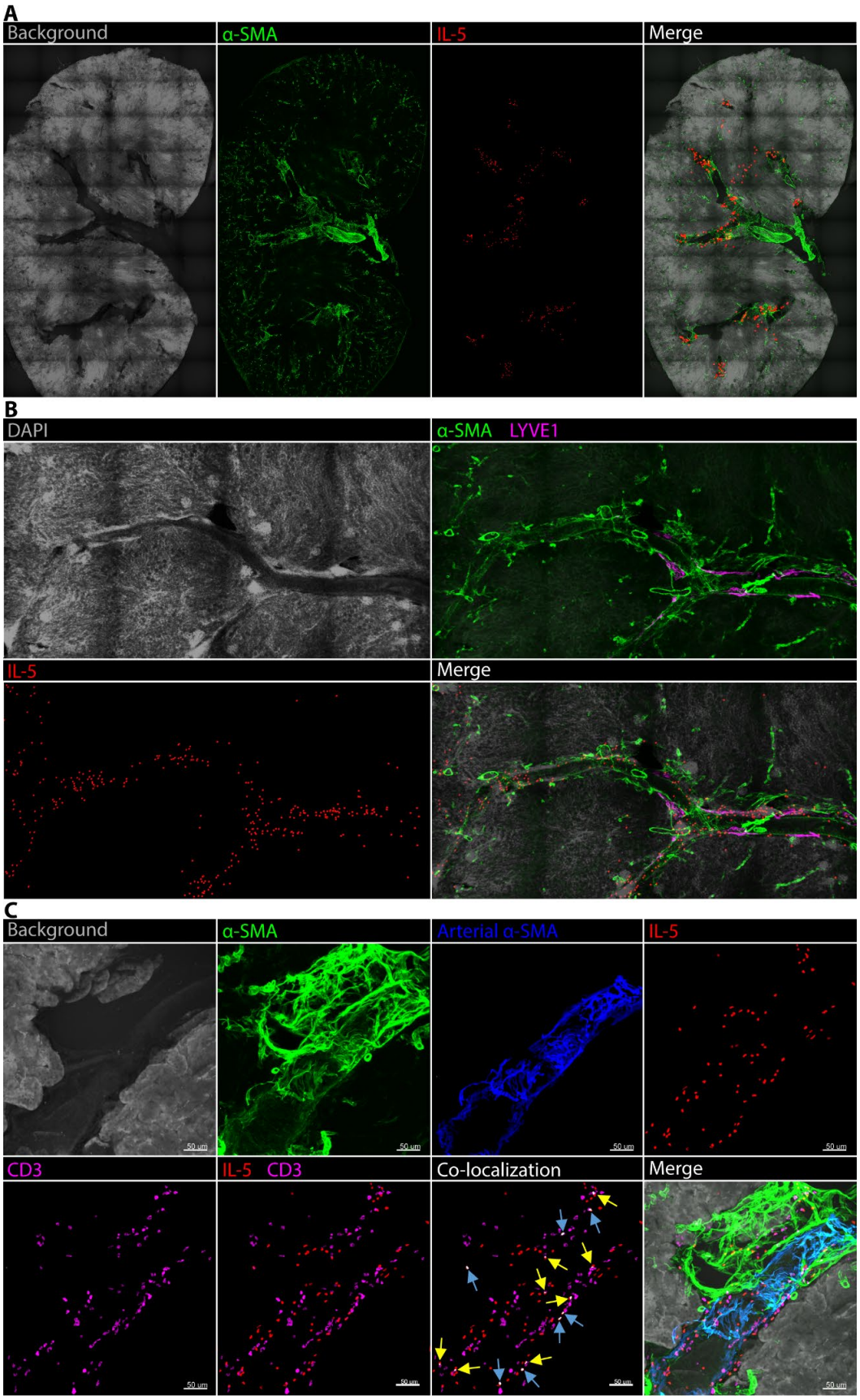

Figure 22: Kidney ILC2 are localised around the vasculature, in the adventitia, under homeostatic conditions

Kidney sections from *Il5*$^{td\text{-}tomatoCre}$; Rosa-CAG-RFP mice were stained for IL-5^{+} cells (predominantly ILC2), the IL-5^{+} pixel surface area was increased to improve clarity, tissue sections were co-stained for α-SMA for structure determination. **(A)** Gross structure of the kidney, ILC2 were located in close proximity to the renal vessels throughout the tissue. **(B)** A magnified view of a vessel spanning regions of the kidney with the addition of DAPI, LYVE1 staining indicates lymphatics which track vasculature in the cortex, ILC2 displayed no preference towards medullary or cortical vessels. **(C)** CD3^{+} cells (predominantly T_H2 cells) contributed negligible IL-5^{+} signal. Background and arterial α-SMA staining demonstrates ILC2 and T_H2 cells are located in the adventitia of the vessel. Blue arrows indicate IL-5 and CD3 co-localization in the same cell, yellow arrows indicate partial co-localization from adjacent cells.

Given ILC2 were present in the kidney and localized to the renal vasculature, the impact of ILC2-reduction, deficiency or depletion on the severity of experimental renal IRI was assessed. This was achieved by using ILC2-reduced (*Rora*$^{fl/+}$*Il7r*$^{cre/+}$), -deficient (*Rora*$^{fl/fl}$*Il7r*$^{cre/+}$) and -depleted (DTx-treated *Icos*$^{dtr/+}$*Cd4*$^{cre/+}$) mice compared to WT and vehicle (saline-treated *Icos*$^{dtr/+}$*Cd4*$^{cre/+}$) controls. These mice have been previously described as appropriate tools for assessing ILC2 function *in vivo* in other organs such as the lung [159, 352]. There were no adverse effects from either treatment, and results were obtained only on the specified endpoints. Here I show that these tools are also appropriate for assessing ILC2 function in the kidney. Indeed, kidney ILC2 were significantly lower in the ILC2-reduced, -deficient and -depleted groups compared to WT or saline-treated controls (**Figure 23A**). Time course analysis of IRI in wild-type mice identified day 7 as the most appropriate time point for the assessment of injury severity due to the presence of histopathological features of acute tubular necrosis, collagen deposition (**Figure 24A,B**); and increased mRNA expression of extracellular matrix,

injury-associated and inflammatory factors (**Figure 25A-K**, **Table 10**). At day 7, 25/84 extracellular matrix factors were increased >2-fold compared to sham controls, whilst 1/84 and 6/84 were increased at day 1 and 3, respectively (**Figure 25A**). IRI induced acute tubular necrosis characterised by dilated tubules and cast formation, compared to sham controls (**Figure 23B**). This was quantified as a tubular injury score and the severity of injury was similar in all genotypes (**Figure 23C**). IRI also induced collagen deposition, marked by methyl blue content between the tubules in the medulla and cortex, compared to sham controls (**Figure 23D**). Collagen deposition was unaffected by the absence of ILC2. IRI also increased the mRNA expression of injury-associated factors, chemokines and pro-inflammatory cytokines (**Figure 23E-J**, **Figure 25C-K**). Neutrophil gelatinase-associated lipocalin, (*Lcn2*; NGAL), a biomarker of renal injury (33,34), was increased by IRI and unaffected by ILC2 reduction, deficiency or depletion (**Figure 23E**). C-X-C motif chemokine ligand 1 (*Cxcl1*) and *Cxcl2* were also significantly increased by IRI in all genotypes (**Figure 23F,G**). Similarly, the pro-inflammatory cytokine tumor necrosis factor (*Tnf*) was increased by IRI, compared to sham controls (**Figure 23H**). Consistent with visible collagen deposition, mRNA expression of the extracellular matrix factors collagen type I alpha 1 chain (*Col1a1*) and fibronectin 1 (*Fn1*) were increased by IRI in all genotypes (**Figure 23I,J**).

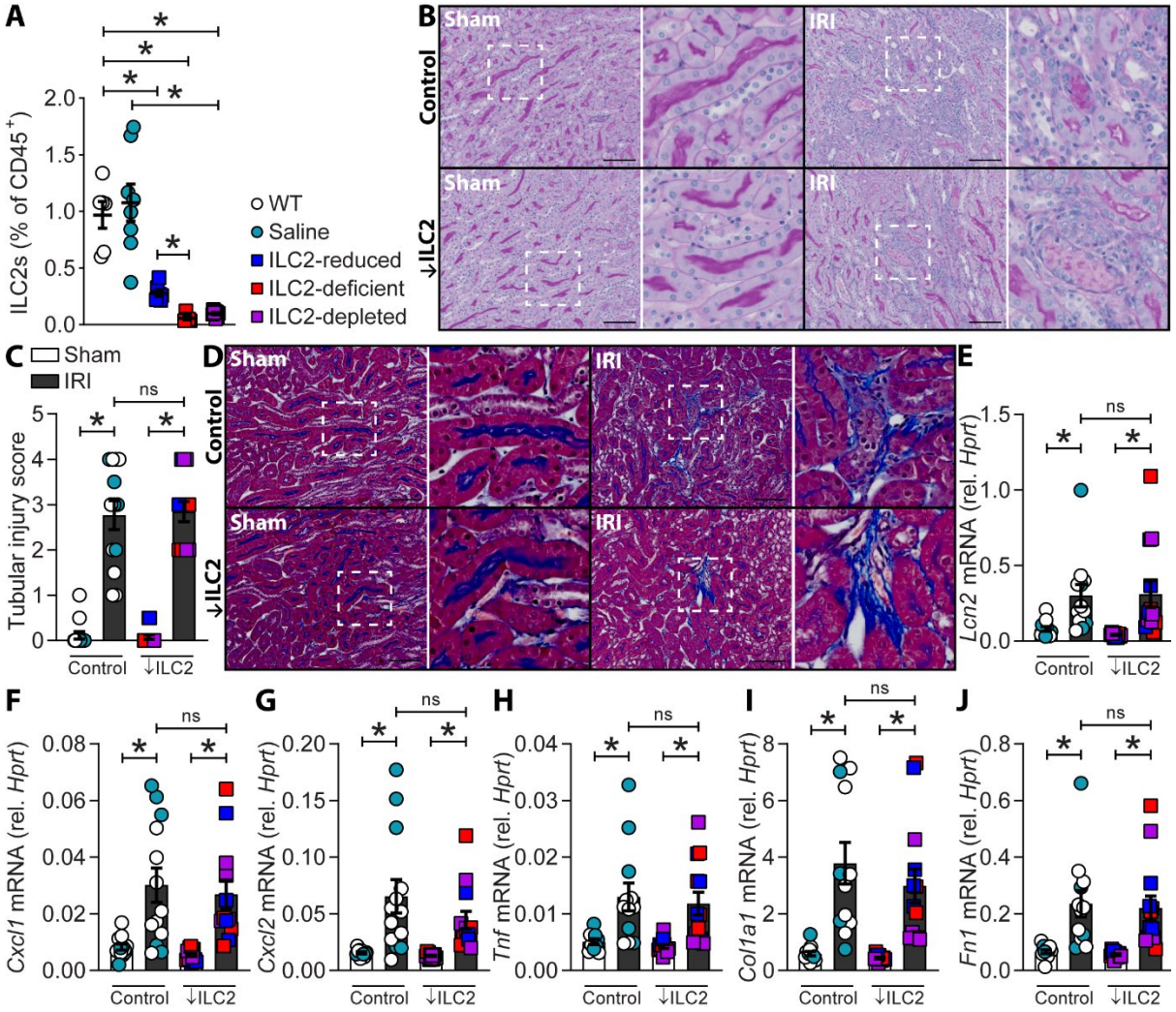

Figure 23: A loss of ILC2 does not alter the severity of experimental renal IRI

All mice were subjected to 29-minute unilateral IRI with contralateral nephrectomy and were assessed compared to sham surgical controls for each genotype. All parameters were assessed 7 days after injury. **(A)** Kidney ILC2 ($CD45^+Lineage^-[TCR^-[TCR\alpha\beta^-TCR\gamma\delta^-CD8^-CD4^-]CD11b^-GR\text{-}1^-B220^-TER\text{-}119^-CD3^-NK\text{-}1.1^-]IL\text{-}7R\alpha^+CD90.2^+ST2^+FSC^{low}SSC^{low}$ single cells) as a percentage of $CD45^+$ single cells from naïve C57BL/6JAusB wild-type (WT, n=6; uncoloured), vehicle (saline-treated *Icos*$^{dtr/+}$*Cd4*$^{cre/+}$, n=8; teal), ILC2-reduced (*Rora*$^{fl/+}$*Il7r*$^{cre/+}$, n=7; blue), ILC2-deficient (*Rora*$^{fl/fl}$*Il7r*$^{cre/+}$, n=5; red) and ILC2-depleted (DTx-treated-*Icos*$^{dtr/+}$*Cd4*$^{cre/+}$, n=8; purple) mice. **(B)** Representative images of periodic acid-Schiff stained kidney sections from control (WT, n=8; Saline, n=5) and ↓ILC2 (ILC2-reduced, n=4; -deficient, n=4 & -depleted, n=5) showing dilated tubules and cast formation. **(C)** Semi-

quantitative tubular injury score indicating injury in terms of the proportion of tubules effected by casts, dilation, apoptosis and/or loss of brush border, where a score of 5 indicates 76-100% of tubules were affected. **(D)** Representative images of Masson's trichrome stained kidney sections following IRI, blue staining indicates collagen deposition. (E-I) mRNA expression of injury (*Lcn2*), inflammatory (*Cxcl1*, *Cxcl2* and *Tnf*) and extracellular matrix (*Col1a1* and *Fn1*) factors in kidney homogenates relative to *Hprt*. Scale bar in each image indicates 100μm. All data are expressed as mean ±SEM. * $P<0.05$, ^{ns} not significant; by Mann-Whitney U-test.

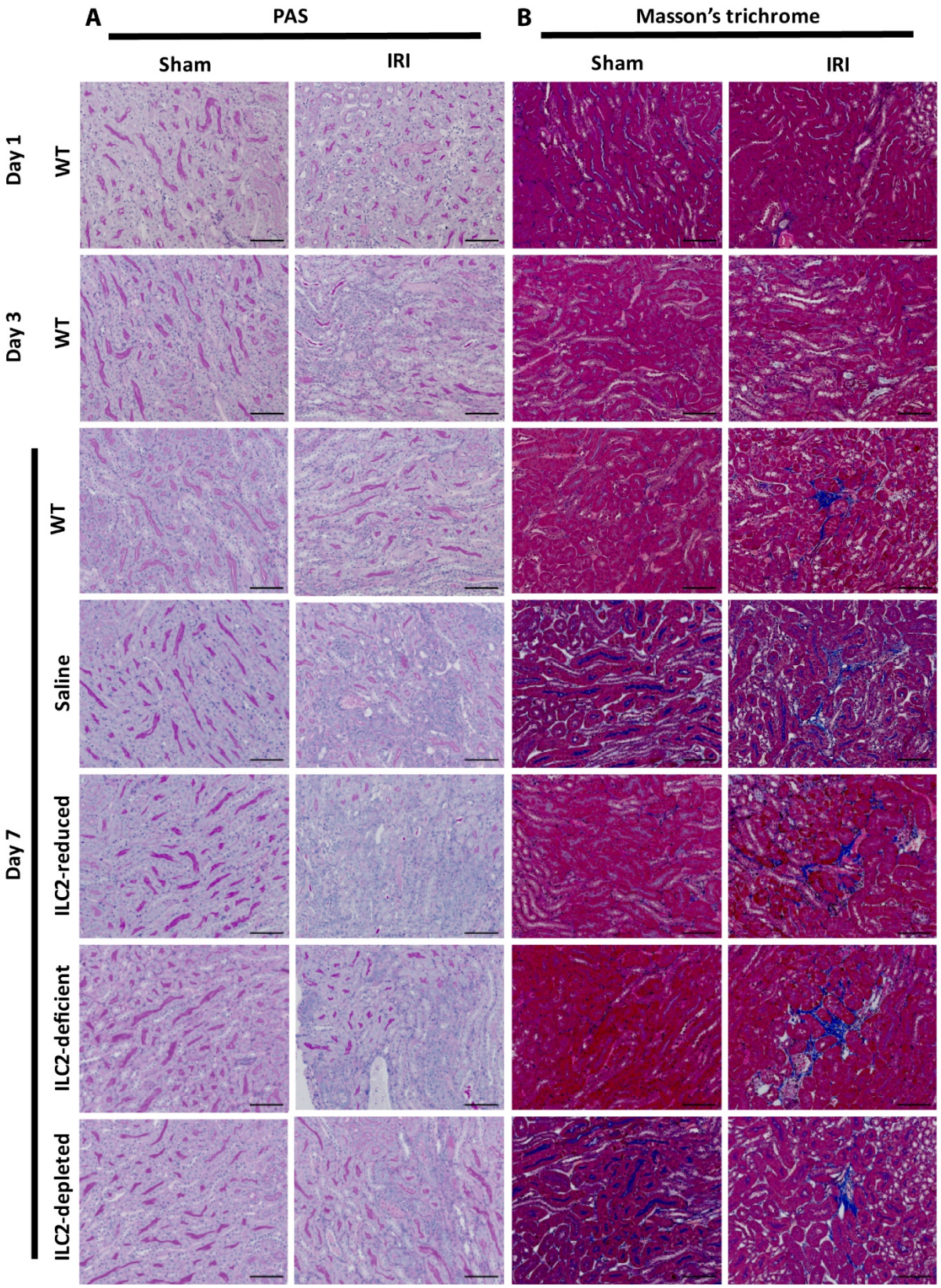

Figure 24: Histopathology following IRI was unaltered by the reduction of ILC2

C57BL/6JAusB wild-type (WT, n=8) mice received a contralateral nephrectomy and 29-minute unilateral IRI and were assessed at 1, 3 and 7-days post-surgery. WT, vehicle

(saline-treated *Icos*$^{dtr/+}$*Cd4*$^{cre/+}$, n=5), ILC2-reduced (*Rora*$^{fl/+}$*Il7r*$^{cre/+}$, n=4), ILC2-deficient (*Rora*$^{fl/fl}$*Il7r*$^{cre/+}$, n=4) and ILC2-depleted (diphtheria toxoid-treated *Icos*$^{dtr/+}$*Cd4*$^{cre/+}$, n=5) were assessed 7-days post-surgery. **(A)** Periodic acid-Schiff and **(B)** Masson's trichrome representative images of stained kidney sections following sham and IRI surgery, blue staining indicates collagen. Scale bar in each image indicates 100µm.

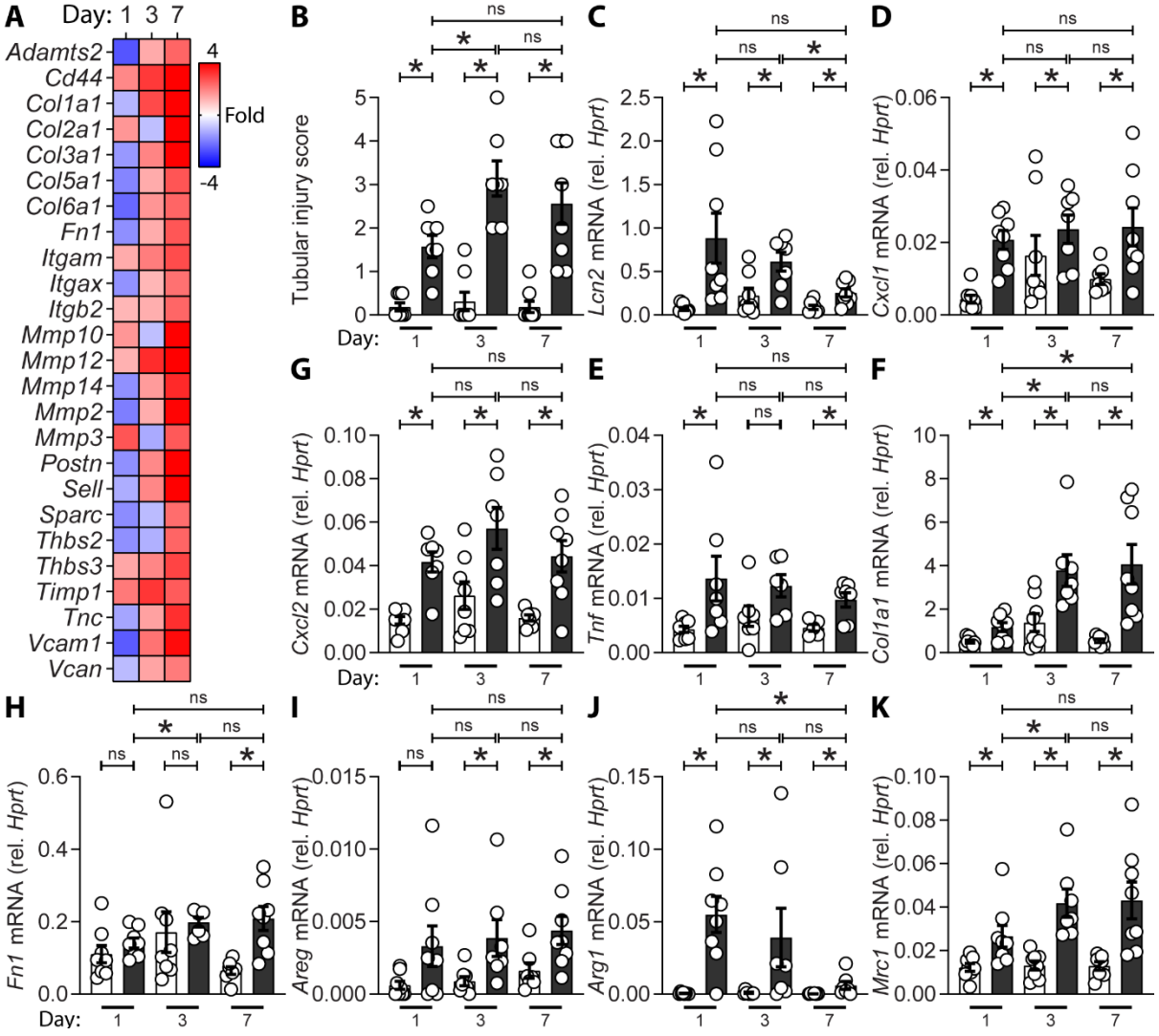

Figure 25: IRI increased mRNA expression and histopathological score

(A) Extracellular Matrix & Adhesion Molecules RT² Profiler PCR Array, truncated to 25/84 targets, which were increased >2 fold in kidney homogenates from C57BL/6JAusB wild-type

(WT, n=8) on day 1, 3 or 7 following IRI (n=8 per timepoint), compared to the average expression across each timepoint following sham surgery (n=24). **(B)** Semi-quantitative tubular injury score indicating injury in terms of the proportion of tubules effected by casts, dilation, apoptosis and/or loss of brush border, where a score of 5 indicates 76-100% of tubules were affected. **(C-K)** mRNA expression of injury (*Lcn2*), inflammatory (*Cxcl1*, *Cxcl2* and *Tnf*), extracellular matrix (*Col1a1* and *Fn1*), ILC2- and M2-macrophage associated factors (*Areg*, *Arg1* and *Mrc1*) relative to *Hprt* expression using the ΔΔCT method in kidney homogenates. All data are expressed as the mean ±SEM. ^{ns} not significant, * P<0.05; by Mann-Whitney U-test.

Table 10: mRNA expression in the kidney following IRI at day 1, 3 and 7 compared to sham controls

Target	Description	Fold regulation from sham		
		Day 1	Day 3	Day 7
Adamts1	A disintegrin-like and metallopeptidase (reprolysin type) with thrombospondin type 1 motif, 1	-1.6113	-1.1035	1.1738
Adamts2	A disintegrin-like and metallopeptidase (reprolysin type) with thrombospondin type 1 motif, 2	-2.6724	1.3323	2.4081
Adamts5	A disintegrin-like and metallopeptidase (reprolysin type) with thrombospondin type 1 motif, 5 (aggrecanase-2)	-2.1000	-1.3803	1.2402
Adamts8	A disintegrin-like and metallopeptidase (reprolysin type) with thrombospondin type 1 motif, 8	-2.4169	1.6815	1.4339
Cd44	CD44 antigen	1.8568	3.0925	4.6425
Cdh1	Cadherin 1	-2.3594	-1.6297	-1.2395
Cdh2	Cadherin 2	-3.0465	-2.0245	-1.3964
Cdh3	Cadherin 3	1.0450	1.2493	1.7628
Cdh4	Cadherin 4	-16.3309	-2.9045	-1.3827
Cntn1	Contactin 1	1.1910	1.0248	1.8196
Col1a1	Collagen, type I, alpha 1	-1.1687	2.8290	7.4719
Col2a1	Collagen, type II, alpha 1	1.6348	-1.0126	6.8394
Col3a1	Collagen, type III, alpha 1	-1.6243	1.9167	6.5845

Col4a1	Collagen, type IV, alpha 1	-2.0894	-1.2016	1.0135
Col4a2	Collagen, type IV, alpha 2	-2.1658	-1.1890	1.2315
Col4a3	Collagen, type IV, alpha 3	-3.8941	-2.0901	-1.3436
Col5a1	Collagen, type V, alpha 1	-1.9210	1.3066	2.6560
Col6a1	Collagen, type VI, alpha 1	-2.3835	1.6603	2.4056
Ctgf	Connective tissue growth factor	-3.1149	-1.7418	-1.4650
Ctnna1	Catenin (cadherin associated protein), alpha 1	-2.3997	-1.7420	-1.2215
Ctnna2	Catenin (cadherin associated protein), alpha 2	-5.0804	-2.1471	1.0287
Ctnnb1	Catenin (cadherin associated protein), beta 1	-2.9810	-1.7725	-1.2896
Ecm1	Extracellular matrix protein 1	-1.9546	-1.5910	-1.0670
Emilin1	Elastin microfibril interfacer 1	-1.4717	-1.0738	1.4703
Entpd1	Ectonucleoside triphosphate diphosphohydrolase 1	-1.3720	-1.1146	1.1752
Fbln1	Fibulin 1	-2.0339	-1.1247	1.2444
Fn1	Fibronectin 1	-1.7684	1.2966	2.6359
Hapln1	Hyaluronan and proteoglycan link protein 1	-4.9031	-6.3906	1.6017
Hc	Hemolytic complement	-3.2884	-1.5036	1.1925
Icam1	Intercellular adhesion molecule 1	-2.2346	-1.1375	1.5280
Itga2	Integrin alpha 2	-3.0395	-1.6365	-1.3171
Itga3	Integrin alpha 3	-1.7038	-1.1117	-1.0317
Itga4	Integrin alpha 4	-2.5647	-1.0717	1.6789
Itga5	Integrin alpha 5 (fibronectin receptor alpha)	-1.4425	1.1516	1.4369
Itgae	Integrin alpha E, epithelial-associated	-6.9649	-1.8227	1.0404
Itgal	Integrin alpha L	-2.4366	-1.1363	1.3132
Itgam	Integrin alpha M	1.3073	2.0285	2.8040
Itgav	Integrin alpha V	-2.2768	-1.4580	-1.1225
Itgax	Integrin alpha X	-1.7234	1.1382	2.2255
Itgb1	Integrin beta 1 (fibronectin receptor beta)	-2.3818	-1.4938	-1.1531
Itgb2	Integrin beta 2	1.1419	1.2649	2.3928
Itgb3	Integrin beta 3	-2.1645	-1.1381	1.0078
Itgb4	Integrin beta 4	-2.1336	-1.1679	-1.1008
Lama1	Laminin, alpha 1	-3.0532	-1.7372	-1.4539
Lama2	Laminin, alpha 2	-2.5274	-1.0978	1.2153
Lama3	Laminin, alpha 3	-3.9016	-1.4041	-1.1558
Lamb2	Laminin, beta 2	-1.6622	-1.1595	-1.1587
Lamb3	Laminin, beta 3	-2.1818	-1.3816	-1.7836
Lamc1	Laminin, gamma 1	-2.9846	-1.4913	-1.1152
Mmp10	Matrix metallopeptidase 10	1.6348	-1.0126	4.2721
Mmp11	Matrix metallopeptidase 11	-2.6080	1.0019	1.5349
Mmp12	Matrix metallopeptidase 12	1.2083	3.3030	8.4504
Mmp13	Matrix metallopeptidase 13	-3.7500	-2.5626	1.0851

Mmp14	Matrix metallopeptidase 14 (membrane-inserted)	-1.7468	1.5680	3.3428
Mmp15	Matrix metallopeptidase 15	-3.5148	-1.1793	1.7931
Mmp1a	Matrix metallopeptidase 1a (interstitial collagenase)	-3.3103	-2.2053	-1.1104
Mmp2	Matrix metallopeptidase 2	-2.0343	1.2714	3.9371
Mmp3	Matrix metallopeptidase 3	2.6568	-1.3486	2.5883
Mmp7	Matrix metallopeptidase 7	-6.9288	-1.1995	1.2644
Mmp8	Matrix metallopeptidase 8	-4.4237	1.1139	1.1115
Mmp9	Matrix metallopeptidase 9	1.2419	1.1493	1.2554
Ncam1	Neural cell adhesion molecule 1	-2.8092	-1.0001	1.7144
Ncam2	Neural cell adhesion molecule 2	-4.1085	-1.9727	-1.1397
Pecam1	Platelet/endothelial cell adhesion molecule 1	-2.2899	-1.4631	-1.1732
Postn	Periostin, osteoblast specific factor	-1.7506	1.8508	10.9844
Sele	Selectin, endothelial cell	1.4145	1.0139	-1.0970
Sell	Selectin, lymphocyte	-1.2951	1.8720	4.6769
Selp	Selectin, platelet	-2.2075	-1.1112	1.1315
Sgce	Sarcoglycan, epsilon	-2.3761	-1.4105	1.0909
Sparc	Secreted acidic cysteine rich glycoprotein	-1.8114	-1.0822	2.2782
Spock1	Sparc/osteonectin, cwcv and kazal-like domains proteoglycan 1	1.7544	-8.2789	1.1235
Spp1	Secreted phosphoprotein 1	1.0493	1.5838	1.5914
Syt1	Synaptotagmin I	-6.5462	-2.4428	1.4732
Tgfbi	Transforming growth factor, beta induced	-1.9456	1.0701	1.3819
Thbs1	Thrombospondin 1	-2.2143	-1.1333	-1.0406
Thbs2	Thrombospondin 2	-1.7437	-1.2456	2.4081
Thbs3	Thrombospondin 3	1.3873	1.8875	2.9234
Timp1	Tissue inhibitor of metalloproteinase 1	2.0943	3.1476	2.5610
Timp2	Tissue inhibitor of metalloproteinase 2	-1.9158	-1.2761	1.4047
Timp3	Tissue inhibitor of metalloproteinase 3	-3.2855	-1.5904	-1.1735
Tnc	Tenascin C	-1.4237	1.4668	3.2574
Vcam1	Vascular cell adhesion molecule 1	-2.5782	2.1930	3.8161
Vcan	Versican	-1.0767	1.4251	2.0607
Vtn	Vitronectin	-2.7040	-2.1430	1.8923
Actb	Actin, beta	-2.0971	-1.5555	-1.1352
B2m	Beta-2 microglobulin	-4.0631	-1.2356	1.3349
Gapdh	Glyceraldehyde-3-phosphate dehydrogenase	-4.6067	-2.3170	-1.5123
Gusb	Glucuronidase, beta	-2.2972	-1.1900	-1.0674
Hsp90ab1	Heat shock protein 90 alpha (cytosolic), class B member 1	-2.4999	-1.6323	-1.0919
MGDC	Mouse Genomic DNA Contamination	1.7689	-1.0126	-1.1574
RTC1	Reverse Transcription Control1	5.9492	-1.0126	-1.1574

RTC2	Reverse Transcription Control2	1.6348	-1.0126	-1.0563
RTC3	Reverse Transcription Control3	6.6231	-1.0126	-1.1574
PPC1	Positive PCR Control1	1.5866	-1.0557	-1.2398
PPC2	Positive PCR Control2	1.6368	1.0317	-1.1147
PPC3	Positive PCR Control3	1.6214	1.0129	-1.1893

3.5 Discussion

ILC2 are critical regulators of tissue homeostasis, but their role in the kidney remains to be fully elucidated. Whilst ILC2 can be induced to proliferate and protect against the deleterious consequences of experimental renal injury, it is not yet known what occurs in the absence of these cells. I first examined whether ILC2 numbers, as a proportion of $CD45^+$ hematopoietic cells, are different in lung and kidney. ILC2 accounted for a greater proportion of $CD45^+$ cells in the kidney than in the lung. t-SNE analysis grouped ILC2 from both sites differently, however the clusters were not entirely distinct between these tissues. There were differences in their cell surface antigen and type 2 cytokine expression, with kidney ILC2 expressing greater amounts of IL-5. Indeed, kidney ILC2 constitutively expressed high levels of IL-5 under homeostatic conditions. ILC2 were also the major source of IL-5 in the kidney, with negligible contribution from T_H2 cells. Therefore, IL-5 was used as a surrogate marker to determine the location of these cells in the kidney.

ILC2 were identified within the kidney and were localized almost exclusively along the renal vasculature. In these studies, an IL-5 linked cre-recombinase was used in conjunction with a flox-stop-flox sequence upstream of a CAG-RFP-WPRE- cassette in the constitutively expressed ROSA26 locus to locate the ILC2. LYVE1, which is expressed by renal lymphatic endothelial cells, was used to further define the location of these cells within the mouse kidney [353, 354]. As expected, LYVE1 staining was embedded within the connective tissue of renal arteries of the cortex, but not within the medulla since no discernible lymphatic network exists

in this region of the kidney [353, 354]. Presumably ILC2 are situated close to the vascular as renal endothelial cells are a major source of IL-33 in the kidney [184, 355]. Confirming my observation by FACS of single cell kidney suspensions, ILC2 were again found to be the major producers of IL-5 in kidney tissue sections, with minimal contribution from $CD3^+$ T cells. Whilst these studies show the location of ILC2 in the kidney using reporter mice, it remains to be determined if ILC2 are also located adjacent to the vasculature in the human kidney, and whether the location of ILC2 is altered in response to renal injury. Although multiple reports have found ILC2 numbers are unchanged by renal injury, their phenotype and activation state following injury requires further elucidation.

Next, I characterised the functional role of ILC2 in the kidney using a loss-of-function approach. To achieve this, I took advantage of ILC2-reduced and -deficient mice, and mice that can be conditionally depleted of ILC2 following the administration of DTx. I validated the use of these tools for knockdown or ablation of ILC2 in the kidney. An experimental model of IRI was chosen, given the proximity of ILC2 to the renal vasculature. Although features of injury were visibly evident following IRI, a reduction, deficiency or depletion in ILC2 did not alter gross histopathology in the kidney, nor did it cause mortality. Indeed, IRI-induced remodelling and collagen deposition occurred independent of ILC2. Whilst it is possible that an earlier time point following injury may have identified differences in histopathology and gene expression, the time point in my study also allowed assessment of collagen deposition, an important feature of remodelling that is regulated by ILC2. It is also plausible that a reduction in ILC2 during AKI could be detrimental to kidney structure and function, when assessed at later time points due to potential maladaptive repair responses in the absence of ILC2. To address this, future studies will need to investigate the role of ILC2 in the progression of AKI to chronic kidney disease [40, 356].

Collectively, this study demonstrates that a reduction, deficiency or depletion in ILC2 does not alter the severity of experimental AKI in mice. Whilst activation of ILC2 and the associated amplification of local type 2 immunity has been previously shown to reduce the deleterious consequences of AKI, comparable injury occurs when ILC2 are reduced, absent or depleted suggesting possible redundancy and compensation by other immune cells, such as T_{reg}, AAM and T_H2 cells. This concept is supported by studies using *Rag1*$^{-/-}$ or *Rag2*$^{-/-}$ mice that lack mature T and B cells, in models of kidney injury. In one study, anti-CD90.2 administration was used to deplete ILC2, however these animals were also deficient in T_{reg} and T_H2 cells. In this model system, despite the depletion of ILC2 with anti-CD90.2, compensation from the T cell compartment is not possible. My data show that a loss of ILC2, when the T cell compartment remains intact, has minimal effects on the severity of IRI. It is possible that the ILC2 in addition to other immune cells, such as T_{reg} and AAM, contribute to AKI, yet this cannot be determined from these data. Indeed, others find that T_{reg} depletion worsened histopathology following IRI. Similarly, studies have found that macrophage polarisation towards AAM promotes the resolution of injury. Further work is required to elucidate the reason for the presence of ILC2 in the kidney, including ascending urinary tract infections and other renal insults as well as in progression to chronic disease.

Chapter 4: Systemic interleukin-33 increased the severity of uropathogenic *Escherichia coli*-induced pyelonephritis and impaired kidney function in mice

At the time of thesis submission, all results in this chapter are unpublished. Descriptions of methods or reagents are recapitulated from **Chapter 3** where the work was performed identically. This work underwent peer review at Kidney International and where possible, reviewer comments have been incorporated. The draft manuscript is:

> **Cameron GJM**, Cautivo KM, Lawrence BM, Loering S, Deshpande AV, Bhatt NP, Collison AM, Foster PS, Deshpande AV, Molofsky AB, Starkey MR. Systemic interleukin-33 increased the severity of uropathogenic *Escherichia coli*-induced pyelonephritis and impaired kidney function in mice. JCI Insight. 2021.

Cameron GJM and Starkey MR conceptualised the manuscript. Cautivo KM and Molofsky AB performed the flow cytometry and immunofluorescence using Il5$^{td\text{-}tomatoCre}$Rosa26-CAG-RFP mice. Cameron GJM performed all other aspects including the infection model, flow cytometry in all other mice, histological assessment, in vivo kidney function, data analysis and drafted the manuscript. Lawrence BM and Loering S assisted with animal monitoring. Loering S assisted with flow cytometry. Bhatt NP assisted with centrifugation of samples. Collison AM, Deshpande AV and Foster PS advised on experimental design.

4.1 Abstract

Here I describe the impact of increased systemic interleukin (IL)-33 on severity of UTI. Wild-type C57BL/6 mice were pre-treated with recombinant mouse IL-33 (rmIL-33) followed by transurethral infection with the uropathogenic *Escherichia coli* clinical isolate UTI89. Pre-treatment with rmIL-33 significantly increased the kidney bacterial load and proportion of mice that developed a kidney infection, termed pyelonephritis. Kidney function was assessed *in vivo* using transcutaneous glomerular filtration rate (*t*GFR) based on FITC-Sinistrin clearance, allowing pair-wise comparisons over time. Pre-treatment with rmIL-33 resulted in more severe kidney function impairment following infection, persisting 4 weeks after infection. These data show that excess exogenous IL-33 drives increased severity of infection marked by increased kidney injury and impaired kidney function.

4.2 Introduction

Uropathogenic *Escherichia coli* causes the majority of urinary bladder infections in humans, termed cystitis [357], and may ascend causing infection of the kidneys, termed pyelonephritis [256]. Whilst antibiotic therapies are sufficient in most cases, the emerging threat of antimicrobial resistance has decreased the effectiveness of such interventions [190]. Several studies have characterised the immunological state of the urinary tract in response to experimental infection in murine models, reviewed in [358]. Yet the function of interleukin (IL)-33 in this context is not well understood. IL-33 is an alarmin, which is released from epithelial cells of the urinary tract upon damage resulting in the activation of subsets of immune cells [203, 359-361]. In the kidney and other organs, IL-33 potently activates multiple cells types including group 2 innate lymphoid cells (ILC2) and $CD4^+$ T helper 2 (T_H2) cells [362-

364]. These cells are known to be strong producers of type II effector cytokines, primarily IL-5 and IL-13, yet the relevance of these cells and cytokines in urinary tract infection is largely unknown [362-364]. Indeed, the immunology of the urinary bladder in particular is significantly limited. However, it is known that elevated IL-5 in human and mouse serum is associated with a persistent and severe urinary tract infection, respectively [213, 365]. There are also diseases whereby type II immunity is enhanced, such as atopic dermatitis and rheumatoid arthritis; interestingly, patients with both of these conditions have a well-known increased risk of developing UTI but to my knowledge the link with type II immunity has not been investigated. Type II immunity is classically known to have critical roles in generation of anti-helminth responses, yet exaggeration of type II immune responses is observed in multiple conditions such as asthma and dermatitis. In recent years, there has been substantial interest in understanding how and why a type II response is initiated in response to a wide array of microbial and non-microbial stimuli. Indeed, there was an explosion of literature enhancing our understanding of these pathways in multiple tissues following the discovery of ILC2. Although there was appreciation that type II immune pathways are important for tissue homeostasis many studies still portrayed these responses as aberrant. Yet these responses are critical drivers of tissue repair following an insult and that the regulation of these responses is important. Therefore, this study aimed to expand on our knowledge of ILC2 in the urinary bladder and kidney in terms of their phenotype and tissue localisation. Additionally, I aimed to investigate the role of IL-33 in the urinary tract by utilizing a murine model of experimental cystitis induced by uropathogenic *Escherichia coli*. I discovered that exogenous IL-33 increased the severity of infection and resulted in substantial impairment to kidney function.

4.3 Methods

4.3.1 Mice

7 to 10-week-old female C57BL/6Jausb wild-type mice were obtained from Australian Bioresources. Each of the described procedures were approved by animal care and ethics committee of the University of Newcastle. As per ethical requirements, animals were culled if they lost >15% body weight (bw). In some experiments, *Icos*$^{dtr/+}$*Cd4*$^{cre/+}$ and *Il5*$^{td\text{-}tomatoCre}$; Rosa26-CAG-RFP reporter-tracker mice were utilised.

4.3.2 Recombinant mouse (rm) treatments

Mice received 0.5µg of rmIL-33 (cat# 580508 [BioLegend, San Diego, United States]) on day -6, -4 and -2 with the infection taking place on day 0, or 200µL of the vehicle phosphate buffered saline (PBS) *via* intraperitoneal injection, as described [338].

4.3.3 ILC2 depletion using diphtheria toxoid (DTx)

ILC2 depletion was performed by pre-treating *Icos*$^{dtr/+}$*Cd4*$^{cre/+}$ mice with 0.025ng kg^{-1} DTx in saline daily by intraperitoneal infection for 7 days, or 200µL of the vehicle saline *via* intraperitoneal injection, as described [159, 366].

4.3.4 Infection model

Uropathogenic *Escherichia coli* clinical isolate UTI89 was prepared, as described [336]. Mice were anaesthetized using isoflurane then transurethrally inoculated with 50µL of the prepared inoculum, as described [336, 337]. Anaesthesia was maintained for exactly 20 minutes following the inoculation to prevent immediate voiding. 20 minutes after inoculation was considered as time 0 for the infection.

4.3.5 Colony forming units (CFU) determination

Urinary bladder and kidney pairs, without kidney capsules, were excised aseptically and physically homogenised in 1000 or 800µL of PBS, respectively, to determine CFU as described [336]. The limit of detection (LOD) was 20 CFU mL^{-1}.

4.3.6 Enzyme-linked immunosorbent assay (ELISA)

200µL of homogenised organs were diluted with 200µL of 2x protein buffer (1 PhosSTOP™ & 1 cOmplete™ in 5mL ddH_2O; Sigma-Aldrich), after centrifugation at 10,000x*g* for 10 minutes at 4°C, the supernatant was assessed for IL-33 (cat# 436407; BioLegend) protein levels. IL-5 (cat# 431204; BioLegend) protein levels were measured in serum. The limit of detection for these assays was 4 and 15pg mL^{-1}, respectively. IL-22 protein levels were measured using quantitative ELISA (cat# 436304 [BioLegend, San Diego, United States]), the limit of detection for this assay was 2pg mL^{-1}.

4.3.7 Flow cytometry and t-distributed stochastic neighbor embedding (t-SNE) analysis

Urinary bladders and kidney pairs were collected from mice. Single-cell suspensions were prepared as described in "Preparation of single-cell suspensions from mouse lung with Collagenase D treatment" (Miltenyi Biotec GmbH, 2008; Bergisch Gladbach, Germany). Cells were blocked with Fc block (purified anti-mouse CD16/32; Biolegend, San Diego, USA) for 30 minutes and stained with fluorescently-conjugated antibodies against target cell surface antigens (**Table 11**, **Table 12**). Staining and washing steps were performed with BSA stain buffer (BD Biosciences, North Ryde, Australia). Samples were acquired on a BD LSR Fortessa X20 flow cytometer. Flow cytometry data were analysed using FlowJo v10.5.3 (Tree Star, Ashland, USA). The t-SNE was performed on ILC ($CD45^+Lineage^-[TCR^-[TCR\alpha\beta^-TCR\gamma\delta^-CD8^-CD4^-]CD11b^-GR\text{-}1^-B220^-TER\text{-}119^-CD3^-NK\text{-}1.1^-]IL7R\alpha^+$ single cells). Using the random down sampling plugin, the number of events in each sample was normalized to equal the lowest, rounded down to the nearest 10 events. All populations were combined into one .fcs file by concatenating the down sampled populations. The t-SNE analysis was performed on the concatenated sample containing the gated populations from all kidney and lung samples combined. For this, the compensated channels that were not used for gating were assessed under the default settings for the native t-SNE FlowJo plugin. Histograms were used to show the differential expression of cell surface antigens and cytokines in the bladder and kidney.

Table 11: Flow cytometry antibodies for assessing group 2 innate lymphoid cells

Antigen	Product code	Clone	Fluorophore	Dilution factor	Source
CD278 (ICOS)	565886	C398.4A	BV421	100	BD Biosciences
TCR-αβ	563221	H57-597	BV510	300	BD Biosciences
TCR-γδ	563218	GL3	BV510	300	BD Biosciences
CD4	563106	RM4-5	BV510	300	BD Biosciences
CD8a	563068	53-6.7	BV510	300	BD Biosciences
KLRG1	740553	2F1	BV650	100	BD Biosciences
CD45	550994	30-F11	PerCP-Cy5.5	200	BD Biosciences
CD127 (IL-7Rα)	562419	SB/199	PE-CF594	100	BD Biosciences
CD25	552880	PC61	PE-Cy7	50	BD Biosciences
IL-33R (ST2)	17-9335-82	RMST2-2	APC	50	eBioscience
CD11b	557960	M1/70	AF700	100	BD Biosciences
LY-6G/C (GR-1)	557979	RB6-8C5	AF700	100	BD Biosciences
CD45R (B220)	557957	RA3-6B2	AF700	100	BD Biosciences
TER-119	560508	TER-119	AF700	100	BD Biosciences
CD3	561388	17A2	AF700	100	BD Biosciences
NK-1.1	560515	PK136	AF700	100	BD Biosciences
CD90.2	561641	53-2.1	APC-Cy7	200	BD Biosciences

Table 12: Flow cytometry antibodies for assessing group 2 innate lymphoid cells in conjunction with T cells

Antigen	Product code	Clone	Fluorophore	Dilution factor	Source
CD45	564279	30-F11	BUV395	400	BD Biosciences
CD90.2	140318	53-2.1	BV605	400	Biolegend
CD3	100236	17A2	APC	100	Biolegend
CD4	100557	RM4-5	BV421	200	Biolegend
CD8a	100750	53-6.7	BV786	200	Biolegend
CD19	115520	6D5	PE-Cy7	200	Biolegend
CD11b	101259	M1/70	FITC	200	Biolegend
NK1.1	108705	PK136	FITC	200	Biolegend
Viability	565388	-	APC-Cy7	1000	BD Biosciences
IL-5	-	-	Td-tomato (PE)	-	Reporter mice

4.3.8 Immunofluorescence

Il5$^{\text{td-tomatoCre}}$; Rosa26-CAG-RFP reporter-tracker mice were euthanised and perfused intracardially with 1x phosphate buffered saline (PBS) and then 4% paraformaldehyde (PFA) in PBS. Kidneys were removed and kept in fresh 4% PFA for 24 hours at 4°C and then washed in 1xPBS. Whole bladder tissue was incubated in permeabilization buffer (1x PBS/0.2% Triton X-100/0.3M glycine) then blocked in PBS/0.2% Triton X-100/5% donkey serum at 4°C overnight. Samples were washed in PBS/0.2% Tween-20 once, then incubated with primary antibodies diluted in PBS/0.2% Tween-20/3% donkey serum at room temperature until the next day. Next, samples were washed in PBS/0.2% Tween-20 for 30 minutes, 3-4 times, then

incubated with secondary antibodies diluted in PBS/0.2% Tween-20/3% donkey serum at room temperature for 6-8 hours. Samples were washed in PBS/0.2% Tween-20 for 1 day and then dehydrated in an ascending ethanol series (20%, 30%, 50%, 70%, 95%, 100%), 10 minutes each step. Finally, whole bladder sections were cleared by soaking in methyl salicylate (M-2047; Sigma-Aldrich) and then mounted in fresh methyl salicylate onto a concave coverslip or chamber. Images were captured with Nikon A1R laser scanning confocal including 405, 488, 561, and 650 laser lines for excitation and imaging with 16X/0.8 or 25X1.1, NA Plan Apo long working distance water immersion objectives. Z steps were acquired every 6μm. The following antibodies and dilutions were used: Living Colors anti-DsRed Rabbit Polyclonal Pan Antibody (1:500; TaKaRa, Mountain View, USA), eFluor 660 LYVE1 monoclonal Antibody (1:300, clone ALY7, eBioscience), Alexa Fluor® 488 donkey anti-goat IgG (H+L), Alexa Fluor® 555 donkey anti-rabbit IgG (H+L) Alexa Fluor® 647 goat anti-hamster IgG (H+L) cross-adsorbed (1:400, ThermoFisher Scientific).

4.3.9 Transcutaneous glomerular filtration rate (*t*GFR) measurement

Dorsal fur was removed using an electric razor and depilation cream. Measurements were obtained by attaching a mini version of the *t*GFR device (MediBeacon gmbH, Mannheim, Germany), as described [340]. Background fluorescence was measured for 3 minutes, an intravenous bolus of 50mg kg^{-1} FITC-Sinistrin (cat# 29389090; MediBeacon gmbH) was administered, and fluorescence decay was measured for 90 minutes. Data was read from the device using MB lab 2 software and was analysed using MB Studio software using a three-compartment model with linear baseline correction to obtain FITC-Sinistrin half-life in minutes (min) which the software used to determine *t*GFR as mL min^{-1} 100g bw^{-1}, using the improved kinetic model as described [341].

4.3.10 Blood urea nitrogen (BUN) measurement

Blood was collected by cardiac puncture; after centrifugation, BUN (cat# 98-11070-01 [IDEXX Laboratories, Rydalmere, Australia]) was measured in serum supernatants using a Catalyst One veterinary chemistry analyser.

4.3.11 Histological assessment

Periodic acid-Schiff (PAS) staining was used for kidney tubular injury scoring using a semi-quantitative method, as described [366]. A score of 0 = 0% of tubules were affected by casts, dilation or remodelling; 1 = 1-10%; 2 = 11-25%; 3 = 26-50%; 4 = 51-75%; 5 = 76-100%. A score was given for each kidney and an average was taken between the kidney pairs, allowing for increments of 0.5.

4.3.12 Statistical analysis

All data were analysed with GraphPad Prism software v9.1.0. Statistical tests, sample size and number of experiments are described in each of the corresponding figure legends.

4.4 Results

To understand what effect rmIL-33 had on the urinary bladder and kidney, flow cytometry was performed on naïve animals after receiving rmIL-33 or vehicle treatment every 2nd day for 6 days (**Figure 26A**). In both tissues, rmIL-33 had a profound effect on the leukocytes characterised as CD45^{+} single cells and in particular greatly increased the proportion of cells

consistent with ILC which did not express lineage markers but did express the IL-7Rα (**Figure 26B-E**). Indeed, rmIL-33 increased $CD45^+$ single cells raw number of events, yet as a proportion of all events they were only significantly increased in the bladder homogenates (**Figure 27A,B**). Likewise, ILC raw numbers of events were increased in both tissues, yet when normalised to total events or to the proportion of $CD45^+$ single cells the statistical significance was only present in the bladder or kidney pair, respectively (**Figure 27C-E**).

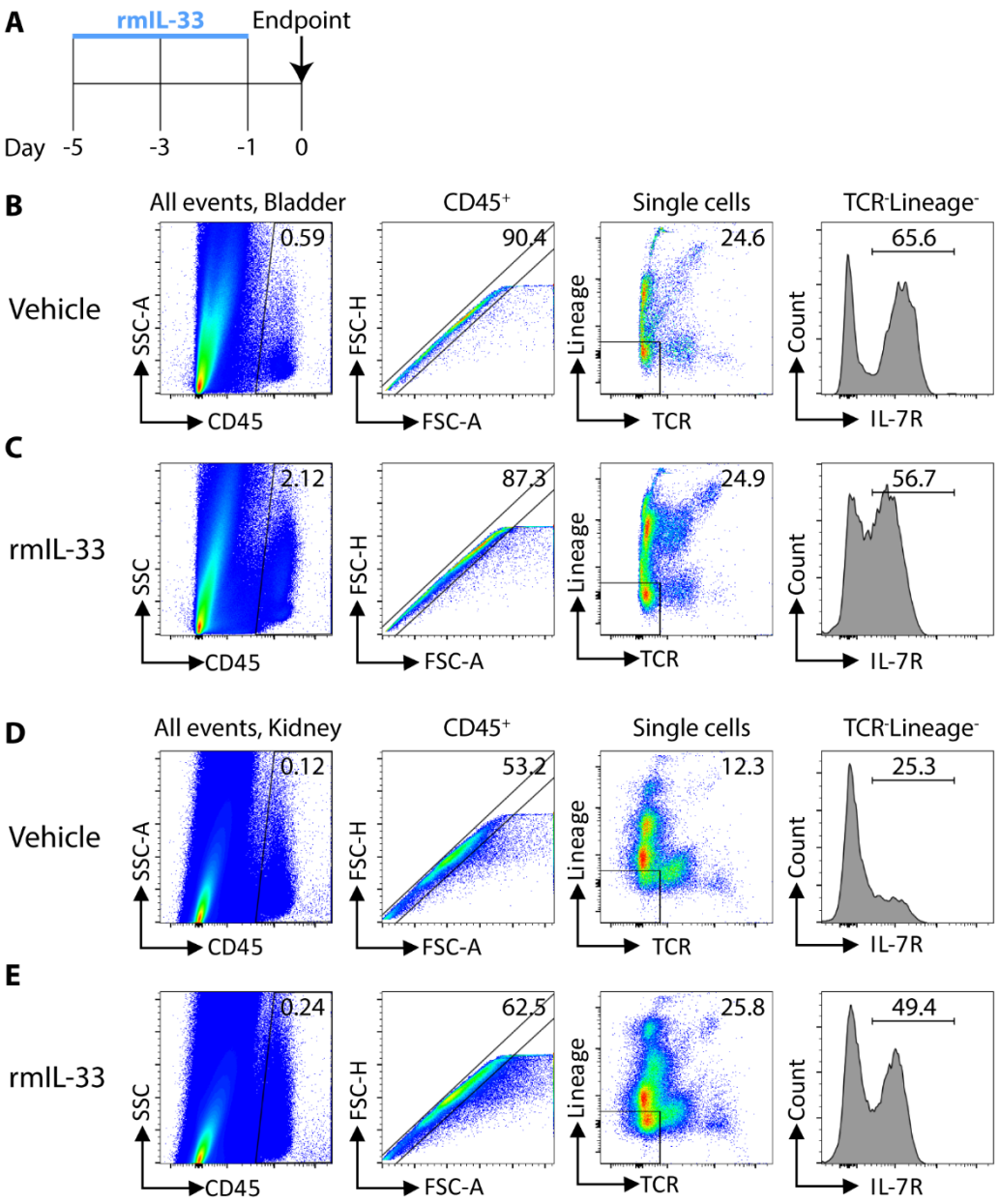

Figure 26: ILC are present in the mouse urinary bladder and kidney in homeostasis

(A) Schematic representation of rmIL-33 pre-treatment model. Representative images from single cell suspensions from female C57BL/6ausb mice, n=6, gated for ILC ($CD45^+Lineage^-$ [TCR^-[$TCR\alpha\beta^-TCR\gamma\delta^-CD8^-CD4^-$]$CD11b^-GR\text{-}1^-B220^-TER\text{-}119^-CD3^-NK\text{-}1.1^-$]$IL\text{-}7R\alpha^+$ single cells) in the urinary bladder after **(B)** vehicle and **(C)** rmIL-33 treatment. ILC2 in the kidneys from the same animals after **(D)** vehicle and **(E)** rmIL-33 treatment. Percentages are indicative of the average from n=6.

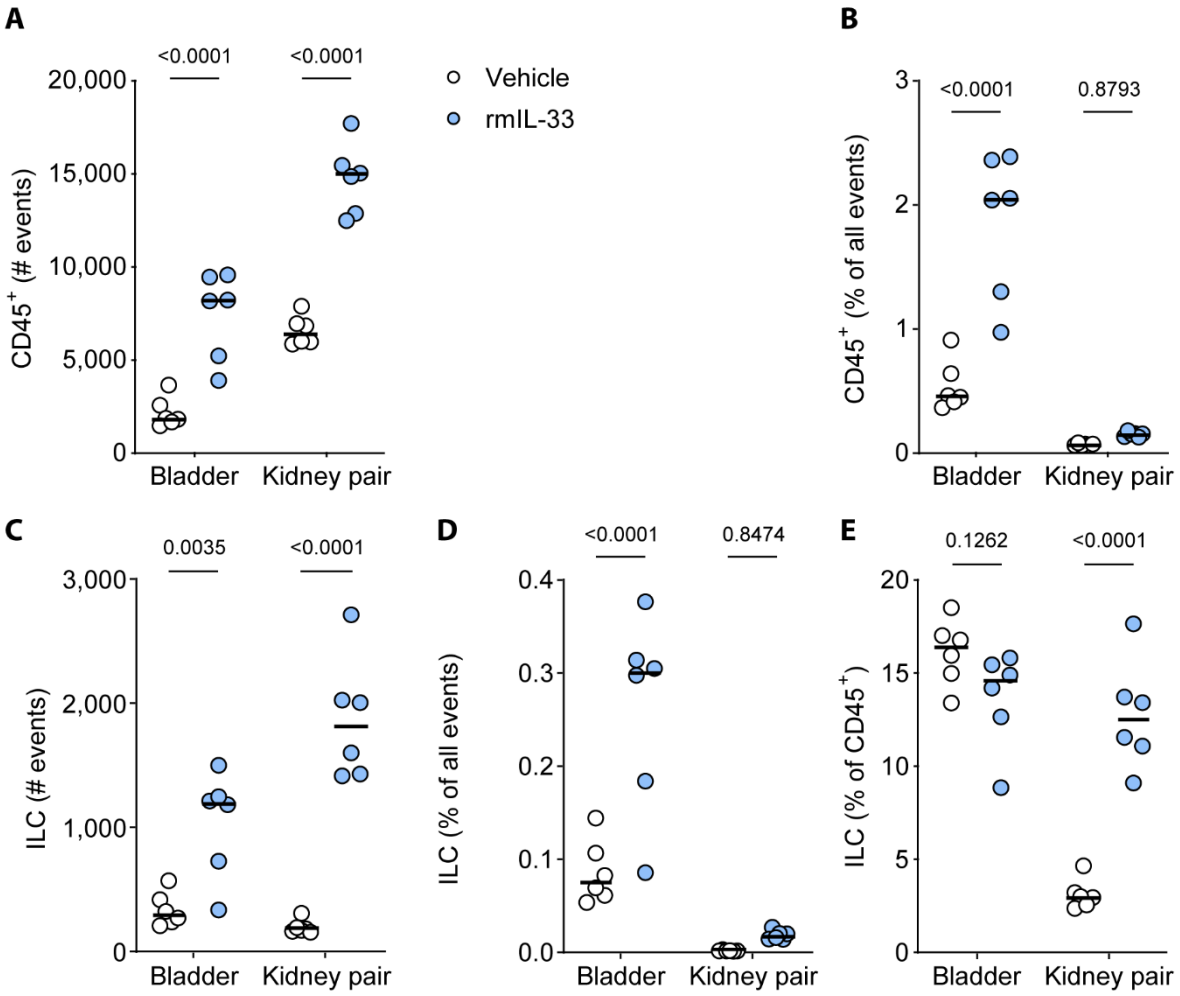

Figure 27: ILC are increased in the urinary bladder and kidney by rmIL-33 treatment

Single cell suspensions from female C57BL/6ausb mice, n=6, urinary bladder and kidneys after vehicle and rmIL-33 treatment were gated for gated for **(A)** $CD45^+$ single cells represented as raw numbers of total events from tissues and **(B)** as a percentage of total events. **(C)** ILC ($CD45^+Lineage^-[TCR^-[TCR\alpha\beta^-TCR\gamma\delta^-CD8^-CD4^-]CD11b^-GR\text{-}1^-B220^-TER\text{-}119^-CD3^-NK\text{-}1.1^-$]$IL\text{-}7R\alpha^+$ single cells) represented as raw numbers, **(D)** as a percentage of total events and **(E)** as a percentage of $CD45^+$ single cells. Percentages are indicative of the average from n=6, *P*-values from unpaired Two-Way ANOVA (Mixed Model) with Šídák correction for multiple comparisons, solid line indicates median.

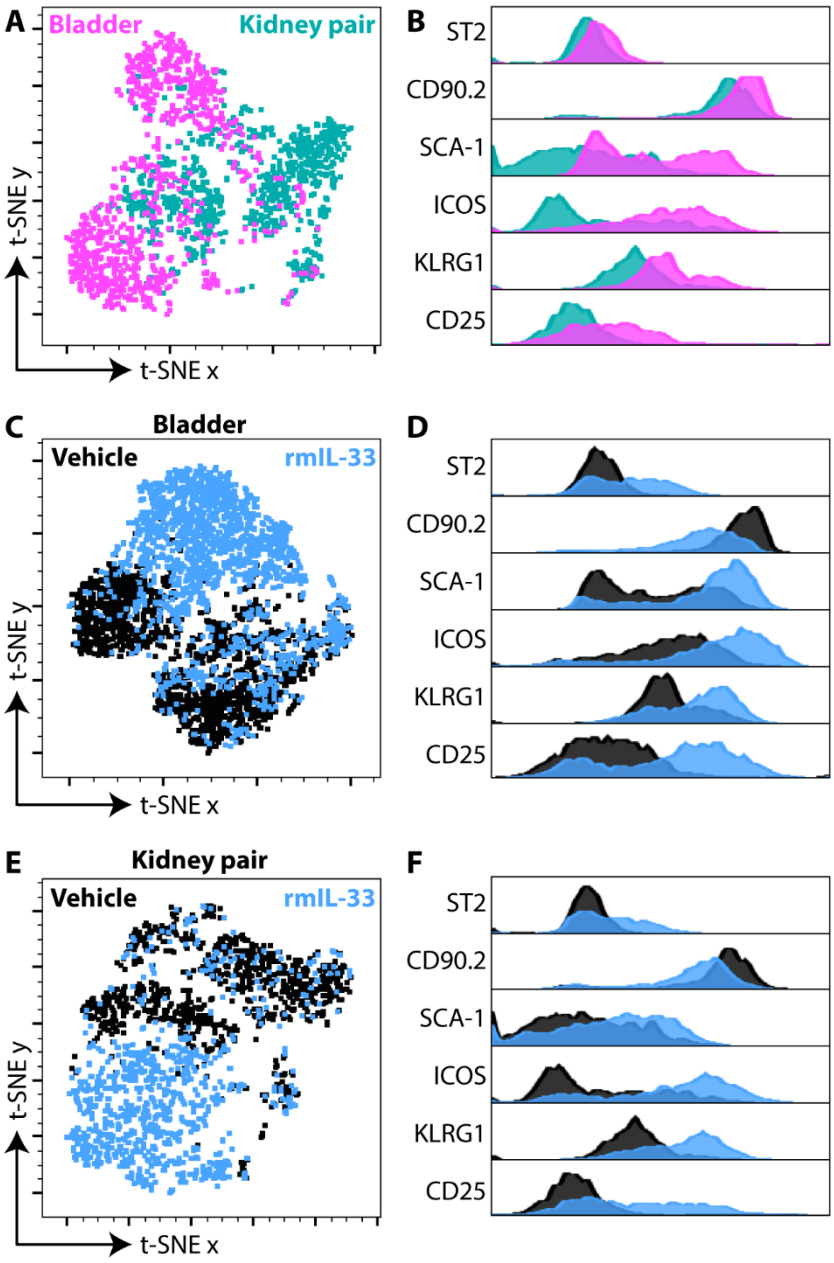

Figure 28: ILC have a unique signature in the urinary bladder compared to the kidney

(A) Single cell suspensions from female C57BL/6ausb mice, n=6, urinary bladder and kidneys were gated for ILC ($CD45^+Lineage^-[TCR^-[TCR\alpha\beta^-TCR\gamma\delta^-CD8^-CD4^-]CD11b^-GR\text{-}1^-B220^-TER\text{-}119^-CD3^-NK\text{-}1.1^-]IL\text{-}7R\alpha^+$ single cells) and compared to one another using t-distributed stochastic neighbor embedding (t-SNE) analysis based on **(B)** their expression of cell surface markers including ST2, CD90.2, SCA-1, ICOS, KLRG1 and CD25. **(C)** Bladder ILC were compared between vehicle and rmIL-33 treatment using t-SNE based on **(D)** their cell surface

expression. **(E)** Kidney ILC were compared between vehicle and rmIL-33 treatment using t-SNE based on **(F)** their cell surface expression. Percentages indicate the average of n=6.

After profiling all ILC, the data was reinterpreted specifically for the ILC2 compartment which are primarily responsive to rmIL-33. ILC2 were gated as $CD45^+$ single cells expressing IL-7Rα, CD90.2 and ST2 but not lineage markers in the bladder and kidney (**Figure 29A-D**). In both tissues, rmIL-33 substantially increased ILC2 in female and male mice, these were represented as proportion of $CD45^+$ single cells as it was most consistent across all experiments; although it is acknowledged that collagenase digestion may not release all immune cells from tissue (**Figure 30A,B**). Additionally, the ILC2 phenotype was altered in both tissues as the median fluorescence intensity (MFI) of ST2, SCA-1, ICOS and CD25 was substantially increased by rmIL-33, yet CD90.2 was significantly decreased in female mice (**Figure 30C-L**).

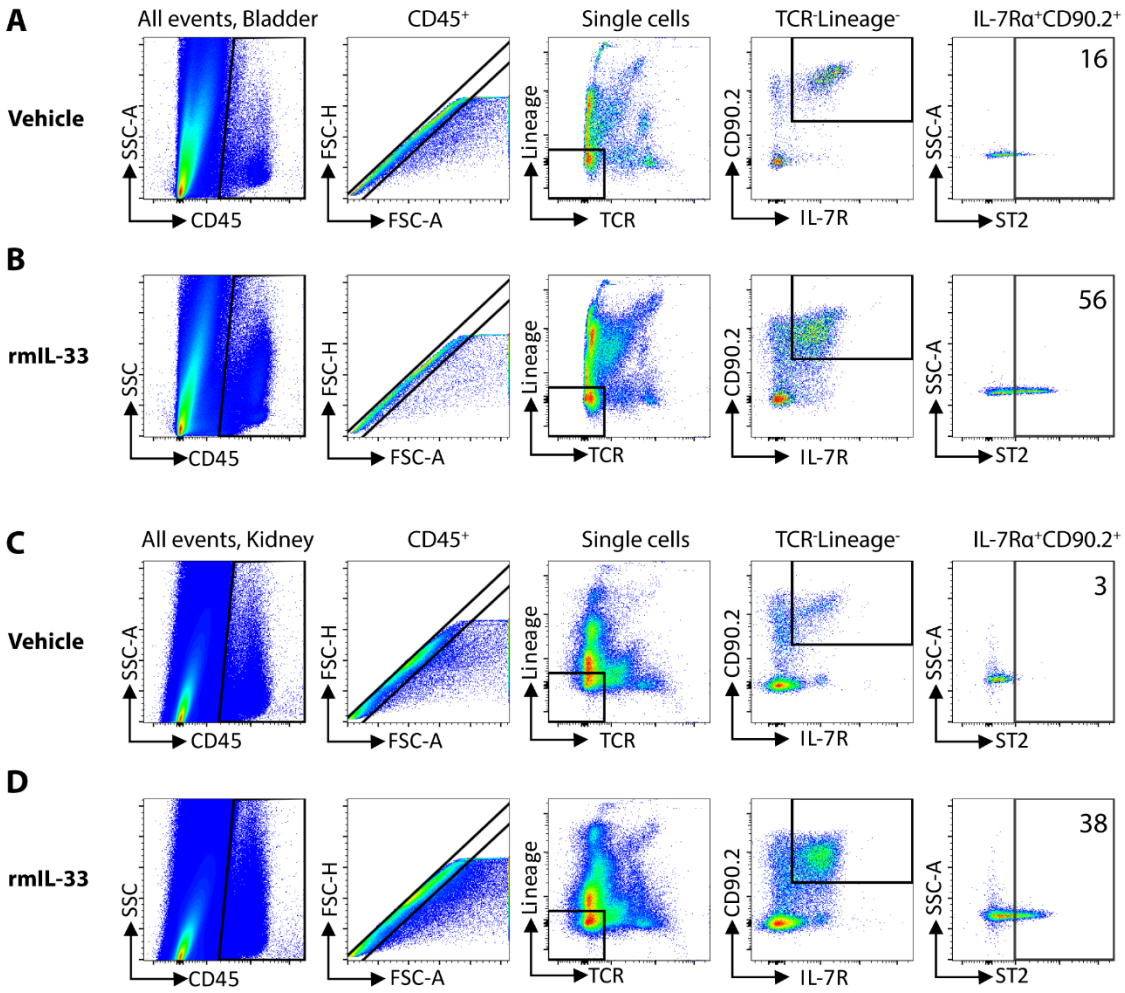

Figure 29: Flow cytometry gating strategy for urinary bladder and kidney mouse ILC2

Representative images from single cell suspensions from female C57BL/6Jausb mice, n=6, gated for ILC2 ($CD45^+Lineage^-[TCR^-[TCR\alpha\beta^-TCR\gamma\delta^-CD8^-CD4^-]CD11b^-GR\text{-}1^-B220^-TER\text{-}119^-CD3^-NK\text{-}1.1^-]IL\text{-}7R\alpha^+CD90.2^+ST2^+$ single cells) in the urinary bladder after **(A)** vehicle and **(B)** rmIL-33 treatment. ILC2 in the kidneys from the same animals after **(C)** vehicle and **(D)** rmIL-33 treatment. Percentages are indicative of the average from n=6.

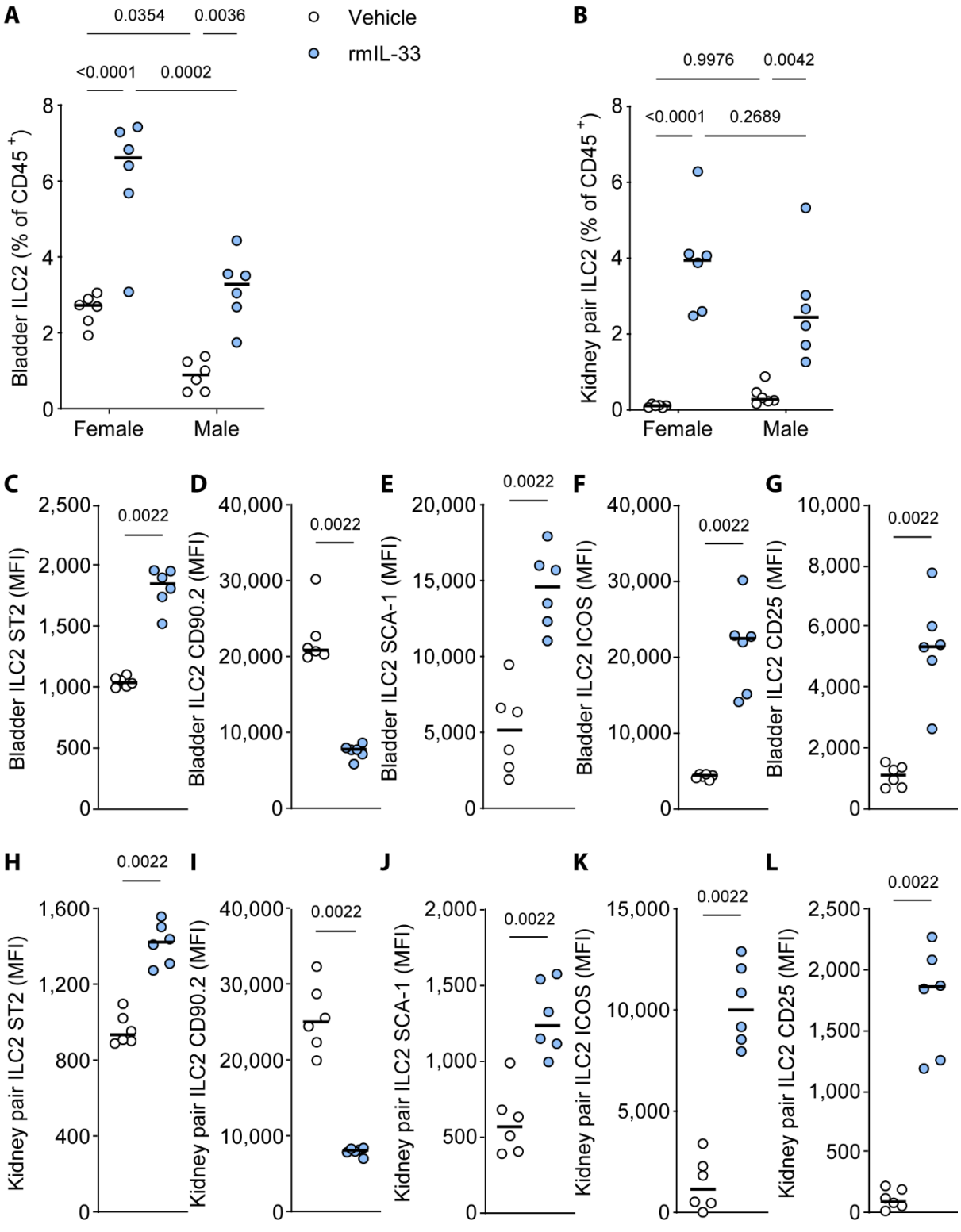

Figure 30: ILC2 number and cell surface markers in mouse bladder and kidney are altered by rmIL-33

Single cell suspensions from male and female C57BL/6Jausb mice, n=6, gated for ILC2 ($CD45^+Lineage^-[TCR^-[TCR\alpha\beta^-TCR\gamma\delta^-CD8^-CD4^-]CD11b^-GR\text{-}1^-B220^-TER\text{-}119^-CD3^-NK\text{-}1.1^-$

]IL-7Rα^{+}CD90.2^{+}ST2^{+} single cells) after rmIL-33 or vehicle in the **(A)** urinary bladder and **(B)** kidney pair, numbers shown as a proportion of CD45^{+} single cells; *P*-values from unpaired Two-Way ANOVA (Mixed Model) with Šídák correction for multiple comparisons. In female mice, the median fluorescence intensity (MFI) of cell surface markers ST2, CD90.2, SCA-1, ICOS and CD25 is shown in the **(C-G)** bladder and **(H-L)** kidney pairs of the same animals; *P*-values from *P*-values from unpaired Mann-Whitney test, solid line indicates median, n=6 (MFI for male mice not shown).

After finding that ILC2 are present in the murine urinary bladder under homeostatic conditions, I set out to determine their localisation within the tissue. My previous work has demonstrated that IL-5 was an effective marker to determine the location of ILC2 in the kidney, therefore I firstly assessed whether this remained true for the bladder [366]. In a preliminary analysis utilizing mice that express an IL-5 linked cre-recombinase crossed to a Rosa-tdtomato lineage tracker, ILC2 were the primary IL-5 expressing cell compared to T-cells which were accountable for <10% of the signal with vehicle or rmIL-33 treatment (**Figure 31A,B**). Therefore, IL-5 was used as a surrogate marker to identify the location of ILC2. IL-5 positive cells, predominantly ILC2, were primarily localized to the vasculature under the luminal surface of the bladder, as visualised with CD31 staining (**Figure 32A,B**). ILC2 were largely not in close proximity with the lymphatics, as visualised with LYVE1 staining (**Figure 32B,C**).

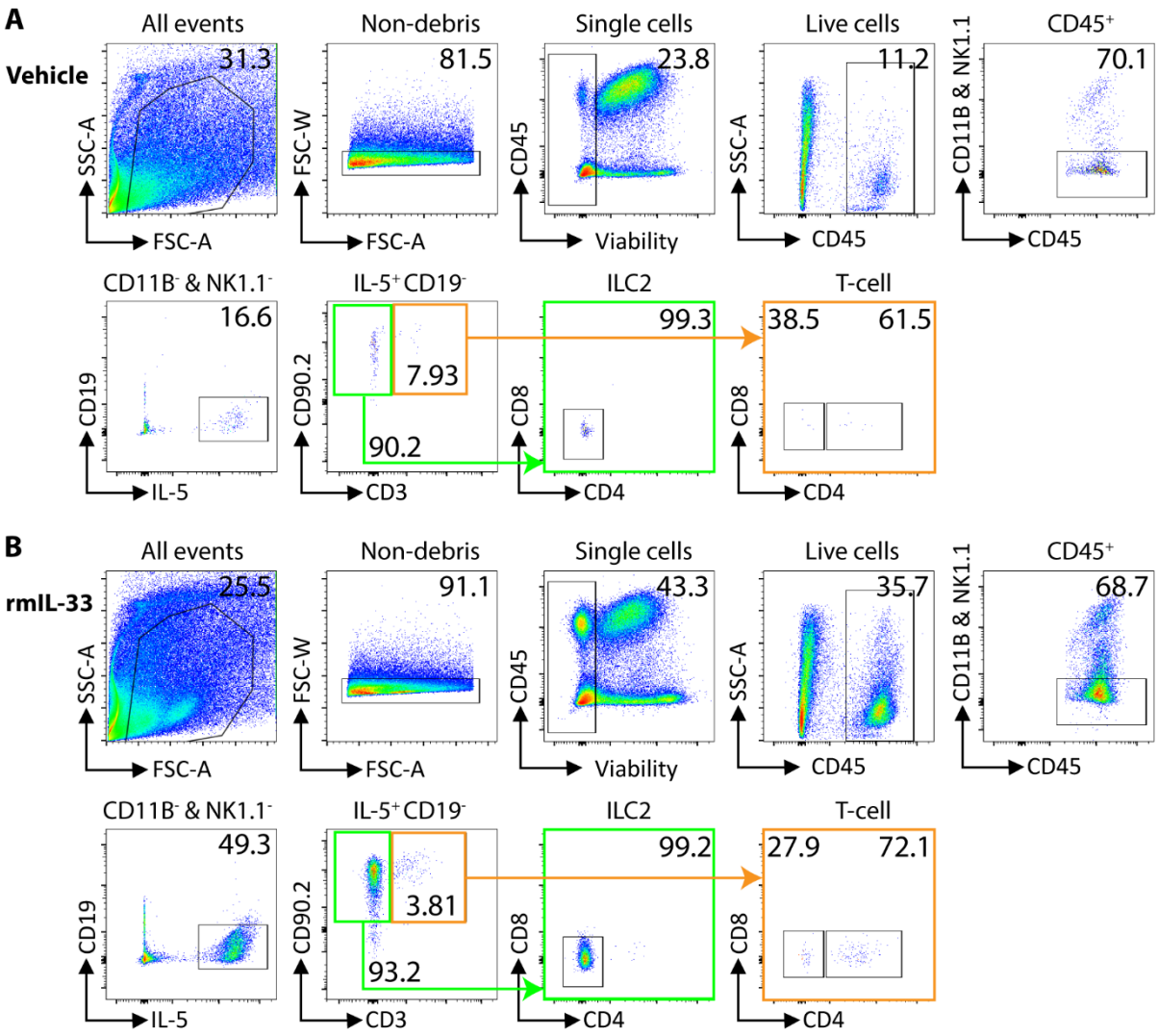

Figure 31: Urinary bladder ILC2 are the primary source of IL-5 compared to T-cells

Single cell suspensions from female *Il5*$^{\text{td-tomatoCre}}$; Rosa-CAG-RFP mice, n=1, gated for ILC2 ($CD45^+CD11B^-NK\text{-}1.1^-IL\text{-}5^+CD19^-CD90.2^+CD3^-CD4^-CD8^-$ single cells) and T-cells ($CD45^+CD11B^-NK\text{-}1.1^-IL\text{-}5^+CD19^-CD90.2^+CD3^+$ single cells) in the urinary bladder after **(A)** vehicle and **(B)** rmIL-33 treatment. Percentages are indicative of n=1.

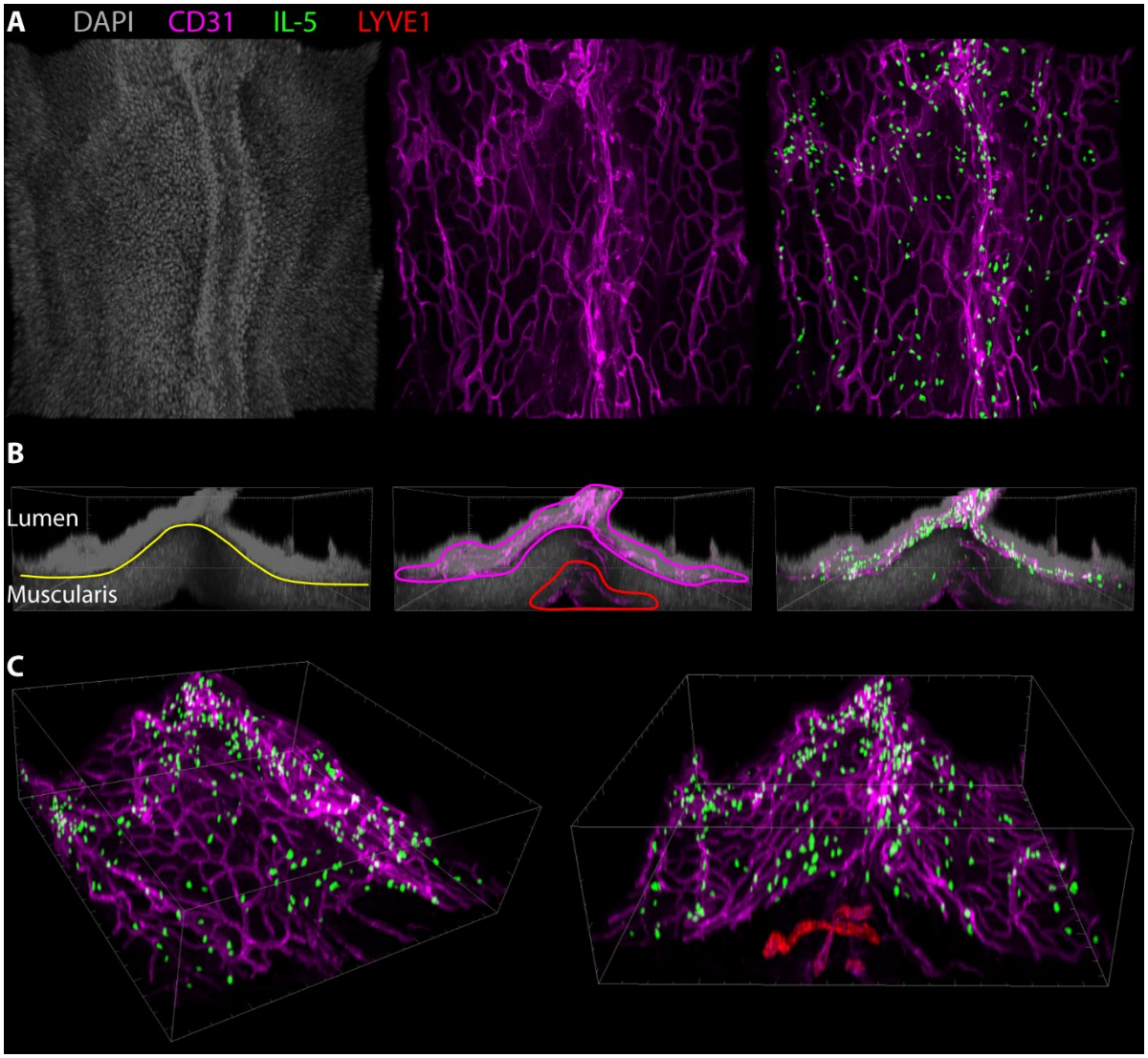

Figure 32: Bladder ILC2 are localised around the vasculature in homeostasis

Bladder sections from *Il5*$^{td\text{-}tomatoCre}$; Rosa-CAG-RFP mice, n=2, were stained for IL-5^{+} cells (predominantly ILC2), the IL-5^{+} pixel surface area was increased to improve clarity, tissue sections were co-stained for DAPI for structure determination, CD31 staining indicates vasculature, and LYVE1 staining indicates lymphatics. **(A)** Top down view of the bladder lumen with DAPI only (left), CD31 only (middle) and CD31 with IL-5 (right) staining. **(B)** Side view with DAPI only (left), DAPI, CD31, LYVE1 (middle) & CD31 and DAPI, CD31 & LYVE1 with IL-5 (right) staining where ILC2 were localised to the bladder lumen, not the muscularis; circled sections show primary location of CD31^{+} stained region (magenta) and

LYVE1^{+} stained region (red). **(C)** Rotated views to clearly demonstrate the tissue architecture (left and right).

Infection of naïve mice with UTI89 resulted in increased IL-33 protein levels in the bladder and kidney (**Figure 33A,B**). Since I had already shown that ILC2 could be increased in the urinary bladder and kidney of female mice, a pilot study was performed to explore whether ILC2-depletion had any impact on UTI. Female *Icos*$^{dtr/+}$*Cd4*$^{cre/+}$ were pre-treated intraperitoneally with 0.5µg rmIL-33 every 2nd day for 6 days or 0.025ng kg^{-1} diphtheria toxoid (DTx) daily for 7 days and were assessed by flow cytometry; vehicle controls received saline. There were no adverse effects from either treatment, and results were obtained only on the specified endpoints. There were no statistical differences in the increase or decrease of ILC2 after rmIL-33 or DTx in the bladder and kidney (**Figure 34A-D**). The UTI model was performed in *Icos*$^{dtr/+}$*Cd4*$^{cre/+}$ with DTx or vehicle, as described above; though there was no obvious differences in the bladder or kidney CFU (**Figure 35A,B**). Since the rmIL-33 treatment seemed to induce a stronger response and associated phenotype, it was focused on instead for future experiments.

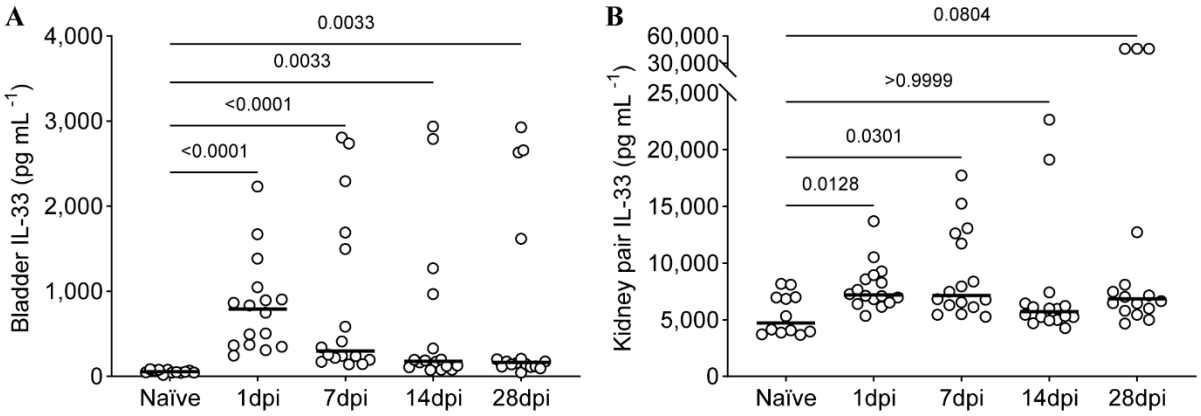

Figure 33: IL-33 is increased in the mouse urinary tract after experimental cystitis

Female C57BL/6Jausb mice were infected *via* transurethral inoculation of uropathogenic *Escherichia coli* clinical isolate UTI89 at ≈10^7 colony forming units (CFU) and were assessed at the specified days post-infection (dpi). **(A)** Bladder and **(B)** kidney pair IL-33 protein levels; data pooled from 4 independent experiments of n=4 (total n=16 per infection timepoint) and 2 experiments of n=3-6 naïve, solid line indicates median, *P*-values from unpaired Kruskal-Wallis test with Dunn's multiple comparisons.

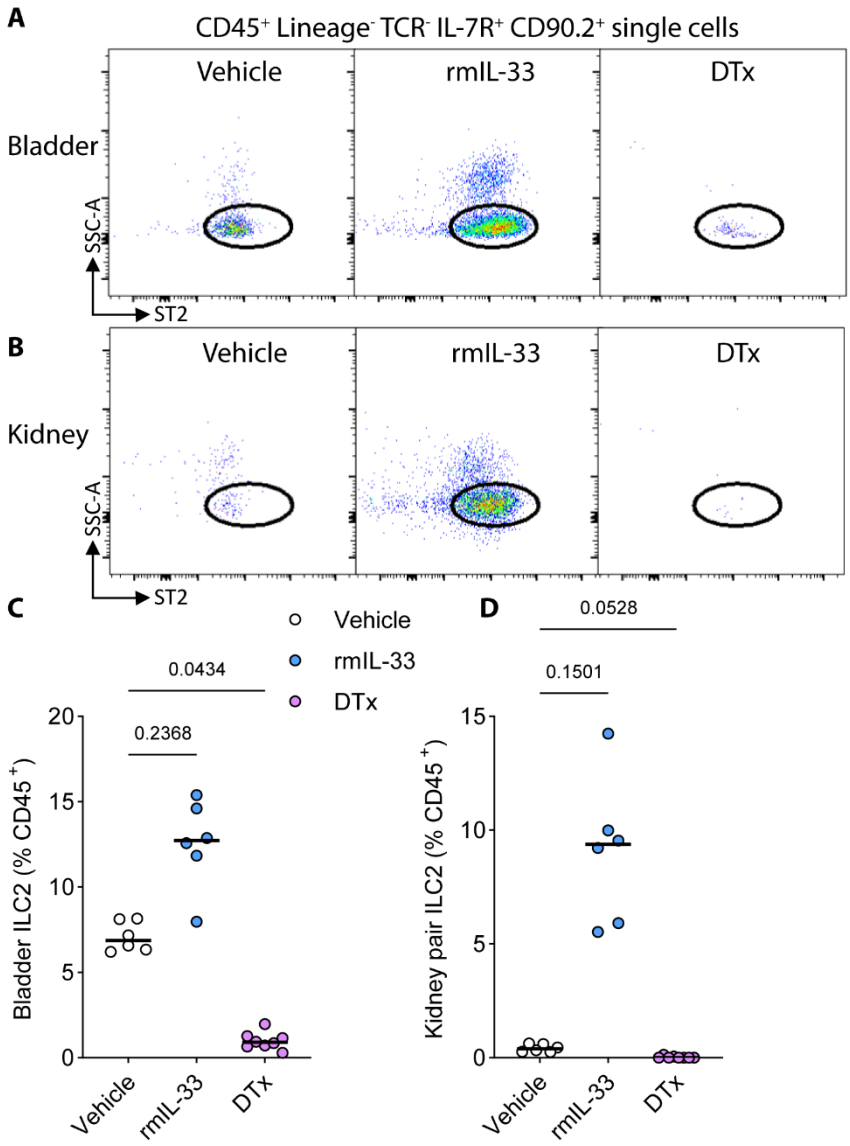

Figure 34: ILC2 expansion and depletion in the urinary bladder and kidney

Representative images from single cell suspensions from female *Icos*$^{dtr/+}$*Cd4*$^{cre/+}$ treated with vehicle, rmIL-33 or diphtheria toxoid (DTx), n=4, and were gated for ILC2 (CD45$^+$Lineage$^-$ [TCR$^-$[TCRαβ$^-$TCRγδ$^-$CD8$^-$CD4$^-$]CD11b$^-$GR-1$^-$B220$^-$TER-119$^-$CD3$^-$NK-1.1$^-$]IL-7Rα$^+$CD90.2$^+$ ST2$^+$ single cells) in the **(A)** urinary bladder and **(B)** kidney and the proportion of ILC2 in the **(C)** urinary bladder and **(D)** kidney; solid line indicates median, *P*-values from unpaired Kruskal-Wallis test with Dunn's multiple comparisons.

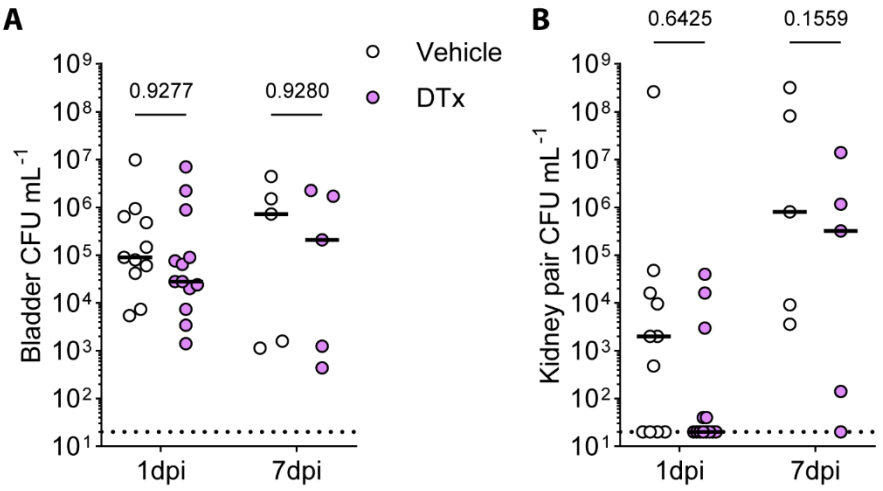

Figure 35: ILC2 depletion does not significantly alter UTI

Female *Icos*$^{dtr/+}$*Cd4*$^{cre/+}$ mice were pre-treated with DTx or vehicle and were infected *via* transurethral inoculation of uropathogenic *Escherichia coli* clinical isolate UTI89 at ≈10^7 colony forming units (CFU) and were assessed at the specified days post-infection (dpi). **(A)** urinary bladder and **(B)** kidney CFU mL^{-1}, n=12 at 1dpi, n=5 at 7dpi; solid line indicates median, *P*-values from unpaired Mann-Whitney test.

In the rmIL-33 UTI model, 9/84 C57BL/6 mice which received rmIL-33 were culled due to weight loss, as per ethical requirements (**Figure 36A,B**). There was a significant difference in weight loss with rmIL-33 pre-treatment compared to vehicle-treated controls throughout the course of infection (**Figure 36C**). There were no statistical differences in bladder CFU (**Figure 36D**). However, kidney CFU were significantly increased by rmIL-33 pre-treatment at 7 days post-infection (dpi) (**Figure 36E**). Similarly, the proportion of animals with an active kidney infection was significantly greater at 7 and 14dpi compared to vehicle-treated controls (**Figure 36F**).

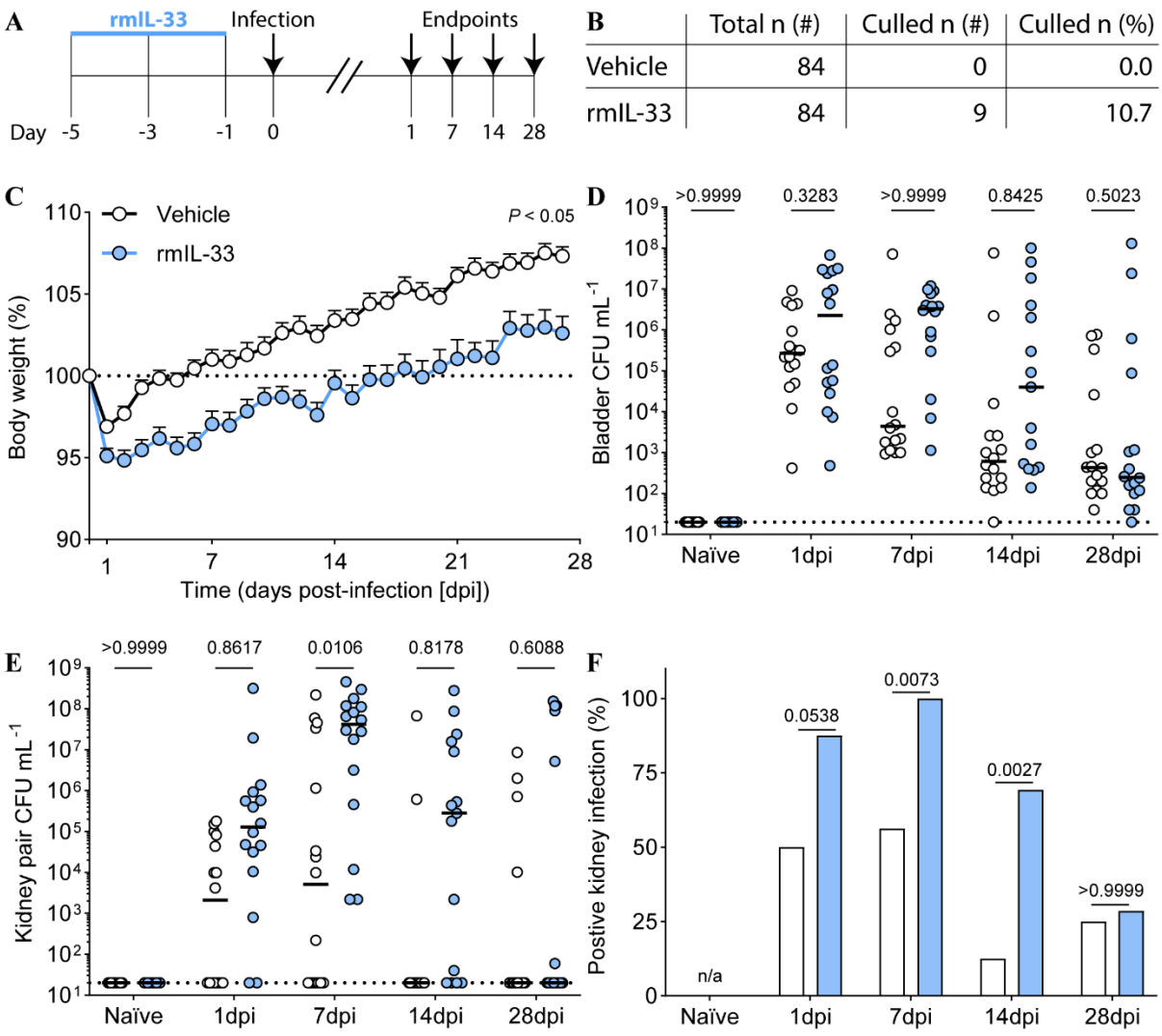

Figure 36: rmIL-33 exaggerated pyelonephritis in a model of experimental cystitis

(A) Schematic of the model whereby female C57BL/6Jausb mice were infected *via* transurethral inoculation of uropathogenic *Escherichia coli* clinical isolate UTI89 at ≈10^7 colony forming units (CFU) and were assessed at the specified days post-infection (dpi). **(B)** 84 animals were randomly allocated to each of the treatment arms (6 independent experiments of at least n=4, total n=16 for 1, 7, 14dpi and n=36 at 28dpi), 9 were culled as per ethical requirements. **(C)** Body weight throughout the infection time course, as a percentage of weight at day 0 prior to infection; bars indicate standard error of the mean, *P*-value from unpaired Two-Way ANOVA (Mixed Model) with Šídák correction for multiple comparisons. **(D)** Bladder and **(E)** kidney pair CFU mL^{-1}; dotted line represents the limit of detection (LOD)

of 20 CFU mL^{-1}, solid line indicates median, *P*-values from unpaired Two-Way ANOVA (Mixed Model) with Šídák correction for multiple comparisons, CFU pooled from 4 independent experiments of n=4 (total n=16 per infection timepoint, per group) and 2 experiments of n=3-6 naïve. **(F)** Percentage of animals which had any level of kidney infection, termed positive kidney infection; data recapitulated from E, *P*-values from individual Chi-squared (Fisher's exact) tests per timepoint.

To assess the effect of exogenous IL-33 on infection, mice were pre-treated with rmIL-33 prior to transurethral inoculation with UTI89. Interestingly, rmIL-33 treatment caused a small, yet consistent and statistically significant increase in body weight (**Figure 37A**). As a consequence, on day 0 of the model, immediately prior to the infection the animals which received rmIL-33 had an increased body weight on average (**Figure 37B**). This observation was only made after completion of the experimental work. In naïve animals, rmIL-33 activity was confirmed by increased serum and bladder IL-5 protein levels, although there was negligible impact in the kidney (**Figure 38A-C**).

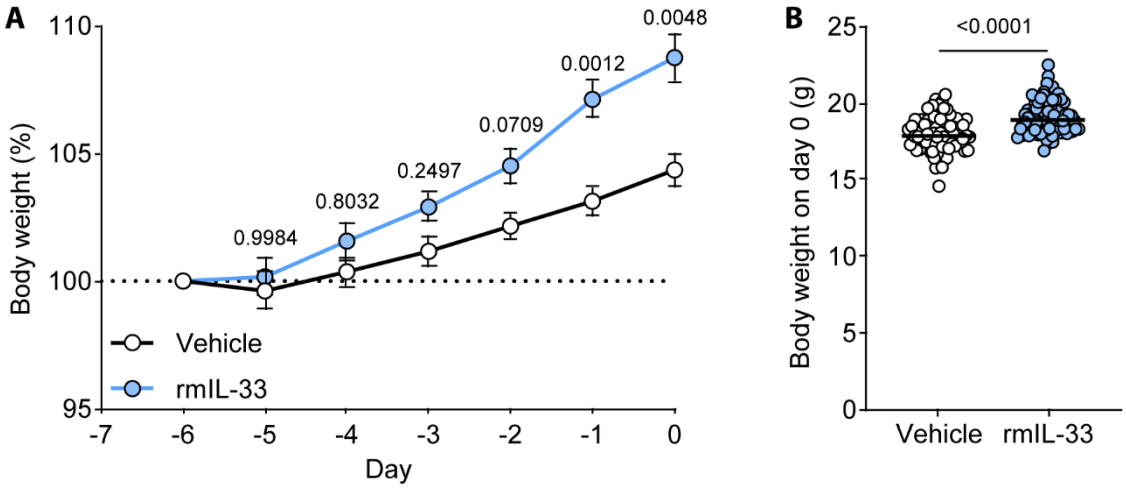

Figure 37: rmIL-33 pre-treatment increased mouse body weight

Female C57BL/6Jausb mice were pre-treated with rmIL-33 or vehicle on day -6, day -4 and day -2, **(A)** body weight was measured immediately prior to treatment and visualised as percentage change from day -6; data pooled from 4 independent experiments of n=4 (total n=16 per group), *P*-values from unpaired Two-Way ANOVA (Mixed Model) with Šídák correction for multiple comparisons. **(B)** Body weight was measured on day 0 of the model, immediately prior to infection; solid line indicates median, data pooled from 4 independent experiments of n=4 (n=16 per timepoint, per group), *P*-value from unpaired parametric T-test.

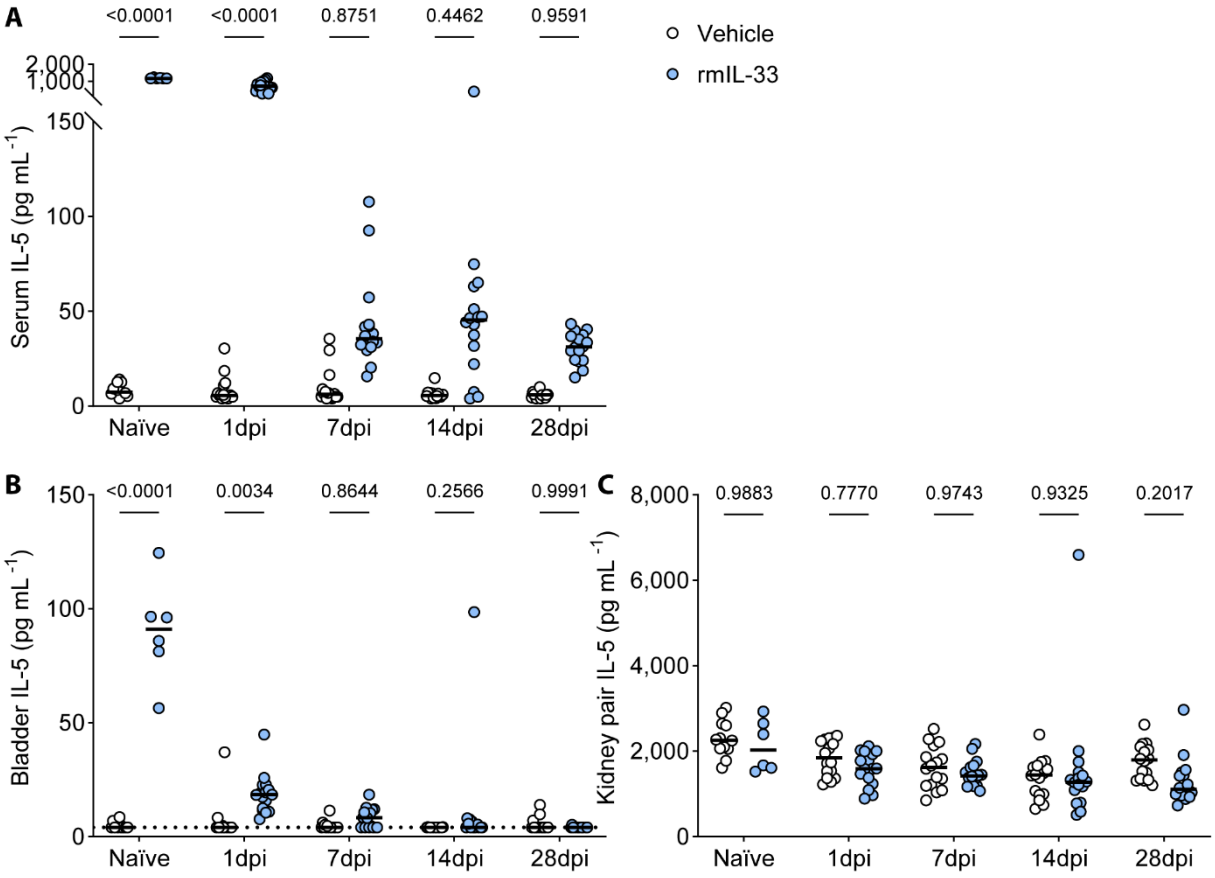

Figure 38: IL-5 is systemically increased by rmIL-33 treatment

Female C57BL/6Jausb mice were infected *via* transurethral inoculation of uropathogenic *Escherichia coli* clinical isolate UTI89 at ≈10^7 colony forming units (CFU) and were assessed at the specified days post-infection (dpi) for **(A)** serum, **(B)** bladder and **(C)** kidney IL-5

protein levels; data pooled from 4 independent experiments of n=4 (total n=16 per infection timepoint, per group) and 2 experiments of n=3-6 naïve, solid line indicates median, *P*-values from unpaired Two-Way ANOVA (Mixed Model) with Šídák correction for multiple comparisons.

To examine the functional impact of pyelonephritis, FITC-Sinistrin clearance was used to measure baseline *t*GFR and changes throughout the course of infection (**Figure 39A**). The clearance of FITC-Sinistrin determined by fluorescent decay prior to infection and weekly after infection was notably different in some animals, especially those that received rmIL-33 pre-treatment (**Figure 39B**). This visual difference was reciprocated by the FITC-Sinistrin half-life and was significantly increased with rmIL-33 at 21 and 28dpi (**Figure 39C**). Likewise, the *t*GFR in these animals was significantly decreased at 14, 21 and 28dpi (**Figure 39D**). However, serum BUN was unable to detect kidney function impairment at 28dpi (**Figure 39E**). rmIL-33 pre-treatment increased kidney histopathology compared to vehicle-treated controls (**Figure 39F**). Semi-quantitative scoring showed a significant increase to tubular injury with rmIL-33 pre-treatment (**Figure 39G**).

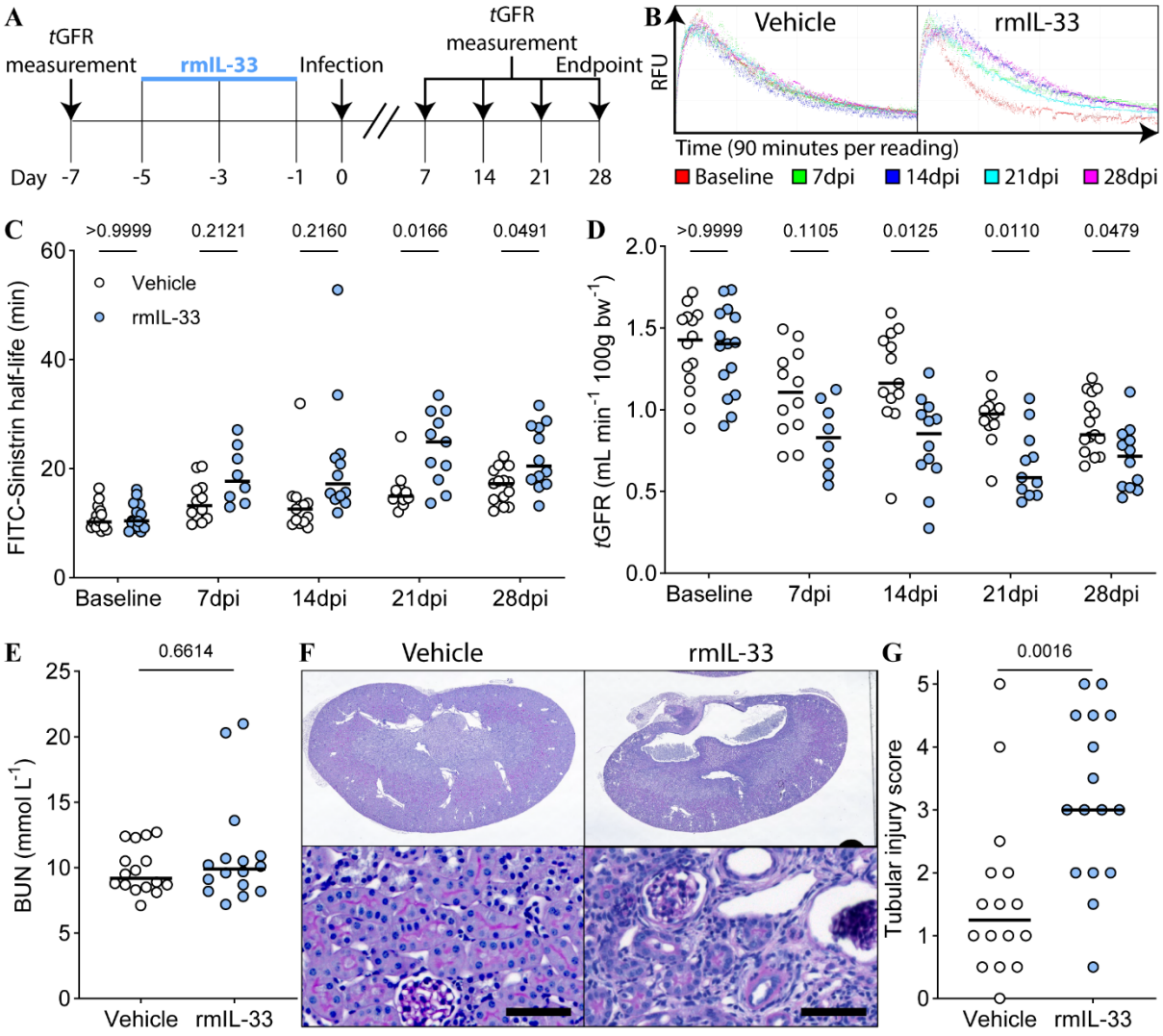

Figure 39: rmIL-33 exaggerated pyelonephritis impaired structure and function of the mouse kidney

(A) Schematic of the model whereby female C57BL/6Jausb mice had their baseline transcutaneous glomerular filtration rate (*t*GFR) measured, were infected *via* transurethral inoculation of uropathogenic *Escherichia coli* clinical isolate UTI89 at ≈10^7 colony forming units (CFU) and the *t*GFR was assessed at the specified days post-infection (dpi). **(B)** Representative images of FITC-Sinistrin clearance over 90 minutes (min) in one mouse from vehicle (left panel) or rmIL-33 (right) at baseline and weekly after infection. **(C)** FITC-Sinistrin half-life in minutes and **(D)** *t*GFR derived from C and corrected for body weight (bw); solid line indicates median, *P*-values from paired Two-Way ANOVA (Mixed-effects analysis)

with Šídák correction for multiple comparisons. **(E)** Blood urea nitrogen (BUN) concentration at 28dpi; solid line indicates median, *P*-values from unpaired Mann-Whitney test. **(F)** Representative images of whole kidneys (top panel) and zoomed in sections of cortex (bottom) from vehicle (left) and rmIL-33 (right), and **(G)** tubular injury score derived from F; solid line indicates median, *P*-values from unpaired Mann-Whitney test. Data pooled from 4 independent experiments of n=4 (total n=16 per group); scale bars indicate 50μm.

To explore why rmIL-33 treatment induced such a deleterious response, the literature was explored to determine which factors should be explored in this model. A critical role for IL-17A was recently discovered for appropriate clearance of uropathogens [203, 297]. However, the functionally similar IL-22 is released by analogous subsets of immune cells such as group 3 innate lymphoid cells, γδ T cells, and T helper 17/22 cells, but IL-22 had not been explored by these studies [203, 290, 297]. Using the rmIL-33 model, IL-22 was found to be increased at 7dpi in the bladder (**Figure 40A**). Intriguingly, IL-22 was decreased in the kidney at 28dpi (**Figure 40B**). These observations were further explored in **Chapter 5**.

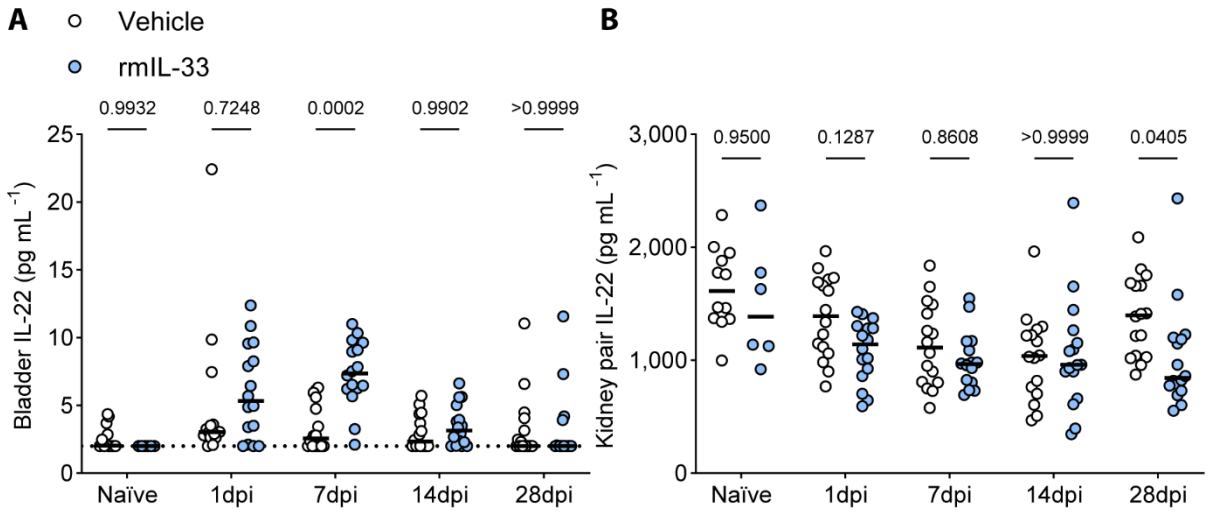

Figure 40: Exogenous IL-33 caused IL-22 levels to increase in the bladder but decrease in the kidney

Female C57BL/6Jausb mice were infected *via* transurethral inoculation of uropathogenic *Escherichia coli* clinical isolate UTI89 at ≈10^7 colony forming units (CFU) and were assessed at the specified days post-infection (dpi). **(A)** Bladder and **(B)** kidney pair IL-22; dotted line represents the limit of detection (LOD) of 4pg mL^1, solid line indicates median, *P*-values from unpaired Two-Way ANOVA (Mixed Model) with Šídák correction for multiple comparisons, data pooled from 4 independent experiments of n=4 (total n=16 per infection timepoint, per group) and 2 experiments of n=3-6 naïve.

4.5 Discussion

Here I describe a body to work around understanding the role of ILC2 in the urinary tract under homeostatic conditions, and in a model of cystitis with rmIL-33 treatment. Flow cytometric profiling revealed that systemic rmIL-33 was sufficient to increase leukocytes in the urinary bladder in addition to the kidney, suggesting that the recombinant cytokine was able to reach the bladder. After determining that ILC were greatly increased in both tissues, the phenotype of these cells was investigated and compared to one another using t-SNE, an unbiased and

unsupervised method to compare the tissues. Although not entirely distinct, there was substantial differences in the cell surface marker profile. In each tissue, the ILC seemed to cluster into two separate areas suggesting there may be two main types of ILC subsets which made up the homeostatic ILC in both tissues, with the other ILC not clustering tightly with either group. Based on my earlier published work, and that of others, I expected to find that ILC2 made up a major population in the kidney and may therefore be the same for the urinary bladder. When comparing and contrasting multiple ILC2 related cell surface markers in both tissues, I determined that ILC2 made up a major ILC population since there was noteworthy expression of ST2 and CD90.2 in particular, but also SCA-1, ICOS, KLRG1 and CD25 which are known to be expressed by ILC2 in other tissue sites. When assessing rmIL-33 treatment in both tissues I noted that the ILC seemed polarised primarily into one cluster rather than the two observed with vehicle treatment, again indicative that the rmIL-33 was causing expansion of the ILC2. Consistent with this theory there were increases to each of the ILC2 surface markers, except for CD90.2 which was significantly decreased. Although I am unable to explain why this has occurred, one theory is that the ILC downregulate CD90.2 to allow increased plasticity towards an ILC2 phenotype, similar to that described for multipotent progenitor cells [367]. Indeed, when reinterpreting these data for ILC2 rather than all ILC subsets I found that ILC2 were indeed present within the urinary bladder and kidney, and that ILC2 were increased by rmIL-33. Again, several ILC2 cell surface markers were increased, yet CD90.2 was considerably lower in line with my previous theory, though speculative at this stage.

Since the ILC2 are located within the urinary tract the next important step was to determine the specific localisation of these cells. My previous work utilised complex genetically modified mice with an IL-5 linked cre-recombinase crossed to a Rosa-tdtomato lineage tracker to determine the location in the kidney, yet this tool had not been validated for the urinary bladder [366]. In the proof-of-principal studies in these mice, ILC2 were the primary IL-5 expressing

cell compared to T-cells which were accountable for negligible IL-5 signal with vehicle or rmIL-33 treatment. Only 1 mouse was able to be allocated to each of the groups, in this experiment ILC2 were a major IL-5 expressing cell with and without exogenous IL-33; but these studies need to be repeated to ensure the data is valid and reproducible. Following on from these studies, the same animal strain provided important insights about the location of these cells in the urinary bladder. The bladder ILC2 were almost exclusively localised around the luminal vasculature which 'lit up' with IL-5 signal, from my preliminary analysis these would predominantly be ILC2. The final piece of the puzzle linking UTI to IL-33 and ILC2 was found during infection of untreated mice. This resulted in increased IL-33 protein levels in the bladder and kidney. Following on from this work, preliminary loss-of-function was performed using genetically modified animals which can be conditionally depleted of ILC2 by the administration of DTx. Whilst this was effective in my earlier work, it only caused a trend to reduce the numbers of ILC2 and did not induce any noteworthy changes to the kinetics of infection, therefore the amplification of ILC2 was utilised for subsequent studies.

Afterwards, the effect of exogenous IL-33 in the context of UTI was investigated using a pre-treatment regime prior to infection. Pre-treatment with rmIL-33 significantly increased bacterial load in the kidneys and the rate of pyelonephritis in the early to mid-phases of infection. Interestingly, IL-5 levels were not changed in the kidney, it is possible that small changes in cytokine levels are hidden by variability in kidney mass and that future experiments may need to optimise a method of normalisation. I also observed weight loss, an important clinical sign of pyelonephritis, although rmIL-33 did cause a small but notable increase to body weight without infection. However, upon further interpretation of these data after the completion of these studies, it became clear that exogenous IL-33 increased the weight of animals prior to infection; therefore, it is quite possible that the weight loss observed the result of the animals returning back to their homeostatic weight. Indeed, circulating levels of IL-33

is elevated by obesity in humans and weight loss improves asthma symptoms in patients [368, 369]. Nonetheless, pyelonephritis was sufficient to drive changes to kidney structure and function as demonstrated by histopathology and *in vivo* kidney function from *t*GFR measurement based on FITC-Sinistrin clearance. Additionally, *t*GFR had the advantage of being measured longitudinally without the need for continuous blood sampling required for BUN or other blood chemistry markers. Importantly, prolonged impairment of kidney function was not able to be recognized using BUN alone. This suggests that the infection-induced kidney injury was not severe enough for detection when using BUN as a biomarker. Clinically, this type of injury would be defined as sub-clinical, since there no biomarker involvement yet the kidney function has been reduced. Thus, I found that *t*GFR was a powerful tool to assess functional consequences of pyelonephritis in this model since pair-wise comparisons could be performed on these data.

There have been numerous studies that demonstrate rmIL-33 is protective against acute kidney injury in pre-clinical models such as ischemia-reperfusion injury with both prophylactic and therapeutic treatment regimes, reviewed in [347]. Whilst these studies are important, my data suggests caution if IL-33 therapeutics are to be considered for clinical use, since it may increase the likelihood of pyelonephritis. Similar to my work, a very recent study characterised T_H2 cells during experimental cystitis and found that type II immunity was detrimental in UTI, and that this biases immune response was exacerbated in subsequent infections, limiting the capacity of clear the infection [360]. Indeed, in my models I found that exogenous IL-33 increased pyelonephritis with a decrease in kidney IL-22 at the late stages of infection and is potentially related to IL-33 'switching off' other forms of immunity. Similarly, others have very recently found that exogenous IL-33 in the gut exacerbates infection and inhibits the protective IL-17A and T_H17 immunity [370]. Additionally, I found that bladder IL-22 levels were increased early in the infection model with exogenous IL-33. Is it plausible that this acts

to stimulate antimicrobial responses, to prevent formation of intracellular reservoirs. Alternatively, it is possible that these responses may act to prevent infection of the upper urinary tract and prevent pyelonephritis; yet it is not possible to determine from these data.

Future studies will need to determine the exact mechanism whereby enhanced type II immunity is detrimental for infection of the urinary tract. Additionally, the mechanism of IL-33-mediated pyelonephritis must be investigated before evaluating the emerging IL-33-mediated immunotherapies, such as those being trialled for atopic dermatitis, as a therapeutic for experimental pyelonephritis. Indeed, anti-IL-33 has been found to be effective in mice during a model of chronic lung inflammation driven by IL-33, and may therefore be effective in other contexts also [371]. In summary, I described a model utilising exogenous IL-33 for exacerbation of pyelonephritis in C57BL/6 mice which also caused impaired kidney function and histopathology.

Chapter 5: Treatment with recombinant interleukin-22 protects against uropathogenic *Escherichia coli*-induced pyelonephritis in mice

At the time of thesis submission, all results in this chapter are unpublished. Descriptions of methods or reagents are recapitulated from **Chapter 3** or **Chapter 4** where the work was performed identically. This work underwent peer review at the American Journal of Physiology - Renal Physiology and where possible, reviewer comments have been incorporated. Some of these results have been used to prepare a draft manuscript:

> **Cameron GJM***, Lawrence BM*, Loering S, Deshpande AV, Bhatt NP, Collison AM, Foster PS, Deshpande AV, Starkey MR. Treatment with recombinant interleukin-22 protects against uropathogenic *Escherichia coli*-induced pyelonephritis in mice. Immunol Cell Biol. 2021. * equal contribution, co-first author

Cameron GJM, Lawrence BM and Starkey MR conceptualised the manuscript. Jones-Freeman B assessed circadian rhythm. Cameron GJM and Lawrence BM performed the infection model, recombinant treatments and ELISA side-by-side with equal contribution. Cameron GJM performed all other aspects including gene expression analysis, data analysis and drafted the manuscript. Loering S assisted with animal monitoring. Bhatt NP assisted with centrifugation of samples. Collison AM, Deshpande AV and Foster PS advised on experimental design and review of the manuscript.

5.1 Abstract

Interleukin (IL)-22 is a multifaceted mucosal cytokine that can act as a double-edged sword, promoting tissue repair/regeneration or inflammation depending on the context. IL-22 is known to have pathological roles in diseases of the urinary tract, yet its role in urinary tract infection and associated kidney injury is largely unknown. Here, I show that low IL-22 protein levels in the kidneys were associated with pyelonephritis in a mouse model of experimental cystitis induced by the uropathogenic *Escherichia coli* clinical isolate UTI89. Under homeostatic conditions, the IL-22 receptor IL-22Rα was restricted to the urothelium of the urinary bladder, and to the tubules of the medulla and cortex of the mouse kidney. Treatment of naïve mice with recombinant mouse IL-22 (rmIL-22) for 3 days resulted in the phosphorylation of signal transducer and activator of transcription 3 (STAT3), a surrogate marker of IL-22 activity, in the kidney but not the urinary bladder. Therefore, the therapeutic effect of rmIL-22 in pyelonephritis was explored. When given prophylactically prior to infection, rmIL-22 was insufficient to cause any significant changes in bacterial burden or the proportion of animals that developed pyelonephritis. However, when administered 12 hours post-infection, rmIL-22 significantly reduced the rate of pyelonephritis at 3 days post-infection. These studies suggest that the timing of intervention is critical, yet future studies will need to expand upon this work to determine the most effective treatment regime. Further studies may also provide preclinical evidence to justify repurposing IL22-targeted immunotherapies, which are currently in phase II clinical trials for other diseases.

5.2 Introduction

Uropathogenic *Escherichia coli* is the causative agent for more than 80% of urinary bladder infections in humans, termed cystitis [357]. These bacteria can rapidly colonise the urothelial lining to establish quiescent intracellular communities and may also ascend causing infection of the kidneys, termed pyelonephritis [247, 256, 270]. Whilst antibiotic therapies are sufficient in most cases [190], the emerging threat of antimicrobial resistance has decreased the effectiveness of such interventions. A future approach for these patients may involve immunotherapies to complement existing antibiotic therapy.

Indeed, several recent studies have characterised the immunological state of the urinary tract in response to experimental infection in murine models, reviewed in [358]. Whilst a critical role for interleukin (IL)-17A has been discovered for appropriate clearance of uropathogens [203, 297], related cytokines are yet to be explored. IL-17A and the functionally similar IL-22 is known to be co-produced by analogous subsets of immune cells including group 3 innate lymphoid cells, γδ T cells, and T helper 17/22 cells [290]. Additionally, IL-17A is increased during experimental cystitis, yet the role of IL-22 in this system is not known [203].

A novel immunotherapy utilizing a recombinant human IL-22 is currently undergoing trial, therefore repurposing this immunotherapy for treating UTI may be a future avenue since IL-22 is known to have tissue protective and antimicrobial functions in other tissues [372-374]. Therefore, this study aimed to investigate whether IL-22 also plays an important role in the urinary tract by utilizing a murine model of experimental cystitis induced by uropathogenic *Escherichia coli*.

5.3 Methods

5.3.1 Mice

All procedures were approved by The University of Newcastle's animal care and ethics committee in accordance with the Australian code for the care and use of animals for scientific purposes. 7 to 10-week-old female C57BL/6Jausb wild-type mice were received from Australian Bioresources (ABR, Moss Vale, Australia). Mice were housed in specific pathogen free, physical containment two conditions, inside individually ventilated enclosures. Mice were allowed at least 5 days to acclimatise before experiments were started and were maintained on a 12-hour day/night cycle with access to standard laboratory chow and water *ad libitum*.

5.3.2 Bacterial preparation

Prior to *in vivo* experiments, uropathogenic *Escherichia coli* clinical isolate UTI89 was cultured using Luria–Bertani (LB) broth & agar plates, incubated statically at 37℃ to induce type 1-piliation, as described [336]. UTI89 was diluted for spectrophotometer assessment in phosphate buffered saline (PBS) to an OD_{600nm} between 0.40 to 0.45 (approximately 10^7 colony forming units [CFU] per 50µL inoculum, as determined empirically for each experiment).

5.3.3 Urinary tract infection model

Mice received 0.05 to 0.1mg°kg^{-1} body weight of buprenorphine diluted in 0.9% saline subcutaneously prior to the procedure for effective analgesia, as per animal ethics requirements. Throughout the procedure, mice were kept on a heat mat set to 37°C. Anaesthesia was induced by 4% isoflurane inhalation and maintained with continuous 1-2% isoflurane

inhalation through a nose cone. Immediately prior to infection, bladder voiding was induced by applying pressure to the lower abdomen. Mice were then transurethrally inoculated with 50µL of the prepared inoculum, as described [336, 337], typically at 9am±1 hour. Anaesthesia was maintained for exactly 20 minutes following the inoculation to prevent immediate voiding, 20 minutes after inoculation was considered as time 0 for the infection. All mice survived to the pre-determined endpoint without signs of pain or distress.

5.3.4 CFU determination

Serial dilutions were performed using 200µL of the inoculum, bladder and kidney homogenates such that the LB agar plates contained 5 replicates of 10µL spots ranging from undiluted to 10^7-fold diluted. LB agar plates were incubated at 37˚C for 16 hours before counting the bacterial colonies and representing as CFU mL^{-1}. The limit of detection for this assay was 20 CFU mL^{-1}.

5.3.5 Tissue homogenization and enzyme-linked immunosorbent assay (ELISA)

Urinary bladder and kidney pairs, minus the kidney capsule, were excised aseptically and physically homogenised in a TissueLyser II™ (Qiagen, Chadstone Centre, Australia) using 5mm stainless steel beads (30Hz for 3 minutes, ≈5400 oscillations) in 1000 or 800µL of PBS, respectively. Homogenization was repeated where required. 200µL of 2xProtein Buffer (1xcOmplete™ tablet and 1xPhosSTOP™ tablet in 5mL of ddH_2O [Sigma-Aldrich, Castle Hill, Australia]) was added to 200µL of the tissue homogenate and vortexed; the remainder of the sample was used for RNA extraction. Following 4˚C centrifugation for 10 minutes at 10,000x*g* the supernatant was kept at -80˚C then later utilized for ELISA using commercially

available kits. STAT3 pY705 was detected and represented as a proportion of total STAT3 in using semi-quantitative ELISA (cat# AB126458 [Abcam, Melbourne, Australia]). IL-17A and IL-22 protein levels were measured using quantitative ELISA (cat# 432504 & 436304, respectively [BioLegend, San Diego, United States]). The limit of detection for these assays were 8 and 2pg per mL, respectively.

5.3.6 RNA extraction, reverse transcription and quantitative real-time polymerase chain reaction (qPCR)

The remainder of the sample was diluted with 1mL of TRI Reagent® (Sigma-Aldrich) and physical homogenisation was repeated. Samples were incubated at room temperature for 5 minutes then centrifuged for 10 minutes at 12,000x*g*. The supernatant was diluted with 500µL of chloroform (Sigma-Aldrich). After vortexing, the samples were incubated at room temperature for 10 minutes then centrifuged for 15 minutes at 12,000x*g*. The supernatant was diluted with 1mL of isopropanol (Sigma-Aldrich). After vortexing, the samples were incubated at room temperature for 10 minutes then centrifuged for 10 minutes at 12,000x*g*. Without disrupting the pellet, the supernatant was discarded. The pellet was carefully washed with 1ml of 75% ethyl alcohol (Sigma-Aldrich), centrifuged for 5 minutes at 10,000x*g*. The washing step was repeated twice before air-drying the pellet at room temperature. The pellet was re-suspended in 10-100µL of UltraPure™ H_2O (Thermo-Fisher Scientific, North Ryde, NSW) for bladders and kidneys, respectively. Samples were kept at -80°C prior to reverse transcription. Immediately prior to reverse transcription, RNA yield was determined by spectrophotometric assessment using a Nanodrop2000™ (Thermo-Fisher Scientific). 5µL of each sample was diluted in ddH_2O such that 1000ng of RNA was loaded per sample. Following DNAse (Sigma-Aldrich) treatment, cDNA was generated using the M-MLV (Thermo-Fisher Scientific, North

Ryde. Australia) enzyme standard operating procedures using a T100™ thermal cycler (BioRad Laboratories, Gladesville, Australia). Using SYBR based methodology, qPCR was performed using CFX384 Touch™ (BioRad Laboratories) as per standard operating procedures. Each primer set was gradient tested to determine the optimal temperature for amplification (**Table 13**). Cycle quantification was interpreted using regression for each target, gene expression was normalized relative to Beta-actin (*Actb*). Melt curves were assessed for signs of primer dimerization and non-specific amplification. On every plate, at least one negative control and no-template control was used for each target to ensure contamination was not present within each master mix or the ddH_2O used.

Table 13: qPCR primer sequences

Target	Forward primer (5`-3`)	Reverse primer (5`-3`)
Actb	GATGTATGAAGGCTTTGGTC	TGTGCACTTTTATTGGTCTC
Il22	ATCAGTGCTACCTGATGAAG	CATTCTTCTGGATGTTCTGG
Il22ra1	CTGTTATCTGGGCTACAAATAC	GTACGTGTTCTTGGATGAAG
Il22ra2	CACTAGAGAAGGAGCAAAAAG	TAGCTGGAATGAGGTATCAG

5.3.7 RT² profiler array

RT² Profiler™ PCR Array Mouse Inflammatory Response & Autoimmunity (Qiagen) was performed as per manufacturer's instructions and data was uploaded then analysed by the online tool, available from: https://dataanalysis.qiagen.com/pcr/arrayanalysis.php. This array allows profiling of 84 genes in a maximum 4 samples, therefore, equal amounts of cDNA for each replicate in a group were pooled from mice at 1, 7 and 14 days post-infection (dpi) following urinary tract infection and sham inoculated controls pooled from each replicate from

each of these timepoints. Sham inoculated controls received transurethral phosphate buffered saline. For each target, the fold change following infection was compared to sham expression in the same tissue.

5.3.8 Immunohistochemistry

Briefly, tissues were fixed with 10% buffered formalin (cat# HT501320-9.5L [Sigma-Aldrich]) for 24 to 48 hours and 4µm thick, longitudinally cut sections were used for IHC. For fluorescent IHC, sections were incubated with primary (cat# MAB42941 [R&D Systems, Minneapolis, United States]) and secondary (cat# AB150157 [Abcam]) antibodies at 1:100 concentration, as described [310]. For standard light microscopy IHC, primary and secondary (cat# MAB42941 & HAF005 [R&D Systems]) were used at 1:100 concentration. DAPI mounting media (cat# 00-4959-52 [Thermo Fisher Scientific) and hematoxylin (cat# MHS1-100ML [Sigma-Aldrich]) counterstain was used for fluorescent and standard IHC, respectively.

5.3.9 Recombinant mouse (rm) treatments

For pre- and post-infection treatments, animals received 0.5µg of rmIL-22 (cat# 582-ML-010/CF [R&D Systems]) daily for 3 days, or 200µL of the vehicle PBS *via* intraperitoneal injection, as described [339]. Treatments which took place at 12hpi typically took place at 9:20pm±1 hour.

5.3.10 Statistical analysis

All data were analysed with GraphPad Prism software v9.1.0. Statistical tests, sample size and number of experiments are described in each of the corresponding figure legends.

5.4 Results

To further explore inflammatory factors which are enhanced during a model of cystitis from uropathogenic *Escherichia coli* clinical isolate UTI89, the mRNA expression was profiled at 1, 7 and 14 days post-infection (dpi) in urinary bladder and kidney pairs using an Inflammatory Response & Autoimmunity RT^2 profiler PCR array (**Figure 41**, **Table 14** & **Table 15**). In the bladder, 34/84 targets were >2 fold increased at 1, 7 or 14dpi compared to sham inoculated controls which received transurethral phosphate buffered saline (**Figure 41A**, **Table 14**). In the kidney pairs, 41/84 targets were increased >2 fold (**Figure 41B**, **Table 15**). Upregulation of chemokine families such as CXCL's and CCL's, (*Cxcl2*, *Cxcl3*, *Cxcl9*, *Ccl3*, *Ccl3*, *Ccl5*) was observed as expected, yet *Il17a* was only upregulated in the kidney and *Il22* mRNA expression was unaltered (**Figure 41**, **Table 14** & **Table 15**). Therefore, protein expression of these factors was assessed in the subsequent experiments to profile their role during experimental UTI.

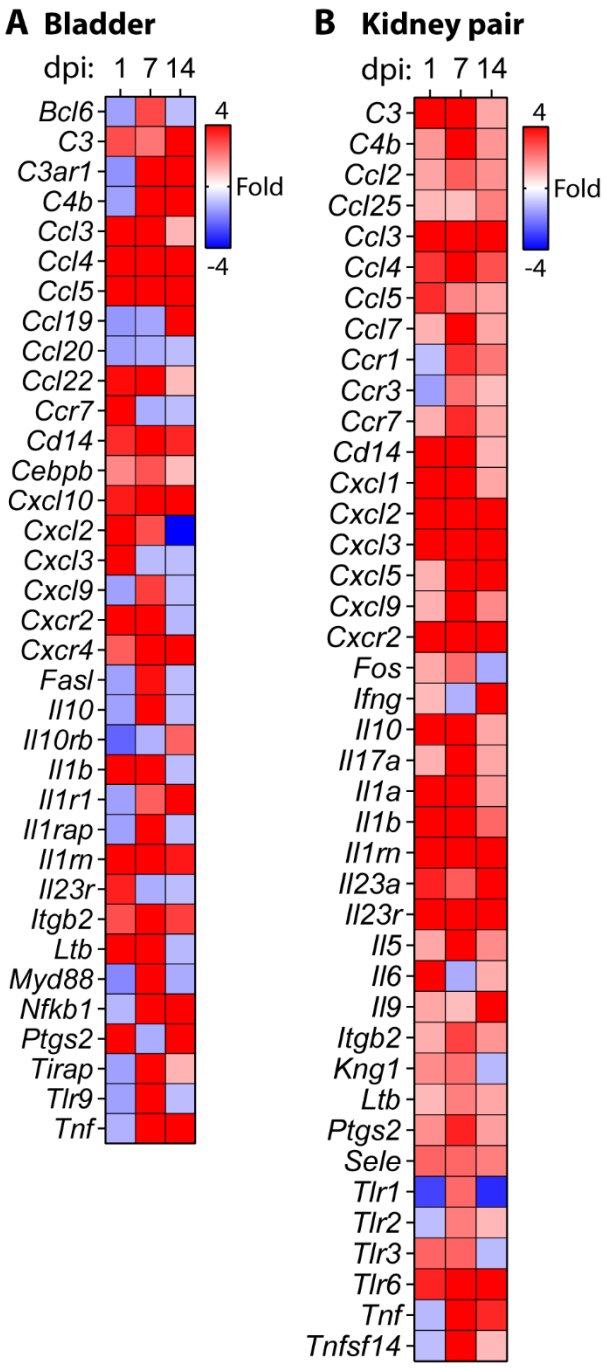

Figure 41: mRNA expression is altered in the urinary bladder and kidney during UTI

Inflammatory Response & Autoimmunity RT² Profiler PCR Array, truncated to targets which were increased >2 fold from at least one timepoint in **(A)** urinary bladder and **(B)** kidney pair homogenates from female C57BL/6Jausb mice infected *via* transurethral inoculation of uropathogenic *Escherichia coli* clinical isolate UTI89 at ≈10^7 colony forming units (CFU) and were assessed at the specified days post infection (dpi), compared to the average expression

across each timepoint following sham inoculation (transurethral phosphate buffered saline); Data pooled from 2 independent experiments of n=4 (n=8 per timepoint).

Table 14: mRNA expression in the urinary bladder within the urinary tract infection model at 1, 7 and 14dpi compared to sham inoculated controls

Target	Description	Fold regulation from sham		
		1dpi	7dpi	14dpi
Bcl6	B-cell leukemia/lymphoma 6	-1.4990	2.8681	-1.0612
C3	Complement component 3	2.8039	2.1789	5.8508
C3ar1	Complement component 3a receptor 1	-1.7254	4.4558	6.9408
C4b	Complement component 4B (Childo blood group)	-1.4990	7.0509	7.9604
Ccl1	Chemokine (C-C motif) ligand 1	-1.4990	-1.2930	-1.0612
Ccl11	Chemokine (C-C motif) ligand 11	-1.4990	-1.2930	-1.0612
Ccl12	Chemokine (C-C motif) ligand 12	-1.4990	-1.2930	1.0893
Ccl17	Chemokine (C-C motif) ligand 17	-1.4990	-1.2930	-1.0612
Ccl19	Chemokine (C-C motif) ligand 19	-1.6546	-1.4272	12.7408
Ccl2	Chemokine (C-C motif) ligand 2	-1.4990	-1.2930	-1.0612
Ccl20	Chemokine (C-C motif) ligand 20	-1.4990	-1.2930	-1.0612
Ccl22	Chemokine (C-C motif) ligand 22	3.8586	7.1982	1.0784
Ccl24	Chemokine (C-C motif) ligand 24	-1.4990	-1.2930	-1.0612
Ccl25	Chemokine (C-C motif) ligand 25	-1.4990	-1.2930	-1.0612
Ccl3	Chemokine (C-C motif) ligand 3	7.2319	8.3855	1.1515
Ccl4	Chemokine (C-C motif) ligand 4	10.7181	6.6070	4.4780
Ccl5	Chemokine (C-C motif) ligand 5	6.2818	22.2037	5.3267
Ccl7	Chemokine (C-C motif) ligand 7	-1.4990	-1.2930	-1.0612
Ccl8	Chemokine (C-C motif) ligand 8	-1.4990	-1.2930	-1.0612
Ccr1	Chemokine (C-C motif) receptor 1	-4.5204	-1.2530	1.0209
Ccr2	Chemokine (C-C motif) receptor 2	-19.5130	1.0622	-1.7761
Ccr3	Chemokine (C-C motif) receptor 3	-1.4990	-1.2930	-1.0612
Ccr4	Chemokine (C-C motif) receptor 4	-1.5077	-1.0857	-1.0673
Ccr7	Chemokine (C-C motif) receptor 7	5.9574	-1.2930	-1.0612
Cd14	CD14 antigen	3.3353	7.6226	3.4151
Cd40	CD40 antigen	-5.6552	-4.8778	-4.0033
Cd40lg	CD40 ligand	-1.4990	-1.2930	-1.0612
Cebpb	CCAAT/enhancer binding protein (C/EBP), beta	1.8684	2.7118	1.0470
Crp	C-reactive protein, pentraxin-related	-1.4990	-1.2930	-1.0612

Csf1	Colony stimulating factor 1 (macrophage)	-4.6686	1.3739	-2.4789
Cxcl1	Chemokine (C-X-C motif) ligand 1	-1.4990	-1.2930	-1.0612
Cxcl10	Chemokine (C-X-C motif) ligand 10	3.5847	15.9495	6.9455
Cxcl11	Chemokine (C-X-C motif) ligand 11	-1.5752	-1.3587	-1.1151
Cxcl2	Chemokine (C-X-C motif) ligand 2	9.1668	2.7665	-5.1404
Cxcl3	Chemokine (C-X-C motif) ligand 3	4.0215	-1.0838	-1.0612
Cxcl5	Chemokine (C-X-C motif) ligand 5	-7.6749	-6.6199	-5.4331
Cxcl9	Chemokine (C-X-C motif) ligand 9	-1.4990	3.0405	-1.0612
Cxcr1	Chemokine (C-X-C motif) receptor 1	-1.4990	-1.2930	-1.0612
Cxcr2	Chemokine (C-X-C motif) receptor 2	7.1992	8.3188	-1.1403
Cxcr4	Chemokine (C-X-C motif) receptor 4	2.5559	23.2226	5.3649
Fasl	Fas ligand (TNF superfamily, member 6)	-1.4990	3.7777	-1.0612
Fos	FBJ osteosarcoma oncogene	-3.0763	-1.9898	-3.4417
Ifng	Interferon gamma	-1.4990	-1.2930	-1.0612
Il10	Interleukin 10	-1.4990	8.1874	-1.0612
Il10rb	Interleukin 10 receptor, beta	-2.4599	-1.2373	2.4517
Il17a	Interleukin 17A	-1.4990	-1.2930	-1.0612
Il18	Interleukin 18	-1.4990	-1.2930	-1.0612
Il1a	Interleukin 1 alpha	-8.4475	-7.2863	-5.9800
Il1b	Interleukin 1 beta	6.8358	27.4081	-1.0612
Il1r1	Interleukin 1 receptor, type I	-1.4990	2.5158	8.4563
Il1rap	Interleukin 1 receptor accessory protein	-1.4990	17.4015	-1.0612
Il1rn	Interleukin 1 receptor antagonist	6.1836	31.0979	3.6283
Il22	Interleukin 22	-1.4990	-1.2930	-1.0612
Il23a	Interleukin 23, alpha subunit p19	-5.5953	-4.8262	-1.0683
Il23r	Interleukin 23 receptor	3.5114	-1.2930	-1.0612
Il5	Interleukin 5	-1.4990	-1.2930	-1.0612
Il6	Interleukin 6	-5.6790	-4.6985	-4.0202
Il6ra	Interleukin 6 receptor, alpha	-16.6317	-2.0239	-3.4144
Il7	Interleukin 7	-1.4990	-1.2930	-1.0612
Il9	Interleukin 9	-1.4990	-1.2930	-1.0612
Itgb2	Integrin beta 2	2.7714	6.8386	3.0194
Kng1	Kininogen 1	-1.4990	-1.2930	-1.0612
Lta	Lymphotoxin A	-1.4990	-1.2930	-1.0612
Ltb	Lymphotoxin B	4.1966	16.0565	-1.1228
Ly96	Lymphocyte antigen 96	-1.4470	-1.2930	-1.0612
Myd88	Myeloid differentiation primary response gene 88	-1.8968	4.9702	-1.3427
Nfkb1	Nuclear factor of kappa light polypeptide gene enhancer in B-cells 1, p105	-1.1510	5.2833	6.6688

Nos2	Nitric oxide synthase 2, inducible	1.1322	1.9453	-1.5235
Nr3c1	Nuclear receptor subfamily 3, group C, member 1	-1.1770	-5.2953	-4.3459
Ptgs2	Prostaglandin-endoperoxide synthase 2	11.6990	-1.2930	11.2687
Ripk2	Receptor (TNFRSF)-interacting serine-threonine kinase 2	-1.4990	-1.2930	-1.0612
Sele	Selectin, endothelial cell	-28.8089	-3.2399	1.0577
Tirap	Toll-interleukin 1 receptor (TIR) domain-containing adaptor protein	-1.4990	3.9726	1.1784
Tlr1	Toll-like receptor 1	-1.4990	-1.2930	-1.0612
Tlr2	Toll-like receptor 2	-9.1654	-4.7625	-33.2772
Tlr3	Toll-like receptor 3	-28.9453	-24.9666	-20.4905
Tlr4	Toll-like receptor 4	-1.4990	-1.2930	-1.0612
Tlr5	Toll-like receptor 5	-1.4990	-1.2930	-1.0612
Tlr6	Toll-like receptor 6	-11.3300	-2.0117	-8.0205
Tlr7	Toll-like receptor 7	-171.1494	-147.6236	-121.1573
Tlr9	Toll-like receptor 9	-1.4990	9.3475	-1.0612
Tnf	Tumor necrosis factor	-1.2254	6.7607	7.5194
Tnfsf14	Tumor necrosis factor (ligand) superfamily, member 14	-1.4990	1.0494	-1.0612
Tollip	Toll interacting protein	-52.8631	-1.5693	-1.8456
Actb	Actin, beta	-1.0711	1.5403	1.2917
B2m	Beta-2 microglobulin	1.3190	3.1505	2.0990
Gapdh	Glyceraldehyde-3-phosphate dehydrogenase	1.0000	1.0000	1.0000
Gusb	Glucuronidase, beta	-2.0338	5.0612	2.5225
Hsp90ab1	Heat shock protein 90 alpha (cytosolic), class B member 1	-2.6796	-1.9643	1.0770
MGDC	Mouse Genomic DNA Contamination	-1.4990	-1.2930	-1.0612
RTC1	Reverse Transcription Control1	-1.4990	-1.2930	-1.0612
RTC2	Reverse Transcription Control2	-1.4990	-1.2930	-1.0612
RTC3	Reverse Transcription Control3	-1.4990	-1.2930	-1.0612
PPC1	Positive PCR Control1	-1.4973	-1.2772	1.0572
PPC2	Positive PCR Control2	-1.4681	-1.2559	1.1306
PPC3	Positive PCR Control3	-1.6092	-1.3345	1.0062

Table 15: mRNA expression in the kidneys within the urinary tract infection model at 1, 7 and 14dpi compared to sham inoculated controls

Target	Description	Fold regulation from sham		
		1dpi	7dpi	14dpi
Bcl6	B-cell leukemia/lymphoma 6	-1.2421	1.0009	-1.1968
C3	Complement component 3	3.9701	7.0928	1.3726
C3ar1	Complement component 3a receptor 1	1.0404	1.1164	1.3018
C4b	Complement component 4B (Childo blood group)	1.6344	4.1931	1.6564
Ccl1	Chemokine (C-C motif) ligand 1	1.2204	1.0507	1.3816
Ccl11	Chemokine (C-C motif) ligand 11	-3.4612	1.7994	-1.5967
Ccl12	Chemokine (C-C motif) ligand 12	1.2813	1.0507	1.5730
Ccl17	Chemokine (C-C motif) ligand 17	-2.0305	1.8539	-1.5906
Ccl19	Chemokine (C-C motif) ligand 19	-4.3368	1.5686	1.2170
Ccl2	Chemokine (C-C motif) ligand 2	1.4217	2.5501	1.7118
Ccl20	Chemokine (C-C motif) ligand 20	1.3589	1.0507	1.6583
Ccl22	Chemokine (C-C motif) ligand 22	-2.7680	-1.5945	-2.3797
Ccl24	Chemokine (C-C motif) ligand 24	1.2204	1.0507	1.3816
Ccl25	Chemokine (C-C motif) ligand 25	1.1260	1.0111	2.0035
Ccl3	Chemokine (C-C motif) ligand 3	9.2238	45.0526	10.1846
Ccl4	Chemokine (C-C motif) ligand 4	3.1959	8.3494	2.7370
Ccl5	Chemokine (C-C motif) ligand 5	3.3287	1.8957	1.4306
Ccl7	Chemokine (C-C motif) ligand 7	1.2204	3.9717	1.3816
Ccl8	Chemokine (C-C motif) ligand 8	-1.3704	-1.6508	-5.2858
Ccr1	Chemokine (C-C motif) receptor 1	-1.0045	3.2471	2.1396
Ccr2	Chemokine (C-C motif) receptor 2	1.0291	-1.0981	-1.3096
Ccr3	Chemokine (C-C motif) receptor 3	-1.5147	2.2331	1.0471
Ccr4	Chemokine (C-C motif) receptor 4	-6.7898	-7.8868	-5.1756
Ccr7	Chemokine (C-C motif) receptor 7	1.2482	3.3536	1.3604
Cd14	CD14 antigen	7.7412	4.3368	1.1800
Cd40	CD40 antigen	-1.1572	1.0442	1.2609
Cd40lg	CD40 ligand	-5.6873	-1.9744	-5.0238
Cebpb	CCAAT/enhancer binding protein (C/EBP), beta	1.3276	1.5007	-1.0093
Crp	C-reactive protein, pentraxin-related	1.2204	1.0507	1.3816
Csf1	Colony stimulating factor 1 (macrophage)	1.0863	1.2016	1.4177
Cxcl1	Chemokine (C-X-C motif) ligand 1	35.9309	4.0504	1.3816
Cxcl10	Chemokine (C-X-C motif) ligand 10	1.3190	1.9731	-1.2396
Cxcl11	Chemokine (C-X-C motif) ligand 11	-2.8706	-3.3344	-2.5357
Cxcl2	Chemokine (C-X-C motif) ligand 2	94.3549	148.4964	48.6730
Cxcl3	Chemokine (C-X-C motif) ligand 3	10.3653	50.7522	5.6711
Cxcl5	Chemokine (C-X-C motif) ligand 5	1.2204	5.1758	13.4069

Cxcl9	Chemokine (C-X-C motif) ligand 9	1.2204	14.2728	1.8496
Cxcr1	Chemokine (C-X-C motif) receptor 1	1.2204	1.0507	1.3816
Cxcr2	Chemokine (C-X-C motif) receptor 2	5.7766	72.4221	4.4512
Cxcr4	Chemokine (C-X-C motif) receptor 4	-1.4865	1.7157	1.1491
Fasl	Fas ligand (TNF superfamily, member 6)	1.2204	1.0507	1.3816
Fos	FBJ osteosarcoma oncogene	1.3429	2.3111	-1.3392
Ifng	Interferon gamma	1.0864	-1.2419	9.8395
Il10	Interleukin 10	8.3898	6.1171	1.3816
Il10rb	Interleukin 10 receptor, beta	-1.1622	-1.1441	-1.0072
Il17a	Interleukin 17A	1.2204	7.2694	1.3816
Il18	Interleukin 18	-1.4662	-2.9009	-1.2632
Il1a	Interleukin 1 alpha	6.2108	52.6441	1.5964
Il1b	Interleukin 1 beta	4.4840	11.3464	2.3788
Il1r1	Interleukin 1 receptor, type I	-1.6147	1.3481	1.1874
Il1rap	Interleukin 1 receptor accessory protein	1.2093	-1.0423	1.5233
Il1rn	Interleukin 1 receptor antagonist	95.7282	303.1494	97.9445
Il22	Interleukin 22	1.2204	1.0507	1.3816
Il23a	Interleukin 23, alpha subunit p19	3.4805	2.5665	5.3167
Il23r	Interleukin 23 receptor	5.8306	5.0898	4.8146
Il5	Interleukin 5	1.3881	5.9754	1.8051
Il6	Interleukin 6	4.0124	-1.3144	1.2747
Il6ra	Interleukin 6 receptor, alpha	-1.4069	1.2943	1.3291
Il7	Interleukin 7	-11.5350	-15.0580	-1.1799
Il9	Interleukin 9	1.3653	1.0507	5.4540
Itgb2	Integrin beta 2	1.2830	2.9677	1.6556
Kng1	Kininogen 1	1.8171	2.2653	-1.1153
Lta	Lymphotoxin A	1.2204	1.0507	1.3816
Ltb	Lymphotoxin B	1.1096	2.0062	1.3918
Ly96	Lymphocyte antigen 96	-1.3877	-1.0051	1.1902
Myd88	Myeloid differentiation primary response gene 88	1.1480	1.3581	-1.1013
Nfkb1	Nuclear factor of kappa light polypeptide gene enhancer in B-cells 1, p105	-1.1783	1.0572	1.0954
Nos2	Nitric oxide synthase 2, inducible	1.3349	1.2096	1.7774
Nr3c1	Nuclear receptor subfamily 3, group C, member 1	-1.4380	-1.3641	1.2506
Ptgs2	Prostaglandin-endoperoxide synthase 2	1.7477	3.4723	1.5137
Ripk2	Receptor (TNFRSF)-interacting serine-threonine kinase 2	-1.9840	-2.8325	-7.6390
Sele	Selectin, endothelial cell	2.4314	2.3751	2.0197
Tirap	Toll-interleukin 1 receptor (TIR) domain-containing adaptor protein	-1.2929	-1.3050	-1.2041
Tlr1	Toll-like receptor 1	-2.9513	2.3487	-3.3549
Tlr2	Toll-like receptor 2	-1.0495	2.0355	1.1215

Tlr3	Toll-like receptor 3	2.4353	2.4353	-1.0894
Tlr4	Toll-like receptor 4	-1.2733	-1.2057	-2.2035
Tlr5	Toll-like receptor 5	-7.4739	-2.7935	-2.0035
Tlr6	Toll-like receptor 6	3.4589	13.4658	10.9071
Tlr7	Toll-like receptor 7	-4.8399	-1.6249	-1.1495
Tlr9	Toll-like receptor 9	-2.9268	1.5791	-2.3930
Tnf	Tumor necrosis factor	-1.1245	5.2998	3.3890
Tnfsf14	Tumor necrosis factor (ligand) superfamily, member 14	-1.0340	11.2086	1.0949
Tollip	Toll interacting protein	-1.2628	1.0534	1.0900
Actb	Actin, beta	1.0561	1.0382	1.0415
B2m	Beta-2 microglobulin	1.0114	1.0197	1.0011
Gapdh	Glyceraldehyde-3-phosphate dehydrogenase	-1.0775	-1.1521	-1.2968
Gusb	Glucuronidase, beta	-1.1896	1.1273	1.2099
Hsp90ab1	Heat shock protein 90 alpha (cytosolic), class B member 1	-1.0724	-1.0620	-1.0452
MGDC	Mouse Genomic DNA Contamination	1.2204	1.0507	1.3816
RTC1	Reverse Transcription Control1	4.5474	1.0507	1.3816
RTC2	Reverse Transcription Control2	1.2204	1.0507	1.3816
RTC3	Reverse Transcription Control3	1.2149	1.0459	1.3754
PPC1	Positive PCR Control1	1.2411	1.0645	1.3960
PPC2	Positive PCR Control2	1.1742	1.0041	1.3598
PPC3	Positive PCR Control3	1.1323	1.0201	1.2595

To explore whether IL-17A or IL-22 levels were regulated by circadian rhythm in the urinary tract, a pilot study was performed whereby a subset of animals were culled at circadian time (CT) intervals of 6 hours (**Figure 42A**). In the urinary bladder, both cytokines were below detection levels, and therefore could not be interpreted. In the kidneys, there was no impact between the sexes of mice, nor between animals culled at differing CT for either cytokine (**Figure 42B-E**).

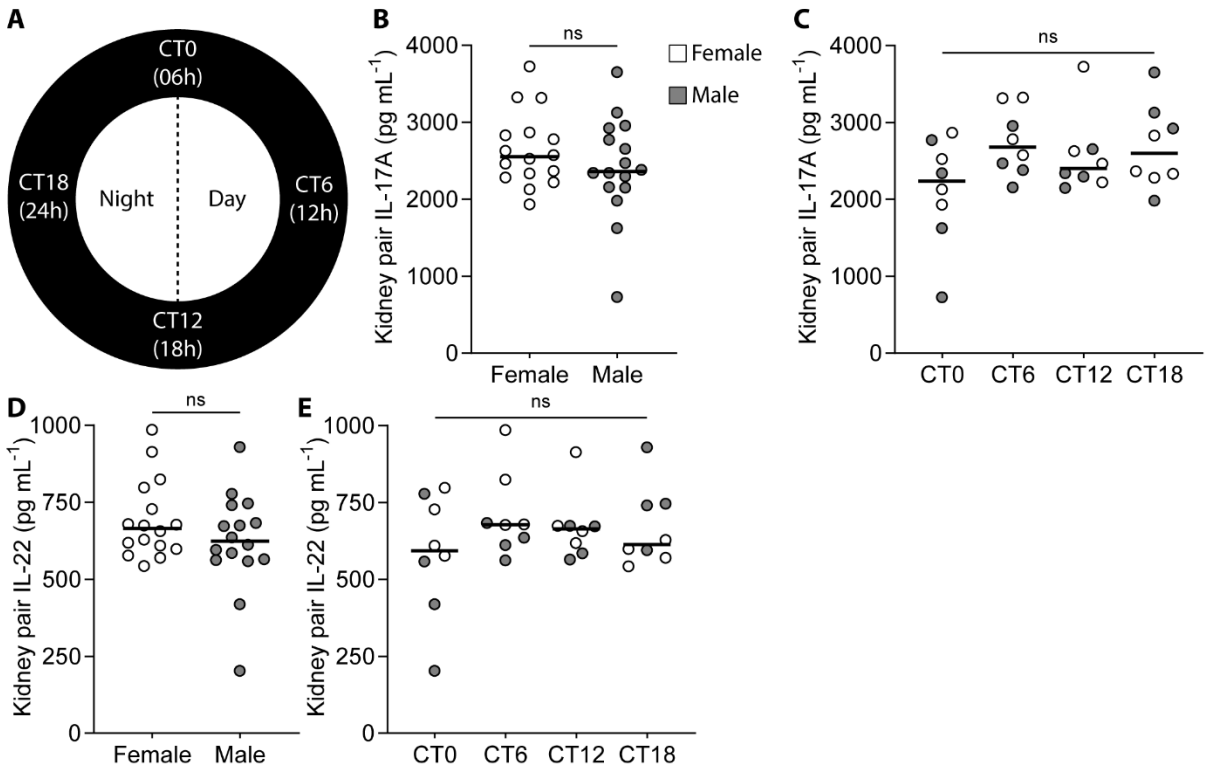

Figure 42: IL 17A and IL 22 protein levels are not altered by sex or circadian rhythm

(A) Schematic representation of circadian time (CT) and comparison to 24-hour (h) time. **(B)** IL 17A protein levels in kidney pairs from naïve female and male C57BL/6Jausb mice. **(C)** IL-17A protein levels at CT increments of 6. **(D)** IL 22 protein levels in kidney pairs from naïve female and male C57BL/6Jausb mice **(E)** IL 22 protein levels in kidney pairs from naïve female and male mice. Urinary bladder cytokine levels were below the limit of detection of 8 and 2pg mL^{-1}, respectively for these assays. Data pooled from 2 independent experiments of n=4 (total n=8 per CT group), solid line indicates median.

To examine the role of IL-22 in response to infection, mice received the uropathogenic *Escherichia coli* clinical isolate UTI89 by transurethral inoculation with approximately 10^7 CFU. The outcomes were evaluated at early endpoints of 0.5, 6, 12 and 24 hours post-infection (hpi), intermediate endpoints at 3 and 7 days dpi and at the later endpoints of 10 and 14dpi. The kinetics resembled a productive infection with the highest levels of infection occurring

between 6 and 24hpi; however, there was no statistical basis for determination of peak of infection (**Figure 43A,B**). Whilst all animals developed a notable infection in the bladder, this model induced a kidney infection in 50% of mice by 6hpi (**Figure 43A,B**). IL-17A and IL-22 protein was undetectable in many of the bladder samples, yet at 24hpi and 3dpi it was detected in the highest proportion of animals, between 5 and 6/8 for each timepoint (**Figure 43C,E**). Kidney IL-22 protein levels displayed a high degree of variability at each timepoint (**Figure 43D,F**).

To further explore the notion of whether IL-17A and IL-22 was associated with pyelonephritis the data was plotted against kidney CFU, and against one another. Levels of IL-17A and IL-22 had no observable correlation with pyelonephritis, but the cytokine levels were strongly correlated with one another (**Figure 44A-C**). Since IL-22 had not yet been investigated during UTI in the literature, these data was interpreted further and data for each timepoint was plotted and labelled with a unique colour (**Figure 44D,E**). At timepoints of 24hpi or lower, there was no association between CFU and IL-22 protein levels (**Figure 44D**). However, kidneys with the highest CFU tended to have the lowest levels of IL-22 protein, especially when looking at the later timepoints of 10 and 14dpi (**Figure 44E**).

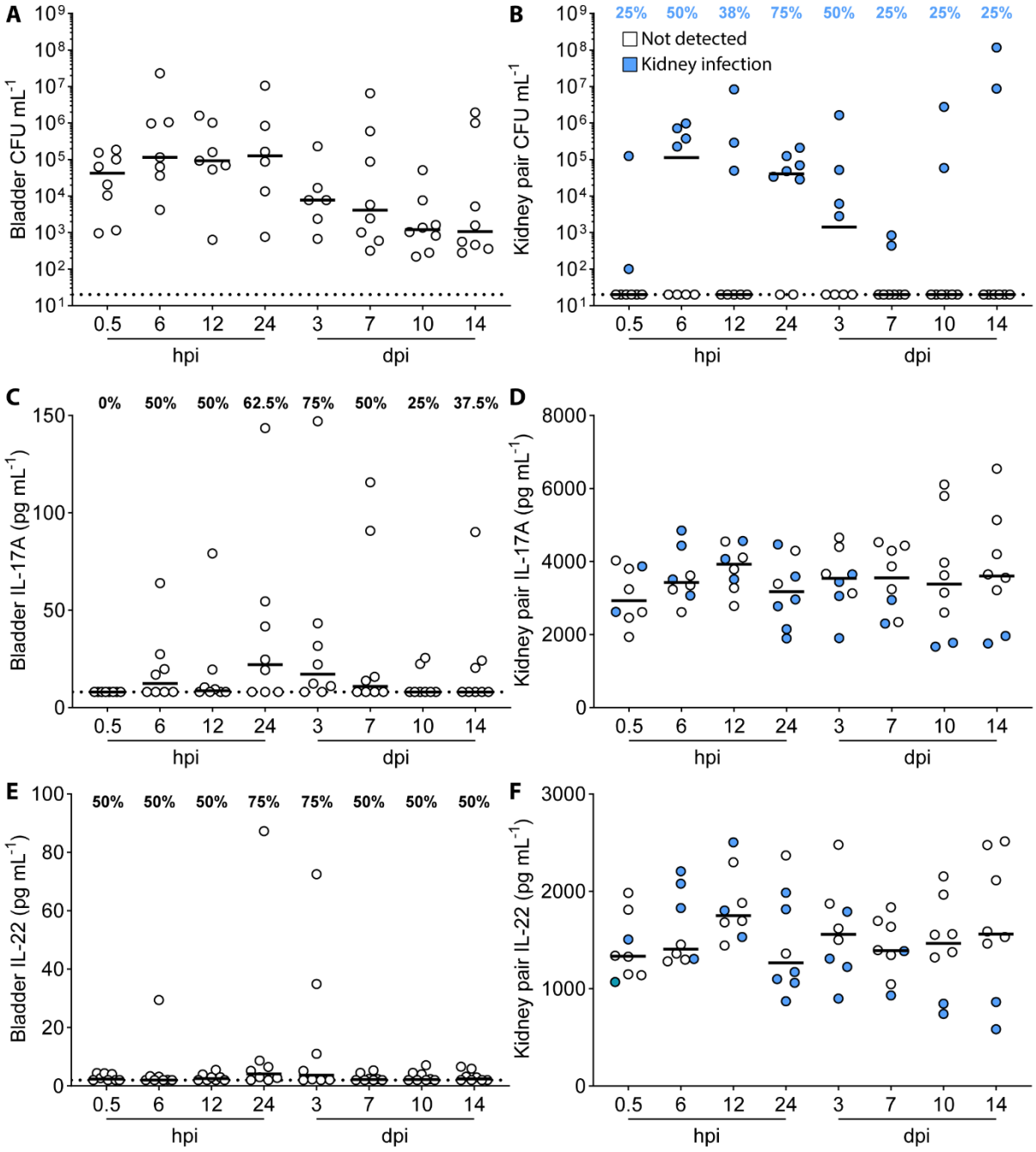

Figure 43: Low IL-17A and IL-22 protein levels were observed alongside pyelonephritis

Female C57BL/6Jausb mice were infected *via* transurethral inoculation of uropathogenic *Escherichia coli* clinical isolate UTI89 at ≈10^7 colony forming units (CFU) and were assessed at the specified hours/days post infection (hpi and dpi, respectively). **(A)** Bladder and **(B)** kidney pair CFU per mL, percentages (blue) indicate proportion with detectable bacteria; dotted line represents the limit of detection (LOD) of 20 CFU mL^{-1}. **(C)** IL-17A protein levels in the bladder and **(D)** kidney pair, percentages indicate proportion with detectable IL-17A;

dotted line represents the LOD of 8pg mL^{-1}. **(E)** IL-22 protein levels in the bladder and **(F)** kidney pair, percentages indicate proportion with detectable IL-22; dotted line represents the LOD of 2pg mL^{-1}. Data pooled from 4 independent experiments of n=2 (total n=8 per group), solid line indicates median.

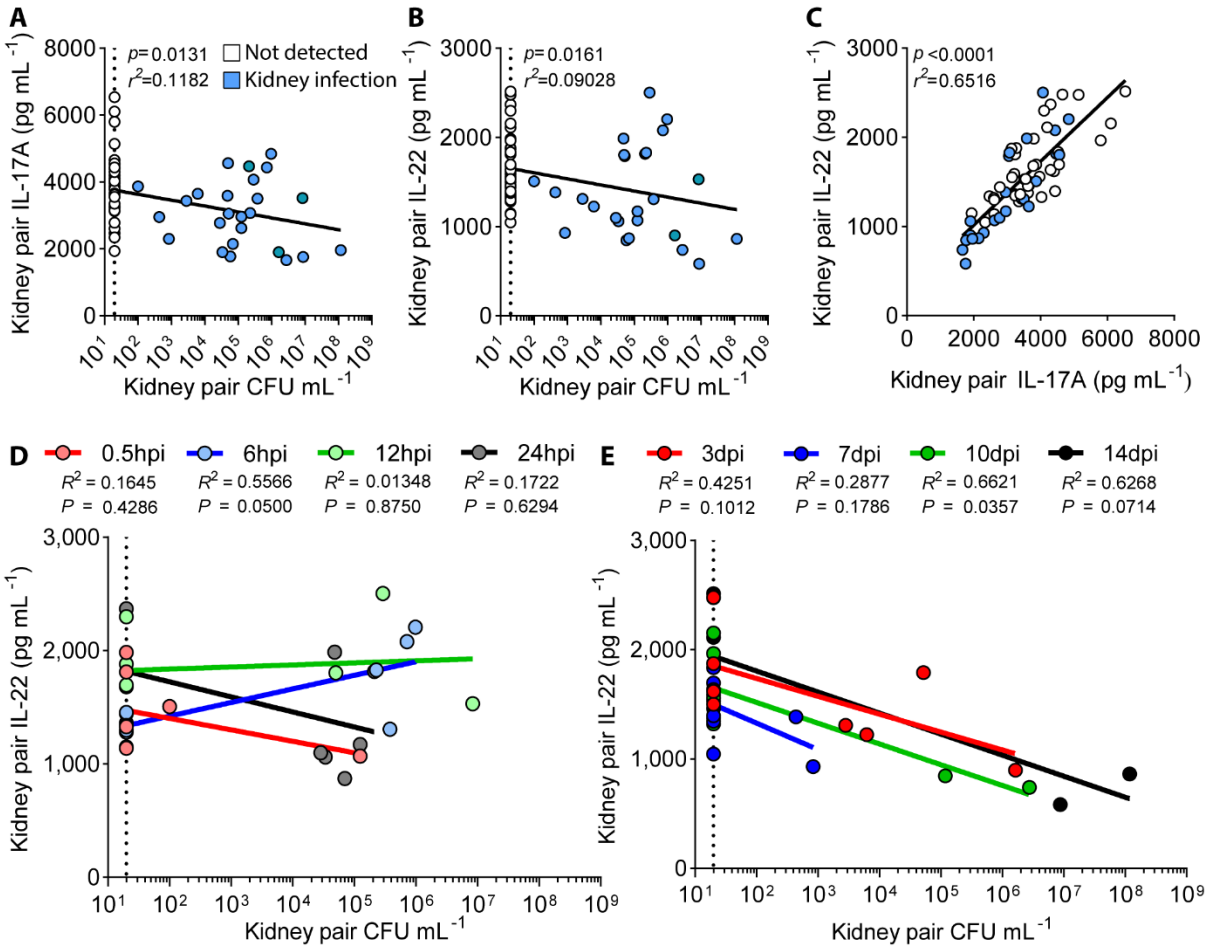

Figure 44: Low IL-22 was correlated with pyelonephritis

Female C57BL/6Jausb mice were infected *via* transurethral inoculation of uropathogenic *Escherichia coli* clinical isolate UTI89 at ≈10^7 colony forming units (CFU) and were assessed at the specified hours/days post-infection (hpi and dpi, respectively). **(A)** Kidney pair CFU mL^{-1} was plotted against cytokine levels of IL-17A and against **(B)** IL-22, collated from all timepoints. **(C)** IL-17A and IL-22 were plotted against one another. Analyses were performed

again for IL-22 levels at each timepoint individually either **(D)** hpi and **(E)** dpi. CFU mL^{-1}; dotted line represents the limit of detection (LOD) of 20 CFU mL^{-1}. Data pooled from 4 independent experiments of n=2 (total n=8 per group) per timepoint; solid line indicates regression, R^2 and *P*-values from regression (logarithmic for CFU data, linear for IL-17A & IL-22) and Spearman-correlation analyses, respectively.

Next, I sought to determine if the tissues of the urinary tract expressed the IL-22 receptor and therefore had the capacity to respond to IL-22. Using fluorescent immunohistochemistry (IHC) IL-22Rα was found to be restricted to the urothelium of the urinary bladder under homeostatic conditions compared to sequential sections processed identically but without the primary antibody (**Figure 45A**). In the kidneys from the same animals, IL-22Rα was ubiquitously expressed by the tubules in the cortex and medulla but was not found in the glomeruli (**Figure 45B,C**). Similar results were achieved using standard IHC methods with light microscopy, where IL-22Rα was present within the urothelium and in the tubules (**Figure 45D-F**). The mRNA expression of *Il22ra1* was also assessed, whilst the target was below detection in the bladder, it was detected within the kidney pairs and was decreased at 14dpi as compared to sham inoculated controls (**Figure 45G**). Additionally, mRNA expression of *Il22*, and *Il22ra2* were assessed but were below detection. To determine whether exogenous IL-22 was able to activate downstream pathways, animals were intraperitoneally administered 3 doses of 0.5µg of rmIL-22 once per day [316], then the urinary bladder and kidneys were collected. In the bladder, there was no change in STAT3 pY705 relative to total STAT3 (**Figure 45H**). In the kidney however, there was a significant increase in STAT3 pY705 following treatment with rmIL-22 (**Figure 45I**).

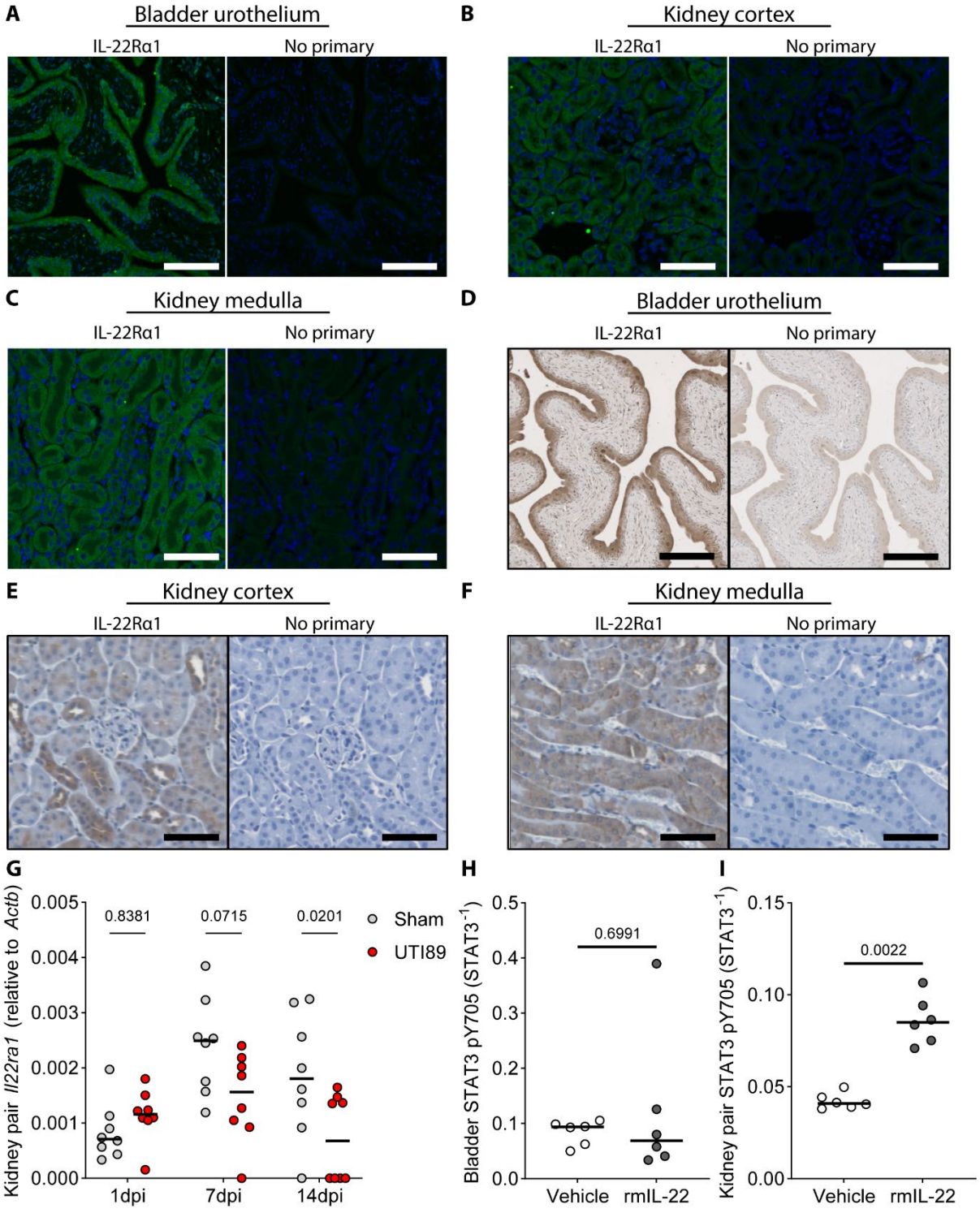

Figure 45: The IL-22 membranous receptor is expressed by the mouse kidney and is responsive to rmIL-22

Female C57BL/6Jausb mice IL-22Rα protein expression in the **(A)** urothelium of the bladder, **(B)** kidney cortex and **(C)** kidney medulla shown in green (left panel), DAPI was used to stain

nuclei in blue; no primary control section (right panel). IL-22Rα protein expression in the **(D)** urothelium, **(E)** kidney cortex and **(F)** kidney medulla in brown (left panel), hematoxylin was used as a structural stain; no primary control section (right panel). Scale bars indicate 50µm, data from 2 independent experiments of n=4 (total n=8). **(G)** *Il22ra1* mRNA levels in kidney pairs relative to *Actb* was measured in female C57BL/6Jausb mice following infection *via* transurethral inoculation of uropathogenic *Escherichia coli* clinical isolate UTI89 at ≈10^7 colony forming units (CFU) or sham inoculation, 2 experiments of n=4. **(H)** Female C57BL/6Jausb mice received 0.5µg of recombinant mouse IL-22 (rmIL-22) daily for 3 days *via* intraperitoneal injection, vehicle treated controls received phosphate buffered saline injections and STAT3 pY705 was measured relative to total STAT3 in the bladder and **(I)** kidney pairs; data from 1 experiment of n=6. *P*-values are from Mann-Whitney U-test.

To explore the therapeutic potential of IL-22, animals were pre-treated with rmIL-22 prior to the infection and outcomes were assessed at 24hpi (**Figure 46A**). Bladder and kidney CFU were relatively consistent between animals which received rmIL-22 and the vehicle treatment, PBS (**Figure 46B,C**). The proportion of animals with pyelonephritis was 5/12 with rmIL-22, whereas there were 8/12 animals with pyelonephritis in the vehicle group (**Figure 46B,C**).

To further explore the potential therapeutic benefit of IL-22 therapy, mice were treated with rmIL-22 after infection, with treatment starting at 12hpi and outcomes assessed at 3dpi (**Figure 46D**). Bladder CFU was unaltered, yet kidney CFU was significantly reduced by rmIL-22 treatment (**Figure 46E,F**). Likewise, the proportion of animals with pyelonephritis decreased with only 5/28 animals that were treated with rmIL-22 having pyelonephritis compared to 12/24 animals that were treated with vehicle (**Figure 46F**). Using the same treatment regime, these outcomes were also assessed at 7dpi (**Figure 46G**). The bladder CFU was identical

between groups and the kidney CFU was not significantly different (**Figure 46H,I**). However, the proportion of mice with pyelonephritis was 1/12 animals when treated with rmIL-22 compared to 4/12 mice in the vehicle treated controls (**Figure 46I**). Data was interpreted visually, without statistics, to select a timepoint to focus on for further study. Since the 12hpi treatment regime induced the strongest response, it was utilised for additional experiments to ensure reproducibility, which is why there are substantially more biological replicates.

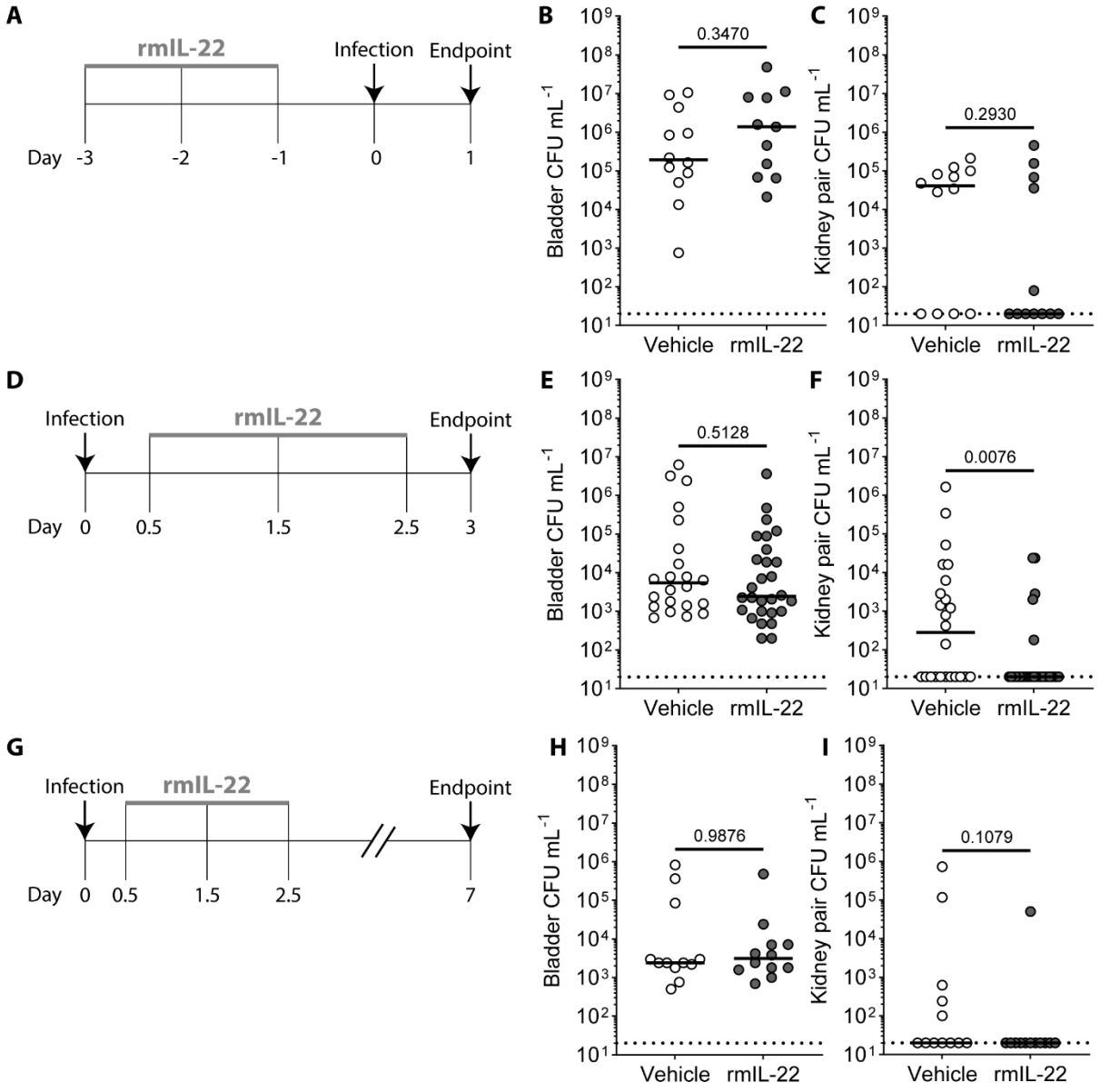

Figure 46: IL-22 treatment post-infection reduced pyelonephritis

Female C57BL/6Jausb mice were infected *via* transurethral inoculation of uropathogenic *Escherichia coli* clinical isolate UTI89 at ≈10^7 colony forming units (CFU). **(A)** Schematic representation of pre-treatment regime whereby 0.5µg rmIL-22 was administered daily *via* intraperitoneal injection starting two days prior to infection, vehicle treated controls received phosphate buffered saline injections. **(B)** Bladder and **(C)** kidney pair CFU mL^{-1} assessed 24 hours post-infection (hpi); dotted line represents the limit of detection (LOD) of 20 CFU mL^{-1}, data was pooled from 3 independent experiments of n=4 (total n=12 per group). **(D)** Schematic representation of post-treatment regime whereby 0.5µg rmIL-22 was administered daily *via* intraperitoneal injection starting at 12hpi. **(E)** Bladder and **(F)** kidney pair CFU mL^{-1} assessed at 3 days post-infection (dpi); LOD of 20 CFU mL^{-1}, data was pooled from 6 independent experiments of n=4-6 (total n=24 vehicle, n=28 rmIL-22). **(G)** Schematic representation of post-treatment regime whereby 0.5µg rmIL-22 was administered daily for 3 days *via* intraperitoneal injection starting at 12hpi. **(H)** Bladder and **(I)** kidney pair CFU mL^{-1} assessed at 7dpi; LOD of 20 CFU mL^{-1}, data was pooled from 3 independent experiments of n=4 (total n=12 per group). *P*-values are from Mann-Whitney U-test.

5.5 Discussion

To assess the function of IL-22 in the urinary tract, mice were subjected to an experimental model of bacterial cystitis induced by transurethral inoculation of uropathogenic *Escherichia coli*. Consistent with the literature, bacterial load in the urinary bladder was highest between 6 to 24hpi and the animals had a persistent infection at 14dpi [203, 213, 247, 270, 297, 336, 337]. Pyelonephritis occurred in approximately half the cases from 6 to 24hpi. Interestingly, the bacteria were not cleared from the kidney in some mice even by 14dpi. This phenomenon has been reported by others in similar proportions [213]. IL-22 was detected at low levels in

kidneys at 7, 10 and 14dpi when an active kidney infection was present, suggesting that an impaired IL-22 response allows the bacteria to colonise the kidney. Yet IL-17A was not detected in the bladder, potentially the signal was reduced by the tissue processing for CFU which was the primary outcome. Since the samples were firstly diluted before homogenisation it is possible that this prevented the detection of cytokines expressed at low levels.

In other tissues, concurrent IL-17A and IL-22 signalling are pro-inflammatory, yet IL-22 can have the opposing function in the absence of IL-17A [375]. Therefore, it is possible that this impaired response allows the bacteria to thrive in the kidney. This may be due to the absence of IL-22-induced production of antimicrobial peptides that requires further exploration. Upregulation of IL-22 may also assist in the maintenance and repair of the bladder urothelium. However, the ability of the urothelium to shed is an effective means of expelling bacteria from the bladder, which has been reviewed extensively [267]. Therefore, I speculate that the protective functions of IL-22 known from other tissues may be detrimental in the bladder if exaggerated; it is plausible that IL-22-mediated tissue maintenance may prevent sufficient shedding of infected cells, potentially increasing bacterial colonization. Consequently, I suggest that the timing, and the regulation of IL-22 signalling, which is crucial for the clearance of uropathogens and not simply the amplitude of cytokine released. To address this, I firstly examined the expression of the IL-22 receptor in these tissues.

Other studies have identified IL-22Rα in the kidney [324], and urinary bladder [325]. I found that expression of IL-22Rα was localized in the urothelium of the bladder and was highly expressed in the tubules of the cortex and medulla regions of the kidney but was not expressed by the glomeruli. This demonstrates the urinary bladder and kidney both have the capacity to respond to IL-22. Next, the therapeutic benefit of IL-22 was explored by administration of the recombinant mouse protein.

IL-22 levels are dependent on sex hormones and fluctuate in response to circadian rhythms in other tissues, such as the gastrointestinal tract [316]. However, this is not well characterised in the urinary bladder. Recent studies found that the levels of IL-22 decreased at night in other tissues such as the lung and gastrointestinal tract [316]. Therefore, the timing of the treatment regime may be critical. Hence, the treatment regime I used started at approximately 12hpi, which corresponded to late at night, where IL-22 protein levels were predicted to be at their lowest based on other organs.

Here, I demonstrated that pre-treatment with rmIL-22 did not alter bacterial load. However, post-infection treatment with rmIL-22 decreased the bacterial load in the kidneys, and a reduced the proportion of mice that developed pyelonephritis. These data support the current evidence from sterile kidney injury models which describe a protective function of IL-22 [324, 333]. Since the proportion of mice that developed a kidney infection decreased with rmIL-22 treatment, it may be that IL-22 is enhancing antimicrobial peptide production, preventing the *Escherichia coli* from colonising the upper urinary tract and preventing pyelonephritis.

Furthermore, this protection showed a trend to be retained out to 7dpi whilst having no impact on bladder bacterial load. Since the 12hpi treatment regime induced the strongest response, the research budget was expended to repeat these experiments to ensure consistency, which is why there was substantially more biological replicates then the other timepoints. Yet the function of IL-22 is context-dependent in other tissue sites and is capable of advantageous or detrimental functions [373]. Therefore, although these data demonstrate exogenous IL-22 therapy is protective when provided early after infection, prolonged treatment may cause uncontrolled inflammation and collateral damage to the host, which may aid the bacterium to replicate. Indeed, evidence suggests IL-22 upregulation could drive favourable conditions for *Escherichia coli* and other facultative anaerobes [376]. Therefore, it is plausible that the kidney

may not be able to effectively repair and prevent the migration of the bacteria if a long-term treatment regime was used.

In conclusion, I show that the protein for IL-22 was increased early after infection in the bladder and was decreased in the kidney at the later phases of infection. I have also shown that a high level of sustained kidney infection correlated with low levels of IL-22. Therefore, reduced IL-22 may be useful as an indicator of sustained kidney infection. I also confirm that the urinary bladder and kidney have the capacity to respond to IL-22 since they express IL-22Rα. Additionally, I show that rmIL-22 is effective at reducing bacterial load in the kidneys using a therapeutic treatment regime, whereas a prophylactic regime was largely ineffective. Unfortunately, it cannot be determined as yet if IL-22 impacts the ability of bacteria to migrate to the kidney, colonise the kidney or whether it alters bacterial replication in this tissue. Studies in other organ systems could suggest that the functionality of IL-22 is likely to be complex, future studies will need to expand upon this work in the kidneys. It is yet to be determined whether the role of IL-22 in the urinary bladder and kidney is primarily antimicrobial or pro-inflammatory. Indeed, further research is required to completely map the function of IL-22 in the urinary tract. Pending further preclinical studies, repurposing immunotherapies which target IL-22 may be a future option since these are currently undergoing clinical trials for other conditions.

Chapter 6: General discussion

6.1 Preface

Ischemic AKI causes acute tubular necrosis and impairs kidney structure and function [17]. Influx of neutrophils and monocytes contribute to the injury, however, other innate immune cells can facilitate the return to homeostasis [343, 344]. ILC2 are potent producers of type II cytokines, predominantly IL-5, and are expanded in response to IL-33 [119, 120]. These cells also promote tissue recovery following insult in multiple organs and have diverse functions *in vivo* [345]. More recently, ILC2 have been investigated in models of surgical IRI, and nephrotoxic chemical-induced injury by doxorubicin or cisplatin. Collectively, these studies show that *in vivo* administration of recombinant mouse cytokines, in particular IL-33, is sufficient to reduce the severity of tubular epithelial cell injury [158, 173, 174, 178, 346]. Similar results were achieved with adoptive transfer of *ex vivo* activated ILC2 [158, 173]. Whilst ILC2 can be artificially induced to proliferate and protect against the deleterious consequences of experimental renal injury, the impact of ILC2-deficiency remained incompletely understood in the kidney. Additionally, the role of ILC2 and IL-33 is largely unexplored in the urinary bladder, and in the context of UTI.

Uropathogenic *Escherichia coli* causes the majority of UTI's and whilst antibiotics are typically sufficient, antimicrobial resistance is increasing. Whilst the immunological state of the urinary tract has been investigated, the role of IL-33 requires further elucidation [358]. Recent studies have highlighted a critical role for IL-17A for appropriate clearance of uropathogens, yet the role of the functionally similar IL-22 in this system was unknown [203, 297]. Therefore, these studies aimed to investigate whether IL-33 and IL-22 also play an important role in the urinary tract by utilizing a murine model of experimental UTI.

6.2 Primary findings

6.2.1 ILC2 were present in the mouse bladder and kidney, were localised around the vasculature; and expansion or ablation of ILC2 was achieved with rmIL-33 and DTx, respectively

Whilst other studies have explored the role of ILC2 in the mouse kidney, they had not previously been investigated in the urinary bladder. Using flow cytometry, ILC2 were demonstrated to be present in the bladder as well as the kidney. The location of ILC2 was investigated in the bladder and kidney using GM mice. In these studies, an IL-5 linked cre-recombinase was used in conjunction with a flox-stop-flox sequence upstream of a CAG-RFP-WPRE- cassette in the constitutively expressed ROSA26 locus to locate the ILC2. In each tissue, I demonstrated that IL-5 reporter systems were suitable for profiling the ILC2 with the T-cell compartment having negligible expression under homeostatic conditions. Whilst a conventional IL-5 reporter strain found similar results, the IL-5 expression by ILC2 was not as robust. In these tissues, ILC2 were found localised to the vasculature using CD31 and α-SMA for bladder and kidney, respectively. Using LYVE1 staining, I demonstrated that the cells were predominantly not associated with areas of the lymphatic network. I also demonstrated that the ILC2 were able to be expanded using rmIL-33 and ablated using DTx in GM mice and validated the use of these tools for targeting ILC2 in the bladder and kidney.

6.2.2 Depleting ILC2 did not alter kidney injury nor urinary tract infection

Kidney ILC2 were investigated in IRI using a loss-of-function approach. To achieve this, I utilised GM mice deficient in ILC2, those that had reduced numbers of ILC2, and those where ablation of ILC2 required DTx. An experimental model of IRI was chosen, given the proximity

of ILC2 to the renal vasculature. Although features of injury were visibly evident following IRI, a reduction, deficiency or depletion in ILC2 did not alter gross histopathology in the kidney, nor did it cause mortality. Indeed, IRI-induced remodelling and collagen deposition occurred independently of ILC2. Collectively, I demonstrated that a reduction, deficiency or depletion in ILC2 does not alter the severity of experimental IRI in mice. My data show that a loss of ILC2, when the T cell compartment remains intact, has minimal effects on the severity of IRI. Indeed, a series of preliminary studies were performed in a model of experimental urinary tract infection, reduction of ILC2 did not alter the kinetics of infection in the urinary bladder, nor was there any change in the kidney.

6.2.3 IL-33 was increased in the bladder and kidney after experimental urinary tract infection, and rmIL-33 exaggerated experimental pyelonephritis which impaired kidney structure and function

Following urinary tract infection, IL-33 was increased in the bladder and kidney of mice. Pre-treatment with rmIL-33 significantly increased bacterial load in the kidneys and the rate of pyelonephritis and induced significant weight loss. Pyelonephritis was sufficient to drive changes to kidney structure and function as demonstrated by histopathology and *in vivo* kidney function from *t*GFR measurement based on FITC-Sinistrin clearance. Importantly, prolonged impairment of kidney function was not able to be recognized using BUN alone. There are now several studies that demonstrate rmIL-33 is protective against acute kidney injury, yet, it drastically increased the likelihood of pyelonephritis in my studies. However, this model may be used to further explore migration of *Escherichia coli*, the consequences and impact on kidney function, and to evaluate new therapeutic options.

6.2.4 IL-22 was decreased during rmIL-33-induced pyelonephritis and low levels of IL-22 was associated with pyelonephritis in the base model

Using the rmIL-33-induced pyelonephritis model, IL-22 was found to be increased in the bladder at the early-mid phase but was decreased in the kidney at the late phase of the model. IL-22 was found to have some correlation with pyelonephritis, and the protein levels were strongly with IL-17A. During the early timepoints, there was no association observed between IL-22 protein levels and CFU in the kidneys. However, kidneys with the lowest IL-22 protein concentration on average were observed to have a high bacterial load. This difference was more profound at the later timepoints, suggesting IL-22 may play an important role in this context.

6.2.5 The IL-22 receptor is expressed in the mouse bladder and kidney, and rmIL-22 treatment after infection protected against pyelonephritis

I found that the expression of IL-22Rα was localized in the urothelium of the bladder and not in the muscularis layer. IL-22Rα was highly expressed in the tubules of the cortex and medulla regions of the kidney but was not expressed by the glomeruli; meaning these tissues have the capacity to respond to IL-22. I demonstrated that post-infection treatment with rmIL-22 caused a decrease bacterial load in the kidney, and a decreased proportion of mice that developed pyelonephritis. Whilst rmIL-22 was effective at reducing bacterial load when administered therapeutically, a prophylactic regime was largely ineffective. These data support the findings from sterile kidney injury models which found a protective function for IL-22, suggesting repurposing existing immunotherapies may have merit.

6.3 Considerations from this thesis in the context of existing literature

Within this thesis, I primarily explored the effect of type II immunity modulation in experimental pre-clinical models of urinary tract insult using mice. Whilst studies exploring the fundamentals critical to enhance our understanding of the mammalian immune system and for the future development of therapeutic strategies, the clinical context needs to be considered. There are a range of situations whereby the human immune system may be biased towards one type or another, which may contribute to why some people are more susceptible to injury, infection or disease development.

It's well established that children have an enhanced capacity for type II responses, the effect of this is best known in the development of allergy and asthma. Additionally, adult women typically have enhanced type II immunity compared to men, partly due to sex hormones. Oestrogens, 17β-oestradiol in particular, can activate oestrogen receptors on ILC, $CD4^+$ and $CD8^+$ T lymphocytes. Whereas androgens, in particular testosterone, have been found to have a suppressive effect on many subsets of lymphocytes through the androgen receptor. The discrepancy of immunity between children and adults may contribute to why children of either sex more often develop UTI, and why men require dialysis more often than women after AKI. Furthermore, this is why my sterile AKI model and uropathogenic UTI model, and those of others, utilise male and female mice, respectively.

There are also diseases whereby type II immunity is enhanced, such as atopic dermatitis and rheumatoid arthritis; interestingly, patients with both of these conditions have a well-known increased risk of developing UTI but to my knowledge, the link with type II immunity has not been investigated. My results, taken together with current literature, demonstrate that type II immunity is protective during sterile injury in the kidney, yet detrimental in an infectious context. Type II immunity is classically known to have critical roles in the generation of anti-

helminth responses. Yet exaggeration of type II immune responses is observed in multiple conditions such as asthma and dermatitis. In recent years, there has been substantial interest in understanding how and why a type II response is initiated in response to a wide array of microbial and non-microbial stimuli. Indeed, there was an explosion of literature enhancing our understanding of these pathways in multiple tissues following the discovery of ILC2 shortly after I began this project. Although there was an appreciation that type II immune pathways are important for tissue homeostasis, many studies still portrayed these responses as aberrant since they focused on the classical literature only. Yet these responses are critical drivers of tissue repair following an insult. The regulation of these responses is important as exacerbation can drive allergy or even and fibrosis within the tissue.

It is plausible that exaggeration of type II immunity by exogenous IL-33 has a dampening effect on other immune pathways. This theory is supported by my results showing decreased type III immunity in the form of low IL-22 during pyelonephritis, and from others showing a dampening of type I immunity and a bias from T_H1 to T_H2 responses in cystitis; yet the exact mechanism remains elusive. These observations lead to my interest in the role of IL-22 in this context. I theorised that type II immunity might act as a double-edged sword in the context of UTI, since it may impair the innate protective features of the urothelial barrier such as exfoliation, and may switch off required immune pathways required to adequately deal with uropathogens. Whilst little effect was seen in the urinary bladder with exogenous IL-33 or IL-22, there was however, an intriguing phenotype in the kidney with the infection being worse with IL-33, but was largely prevented with IL-22 post-infection regime.

In the gastrointestinal tract, IL-22 has key functions in defence against bacteria by stimulating mucins, but also by inducing the generation of antimicrobial peptides. Together these factors explain how IL-22 improves barrier integrity. The urinary microbiome is poorly understood at present and it is possible that we do not fully appreciate its role in the protection of the urinary

tract against infection from uropathogens. Whilst antibiotics are effective in most cases of UTI, the effect on dysbiosis of the urinary microbiome is not yet understood. In this thesis I describe immune factors which exaggerate and protect against pyelonephritis, these factors can be modulated by existing immunotherapies. However, further investigation of the immune pathways is required before we can speculate on the clinical effectiveness.

6.4 Strengths and limitations of this thesis

These studies were largely carried out in a newly established group with no major funding for this specific project. Resources required for establishment of the *in vivo* models came from institutional pilot/seed funding. Whilst this allowed for the freedom to explore interesting observations and perform discovery-driven research, there were limitations on the types of experiments that were possible. The study of the kidney and bladder was entirely new for the group, the strength is that it was new and exciting, yet it was limited by the need to establish all of the protocols, models, safety and ethics applications within the thesis timeframe.

During the project conceptualisation in 2017, the knowledge of ILC2 in the urinary tract was immature. At this time, there was one paper describing ILC2 being renoprotective through IL-25. Yet whilst setting up this project in 2018, there was an explosion of literature about IL-33 and ILC2, specifically the work involved very similar models of kidney injury with ILC2 expansion, many of the studies using rmIL-33. These studies demonstrated the project was based on a solid hypothesis, yet it meant I then needed to take the project in another direction to maintain novelty; hence, I focused on a loss-of-function in these models of surgical kidney injury instead of ILC2 expansion. Although the impact of the work was somewhat limited by this, I identified that depletion of the cells did not alter the severity of injury. A major strength

was that these studies contributed to the current literature with an in-depth analysis of ILC2 phenotype and localisation in the kidney.

A number of complex GM mouse strains were utilised in this project. These allowed investigation of the role of ILC2 in the kidney using an experimental IRI model and a loss-of-function approach; and to perform a pilot study to investigate these cells in the bladder during UTI. A limitation is that the animals were not bred specifically for this project and had to be utilised in the numbers available surplus to the requirement of the funded project, hence the differing numbers of replicates. In an ideal world, at least twice the number of replicates would have been used for these studies to increase the power of the statistical analysis. However, this approach meant that every litter of pups was able to be assigned to research experiments without any waste, making the project ethical. Additionally, with further funding it would have been possible to perform many assessments at additional timepoints and in different disease models. The effect of ILC2 depletion or exaggeration, localisation of ILC2 in the tissue, distribution of the IL-22 receptor, effect of IL-22 treatment at earlier and later phases of challenge, and many other outcomes were not assessed in the tissues at different timepoints following sterile injury or infection, which is a limitation of the work.

Another limitation is the use of Buprenorphine, an opioid, in each of the *in vivo* models for effective analgesia. Indeed, chronic opioid use is known to decrease the proliferative capacity of subsets of innate and adaptive immune cells in humans and mice, including monocytes and lymphocytes. Although this was an ethical requirement imposed by the institutional animal care and ethics committee, the use of Buprenorphine undoubtably confounded the results. However, it is important to note that all control animals, including sham surgeries, sham infections and vehicle treatment groups, received identical analgesic regime thus somewhat limiting the impact on the conclusions made from these data.

There were several experiments which, to the best of my knowledge, had entirely novel and important observations. In particular, the profiling of ILC2 location and validation of tools to modulate their numbers in the urinary bladder. Additionally, the assessment of conscious kidney function repetitively in the same animals over time had not yet been performed in the context of UTI. Additionally, the serendipitous discovery that rmIL-33 pre-treatment exaggerated pyelonephritis in the cystitis UTI model may have future implications for patients with diseases characterised by exaggerated IL-33. Furthermore, the discovery that a therapeutic treatment regime of rmIL-22 was sufficient to protect against pyelonephritis is likely to be of future interest. These strengths all have the same limitation, these observations are from mice and may not the directly relevant or indicative to human pathophysiology.

In hindsight, a pyelonephritis strain of uropathogen, such as CFT073, would be interesting as a comparison to my results using UTI89. Additionally, studies involving the various strains of C3H mice may yield further insight. Unfortunately, these experiments were not possible in the timeframe of the thesis, nor was there sufficient funding available to perform these supplementary studies.

6.5 Future directions and emerging therapeutics

Further studies are required to elucidate the reason for the presence of ILC2 in the urinary tract, in particular, examining the role of these cells past the acute injury in the progression to chronic disease. These current studies demonstrate that ILC2 are present in the bladder and kidney, that rmIL-33 is effective to increase these cells, and that rmIL-33 has a substantial effect in the context of UTI; future studies will need to perform a more in-depth analysis to hone in on the exact mechanism. It is plausible that it's the increased ILC2 which is responsible for the

pyelonephritis, yet future studies may demonstrate that the type II environment prevents an effective anti-bacterial response in the kidney independent of ILC2 presence. It is essential that the mechanism of IL-33-mediated pyelonephritis is determined before evaluating the emerging IL-33-mediated immunotherapies as a therapeutic for experimental pyelonephritis. Furthermore, a detailed assessment of the immune cell composition by flow cytometry during the various stages of infection would help determine mechanisms and identify the cells producing IL-22, which may be reduced during UTI. It is currently unknown whether IL-22 impacts the ability of bacteria to migrate to the kidney, colonise the kidney or whether it alters bacterial replication in this tissue; therefore, future studies will need to expand upon this work. It is yet to be determined whether the role of IL-22 in the urinary bladder and kidney is primarily antimicrobial or pro-inflammatory. Further study is needed to gain a deeper understanding around the role of IL-22 in the urinary tract. Additionally, future studies will need to determine the most effective treatment regime for IL-22 intervention.

In future studies, there may be sufficient pre-clinical evidence to support the repurposing of existing immunotherapies. REGN3500 (Regeneron Pharmaceuticals) is a monoclonal antibody that inhibits the human IL-33 protein. REGN3500 is currently under investigation in a phase 4 clinical trial (trial # NCT04701983) for the treatment of chronic obstructive pulmonary disease. Clinical safety and pharmacokinetic studies have already been completed as well as trials in atopic dermatitis (trial # NCT03738423) and asthma (trial # NCT02999711). Likewise, an emerging immunotherapy exists in the form of a human recombinant IL-22 IgG2-Fc named F-652 (Generon BioMed), which aims to mimic the protective effects of endogenous IL-22. F-652 is currently under investigation in a phase IIa clinical trial (trial # NCT02406651) for the treatment of graft vs host disease. Clinical safety and pharmacokinetic studies have already been completed as well as a trial in alcoholic hepatitis (trial # NCT02655510). IL-22 may be an attractive novel therapeutic target for severe UTI due to its dual antimicrobial and tissue-

protective effects in other tissue sites. Yet before considering repurposing of either immunotherapy, additional preclinical *in vivo* evidence is required to determine if an IL-33 antibody, or a recombinant form of IL-22 may be suitable as a novel therapy for the treatment of cystitis and pyelonephritis.

6.6 Epilogue

Within this thesis, several knowledge gaps were addressed in the urinary bladder and kidney. In **Chapter 3**, the studies demonstrated the phenotype and location of ILC2 in the kidney under homeostatic conditions, and IRI was used and the severity of injury was assessed using a loss-of-function approach. In **Chapter 4**, the location of ILC2 was demonstrated in the urinary bladder and exogenous IL-33 was sufficient to drive pyelonephritis, impair kidney structure and function, and also decrease kidney IL-22. In **Chapter 5**, low IL-22 was found to be associated with high bacterial load in the kidneys, and exogenous IL-22 was sufficient to prevent pyelonephritis (**Figure 47**).

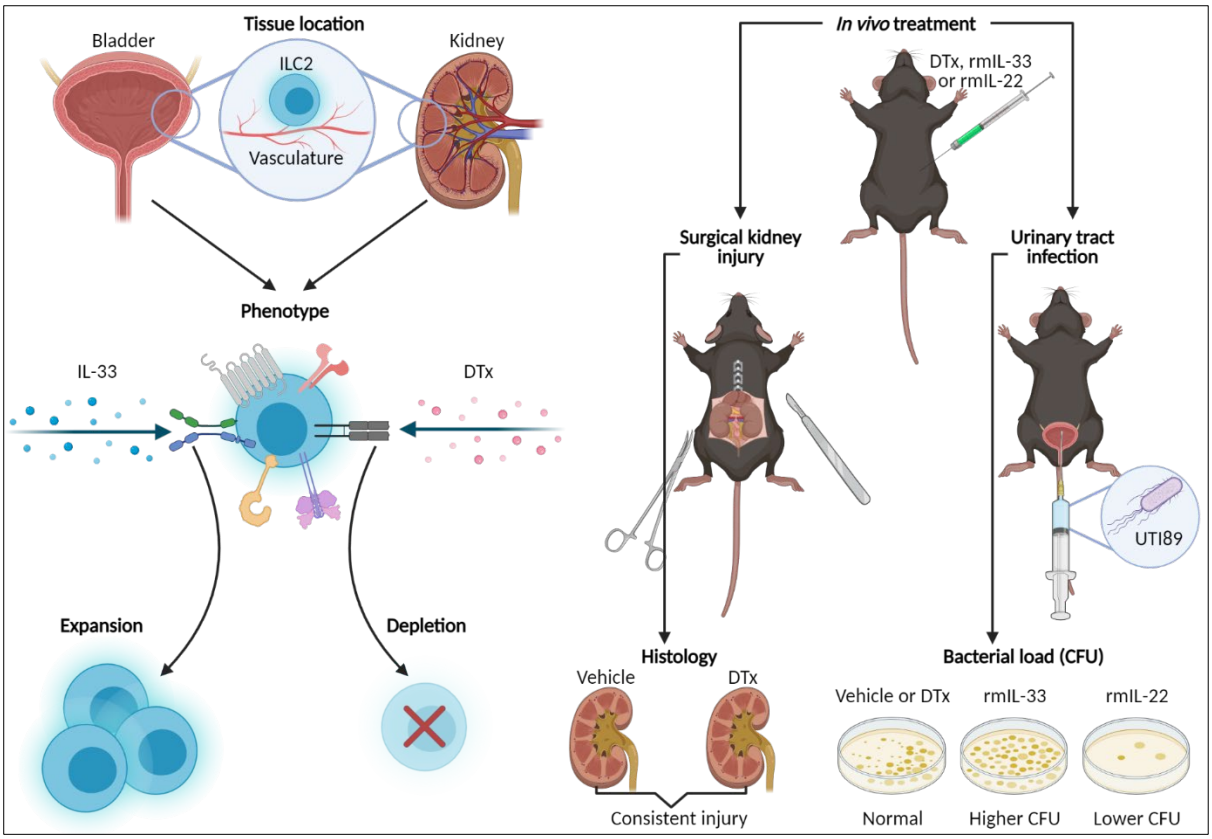

Figure 47: Concluding schematic summarising the knowledge gained from this thesis

Recombinant mouse (rm), interleukin (IL), diphtheria toxoid (DTx), uropathogenic *Escherichia coli* (UTI89). Created with Biorender.com.

References

1. Wallace MA. Anatomy and physiology of the kidney. Aorn j. 1998;68(5):800, 3-16, 19-20; quiz 21-4.

2. Baum M. Role of the kidney in the prenatal and early postnatal programming of hypertension. Am J Physiol Renal Physiol. 2010;298(2):F235-47.

3. Hinchliffe SA, Sargent PH, Howard CV, Chan YF, van Velzen D. Human intrauterine renal growth expressed in absolute number of glomeruli assessed by the disector method and Cavalieri principle. Lab Invest. 1991;64(6):777-84.

4. Levey AS, Coresh J. Chronic kidney disease. Lancet. 2012;379(9811):165-80.

5. Lewington AJ, Cerdá J, Mehta RL. Raising awareness of acute kidney injury: a global perspective of a silent killer. Kidney Int. 2013;84(3):457-67.

6. Bellomo R, Kellum JA, Ronco C. Acute kidney injury. Lancet. 2012;380(9843):756-66.

7. Murugan R, Kellum JA. Acute kidney injury: what's the prognosis? Nat Rev Nephrol. 2011;7(4):209-17.

8. Schrier RW, Wang W, Poole B, Mitra A. Acute renal failure: definitions, diagnosis, pathogenesis, and therapy. J Clin Invest. 2004;114(1):5-14.

9. Ali T, Khan I, Simpson W, Prescott G, Townend J, Smith W, et al. Incidence and outcomes in acute kidney injury: a comprehensive population-based study. J Am Soc Nephrol. 2007;18(4):1292-8.

10. Susantitaphong P, Cruz DN, Cerda J, Abulfaraj M, Alqahtani F, Koulouridis I, et al. World incidence of AKI: a meta-analysis. Clin J Am Soc Nephrol. 2013;8(9):1482-93.

11. Mehta RL, Cerdá J, Burdmann EA, Tonelli M, García-García G, Jha V, et al. International Society of Nephrology's 0by25 initiative for acute kidney injury (zero preventable deaths by 2025): a human rights case for nephrology. Lancet. 2015;385(9987):2616-43.

12. Chertow GM, Burdick E, Honour M, Bonventre JV, Bates DW. Acute kidney injury, mortality, length of stay, and costs in hospitalized patients. J Am Soc Nephrol. 2005;16(11):3365-70.

13. Hsu CY, Ordoñez JD, Chertow GM, Fan D, McCulloch CE, Go AS. The risk of acute renal failure in patients with chronic kidney disease. Kidney Int. 2008;74(1):101-7.

14. Hall AM, Unwin RJ, Parker N, Duchen MR. Multiphoton imaging reveals differences in mitochondrial function between nephron segments. J Am Soc Nephrol. 2009;20(6):1293-302.

15. Devarajan P. Update on mechanisms of ischemic acute kidney injury. J Am Soc Nephrol. 2006;17(6):1503-20.

16. Jang HR, Rabb H. The innate immune response in ischemic acute kidney injury. Clin Immunol. 2009;130(1):41-50.

17. Bonventre JV, Yang L. Cellular pathophysiology of ischemic acute kidney injury. J Clin Invest. 2011;121(11):4210-21.

18. Myers BD, Moran SM. Hemodynamically mediated acute renal failure. N Engl J Med. 1986;314(2):97-105.

19. Brezis M, Rosen S, Silva P, Epstein FH. Renal ischemia: a new perspective. Kidney Int. 1984;26(4):375-83.

20. Eckardt KU, Kasiske BL. Kidney disease: improving global outcomes. Nat Rev Nephrol. 2009;5(11):650-7.

21. Bellomo R, Ronco C, Kellum JA, Mehta RL, Palevsky P. Acute renal failure - definition, outcome measures, animal models, fluid therapy and information technology needs: the Second International Consensus Conference of the Acute Dialysis Quality Initiative (ADQI) Group. Crit Care. 2004;8(4):R204-12.

22. K/DOQI clinical practice guidelines for chronic kidney disease: evaluation, classification, and stratification. Am J Kidney Dis. 2002;39(2 Suppl 1):S1-266.

23. Uchino S, Kellum JA, Bellomo R, Doig GS, Morimatsu H, Morgera S, et al. Acute renal failure in critically ill patients: a multinational, multicenter study. Jama. 2005;294(7):813-8.

24. Hoste EA, Clermont G, Kersten A, Venkataraman R, Angus DC, De Bacquer D, et al. RIFLE criteria for acute kidney injury are associated with hospital mortality in critically ill patients: a cohort analysis. Crit Care. 2006;10(3):R73.

25. Chawla LS, Eggers PW, Star RA, Kimmel PL. Acute kidney injury and chronic kidney disease as interconnected syndromes. N Engl J Med. 2014;371(1):58-66.

26. Chawla LS, Kimmel PL. Acute kidney injury and chronic kidney disease: an integrated clinical syndrome. Kidney Int. 2012;82(5):516-24.

27. Lameire NH, Bagga A, Cruz D, De Maeseneer J, Endre Z, Kellum JA, et al. Acute kidney injury: an increasing global concern. Lancet. 2013;382(9887):170-9.

28. Australian Bureau of Statistics. Australian Health Survey: Biomedical Results for Chronic Diseases, 2011-12, ABS cat. no. 4364.0.55.005. 31–36. 2013.

29. Gong Y, Zhang F, Ding F, Gu Y. Elderly patients with acute kidney injury (AKI): clinical features and risk factors for mortality. Arch Gerontol Geriatr. 2012;54(2):e47-51.

30. Hodeify R, Megyesi J, Tarcsafalvi A, Mustafa HI, Hti Lar Seng NS, Price PM. Gender differences control the susceptibility to ER stress-induced acute kidney injury. Am J Physiol Renal Physiol. 2013;304(7):F875-82.

31. Liangos O, Wald R, O'Bell JW, Price L, Pereira BJ, Jaber BL. Epidemiology and outcomes of acute renal failure in hospitalized patients: a national survey. Clin J Am Soc Nephrol. 2006;1(1):43-51.

32. Obialo CI, Okonofua EC, Tayade AS, Riley LJ. Epidemiology of de novo acute renal failure in hospitalized African Americans: comparing community-acquired vs hospital-acquired disease. Arch Intern Med. 2000;160(9):1309-13.

33. Roberts G, Phillips D, McCarthy R, Bolusani H, Mizen P, Hassan M, et al. Acute kidney injury risk assessment at the hospital front door: what is the best measure of risk? Clin Kidney J. 2015;8(6):673-80.

34. Talabani B, Zouwail S, Pyart RD, Meran S, Riley SG, Phillips AO. Epidemiology and outcome of community-acquired acute kidney injury. Nephrology (Carlton). 2014;19(5):282-7.

35. Kaddourah A, Basu RK, Bagshaw SM, Goldstein SL. Epidemiology of Acute Kidney Injury in Critically Ill Children and Young Adults. N Engl J Med. 2017;376(1):11-20.

36. Thakar CV, Christianson A, Freyberg R, Almenoff P, Render ML. Incidence and outcomes of acute kidney injury in intensive care units: a Veterans Administration study. Crit Care Med. 2009;37(9):2552-8.

37. Kellum JA, Levin N, Bouman C, Lameire N. Developing a consensus classification system for acute renal failure. Curr Opin Crit Care. 2002;8(6):509-14.

38. Kidney Disease: Improving Global Outcomes (KDIGO) Acute Kidney Injury Work Group. KDIGO Clinical Practice Guideline for Acute Kidney Injury. Kidney international supplements. 2012;2(1):1-138.

39. Lieberthal W, Nigam SK. Acute renal failure. II. Experimental models of acute renal failure: imperfect but indispensable. Am J Physiol Renal Physiol. 2000;278(1):F1-f12.

40. Liu J, Kumar S, Dolzhenko E, Alvarado GF, Guo J, Lu C, et al. Molecular characterization of the transition from acute to chronic kidney injury following ischemia/reperfusion. JCI Insight. 2017;2(18).

41. National Kidney Foundation. K/DOQI clinical practice guidelines for chronic kidney disease: evaluation, classification, and stratification. Am J Kidney Dis. 2002;39(2 Suppl 1):S1-266.

42. Kiss N, Hamar P. Histopathological Evaluation of Contrast-Induced Acute Kidney Injury Rodent Models. Biomed Res Int. 2016;2016:3763250.

43. Zuk A, Bonventre JV. Acute Kidney Injury. Annu Rev Med. 2016;67:293-307.

44. Baxmann AC, Ahmed MS, Marques NC, Menon VB, Pereira AB, Kirsztajn GM, et al. Influence of muscle mass and physical activity on serum and urinary creatinine and serum cystatin C. Clin J Am Soc Nephrol. 2008;3(2):348-54.

45. Dirks J, Remuzzi G, Horton S, Schieppati A, Rizvi SAH. Diseases of the Kidney and the Urinary System. In: Jamison DT, Breman JG, Measham AR, Alleyne G, Claeson M, Evans DB, et al., editors. Disease Control Priorities in Developing Countries. Washington (DC), New York: Oxford University Press; 2006.

46. Luke RG. Uremia and the BUN. N Engl J Med. 1981;305(20):1213-5.

47. Lyman JL. Blood urea nitrogen and creatinine. Emerg Med Clin North Am. 1986;4(2):223-33.

48. Amdur RL, Chawla LS, Amodeo S, Kimmel PL, Palant CE. Outcomes following diagnosis of acute renal failure in U.S. veterans: focus on acute tubular necrosis. Kidney Int. 2009;76(10):1089-97.

49. Chawla LS, Amdur RL, Amodeo S, Kimmel PL, Palant CE. The severity of acute kidney injury predicts progression to chronic kidney disease. Kidney Int. 2011;79(12):1361-9.

50. Ishani A, Xue JL, Himmelfarb J, Eggers PW, Kimmel PL, Molitoris BA, et al. Acute kidney injury increases risk of ESRD among elderly. J Am Soc Nephrol. 2009;20(1):223-8.

51. James MT, Ghali WA, Knudtson ML, Ravani P, Tonelli M, Faris P, et al. Associations between acute kidney injury and cardiovascular and renal outcomes after coronary angiography. Circulation. 2011;123(4):409-16.

52. Lo LJ, Go AS, Chertow GM, McCulloch CE, Fan D, Ordoñez JD, et al. Dialysis-requiring acute renal failure increases the risk of progressive chronic kidney disease. Kidney Int. 2009;76(8):893-9.

53. Wald R, Quinn RR, Luo J, Li P, Scales DC, Mamdani MM, et al. Chronic dialysis and death among survivors of acute kidney injury requiring dialysis. Jama. 2009;302(11):1179-85.

54. Murray PT, Devarajan P, Levey AS, Eckardt KU, Bonventre JV, Lombardi R, et al. A framework and key research questions in AKI diagnosis and staging in different environments. Clin J Am Soc Nephrol. 2008;3(3):864-8.

55. Palm CA, Segev G, Cowgill LD, LeRoy BE, Kowalkowski KL, Kanakubo K, et al. Urinary Neutrophil Gelatinase-associated Lipocalin as a Marker for Identification of Acute Kidney Injury and Recovery in Dogs with Gentamicin-induced Nephrotoxicity. J Vet Intern Med. 2016;30(1):200-5.

56. Yatsu T, Arai Y, Takizawa K, Kasai-Nakagawa C, Takanashi M, Uchida W, et al. Effect of YM435, a dopamine DA1 receptor agonist, in a canine model of ischemic acute renal failure. Gen Pharmacol. 1998;31(5):803-7.

57. Park KM, Kim JI, Ahn Y, Bonventre AJ, Bonventre JV. Testosterone is responsible for enhanced susceptibility of males to ischemic renal injury. J Biol Chem. 2004;279(50):52282-92.

58. Wei Q, Dong Z. Mouse model of ischemic acute kidney injury: technical notes and tricks. Am J Physiol Renal Physiol. 2012;303(11):F1487-94.

59. Singh AP, Junemann A, Muthuraman A, Jaggi AS, Singh N, Grover K, et al. Animal models of acute renal failure. Pharmacol Rep. 2012;64(1):31-44.

60. Hesketh EE, Czopek A, Clay M, Borthwick G, Ferenbach D, Kluth D, et al. Renal ischaemia reperfusion injury: a mouse model of injury and regeneration. J Vis Exp. 2014(88).

61. Skrypnyk NI, Harris RC, de Caestecker MP. Ischemia-reperfusion model of acute kidney injury and post injury fibrosis in mice. J Vis Exp. 2013(78).

62. Bascands JL, Schanstra JP. Obstructive nephropathy: insights from genetically engineered animals. Kidney Int. 2005;68(3):925-37.

63. Ucero AC, Benito-Martin A, Izquierdo MC, Sanchez-Niño MD, Sanz AB, Ramos AM, et al. Unilateral ureteral obstruction: beyond obstruction. Int Urol Nephrol. 2014;46(4):765-76.

64. Choi SY, Piao ZH, Jin L, Kim JH, Kim GR, Ryu Y, et al. Piceatannol Attenuates Renal Fibrosis Induced by Unilateral Ureteral Obstruction via Downregulation of Histone Deacetylase 4/5 or p38-MAPK Signaling. PLoS One. 2016;11(11):e0167340.

65. Chung S, Kim S, Kim M, Koh ES, Yoon HE, Kim HS, et al. T-type calcium channel blocker attenuates unilateral ureteral obstruction-induced renal interstitial fibrosis by activating the Nrf2 antioxidant pathway. Am J Transl Res. 2016;8(11):4574-85.

66. Chung S, Yoon HE, Kim SJ, Kim SJ, Koh ES, Hong YA, et al. Oleanolic acid attenuates renal fibrosis in mice with unilateral ureteral obstruction via facilitating nuclear translocation of Nrf2. Nutr Metab (Lond). 2014;11(1):2.

67. Kim S, Kim SJ, Yoon HE, Chung S, Choi BS, Park CW, et al. Fimasartan, a Novel Angiotensin-Receptor Blocker, Protects against Renal Inflammation and Fibrosis in Mice with Unilateral Ureteral Obstruction: the Possible Role of Nrf2. Int J Med Sci. 2015;12(11):891-904.

68. Tian S, Li C, Ran R, Chen SY. Surfactant protein A deficiency exacerbates renal interstitial fibrosis following obstructive injury in mice. Biochim Biophys Acta Mol Basis Dis. 2017;1863(2):509-17.

69. Zhang G, Kim H, Cai X, López-Guisa JM, Alpers CE, Liu Y, et al. Urokinase receptor deficiency accelerates renal fibrosis in obstructive nephropathy. J Am Soc Nephrol. 2003;14(5):1254-71.

70. Kim JS, Han BG, Choi SO, Cha SK. Secondary Focal Segmental Glomerulosclerosis: From Podocyte Injury to Glomerulosclerosis. Biomed Res Int. 2016;2016:1630365.

71. Lee VW, Harris DC. Adriamycin nephropathy: a model of focal segmental glomerulosclerosis. Nephrology (Carlton). 2011;16(1):30-8.

72. Chen YM, Liapis H. Focal segmental glomerulosclerosis: molecular genetics and targeted therapies. BMC Nephrol. 2015;16:101.

73. Fogo AB. Causes and pathogenesis of focal segmental glomerulosclerosis. Nat Rev Nephrol. 2015;11(2):76-87.

74. Kiffel J, Rahimzada Y, Trachtman H. Focal segmental glomerulosclerosis and chronic kidney disease in pediatric patients. Adv Chronic Kidney Dis. 2011;18(5):332-8.

75. Brooks C, Wei Q, Cho SG, Dong Z. Regulation of mitochondrial dynamics in acute kidney injury in cell culture and rodent models. J Clin Invest. 2009;119(5):1275-85.

76. Che R, Yuan Y, Huang S, Zhang A. Mitochondrial dysfunction in the pathophysiology of renal diseases. Am J Physiol Renal Physiol. 2014;306(4):F367-78.

77. Dröse S, Brandt U. Molecular mechanisms of superoxide production by the mitochondrial respiratory chain. Adv Exp Med Biol. 2012;748:145-69.

78. Stallons LJ, Funk JA, Schnellmann RG. Mitochondrial Homeostasis in Acute Organ Failure. Curr Pathobiol Rep. 2013;1(3).

79. Zhan M, Brooks C, Liu F, Sun L, Dong Z. Mitochondrial dynamics: regulatory mechanisms and emerging role in renal pathophysiology. Kidney Int. 2013;83(4):568-81.

80. Duann P, Lianos EA, Ma J, Lin PH. Autophagy, Innate Immunity and Tissue Repair in Acute Kidney Injury. Int J Mol Sci. 2016;17(5).

81. Hammad H, Lambrecht BN. Barrier Epithelial Cells and the Control of Type 2 Immunity. Immunity. 2015;43(1):29-40.

82. Kurts C, Panzer U, Anders HJ, Rees AJ. The immune system and kidney disease: basic concepts and clinical implications. Nat Rev Immunol. 2013;13(10):738-53.

83. Carriere V, Roussel L, Ortega N, Lacorre DA, Americh L, Aguilar L, et al. IL-33, the IL-1-like cytokine ligand for ST2 receptor, is a chromatin-associated nuclear factor in vivo. Proc Natl Acad Sci U S A. 2007;104(1):282-7.

84. Moussion C, Ortega N, Girard JP. The IL-1-like cytokine IL-33 is constitutively expressed in the nucleus of endothelial cells and epithelial cells in vivo: a novel 'alarmin'? PLoS One. 2008;3(10):e3331.

85. Pichery M, Mirey E, Mercier P, Lefrancais E, Dujardin A, Ortega N, et al. Endogenous IL-33 is highly expressed in mouse epithelial barrier tissues, lymphoid organs, brain, embryos, and inflamed tissues: in situ analysis using a novel Il-33-LacZ gene trap reporter strain. J Immunol. 2012;188(7):3488-95.

86. Küchler AM, Pollheimer J, Balogh J, Sponheim J, Manley L, Sorensen DR, et al. Nuclear interleukin-33 is generally expressed in resting endothelium but rapidly lost upon angiogenic or proinflammatory activation. Am J Pathol. 2008;173(4):1229-42.

87. Baekkevold ES, Roussigné M, Yamanaka T, Johansen FE, Jahnsen FL, Amalric F, et al. Molecular characterization of NF-HEV, a nuclear factor preferentially expressed in human high endothelial venules. Am J Pathol. 2003;163(1):69-79.

88. Lingel A, Weiss TM, Niebuhr M, Pan B, Appleton BA, Wiesmann C, et al. Structure of IL-33 and its interaction with the ST2 and IL-1RAcP receptors--insight into heterotrimeric IL-1 signaling complexes. Structure. 2009;17(10):1398-410.

89. Liu X, Hammel M, He Y, Tainer JA, Jeng US, Zhang L, et al. Structural insights into the interaction of IL-33 with its receptors. Proc Natl Acad Sci U S A. 2013;110(37):14918-23.

90. Roussel L, Erard M, Cayrol C, Girard JP. Molecular mimicry between IL-33 and KSHV for attachment to chromatin through the H2A-H2B acidic pocket. EMBO Rep. 2008;9(10):1006-12.

91. Cayrol C, Girard JP. IL-33: an alarmin cytokine with crucial roles in innate immunity, inflammation and allergy. Curr Opin Immunol. 2014;31:31-7.

92. Cayrol C, Girard JP. Interleukin-33 (IL-33): A nuclear cytokine from the IL-1 family. Immunol Rev. 2018;281(1):154-68.

93. Liew FY, Girard JP, Turnquist HR. Interleukin-33 in health and disease. Nat Rev Immunol. 2016;16(11):676-89.

94. Zhou Z, Yan F, Liu O. Interleukin (IL)-33: an orchestrator of immunity from host defence to tissue homeostasis. Clin Transl Immunology. 2020;9(6):e1146.

95. Smithgall MD, Comeau MR, Yoon BR, Kaufman D, Armitage R, Smith DE. IL-33 amplifies both Th1- and Th2-type responses through its activity on human basophils, allergen-reactive Th2 cells, iNKT and NK cells. Int Immunol. 2008;20(8):1019-30.

96. Bonilla WV, Fröhlich A, Senn K, Kallert S, Fernandez M, Johnson S, et al. The alarmin interleukin-33 drives protective antiviral $CD8^+$ T cell responses. Science. 2012;335(6071):984-9.

97. Bourgeois E, Van LP, Samson M, Diem S, Barra A, Roga S, et al. The pro-Th2 cytokine IL-33 directly interacts with invariant NKT and NK cells to induce IFN-gamma production. Eur J Immunol. 2009;39(4):1046-55.

98. Kearley J, Silver JS, Sanden C, Liu Z, Berlin AA, White N, et al. Cigarette smoke silences innate lymphoid cell function and facilitates an exacerbated type I interleukin-33-dependent response to infection. Immunity. 2015;42(3):566-79.

99. Peine M, Marek RM, Löhning M. IL-33 in T Cell Differentiation, Function, and Immune Homeostasis. Trends Immunol. 2016;37(5):321-33.

100. Alves-Filho JC, Sônego F, Souto FO, Freitas A, Verri WA, Jr., Auxiliadora-Martins M, et al. Interleukin-33 attenuates sepsis by enhancing neutrophil influx to the site of infection. Nat Med. 2010;16(6):708-12.

101. Arpaia N, Green JA, Moltedo B, Arvey A, Hemmers S, Yuan S, et al. A Distinct Function of Regulatory T Cells in Tissue Protection. Cell. 2015;162(5):1078-89.

102. Bouchery T, Kyle R, Camberis M, Shepherd A, Filbey K, Smith A, et al. ILC2s and T cells cooperate to ensure maintenance of M2 macrophages for lung immunity against hookworms. Nat Commun. 2015;6:6970.

103. Cherry WB, Yoon J, Bartemes KR, Iijima K, Kita H. A novel IL-1 family cytokine, IL-33, potently activates human eosinophils. J Allergy Clin Immunol. 2008;121(6):1484-90.

104. de Kleer IM, Kool M, de Bruijn MJ, Willart M, van Moorleghem J, Schuijs MJ, et al. Perinatal Activation of the Interleukin-33 Pathway Promotes Type 2 Immunity in the Developing Lung. Immunity. 2016;45(6):1285-98.

105. Eissmann MF, Dijkstra C, Jarnicki A, Phesse T, Brunnberg J, Poh AR, et al. IL-33-mediated mast cell activation promotes gastric cancer through macrophage mobilization. Nat Commun. 2019;10(1):2735.

106. Emi-Sugie M, Toyama S, Matsuda A, Saito H, Matsumoto K. IL-33 induces functional CCR7 expression in human mast cells. J Allergy Clin Immunol. 2018;142(4):1341-4.

107. Espinassous Q, Garcia-de-Paco E, Garcia-Verdugo I, Synguelakis M, von Aulock S, Sallenave JM, et al. IL-33 enhances lipopolysaccharide-induced inflammatory cytokine production from mouse macrophages by regulating lipopolysaccharide receptor complex. J Immunol. 2009;183(2):1446-55.

108. Fu AK, Hung KW, Yuen MY, Zhou X, Mak DS, Chan IC, et al. IL-33 ameliorates Alzheimer's disease-like pathology and cognitive decline. Proc Natl Acad Sci U S A. 2016;113(19):E2705-13.

109. Gadani SP, Smirnov I, Smith AT, Overall CC, Kipnis J. Characterization of meningeal type 2 innate lymphocytes and their response to CNS injury. J Exp Med. 2017;214(2):285-96.

110. Göpfert C, Andreas N, Weber F, Häfner N, Yakovleva T, Gaestel M, et al. The p38-MK2/3 Module Is Critical for IL-33-Induced Signaling and Cytokine Production in Dendritic Cells. J Immunol. 2018;200(3):1198-206.

111. Haenuki Y, Matsushita K, Futatsugi-Yumikura S, Ishii KJ, Kawagoe T, Imoto Y, et al. A critical role of IL-33 in experimental allergic rhinitis. J Allergy Clin Immunol. 2012;130(1):184-94.e11.

112. Joulia R, L'Faqihi FE, Valitutti S, Espinosa E. IL-33 fine tunes mast cell degranulation and chemokine production at the single-cell level. J Allergy Clin Immunol. 2017;140(2):497-509.e10.

113. Kolodin D, van Panhuys N, Li C, Magnuson AM, Cipolletta D, Miller CM, et al. Antigen- and cytokine-driven accumulation of regulatory T cells in visceral adipose tissue of lean mice. Cell Metab. 2015;21(4):543-57.

114. Krishack PA, Louviere TJ, Decker TS, Kuzel TG, Greenberg JA, Camacho DF, et al. Protection against Staphylococcus aureus bacteremia-induced mortality depends on ILC2s and eosinophils. JCI Insight. 2019;4(6).

115. Li D, Guabiraba R, Besnard AG, Komai-Koma M, Jabir MS, Zhang L, et al. IL-33 promotes ST2-dependent lung fibrosis by the induction of alternatively activated macrophages and innate lymphoid cells in mice. J Allergy Clin Immunol. 2014;134(6):1422-32.e11.

116. Matta BM, Reichenbach DK, Zhang X, Mathews L, Koehn BH, Dwyer GK, et al. Peri-alloHCT IL-33 administration expands recipient T-regulatory cells that protect mice against acute GVHD. Blood. 2016;128(3):427-39.

117. Mjösberg JM, Trifari S, Crellin NK, Peters CP, van Drunen CM, Piet B, et al. Human IL-25- and IL-33-responsive type 2 innate lymphoid cells are defined by expression of CRTH2 and CD161. Nat Immunol. 2011;12(11):1055-62.

118. Molofsky AB, Van Gool F, Liang HE, Van Dyken SJ, Nussbaum JC, Lee J, et al. Interleukin-33 and Interferon-γ Counter-Regulate Group 2 Innate Lymphoid Cell Activation during Immune Perturbation. Immunity. 2015;43(1):161-74.

119. Moro K, Yamada T, Tanabe M, Takeuchi T, Ikawa T, Kawamoto H, et al. Innate production of T(H)2 cytokines by adipose tissue-associated c-Kit(+)Sca-1(+) lymphoid cells. Nature. 2010;463(7280):540-4.

120. Neill DR, Wong SH, Bellosi A, Flynn RJ, Daly M, Langford TK, et al. Nuocytes represent a new innate effector leukocyte that mediates type-2 immunity. Nature. 2010;464(7293):1367-70.

121. Nobs SP, Natali S, Pohlmeier L, Okreglicka K, Schneider C, Kurrer M, et al. PPARγ in dendritic cells and T cells drives pathogenic type-2 effector responses in lung inflammation. J Exp Med. 2017;214(10):3015-35.

122. Price AE, Liang HE, Sullivan BM, Reinhardt RL, Eisley CJ, Erle DJ, et al. Systemically dispersed innate IL-13-expressing cells in type 2 immunity. Proc Natl Acad Sci U S A. 2010;107(25):11489-94.

123. Schiering C, Krausgruber T, Chomka A, Fröhlich A, Adelmann K, Wohlfert EA, et al. The alarmin IL-33 promotes regulatory T-cell function in the intestine. Nature. 2014;513(7519):564-8.

124. Sun B, Zhu L, Tao Y, Sun HX, Li Y, Wang P, et al. Characterization and allergic role of IL-33-induced neutrophil polarization. Cell Mol Immunol. 2018;15(8):782-93.

125. Tran VG, Kim HJ, Kim J, Kang SW, Moon UJ, Cho HR, et al. IL-33 Enhances Host Tolerance to Candida albicans Kidney Infections through Induction of IL-13 Production by CD4+ T Cells. J Immunol. 2015;194(10):4871-9.

126. Turnquist HR, Zhao Z, Rosborough BR, Liu Q, Castellaneta A, Isse K, et al. IL-33 expands suppressive CD11b+ Gr-1(int) and regulatory T cells, including ST2L+ Foxp3+ cells, and mediates regulatory T cell-dependent promotion of cardiac allograft survival. J Immunol. 2011;187(9):4598-610.

127. Vasanthakumar A, Moro K, Xin A, Liao Y, Gloury R, Kawamoto S, et al. The transcriptional regulators IRF4, BATF and IL-33 orchestrate development and maintenance of adipose tissue-resident regulatory T cells. Nat Immunol. 2015;16(3):276-85.

128. Wang JX, Kaieda S, Ameri S, Fishgal N, Dwyer D, Dellinger A, et al. IL-33/ST2 axis promotes mast cell survival via BCLXL. Proc Natl Acad Sci U S A. 2014;111(28):10281-6.

129. Spits H, Artis D, Colonna M, Diefenbach A, Di Santo JP, Eberl G, et al. Innate lymphoid cells--a proposal for uniform nomenclature. Nat Rev Immunol. 2013;13(2):145-9.

130. Daussy C, Faure F, Mayol K, Viel S, Gasteiger G, Charrier E, et al. T-bet and Eomes instruct the development of two distinct natural killer cell lineages in the liver and in the bone marrow. J Exp Med. 2014;211(3):563-77.

131. Cella M, Fuchs A, Vermi W, Facchetti F, Otero K, Lennerz JK, et al. A human natural killer cell subset provides an innate source of IL-22 for mucosal immunity. Nature. 2009;457(7230):722-5.

132. Takatori H, Kanno Y, Watford WT, Tato CM, Weiss G, Ivanov, II, et al. Lymphoid tissue inducer-like cells are an innate source of IL-17 and IL-22. J Exp Med. 2009;206(1):35-41.

133. Halim TY, Steer CA, Mathä L, Gold MJ, Martinez-Gonzalez I, McNagny KM, et al. Group 2 innate lymphoid cells are critical for the initiation of adaptive T helper 2 cell-mediated allergic lung inflammation. Immunity. 2014;40(3):425-35.

134. Huang Y, Paul WE. Inflammatory group 2 innate lymphoid cells. Int Immunol. 2016;28(1):23-8.

135. Molofsky AB, Nussbaum JC, Liang HE, Van Dyken SJ, Cheng LE, Mohapatra A, et al. Innate lymphoid type 2 cells sustain visceral adipose tissue eosinophils and alternatively activated macrophages. J Exp Med. 2013;210(3):535-49.

136. Huang Y, Guo L, Qiu J, Chen X, Hu-Li J, Siebenlist U, et al. IL-25-responsive, lineage-negative KLRG1(hi) cells are multipotential 'inflammatory' type 2 innate lymphoid cells. Nat Immunol. 2015;16(2):161-9.

137. Koyasu S. Inflammatory ILC2 cells: disguising themselves as progenitors? Nat Immunol. 2015;16(2):133-4.

138. Nussbaum JC, Van Dyken SJ, von Moltke J, Cheng LE, Mohapatra A, Molofsky AB, et al. Type 2 innate lymphoid cells control eosinophil homeostasis. Nature. 2013;502(7470):245-8.

139. Drake LY, Iijima K, Kita H. Group 2 innate lymphoid cells and CD4+ T cells cooperate to mediate type 2 immune response in mice. Allergy. 2014;69(10):1300-7.

140. Pelly VS, Kannan Y, Coomes SM, Entwistle LJ, Rückerl D, Seddon B, et al. IL-4-producing ILC2s are required for the differentiation of T(H)2 cells following Heligmosomoides polygyrus infection. Mucosal Immunol. 2016;9(6):1407-17.

141. Motomura Y, Morita H, Moro K, Nakae S, Artis D, Endo TA, et al. Basophil-derived interleukin-4 controls the function of natural helper cells, a member of ILC2s, in lung inflammation. Immunity. 2014;40(5):758-71.

142. Pastor-Soler NM, Sutton TA, Mang HE, Kinlough CL, Gendler SJ, Madsen CS, et al. Muc1 is protective during kidney ischemia-reperfusion injury. Am J Physiol Renal Physiol. 2015;308(12):F1452-62.

143. Al-Bataineh MM, Kinlough CL, Poland PA, Pastor-Soler NM, Sutton TA, Mang HE, et al. Muc1 enhances the β-catenin protective pathway during ischemia-reperfusion injury. Am J Physiol Renal Physiol. 2016;310(6):F569-79.

144. Gibier JB, Hémon B, Fanchon M, Gaudelot K, Pottier N, Ringot B, et al. Dual role of MUC1 mucin in kidney ischemia-reperfusion injury: Nephroprotector in early phase, but pro-fibrotic in late phase. Biochim Biophys Acta Mol Basis Dis. 2017;1863(6):1336-49.

145. Lech M, Gröbmayr R, Ryu M, Lorenz G, Hartter I, Mulay SR, et al. Macrophage phenotype controls long-term AKI outcomes--kidney regeneration versus atrophy. J Am Soc Nephrol. 2014;25(2):292-304.

146. Van Dyken SJ, Locksley RM. Interleukin-4- and interleukin-13-mediated alternatively activated macrophages: roles in homeostasis and disease. Annu Rev Immunol. 2013;31:317-43.

147. Maazi H, Patel N, Sankaranarayanan I, Suzuki Y, Rigas D, Soroosh P, et al. ICOS:ICOS-ligand interaction is required for type 2 innate lymphoid cell function, homeostasis, and induction of airway hyperreactivity. Immunity. 2015;42(3):538-51.

148. Kamachi F, Isshiki T, Harada N, Akiba H, Miyake S. ICOS promotes group 2 innate lymphoid cell activation in lungs. Biochem Biophys Res Commun. 2015;463(4):739-45.

149. Rigas D, Lewis G, Aron JL, Wang B, Banie H, Sankaranarayanan I, et al. Type 2 innate lymphoid cell suppression by regulatory T cells attenuates airway hyperreactivity and requires inducible T-cell costimulator-inducible T-cell costimulator ligand interaction. J Allergy Clin Immunol. 2017;139(5):1468-77.e2.

150. Halim TYF, Rana BMJ, Walker JA, Kerscher B, Knolle MD, Jolin HE, et al. Tissue-Restricted Adaptive Type 2 Immunity Is Orchestrated by Expression of the Costimulatory Molecule OX40L on Group 2 Innate Lymphoid Cells. Immunity. 2018;48(6):1195-207.e6.

151. Halim TY, Hwang YY, Scanlon ST, Zaghouani H, Garbi N, Fallon PG, et al. Group 2 innate lymphoid cells license dendritic cells to potentiate memory TH2 cell responses. Nat Immunol. 2016;17(1):57-64.

152. Mirchandani AS, Besnard AG, Yip E, Scott C, Bain CC, Cerovic V, et al. Type 2 innate lymphoid cells drive CD4+ Th2 cell responses. J Immunol. 2014;192(5):2442-8.

153. Zaiss DMW, Gause WC, Osborne LC, Artis D. Emerging functions of amphiregulin in orchestrating immunity, inflammation, and tissue repair. Immunity. 2015;42(2):216-26.

154. Rak GD, Osborne LC, Siracusa MC, Kim BS, Wang K, Bayat A, et al. IL-33-Dependent Group 2 Innate Lymphoid Cells Promote Cutaneous Wound Healing. J Invest Dermatol. 2016;136(2):487-96.

155. Monticelli LA, Sonnenberg GF, Abt MC, Alenghat T, Ziegler CG, Doering TA, et al. Innate lymphoid cells promote lung-tissue homeostasis after infection with influenza virus. Nat Immunol. 2011;12(11):1045-54.

156. Zhou Y, Lee JY, Lee CM, Cho WK, Kang MJ, Koff JL, et al. Amphiregulin, an epidermal growth factor receptor ligand, plays an essential role in the pathogenesis of transforming growth factor-β-induced pulmonary fibrosis. J Biol Chem. 2012;287(50):41991-2000.

157. Kefaloyianni E, Muthu ML, Kaeppler J, Sun X, Sabbisetti V, Chalaris A, et al. ADAM17 substrate release in proximal tubule drives kidney fibrosis. JCI Insight. 2016;1(13).

158. Cao Q, Wang Y, Niu Z, Wang C, Wang R, Zhang Z, et al. Potentiating Tissue-Resident Type 2 Innate Lymphoid Cells by IL-33 to Prevent Renal Ischemia-Reperfusion Injury. J Am Soc Nephrol. 2018;29(3):961-76.

159. Oliphant CJ, Hwang YY, Walker JA, Salimi M, Wong SH, Brewer JM, et al. MHCII-mediated dialog between group 2 innate lymphoid cells and CD4(+) T cells potentiates type 2 immunity and promotes parasitic helminth expulsion. Immunity. 2014;41(2):283-95.

160. Klose CSN, Mahlakõiv T, Moeller JB, Rankin LC, Flamar AL, Kabata H, et al. The neuropeptide neuromedin U stimulates innate lymphoid cells and type 2 inflammation. Nature. 2017;549(7671):282-6.

161. Cardoso V, Chesné J, Ribeiro H, García-Cassani B, Carvalho T, Bouchery T, et al. Neuronal regulation of type 2 innate lymphoid cells via neuromedin U. Nature. 2017;549(7671):277-81.

162. Wallrapp A, Riesenfeld SJ, Burkett PR, Abdulnour RE, Nyman J, Dionne D, et al. The neuropeptide NMU amplifies ILC2-driven allergic lung inflammation. Nature. 2017;549(7672):351-6.

163. Laffont S, Blanquart E, Savignac M, Cénac C, Laverny G, Metzger D, et al. Androgen signaling negatively controls group 2 innate lymphoid cells. J Exp Med. 2017;214(6):1581-92.

164. Warren KJ, Sweeter JM, Pavlik JA, Nelson AJ, Devasure JM, Dickinson JD, et al. Sex differences in activation of lung-related type 2 innate lymphoid cells in experimental asthma. Ann Allergy Asthma Immunol. 2017;118(2):233-4.

165. Cephus JY, Stier MT, Fuseini H, Yung JA, Toki S, Bloodworth MH, et al. Testosterone Attenuates Group 2 Innate Lymphoid Cell-Mediated Airway Inflammation. Cell Rep. 2017;21(9):2487-99.

166. Bartemes K, Chen CC, Iijima K, Drake L, Kita H. IL-33-Responsive Group 2 Innate Lymphoid Cells Are Regulated by Female Sex Hormones in the Uterus. J Immunol. 2018;200(1):229-36.

167. Kadel S, Ainsua-Enrich E, Hatipoglu I, Turner S, Singh S, Khan S, et al. A Major Population of Functional KLRG1(-) ILC2s in Female Lungs Contributes to a Sex Bias in ILC2 Numbers. Immunohorizons. 2018;2(2):74-86.

168. Kang KP, Lee JE, Lee AS, Jung YJ, Kim D, Lee S, et al. Effect of gender differences on the regulation of renal ischemia-reperfusion-induced inflammation in mice. Mol Med Rep. 2014;9(6):2061-8.

169. Duerr CU, McCarthy CD, Mindt BC, Rubio M, Meli AP, Pothlichet J, et al. Type I interferon restricts type 2 immunopathology through the regulation of group 2 innate lymphoid cells. Nat Immunol. 2016;17(1):65-75.

170. Stier MT, Goleniewska K, Cephus JY, Newcomb DC, Sherrill TP, Boyd KL, et al. STAT1 Represses Cytokine-Producing Group 2 and Group 3 Innate Lymphoid Cells during Viral Infection. J Immunol. 2017;199(2):510-9.

171. Moro K, Kabata H, Tanabe M, Koga S, Takeno N, Mochizuki M, et al. Interferon and IL-27 antagonize the function of group 2 innate lymphoid cells and type 2 innate immune responses. Nat Immunol. 2016;17(1):76-86.

172. Hansbro PM, Scott GV, Essilfie AT, Kim RY, Starkey MR, Nguyen DH, et al. Th2 cytokine antagonists: potential treatments for severe asthma. Expert Opin Investig Drugs. 2013;22(1):49-69.

173. Huang Q, Niu Z, Tan J, Yang J, Liu Y, Ma H, et al. IL-25 Elicits Innate Lymphoid Cells and Multipotent Progenitor Type 2 Cells That Reduce Renal Ischemic/Reperfusion Injury. J Am Soc Nephrol. 2015;26(9):2199-211.

174. Riedel JH, Becker M, Kopp K, Düster M, Brix SR, Meyer-Schwesinger C, et al. IL-33-Mediated Expansion of Type 2 Innate Lymphoid Cells Protects from Progressive Glomerulosclerosis. J Am Soc Nephrol. 2017;28(7):2068-80.

175. Ali S, Huber M, Kollewe C, Bischoff SC, Falk W, Martin MU. IL-1 receptor accessory protein is essential for IL-33-induced activation of T lymphocytes and mast cells. Proc Natl Acad Sci U S A. 2007;104(47):18660-5.

176. Suzukawa M, Iikura M, Koketsu R, Nagase H, Tamura C, Komiya A, et al. An IL-1 cytokine member, IL-33, induces human basophil activation via its ST2 receptor. J Immunol. 2008;181(9):5981-9.

177. Stolarski B, Kurowska-Stolarska M, Kewin P, Xu D, Liew FY. IL-33 exacerbates eosinophil-mediated airway inflammation. J Immunol. 2010;185(6):3472-80.

178. Stremska ME, Jose S, Sabapathy V, Huang L, Bajwa A, Kinsey GR, et al. IL233, A Novel IL-2 and IL-33 Hybrid Cytokine, Ameliorates Renal Injury. J Am Soc Nephrol. 2017;28(9):2681-93.

179. Starkey MR, McKenzie AN, Belz GT, Hansbro PM. Pulmonary group 2 innate lymphoid cells: surprises and challenges. Mucosal Immunol. 2019;12(2):299-311.

180. Vély F, Barlogis V, Vallentin B, Neven B, Piperoglou C, Ebbo M, et al. Evidence of innate lymphoid cell redundancy in humans. Nat Immunol. 2016;17(11):1291-9.

181. Akcay A, Nguyen Q, He Z, Turkmen K, Won Lee D, Hernando AA, et al. IL-33 exacerbates acute kidney injury. J Am Soc Nephrol. 2011;22(11):2057-67.

182. Liang H, Xu F, Wen XJ, Liu HZ, Wang HB, Zhong JY, et al. Interleukin-33 signaling contributes to renal fibrosis following ischemia reperfusion. Eur J Pharmacol. 2017;812:18-27.

183. Chen WY, Chang YJ, Su CH, Tsai TH, Chen SD, Hsing CH, et al. Upregulation of Interleukin-33 in obstructive renal injury. Biochem Biophys Res Commun. 2016;473(4):1026-32.

184. Ferhat M, Robin A, Giraud S, Sena S, Goujon JM, Touchard G, et al. Endogenous IL-33 Contributes to Kidney Ischemia-Reperfusion Injury as an Alarmin. J Am Soc Nephrol. 2018;29(4):1272-88.

185. J. Gordon Betts, Kelly A. Young, James A. Wise, Eddie Johnson, Brandon Poe, Dean H. Kruse, et al. Anatomy and Physiology, The Urinary System and Homeostasis. OpenStax; 2013.

186. Sugaya K, Nishijima S, Miyazato M, Ogawa Y. Central nervous control of micturition and urine storage. J Smooth Muscle Res. 2005;41(3):117-32.

187. Varley C, Hill G, Pellegrin S, Shaw NJ, Selby PJ, Trejdosiewicz LK, et al. Autocrine regulation of human urothelial cell proliferation and migration during regenerative responses in vitro. Exp Cell Res. 2005;306(1):216-29.

188. Lazzeri M. The physiological function of the urothelium--more than a simple barrier. Urol Int. 2006;76(4):289-95.

189. Whiteside SA, Razvi H, Dave S, Reid G, Burton JP. The microbiome of the urinary tract--a role beyond infection. Nat Rev Urol. 2015;12(2):81-90.

190. Kolman KB. Cystitis and Pyelonephritis: Diagnosis, Treatment, and Prevention. Prim Care. 2019;46(2):191-202.

191. Simões e Silva AC, Oliveira EA. Update on the approach of urinary tract infection in childhood. J Pediatr (Rio J). 2015;91(6 Suppl 1):S2-10.

192. Stamm WE, Norrby SR. Urinary tract infections: disease panorama and challenges. J Infect Dis. 2001;183 Suppl 1:S1-4.

193. Shaikh N, Morone NE, Bost JE, Farrell MH. Prevalence of urinary tract infection in childhood: a meta-analysis. Pediatr Infect Dis J. 2008;27(4):302-8.

194. Keren R, Shaikh N, Pohl H, Gravens-Mueller L, Ivanova A, Zaoutis L, et al. Risk Factors for Recurrent Urinary Tract Infection and Renal Scarring. Pediatrics. 2015;136(1):e13-21.

195. Foxman B. Epidemiology of urinary tract infections: incidence, morbidity, and economic costs. Am J Med. 2002;113 Suppl 1A:5s-13s.

196. Dwyer PL, O'Reilly M. Recurrent urinary tract infection in the female. Curr Opin Obstet Gynecol. 2002;14(5):537-43.

197. Shaikh N, Haralam MA, Kurs-Lasky M, Hoberman A. Association of Renal Scarring With Number of Febrile Urinary Tract Infections in Children. JAMA Pediatr. 2019;173(10):949-52.

198. Price E, Pallett A, Gilbert RD, Williams C. Microbiological aspects of the UK National Institute for Health and Clinical Excellence (NICE) guidance on urinary tract infection in children. J Antimicrob Chemother. 2010;65(5):836-41.

199. Kohler TS, Yadven M, Manvar A, Liu N, Monga M. The length of the male urethra. Int Braz J Urol. 2008;34(4):451-4; discussion 5-6.

200. Lacerda Mariano L, Ingersoll MA. The immune response to infection in the bladder. Nat Rev Urol. 2020;17(8):439-58.

201. Raz R. Urinary tract infection in postmenopausal women. Korean J Urol. 2011;52(12):801-8.

202. Scholes D, Hooton TM, Roberts PL, Stapleton AE, Gupta K, Stamm WE. Risk factors for recurrent urinary tract infection in young women. J Infect Dis. 2000;182(4):1177-82.

203. Zychlinsky Scharff A, Rousseau M, Lacerda Mariano L, Canton T, Consiglio CR, Albert ML, et al. Sex differences in IL-17 contribute to chronicity in male versus female urinary tract infection. JCI Insight. 2019;5(13).

204. Kofteridis DP, Papadimitraki E, Mantadakis E, Maraki S, Papadakis JA, Tzifa G, et al. Effect of diabetes mellitus on the clinical and microbiological features of hospitalized elderly patients with acute pyelonephritis. J Am Geriatr Soc. 2009;57(11):2125-8.

205. Ronald A, Ludwig E. Urinary tract infections in adults with diabetes. Int J Antimicrob Agents. 2001;17(4):287-92.

206. Walker E, Lyman A, Gupta K, Mahoney MV, Snyder GM, Hirsch EB. Clinical Management of an Increasing Threat: Outpatient Urinary Tract Infections Due to Multidrug-Resistant Uropathogens. Clin Infect Dis. 2016;63(7):960-5.

207. Miano R, Germani S, Vespasiani G. Stones and urinary tract infections. Urol Int. 2007;79 Suppl 1:32-6.

208. Horan TC, Andrus M, Dudeck MA. CDC/NHSN surveillance definition of health care-associated infection and criteria for specific types of infections in the acute care setting. Am J Infect Control. 2008;36(5):309-32.

209. Rubin RH, Shapiro ED, Andriole VT, Davis RJ, Stamm WE. Evaluation of new anti-infective drugs for the treatment of urinary tract infection. Infectious Diseases Society of America and the Food and Drug Administration. Clin Infect Dis. 1992;15 Suppl 1:S216-27.

210. Johansen TE, Botto H, Cek M, Grabe M, Tenke P, Wagenlehner FM, et al. Critical review of current definitions of urinary tract infections and proposal of an EAU/ESIU classification system. Int J Antimicrob Agents. 2011;38 Suppl:64-70.

211. Bonkat G, Bartoletti R, Bruyère F, Cai T, Geerlings SE, Köves B, et al. EAU Urological Infections Guidelines 2021. ISBN 978-94-92671-13-4. Available from: https://uroweb.org/wp-content/uploads/EAU-Guidelines-on-Urological-infections-2021.pdf.

212. O'Brien VP, Dorsey DA, Hannan TJ, Hultgren SJ. Host restriction of Escherichia coli recurrent urinary tract infection occurs in a bacterial strain-specific manner. PLoS Pathog. 2018;14(12):e1007457.

213. Hannan TJ, Mysorekar IU, Hung CS, Isaacson-Schmid ML, Hultgren SJ. Early severe inflammatory responses to uropathogenic E. coli predispose to chronic and recurrent urinary tract infection. PLoS Pathog. 2010;6(8):e1001042.

214. Hoberman A, Wald ER, Reynolds EA, Penchansky L, Charron M. Pyuria and bacteriuria in urine specimens obtained by catheter from young children with fever. J Pediatr. 1994;124(4):513-9.

215. Wolfe AJ, Toh E, Shibata N, Rong R, Kenton K, Fitzgerald M, et al. Evidence of uncultivated bacteria in the adult female bladder. J Clin Microbiol. 2012;50(4):1376-83.

216. Hilt EE, McKinley K, Pearce MM, Rosenfeld AB, Zilliox MJ, Mueller ER, et al. Urine is not sterile: use of enhanced urine culture techniques to detect resident bacterial flora in the adult female bladder. J Clin Microbiol. 2014;52(3):871-6.

217. Flores-Mireles AL, Walker JN, Caparon M, Hultgren SJ. Urinary tract infections: epidemiology, mechanisms of infection and treatment options. Nat Rev Microbiol. 2015;13(5):269-84.

218. Foxman B. Urinary tract infection syndromes: occurrence, recurrence, bacteriology, risk factors, and disease burden. Infect Dis Clin North Am. 2014;28(1):1-13.

219. Ramakrishnan K, Scheid DC. Diagnosis and management of acute pyelonephritis in adults. Am Fam Physician. 2005;71(5):933-42.

220. Jakobsson B, Berg U, Svensson L. Renal scarring after acute pyelonephritis. Arch Dis Child. 1994;70(2):111-5.

221. Jacobson SH, Eklöf O, Lins LE, Wikstad I, Winberg J. Long-term prognosis of post-infectious renal scarring in relation to radiological findings in childhood--a 27-year follow-up. Pediatr Nephrol. 1992;6(1):19-24.

222. Berry SH, Elliott MN, Suttorp M, Bogart LM, Stoto MA, Eggers P, et al. Prevalence of symptoms of bladder pain syndrome/interstitial cystitis among adult females in the United States. J Urol. 2011;186(2):540-4.

223. Clemens JQ, Meenan RT, O'Keeffe Rosetti MC, Brown SO, Gao SY, Calhoun EA. Prevalence of interstitial cystitis symptoms in a managed care population. J Urol. 2005;174(2):576-80.

224. Belyayeva M, Jeong JM. Acute Pyelonephritis. StatPearls. Treasure Island (FL): StatPearls Publishing; 2020.

225. Wennerström M, Hansson S, Hedner T, Himmelmann A, Jodal U. Ambulatory blood pressure 16-26 years after the first urinary tract infection in childhood. J Hypertens. 2000;18(4):485-91.

226. Hsiao CY, Yang HY, Hsiao MC, Hung PH, Wang MC. Risk Factors for Development of Acute Kidney Injury in Patients with Urinary Tract Infection. PLoS One. 2015;10(7):e0133835.

227. Wagenlehner FM, Tandogdu Z, Bjerklund Johansen TE. An update on classification and management of urosepsis. Curr Opin Urol. 2017;27(2):133-7.

228. Ferry SA, Holm SE, Stenlund H, Lundholm R, Monsen TJ. The natural course of uncomplicated lower urinary tract infection in women illustrated by a randomized placebo controlled study. Scand J Infect Dis. 2004;36(4):296-301.

229. Bryce A, Hay AD, Lane IF, Thornton HV, Wootton M, Costelloe C. Global prevalence of antibiotic resistance in paediatric urinary tract infections caused by Escherichia coli and association with routine use of antibiotics in primary care: systematic review and meta-analysis. Bmj. 2016;352:i939.

230. Matthews PC, Barrett LK, Warren S, Stoesser N, Snelling M, Scarborough M, et al. Oral fosfomycin for treatment of urinary tract infection: a retrospective cohort study. BMC Infect Dis. 2016;16(1):556.

231. Asadi Karam MR, Habibi M, Bouzari S. Urinary tract infection: Pathogenicity, antibiotic resistance and development of effective vaccines against Uropathogenic Escherichia coli. Mol Immunol. 2019;108:56-67.

232. Bitew A, Molalign T, Chanie M. Species distribution and antibiotic susceptibility profile of bacterial uropathogens among patients complaining urinary tract infections. BMC Infect Dis. 2017;17(1):654.

233. Hay AD, Costelloe C. Antibiotics for childhood urinary tract infection: can we be smarter? Br J Gen Pract. 2013;63(609):175-6.

234. Gupta K, Hooton TM, Naber KG, Wullt B, Colgan R, Miller LG, et al. International clinical practice guidelines for the treatment of acute uncomplicated cystitis and pyelonephritis

in women: A 2010 update by the Infectious Diseases Society of America and the European Society for Microbiology and Infectious Diseases. Clin Infect Dis. 2011;52(5):e103-20.

235. Smellie JM, Grüneberg RN, Leakey A, Atkin WS. Long-term low-dose co-trimoxazole in prophylaxis of childhood urinary tract infection: clinical aspects. Br Med J. 1976;2(6029):203-6.

236. Roustit M, Blondel E, Villier C, Fonrose X, Mallaret MP. Symptomatic hypoglycemia associated with trimethoprim/sulfamethoxazole and repaglinide in a diabetic patient. Ann Pharmacother. 2010;44(4):764-7.

237. Greenberg S, Reiser IW, Chou SY, Porush JG. Trimethoprim-sulfamethoxazole induces reversible hyperkalemia. Ann Intern Med. 1993;119(4):291-5.

238. Fischer HD, Juurlink DN, Mamdani MM, Kopp A, Laupacis A. Hemorrhage during warfarin therapy associated with cotrimoxazole and other urinary tract anti-infective agents: a population-based study. Arch Intern Med. 2010;170(7):617-21.

239. Williams G, Craig JC. Long-term antibiotics for preventing recurrent urinary tract infection in children. Cochrane Database Syst Rev. 2019;4(4):Cd001534.

240. Novelli A, Rosi E. Pharmacological properties of oral antibiotics for the treatment of uncomplicated urinary tract infections. J Chemother. 2017;29(sup1):10-8.

241. Palou J, Angulo JC, Ramón de Fata F, García-Tello A, González-Enguita C, Boada A, et al. Randomized comparative study for the assessment of a new therapeutic schedule of fosfomycin trometamol in postmenopausal women with uncomplicated lower urinary tract infection. Actas Urol Esp (English Edition). 2013;37(3):147-55.

242. Schilling JD, Lorenz RG, Hultgren SJ. Effect of trimethoprim-sulfamethoxazole on recurrent bacteriuria and bacterial persistence in mice infected with uropathogenic Escherichia coli. Infect Immun. 2002;70(12):7042-9.

243. Terlizzi ME, Gribaudo G, Maffei ME. UroPathogenic Escherichia coli (UPEC) Infections: Virulence Factors, Bladder Responses, Antibiotic, and Non-antibiotic Antimicrobial Strategies. Front Microbiol. 2017;8:1566.

244. Manges AR, Johnson JR, Foxman B, O'Bryan TT, Fullerton KE, Riley LW. Widespread distribution of urinary tract infections caused by a multidrug-resistant Escherichia coli clonal group. N Engl J Med. 2001;345(14):1007-13.

245. Blango MG, Mulvey MA. Persistence of uropathogenic Escherichia coli in the face of multiple antibiotics. Antimicrob Agents Chemother. 2010;54(5):1855-63.

246. Hvidberg H, Struve C, Krogfelt KA, Christensen N, Rasmussen SN, Frimodt-Møller N. Development of a long-term ascending urinary tract infection mouse model for antibiotic treatment studies. Antimicrob Agents Chemother. 2000;44(1):156-63.

247. Wright KJ, Seed PC, Hultgren SJ. Development of intracellular bacterial communities of uropathogenic Escherichia coli depends on type 1 pili. Cell Microbiol. 2007;9(9):2230-41.

248. Demir M, Kazanasmaz H. Uropathogens and antibiotic resistance in the community and hospital-induced urinary tract infected children. J Glob Antimicrob Resist. 2020;20:68-73.

249. Gaspari RJ, Dickson E, Karlowsky J, Doern G. Antibiotic resistance trends in paediatric uropathogens. Int J Antimicrob Agents. 2005;26(4):267-71.

250. Pratt LA, Kolter R. Genetic analysis of Escherichia coli biofilm formation: roles of flagella, motility, chemotaxis and type I pili. Mol Microbiol. 1998;30(2):285-93.

251. Thumbikat P, Berry RE, Zhou G, Billips BK, Yaggie RE, Zaichuk T, et al. Bacteria-induced uroplakin signaling mediates bladder response to infection. PLoS Pathog. 2009;5(5):e1000415.

252. Thomas WE, Trintchina E, Forero M, Vogel V, Sokurenko EV. Bacterial adhesion to target cells enhanced by shear force. Cell. 2002;109(7):913-23.

253. Mysorekar IU, Hultgren SJ. Mechanisms of uropathogenic Escherichia coli persistence and eradication from the urinary tract. Proc Natl Acad Sci U S A. 2006;103(38):14170-5.

254. Martinez JJ, Mulvey MA, Schilling JD, Pinkner JS, Hultgren SJ. Type 1 pilus-mediated bacterial invasion of bladder epithelial cells. Embo j. 2000;19(12):2803-12.

255. Song J, Bishop BL, Li G, Duncan MJ, Abraham SN. TLR4-initiated and cAMP-mediated abrogation of bacterial invasion of the bladder. Cell Host Microbe. 2007;1(4):287-98.

256. Lane MC, Alteri CJ, Smith SN, Mobley HL. Expression of flagella is coincident with uropathogenic Escherichia coli ascension to the upper urinary tract. Proc Natl Acad Sci U S A. 2007;104(42):16669-74.

257. Wiles TJ, Kulesus RR, Mulvey MA. Origins and virulence mechanisms of uropathogenic Escherichia coli. Exp Mol Pathol. 2008;85(1):11-9.

258. Watts RE, Totsika M, Challinor VL, Mabbett AN, Ulett GC, De Voss JJ, et al. Contribution of siderophore systems to growth and urinary tract colonization of asymptomatic bacteriuria Escherichia coli. Infect Immun. 2012;80(1):333-44.

259. Keane WF, Welch R, Gekker G, Peterson PK. Mechanism of Escherichia coli alpha-hemolysin-induced injury to isolated renal tubular cells. Am J Pathol. 1987;126(2):350-7.

260. Spurbeck RR, Dinh PC, Jr., Walk ST, Stapleton AE, Hooton TM, Nolan LK, et al. Escherichia coli isolates that carry vat, fyuA, chuA, and yfcV efficiently colonize the urinary tract. Infect Immun. 2012;80(12):4115-22.

261. Mills M, Meysick KC, O'Brien AD. Cytotoxic necrotizing factor type 1 of uropathogenic Escherichia coli kills cultured human uroepithelial 5637 cells by an apoptotic mechanism. Infect Immun. 2000;68(10):5869-80.

262. Bower JM, Eto DS, Mulvey MA. Covert operations of uropathogenic Escherichia coli within the urinary tract. Traffic. 2005;6(1):18-31.

263. Guyer DM, Radulovic S, Jones FE, Mobley HL. Sat, the secreted autotransporter toxin of uropathogenic Escherichia coli, is a vacuolating cytotoxin for bladder and kidney epithelial cells. Infect Immun. 2002;70(8):4539-46.

264. Horwitz MA, Silverstein SC. Influence of the Escherichia coli capsule on complement fixation and on phagocytosis and killing by human phagocytes. J Clin Invest. 1980;65(1):82-94.

265. Aguiniga LM, Yaggie RE, Schaeffer AJ, Klumpp DJ. Lipopolysaccharide Domains Modulate Urovirulence. Infect Immun. 2016;84(11):3131-40.

266. Zhang G, Meredith TC, Kahne D. On the essentiality of lipopolysaccharide to Gram-negative bacteria. Curr Opin Microbiol. 2013;16(6):779-85.

267. Kaper JB, Nataro JP, Mobley HL. Pathogenic Escherichia coli. Nat Rev Microbiol. 2004;2(2):123-40.

268. Abraham SN, Miao Y. The nature of immune responses to urinary tract infections. Nat Rev Immunol. 2015;15(10):655-63.

269. Mysorekar IU, Isaacson-Schmid M, Walker JN, Mills JC, Hultgren SJ. Bone morphogenetic protein 4 signaling regulates epithelial renewal in the urinary tract in response to uropathogenic infection. Cell Host Microbe. 2009;5(5):463-75.

270. Mulvey MA, Schilling JD, Hultgren SJ. Establishment of a persistent Escherichia coli reservoir during the acute phase of a bladder infection. Infect Immun. 2001;69(7):4572-9.

271. Miguel DF, Terreri MT, Pereira RMR, Bonfá E, Silva CAA, Corrente JE, et al. Comparison of urinary parameters, biomarkers, and outcome of childhood systemic lupus erythematosus early onset-lupus nephritis. Adv Rheumatol. 2020;60(1):10.

272. Olson PD, McLellan LK, Liu A, Briden KE, Tiemann KM, Daugherty AL, et al. Renal scar formation and kidney function following antibiotic-treated murine pyelonephritis. Dis Model Mech. 2017;10(11):1371-9.

273. Schilling JD, Martin SM, Hunstad DA, Patel KP, Mulvey MA, Justice SS, et al. CD14- and Toll-like receptor-dependent activation of bladder epithelial cells by lipopolysaccharide and type 1 piliated Escherichia coli. Infect Immun. 2003;71(3):1470-80.

274. Cunningham PN, Wang Y, Guo R, He G, Quigg RJ. Role of Toll-like receptor 4 in endotoxin-induced acute renal failure. J Immunol. 2004;172(4):2629-35.

275. Samuelsson P, Hang L, Wullt B, Irjala H, Svanborg C. Toll-like receptor 4 expression and cytokine responses in the human urinary tract mucosa. Infect Immun. 2004;72(6):3179-86.

276. Krzemień G, Szmigielska A, Turczyn A, Pańczyk-Tomaszewska M. Urine interleukin-6, interleukin-8 and transforming growth factor β1 in infants with urinary tract infection and asymptomatic bacteriuria. Cent Eur J Immunol. 2016;41(3):260-7.

277. Engelsöy U, Rangel I, Demirel I. Impact of Proinflammatory Cytokines on the Virulence of Uropathogenic Escherichia coli. Front Microbiol. 2019;10:1051.

278. Valore EV, Park CH, Quayle AJ, Wiles KR, McCray PB, Jr., Ganz T. Human beta-defensin-1: an antimicrobial peptide of urogenital tissues. J Clin Invest. 1998;101(8):1633-42.

279. Chromek M, Slamová Z, Bergman P, Kovács L, Podracká L, Ehrén I, et al. The antimicrobial peptide cathelicidin protects the urinary tract against invasive bacterial infection. Nat Med. 2006;12(6):636-41.

280. Schiwon M, Weisheit C, Franken L, Gutweiler S, Dixit A, Meyer-Schwesinger C, et al. Crosstalk between sentinel and helper macrophages permits neutrophil migration into infected uroepithelium. Cell. 2014;156(3):456-68.

281. Ingersoll MA, Kline KA, Nielsen HV, Hultgren SJ. G-CSF induction early in uropathogenic Escherichia coli infection of the urinary tract modulates host immunity. Cell Microbiol. 2008;10(12):2568-78.

282. Mora-Bau G, Platt AM, van Rooijen N, Randolph GJ, Albert ML, Ingersoll MA. Macrophages Subvert Adaptive Immunity to Urinary Tract Infection. PLoS Pathog. 2015;11(7):e1005044.

283. Duell BL, Carey AJ, Tan CK, Cui X, Webb RI, Totsika M, et al. Innate transcriptional networks activated in bladder in response to uropathogenic Escherichia coli drive diverse biological pathways and rapid synthesis of IL-10 for defense against bacterial urinary tract infection. J Immunol. 2012;188(2):781-92.

284. Ko YC, Mukaida N, Ishiyama S, Tokue A, Kawai T, Matsushima K, et al. Elevated interleukin-8 levels in the urine of patients with urinary tract infections. Infect Immun. 1993;61(4):1307-14.

285. Hang L, Haraoka M, Agace WW, Leffler H, Burdick M, Strieter R, et al. Macrophage inflammatory protein-2 is required for neutrophil passage across the epithelial barrier of the infected urinary tract. J Immunol. 1999;162(5):3037-44.

286. Bowen SE, Watt CL, Murawski IJ, Gupta IR, Abraham SN. Interplay between vesicoureteric reflux and kidney infection in the development of reflux nephropathy in mice. Dis Model Mech. 2013;6(4):934-41.

287. Mobley HL, Green DM, Trifillis AL, Johnson DE, Chippendale GR, Lockatell CV, et al. Pyelonephritogenic Escherichia coli and killing of cultured human renal proximal tubular epithelial cells: role of hemolysin in some strains. Infect Immun. 1990;58(5):1281-9.

288. Schwartz DJ, Conover MS, Hannan TJ, Hultgren SJ. Uropathogenic Escherichia coli superinfection enhances the severity of mouse bladder infection. PLoS Pathog. 2015;11(1):e1004599.

289. Mühl H. Pro-Inflammatory Signaling by IL-10 and IL-22: Bad Habit Stirred Up by Interferons? Front Immunol. 2013;4:18.

290. Jee MH, Johansen JD, Buus TB, Petersen TH, Gadsbøll A, Woetmann A, et al. Increased Production of IL-17A-Producing γδ T Cells in the Thymus of Filaggrin-Deficient Mice. Front Immunol. 2018;9:988.

291. Kleinschek MA, Boniface K, Sadekova S, Grein J, Murphy EE, Turner SP, et al. Circulating and gut-resident human Th17 cells express CD161 and promote intestinal inflammation. J Exp Med. 2009;206(3):525-34.

292. Lockhart E, Green AM, Flynn JL. IL-17 production is dominated by gammadelta T cells rather than CD4 T cells during Mycobacterium tuberculosis infection. J Immunol. 2006;177(7):4662-9.

293. Umemura M, Yahagi A, Hamada S, Begum MD, Watanabe H, Kawakami K, et al. IL-17-mediated regulation of innate and acquired immune response against pulmonary Mycobacterium bovis bacille Calmette-Guerin infection. J Immunol. 2007;178(6):3786-96.

294. Hamada S, Umemura M, Shiono T, Tanaka K, Yahagi A, Begum MD, et al. IL-17A produced by gammadelta T cells plays a critical role in innate immunity against listeria monocytogenes infection in the liver. J Immunol. 2008;181(5):3456-63.

295. Kolls JK, Lindén A. Interleukin-17 family members and inflammation. Immunity. 2004;21(4):467-76.

296. Langrish CL, Chen Y, Blumenschein WM, Mattson J, Basham B, Sedgwick JD, et al. IL-23 drives a pathogenic T cell population that induces autoimmune inflammation. J Exp Med. 2005;201(2):233-40.

297. Sivick KE, Schaller MA, Smith SN, Mobley HL. The innate immune response to uropathogenic Escherichia coli involves IL-17A in a murine model of urinary tract infection. J Immunol. 2010;184(4):2065-75.

298. Dixon BR, Radin JN, Piazuelo MB, Contreras DC, Algood HM. IL-17a and IL-22 Induce Expression of Antimicrobials in Gastrointestinal Epithelial Cells and May Contribute to Epithelial Cell Defense against Helicobacter pylori. PLoS One. 2016;11(2):e0148514.

299. Ouyang W, Rutz S, Crellin NK, Valdez PA, Hymowitz SG. Regulation and functions of the IL-10 family of cytokines in inflammation and disease. Annu Rev Immunol. 2011;29:71-109.

300. Radaeva S, Sun R, Pan HN, Hong F, Gao B. Interleukin 22 (IL-22) plays a protective role in T cell-mediated murine hepatitis: IL-22 is a survival factor for hepatocytes via STAT3 activation. Hepatology. 2004;39(5):1332-42.

301. Nagalakshmi ML, Rascle A, Zurawski S, Menon S, de Waal Malefyt R. Interleukin-22 activates STAT3 and induces IL-10 by colon epithelial cells. Int Immunopharmacol. 2004;4(5):679-91.

302. Pickert G, Neufert C, Leppkes M, Zheng Y, Wittkopf N, Warntjen M, et al. STAT3 links IL-22 signaling in intestinal epithelial cells to mucosal wound healing. J Exp Med. 2009;206(7):1465-72.

303. Sonnenberg GF, Monticelli LA, Alenghat T, Fung TC, Hutnick NA, Kunisawa J, et al. Innate lymphoid cells promote anatomical containment of lymphoid-resident commensal bacteria. Science. 2012;336(6086):1321-5.

304. Dudakov JA, Hanash AM, van den Brink MR. Interleukin-22: immunobiology and pathology. Annu Rev Immunol. 2015;33:747-85.

305. Rutz S, Eidenschenk C, Ouyang W. IL-22, not simply a Th17 cytokine. Immunol Rev. 2013;252(1):116-32.

306. Zheng Y, Valdez PA, Danilenko DM, Hu Y, Sa SM, Gong Q, et al. Interleukin-22 mediates early host defense against attaching and effacing bacterial pathogens. Nat Med. 2008;14(3):282-9.

307. Mulcahy ME, Leech JM, Renauld JC, Mills KH, McLoughlin RM. Interleukin-22 regulates antimicrobial peptide expression and keratinocyte differentiation to control Staphylococcus aureus colonization of the nasal mucosa. Mucosal Immunol. 2016;9(6):1429-41.

308. Andoh A, Zhang Z, Inatomi O, Fujino S, Deguchi Y, Araki Y, et al. Interleukin-22, a member of the IL-10 subfamily, induces inflammatory responses in colonic subepithelial myofibroblasts. Gastroenterology. 2005;129(3):969-84.

309. Zheng Y, Danilenko DM, Valdez P, Kasman I, Eastham-Anderson J, Wu J, et al. Interleukin-22, a T(H)17 cytokine, mediates IL-23-induced dermal inflammation and acanthosis. Nature. 2007;445(7128):648-51.

310. Starkey MR, Plank MW, Casolari P, Papi A, Pavlidis S, Guo Y, et al. IL-22 and its receptors are increased in human and experimental COPD and contribute to pathogenesis. Eur Respir J. 2019;54(1).

311. Wolk K, Warszawska K, Hoeflich C, Witte E, Schneider-Burrus S, Witte K, et al. Deficiency of IL-22 contributes to a chronic inflammatory disease: pathogenetic mechanisms in acne inversa. J Immunol. 2011;186(2):1228-39.

312. Geboes L, Dumoutier L, Kelchtermans H, Schurgers E, Mitera T, Renauld JC, et al. Proinflammatory role of the Th17 cytokine interleukin-22 in collagen-induced arthritis in C57BL/6 mice. Arthritis Rheum. 2009;60(2):390-5.

313. Brand S, Beigel F, Olszak T, Zitzmann K, Eichhorst ST, Otte JM, et al. IL-22 is increased in active Crohn's disease and promotes proinflammatory gene expression and intestinal epithelial cell migration. Am J Physiol Gastrointest Liver Physiol. 2006;290(4):G827-38.

314. Barros-Martins J, Schmolka N, Fontinha D, Pires de Miranda M, Simas JP, Brok I, et al. Effector γδ T Cell Differentiation Relies on Master but Not Auxiliary Th Cell Transcription Factors. J Immunol. 2016;196(9):3642-52.

315. Reinhardt A, Prinz I. Whodunit? The Contribution of Interleukin (IL)-17/IL-22-Producing γδ T Cells, αβ T Cells, and Innate Lymphoid Cells to the Pathogenesis of Spondyloarthritis. Front Immunol. 2018;9:885.

316. Seillet C, Luong K, Tellier J, Jacquelot N, Shen RD, Hickey P, et al. The neuropeptide VIP confers anticipatory mucosal immunity by regulating ILC3 activity. Nat Immunol. 2020;21(2):168-77.

317. Engel D, Dobrindt U, Tittel A, Peters P, Maurer J, Gütgemann I, et al. Tumor necrosis factor alpha- and inducible nitric oxide synthase-producing dendritic cells are rapidly recruited to the bladder in urinary tract infection but are dispensable for bacterial clearance. Infect Immun. 2006;74(11):6100-7.

318. Jones-Carson J, Balish E, Uehling DT. Susceptibility of immunodeficient gene-knockout mice to urinary tract infection. J Urol. 1999;161(1):338-41.

319. Kotenko SV, Izotova LS, Mirochnitchenko OV, Esterova E, Dickensheets H, Donnelly RP, et al. Identification of the functional interleukin-22 (IL-22) receptor complex: the IL-10R2 chain (IL-10Rbeta) is a common chain of both the IL-10 and IL-22 (IL-10-related T cell-derived inducible factor, IL-TIF) receptor complexes. J Biol Chem. 2001;276(4):2725-32.

320. Dumoutier L, Leemans C, Lejeune D, Kotenko SV, Renauld JC. Cutting edge: STAT activation by IL-19, IL-20 and mda-7 through IL-20 receptor complexes of two types. J Immunol. 2001;167(7):3545-9.

321. Pestka S, Krause CD, Sarkar D, Walter MR, Shi Y, Fisher PB. Interleukin-10 and related cytokines and receptors. Annu Rev Immunol. 2004;22:929-79.

322. Li J, Tomkinson KN, Tan XY, Wu P, Yan G, Spaulding V, et al. Temporal associations between interleukin 22 and the extracellular domains of IL-22R and IL-10R2. Int Immunopharmacol. 2004;4(5):693-708.

323. Yoon SI, Jones BC, Logsdon NJ, Harris BD, Deshpande A, Radaeva S, et al. Structure and mechanism of receptor sharing by the IL-10R2 common chain. Structure. 2010;18(5):638-48.

324. Xu MJ, Feng D, Wang H, Guan Y, Yan X, Gao B. IL-22 ameliorates renal ischemia-reperfusion injury by targeting proximal tubule epithelium. J Am Soc Nephrol. 2014;25(5):967-77.

325. Le PT, Pearce MM, Zhang S, Campbell EM, Fok CS, Mueller ER, et al. IL22 regulates human urothelial cell sensory and innate functions through modulation of the acetylcholine response, immunoregulatory cytokines and antimicrobial peptides: assessment of an in vitro model. PLoS One. 2014;9(10):e111375.

326. Martin JC, Bériou G, Heslan M, Chauvin C, Utriainen L, Aumeunier A, et al. Interleukin-22 binding protein (IL-22BP) is constitutively expressed by a subset of conventional dendritic cells and is strongly induced by retinoic acid. Mucosal Immunol. 2014;7(1):101-13.

327. Xu W, Presnell SR, Parrish-Novak J, Kindsvogel W, Jaspers S, Chen Z, et al. A soluble class II cytokine receptor, IL-22RA2, is a naturally occurring IL-22 antagonist. Proc Natl Acad Sci U S A. 2001;98(17):9511-6.

328. Mizoguchi A, Yano A, Himuro H, Ezaki Y, Sadanaga T, Mizoguchi E. Clinical importance of IL-22 cascade in IBD. J Gastroenterol. 2018;53(4):465-74.

329. Pelczar P, Witkowski M, Perez LG, Kempski J, Hammel AG, Brockmann L, et al. A pathogenic role for T cell-derived IL-22BP in inflammatory bowel disease. Science. 2016;354(6310):358-62.

330. Jinnohara T, Kanaya T, Hase K, Sakakibara S, Kato T, Tachibana N, et al. IL-22BP dictates characteristics of Peyer's patch follicle-associated epithelium for antigen uptake. J Exp Med. 2017;214(6):1607-18.

331. Pan CX, Tang J, Wang XY, Wu FR, Ge JF, Chen FH. Role of interleukin-22 in liver diseases. Inflamm Res. 2014;63(7):519-25.

332. Demirel I, Säve S, Kruse R, Persson K. Expression of suppressor of cytokine signalling 3 (SOCS3) in human bladder epithelial cells infected with uropathogenic Escherichia coli. Apmis. 2013;121(2):158-67.

333. Weidenbusch M, Song S, Iwakura T, Shi C, Rodler S, Kobold S, et al. IL-22 sustains epithelial integrity in progressive kidney remodeling and fibrosis. Physiol Rep. 2018;6(16):e13817.

334. Gnirck AC, Wunderlich M, Becker M, Xiong T, Weinert E, Meyer-Schwesinger C, et al. Endogenous IL-22 is dispensable for experimental glomerulonephritis. Am J Physiol Renal Physiol. 2019;316(4):F712-f22.

335. Ingersoll MA, Starkey MR. Interleukin-22 in urinary tract disease - new experimental directions. Clin Transl Immunology. 2020;9(6):e1143.

336. Hung CS, Dodson KW, Hultgren SJ. A murine model of urinary tract infection. Nat Protoc. 2009;4(8):1230-43.

337. Zychlinsky Scharff A, Albert ML, Ingersoll MA. Urinary Tract Infection in a Small Animal Model: Transurethral Catheterization of Male and Female Mice. J Vis Exp. 2017(130).

338. Dahlgren MW, Jones SW, Cautivo KM, Dubinin A, Ortiz-Carpena JF, Farhat S, et al. Adventitial Stromal Cells Define Group 2 Innate Lymphoid Cell Tissue Niches. Immunity. 2019;50(3):707-22.e6.

339. Mielke LA, Jones SA, Raverdeau M, Higgs R, Stefanska A, Groom JR, et al. Retinoic acid expression associates with enhanced IL-22 production by γδ T cells and innate lymphoid cells and attenuation of intestinal inflammation. J Exp Med. 2013;210(6):1117-24.

340. Scarfe L, Schock-Kusch D, Ressel L, Friedemann J, Shulhevich Y, Murray P, et al. Transdermal Measurement of Glomerular Filtration Rate in Mice. J Vis Exp. 2018(140).

341. Friedemann J, Heinrich R, Shulhevich Y, Raedle M, William-Olsson L, Pill J, et al. Improved kinetic model for the transcutaneous measurement of glomerular filtration rate in experimental animals. Kidney Int. 2016;90(6):1377-85.

342. Shih W, Hines WH, Neilson EG. Effects of cyclosporin A on the development of immune-mediated interstitial nephritis. Kidney Int. 1988;33(6):1113-8.

343. Lee S, Huen S, Nishio H, Nishio S, Lee HK, Choi BS, et al. Distinct macrophage phenotypes contribute to kidney injury and repair. J Am Soc Nephrol. 2011;22(2):317-26.

344. Friedewald JJ, Rabb H. Inflammatory cells in ischemic acute renal failure. Kidney Int. 2004;66(2):486-91.

345. Loering S, Cameron GJM, Starkey MR, Hansbro PM. Lung development and emerging roles for type 2 immunity. J Pathol. 2019;247(5):686-96.

346. Sabapathy V, Cheru NT, Corey R, Mohammad S, Sharma R. A Novel Hybrid Cytokine IL233 Mediates regeneration following Doxorubicin-Induced Nephrotoxic Injury. Sci Rep. 2019;9(1):3215.

347. Cameron GJM, Jiang SH, Loering S, Deshpande AV, Hansbro PM, Starkey MR. Emerging therapeutic potential of group 2 innate lymphoid cells in acute kidney injury. J Pathol. 2019;248(1):9-15.

348. Ramesh G, Ranganathan P. Mouse models and methods for studying human disease, acute kidney injury (AKI). Methods Mol Biol. 2014;1194:421-36.

349. Jang HR, Rabb H. Immune cells in experimental acute kidney injury. Nat Rev Nephrol. 2015;11(2):88-101.

350. Turner JE, Becker M, Mittrücker HW, Panzer U. Tissue-Resident Lymphocytes in the Kidney. J Am Soc Nephrol. 2018;29(2):389-99.

351. Langford DJ, Bailey AL, Chanda ML, Clarke SE, Drummond TE, Echols S, et al. Coding of facial expressions of pain in the laboratory mouse. Nat Methods. 2010;7(6):447-9.

352. Donovan C, Starkey MR, Kim RY, Rana BMJ, Barlow JL, Jones B, et al. Roles for T/B lymphocytes and ILC2s in experimental chronic obstructive pulmonary disease. J Leukoc Biol. 2019;105(1):143-50.

353. Banerji S, Ni J, Wang SX, Clasper S, Su J, Tammi R, et al. LYVE-1, a new homologue of the CD44 glycoprotein, is a lymph-specific receptor for hyaluronan. J Cell Biol. 1999;144(4):789-801.

354. Lee HW, Qin YX, Kim YM, Park EY, Hwang JS, Huo GH, et al. Expression of lymphatic endothelium-specific hyaluronan receptor LYVE-1 in the developing mouse kidney. Cell Tissue Res. 2011;343(2):429-44.

355. Shelite TR, Liang Y, Wang H, Mendell NL, Trent BJ, Sun J, et al. IL-33-Dependent Endothelial Activation Contributes to Apoptosis and Renal Injury in Orientia tsutsugamushi-Infected Mice. PLoS Negl Trop Dis. 2016;10(3):e0004467.

356. Sharp CN, Doll MA, Megyesi J, Oropilla GB, Beverly LJ, Siskind LJ. Subclinical kidney injury induced by repeated cisplatin administration results in progressive chronic kidney disease. Am J Physiol Renal Physiol. 2018;315(1):F161-f72.

357. Foxman B, Brown P. Epidemiology of urinary tract infections: transmission and risk factors, incidence, and costs. Infect Dis Clin North Am. 2003;17(2):227-41.

358. Klein RD, Hultgren SJ. Urinary tract infections: microbial pathogenesis, host-pathogen interactions and new treatment strategies. Nat Rev Microbiol. 2020;18(4):211-26.

359. Mulvey MA, Lopez-Boado YS, Wilson CL, Roth R, Parks WC, Heuser J, et al. Induction and evasion of host defenses by type 1-piliated uropathogenic Escherichia coli. Science. 1998;282(5393):1494-7.

360. Wu J, Hayes BW, Phoenix C, Macias GS, Miao Y, Choi HW, et al. A highly polarized T(H)2 bladder response to infection promotes epithelial repair at the expense of preventing new infections. Nat Immunol. 2020;21(6):671-83.

361. O'Brien VP, Hannan TJ, Yu L, Livny J, Roberson ED, Schwartz DJ, et al. A mucosal imprint left by prior Escherichia coli bladder infection sensitizes to recurrent disease. Nat Microbiol. 2016;2:16196.

362. Divekar R, Kita H. Recent advances in epithelium-derived cytokines (IL-33, IL-25, and thymic stromal lymphopoietin) and allergic inflammation. Curr Opin Allergy Clin Immunol. 2015;15(1):98-103.

363. Fort MM, Cheung J, Yen D, Li J, Zurawski SM, Lo S, et al. IL-25 induces IL-4, IL-5, and IL-13 and Th2-associated pathologies in vivo. Immunity. 2001;15(6):985-95.

364. Walker JA, McKenzie AN. Development and function of group 2 innate lymphoid cells. Curr Opin Immunol. 2013;25(2):148-55.

365. Hannan TJ, Roberts PL, Riehl TE, van der Post S, Binkley JM, Schwartz DJ, et al. Inhibition of Cyclooxygenase-2 Prevents Chronic and Recurrent Cystitis. EBioMedicine. 2014;1(1):46-57.

366. Cameron GJM, Cautivo KM, Loering S, Jiang SH, Deshpande AV, Foster PS, et al. Group 2 Innate Lymphoid Cells Are Redundant in Experimental Renal Ischemia-Reperfusion Injury. Front Immunol. 2019;10:826.

367. Moraes DA, Sibov TT, Pavon LF, Alvim PQ, Bonadio RS, Da Silva JR, et al. A reduction in CD90 (THY-1) expression results in increased differentiation of mesenchymal stromal cells. Stem Cell Res Ther. 2016;7(1):97.

368. Tang H, Liu N, Feng X, Yang Y, Fang Y, Zhuang S, et al. Circulating levels of IL-33 are elevated by obesity and positively correlated with metabolic disorders in Chinese adults. J Transl Med. 2021;19(1):52.

369. Dias-Júnior SA, Reis M, de Carvalho-Pinto RM, Stelmach R, Halpern A, Cukier A. Effects of weight loss on asthma control in obese patients with severe asthma. Eur Respir J. 2014;43(5):1368-77.

370. Palmieri V, Ebel JF, Ngo Thi Phuong N, Klopfleisch R, Vu VP, Adamczyk A, et al. Interleukin-33 signaling exacerbates experimental infectious colitis by enhancing gut permeability and inhibiting protective Th17 immunity. Mucosal Immunol. 2021.

371. Allinne J, Scott G, Lim WK, Birchard D, Erjefält JS, Sandén C, et al. IL-33 blockade affects mediators of persistence and exacerbation in a model of chronic airway inflammation. J Allergy Clin Immunol. 2019;144(6):1624-37.e10.

372. Tang KY, Lickliter J, Huang ZH, Xian ZS, Chen HY, Huang C, et al. Safety, pharmacokinetics, and biomarkers of F-652, a recombinant human interleukin-22 dimer, in healthy subjects. Cell Mol Immunol. 2019;16(5):473-82.

373. Ouyang W, O'Garra A. IL-10 Family Cytokines IL-10 and IL-22: from Basic Science to Clinical Translation. Immunity. 2019;50(4):871-91.

374. Ingersoll MA, Starkey MR. Interleukin 22 in urinary tract disease – new experimental directions. Clin Transl Immunology. (In press).

375. Sonnenberg GF, Nair MG, Kirn TJ, Zaph C, Fouser LA, Artis D. Pathological versus protective functions of IL-22 in airway inflammation are regulated by IL-17A. J Exp Med. 2010;207(6):1293-305.

376. Behnsen J, Jellbauer S, Wong CP, Edwards RA, George MD, Ouyang W, et al. The cytokine IL-22 promotes pathogen colonization by suppressing related commensal bacteria. Immunity. 2014;40(2):262-73.